

CONTROLLER DESIGN FOR RCTA AIRCRAFT USING PARAMETER ESTIMATION TO INTEGRATE NAVIGATIONAL TECHNIQUE

A Thesis submitted to the
UPES

For the Award of
Doctor of Philosophy
in
Aerospace Engineering

By
Roli Jaiswal

Dec. 2022

SUPERVISOR (s)

Dr. Om Prakash
Professor
Dr. Sudhir Kumar Chaturvedi
Associate Professor
Department of Aerospace Engineering, UPES



Department of Aerospace Engineering
School of Engineering (SOE)
UPES
Dehradun: 248007, Uttarakhand

CONTROLLER DESIGN FOR RCTA AIRCRAFT USING PARAMETER ESTIMATION TO INTEGRATE NAVIGATIONAL TECHNIQUE

A Thesis submitted to the
UPES

For the Award of
Doctor of Philosophy
in
Aerospace Engineering

By
Roli Jaiswal
SAP ID: 500065475

Oct. 2023

SUPERVISOR (s)

Dr. Om Prakash
Professor
Dr. Sudhir Kumar Chaturvedi
Associate Professor
Department of Aerospace Engineering, UPES



Department of Aerospace Engineering
School of Engineering (SOE)
UPES
Dehradun: 248007, Uttarakhand

Oct.2023

DECLARATION

I declare that the thesis entitled “**CONTROLLER DESIGN FOR RCTA AIRCRAFT USING PARAMETER ESTIMATION TO INTEGRATE NAVIGATIONAL TECHNIQUE**” has been prepared by me under the guidance of D r. Om Prakash, Professor, Department of Aerospace Engineering, UPES, and D r. Sudhir Kumar Chaturvedi, Associate Professor, Department of Aerospace Engineering, UPES. No part of this thesis has formed the basis for the award of any degree or fellowship previously.



Roli Jaiswal

School of Engineering [SOE]

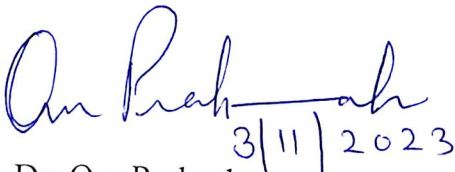
UPES

Dehradun: 248007, Uttarakhand

Nov.2023

CERTIFICATE

I certify that Roli Jaiswal has prepared her thesis entitled “**CONTROLLER DESIGN FOR RCTA AIRCRAFT USING PARAMETER ESTIMATION TO INTEGRATE NAVIGATIONAL TECHNIQUE**”, for the award of PhD degree of the UPES, under my guidance. She has carried out the work at School of Engineering, UPES.


3/11/2023
Dr. Om Prakash

School of Engineering,

UPES

Dehradun: 248007, Uttarakhand

Date: November 2023

CERTIFICATE

I certify that Roli Jaiswal has prepared her thesis entitled “**CONTROLLER DESIGN FOR RCTA AIRCRAFT USING PARAMETER ESTIMATION TO INTEGRATE NAVIGATIONAL TECHNIQUE**”, for the award of PhD degree of the UPES, under my guidance. She has carried out the work at School of Engineering, UPES.



Sudhir Kumar
Chaturvedi
3/11/2023

Dr. Sudhir Kumar Chaturvedi

School of Engineering

UPES

Dehradun: 248007, Uttarakhand

Date: November 2023

Dedicated to My family.

Motivated by My Beloved Husband

ABSTRACT

System Identification is the input /output model interface to develop a mathematical model in presence of noise, disruptions, etc. These random observations in terms of process and measurement noise are distorted due to sensors, and external disturbances. Handling imperfect measurements is simplified by evaluating the parameters of the system using statistical techniques. In the past years, system Identification has expanded its growth due to its application in designing controllers, health monitoring, and analysis of dynamic systems, making system fully autonomous, and fault-tolerant. Some of the traditional methods for linear systems in the frequency/ time domain are FFT, ML, and LS. System Id is applied to study the time-variant tracking behavior of vehicle subsystems in real time to update system modeling by parameter estimation in a continuous interval to detect sensor fault, and system failure [1][2][3]. The research work displays the result of the aerodynamic parameters of Hansa-III evaluated by applying the Maximum Likelihood algorithm.

Multiple numbers datasets were collected during the flight test of Hansa-III whereas, eight data sets were finalized for parameter estimation[10]. The Terminology HA resembles ‘Hansa-III’, L is Longitudinal, and numerals ‘1-8’ defines the number of data sets such as HAL1, HAL2, HAL3..... and so on. The Flight test was conducted by executing several control input forms such as Multi-step 3211 Input, Doublet Input, and Pulse Input. For longitudinal, the letter(s) accompanied by ‘L’ such as ‘M’ correspond to multi-step, ‘D’ as a doublet, and ‘P’ as pulse elevator control inputs.

The result exhibited in form of non-dimensional derivatives using the Maximum Likelihood method are considerably accurate and the value of the larger number of datasets are found close to wind tunnel values as correct calibration of the sensors before the flight test is the necessary step that needs to be executed to acquire a good quality of flight data. File processing of generated data gives information that $C_{L\alpha}$, $C_{m\alpha}$, $C_{m\delta_e}$, C_{D_0} , C_{m_0} , C_{m_q} are termed as strong derivatives whereas weak parameters $C_{L\delta_e}$, C_{Lq} , $C_{D\delta_e}$ affects in negligible amount as compared to strong so deviation in the value from wind-tunnel is neglected. It is found that there is a maximum departure in the wind-tunnel values for the Pulse Input form when comparing with Multi-step and

Doublet therefore Multi-step Input is more appropriate among all three Input forms. The type of control input (Multi-step, Doublet or Pulse) influences the estimates negligibly if the control input is appropriately excited to generate the data with proper information and frequency contents. Once the values of strong and weak derivatives are estimated then the Validation process is exercised to validate the result of derivatives that came from the wind tunnel and Maximum Likelihood methodology.

As system Identification expanded its application to design controllers thus the development of an autopilot for applications in defence, aerial surveillance, and transportation is a cause of to design of PID Controller. In the context of attitude controller design, the aircraft is modelled in longitudinal motion and the state-space matrix is formulated, and the PID controller is designed on MATLAB environment using Control System Toolbox satisfying design requirement. The time and frequency domain characteristics of different approaches such as Pole-Placement, Root-Locus, and Linear Quadratic Regulator are compared to get fruitful results. The gain parameters are optimized by comparing closed-loop PID tuning approaches such as ZN, Modified ZN, Tyreus- luyben, Astrum- Haglund for pitch control. The solution of these tuning approaches is analysed in form of gains K_p , K_i , K_d as The constant steady-state error is brought on by K_p , which also improves steady-state tracking fidelity and lessens the system's sensitivity while parameter variation. K_d refers to the system- stability but acquires poor steady-state feedback, and K_I have the characteristic of good steady-state response but leads to system instability. The Transfer function of PID consists of two zeros in the numerator, one pole is located at the origin in the denominator which makes the overall system highly stable. The response of the tuning technique, Astrum -Haglund is undamped oscillatory motion as it does not contain a derivative filter that leads to system instability. The response of Tyreus-Luyben experiences the larger value of K_d that influences overall system parameters thus aircraft stability is increased but the steady-state value is difficult to attain. The gain values of ZN and Modified ZN are compared and depict that both controllers approach steady state rapidly and features of stability but modified ZN exhibits the finest result as the controller satisfies design requirements and approaches steady state close to zero.

The Design of the Flight control System involves classical and modern approaches. The simplest way to design a controller is using SISO (Single Input Single Output) Systems but systems applicable for industries are MIMO (Multi Input Multi Output), which are more complex[1]

[2].The foremost classical technique is Root-locus which solves control system performance by adjusting the location of closed-loop poles to attain system performance by varying system parameters as per the control design requirement applied. The Classical approach (Root-Locus) has certain limitations to SISO Systems whereas modern control techniques can be applied to MIMO time-variant, linear/ non-linear systems. The Pole-placement and Linear Quadratic Regulator are proposed for the estimation of the gain matrix. The Simulated results acquired using LQR and Pole-Placement are analysed and conclude that the settling time of the LQR Controller is 0.44s as compared to 3.08s for Pole-Placement and has the excellent feature of eliminating steady-state error to zero. The peak overshoot value gives information about deviated peak time response concerning the final one which is 0.332 which exemplifies that LQR provides more stability and deviates minutely. Simulation results prove efficacious for the LQR approach used for designing the vigorous controller.

The study also investigates the problem statement connected to parameter estimation for the aircraft positioning systems subjected to inertial sensor measurements purveyed by Hansa-III aircraft. The Integration of the D.R algorithm in Hansa-III aircraft assists in estimating longitude, latitude, and altitude (θ , ϕ , h). The Dead Reckoning method determines the current position by utilizing the previously determined position over elapsed time on estimated speed. The research study incorporates the implementation of the navigational approach to estimate aircraft position. Dead- Reckoning is operated for cartesian coordinate estimation using real flight data and gives precise navigational details of aircraft at lost time signal connectivity. The results are validated with exponential smoothing in graphical/ tabulated form and summarize that percentage error of Latitude, Longitude is deemed to be very less that justifies the result dominantly.

ACKNOWLEDGEMENT

At the very beginning of the report, before acknowledging the support and the contribution of the countless personalities during the period of research work, I feel to take blessings from my father, Late Pramod Kumar Jaiswal, and almighty god for providing strength to proceed out the research study smoothly without any hindrance.

With deepest gratitude, I would like to express my heartfelt thanks to my mentor **Dr. Om Prakash** for his valuable time, active support, and guidance at every phase of the PhD work. Modeling and Simulation of any vehicular object in space is his specialty. His simplicity, generosity, and active enthusiasm all along the journey is highly commendable. I am privileged and indebted for his esteemed support and technical insights in flight mechanics. I would like to appreciate **Dr. Sudhir Kumar Chaturvedi**, my co-supervisor for helping me with publications and making it possible to complete my research study within the timeframe. With his simplicity, offering freedom to his research students, level of support, and follow-ups the research was a fruitful experience.

My Sincere thanks to **Prof Rakesh Kumar** who helped me by providing flight data for Hansa-III. A Person of simplicity, humility, and enthusiasm toward research in the area of Parameter estimation inspired me to opt for my research topic in the same area. I am indebted throughout my life as he was the one to introduce me to the concept of System Identification. His valuable suggestions, encouragement, and constant guidance throughout my life make me a good researcher.

I would take the opportunity to express my gratitude to **Dr. Ambuj Srivastava**, Chief Manager (Transport Aircraft Research and Design Centre), and **Abhishek Nigam**, Assistant Director (Directorate General of Civil Aviation, Ministry of Civil Aviation, India) for their constant encouragement during the initial days of my career in HAL. I've always be infatuated with them because of the vast information we shared.

Many pleasant recollections come to mind if I talk about UPES Workaholic life, it was an immense pleasure to work with and benefit from conversations with Dr. Om Prakash, Dr. M. Raja, and Dr. Vindhya Devella related to flight mechanics, and Control Systems. I would like

to express my gratitude to Dr. Ashish Mishra Dr. Rajesh Yadav, Dr. Aslesha Bodavula, Shikhar Purohit, and all the members of the Aerospace department as well as Manisha Yadav of Academic planning and Operations for their support and guidance throughout my PhD.

The entire PhD work is inspired by my beloved husband, **Atanu Sadhukhan** who played a significant role in my pedagogical endeavors. He is the one who encouraged me to opt for PhD. The technical knowledge of him in the aerospace industry assisted me during my research work. He is always standing at my back for constant support, and guidance. His patience, faith, and love is the reason for finishing research work within timeframe. I am utmost thankful to him for his unflinching support during the entire curriculum.

I acknowledge my thank to my mother-in-law for her boundless support, and the efforts she took without giving burden to me in performing house-hold chores. She never allowed me in the kitchen for cooking during the entire course. My heart-felt thanks to my father-in-law for his unflinching support, esteem love, and faith in me to finish my studies so that he could give me the title of Doctor in the prefix of my name.

I am exceptionally thankful to my mother for her sacrifices, and prayers throughout my educational pursuits as without her blessings, I cannot imagine reaching this stage. I am thankful to my brother-in-law, Pronoy Das who helped me to understand the Advance level of Excel which is useful in attaining my third research objective.

I am immensely thankful to my siblings - Neha Jaiswal, Kushagra, Sanju Bhai, Anoop Bhai, Mayank Bhai, Priyanka Das, Preeti Jaiswal, Vedika, and brother-in-law Sukhwinder Singh for their appreciation and constant encouragement. I would like to thank my BFF Sunaina Sharma for the invisible support, and unforgettable memories while sharing the room.

I am indebted to all the family members: my Uncle, Aunt, Balwinder Aunty, sister-in-law, and brother-in-law for their belief, positive thinking, and support during the PhD work.

I owe an apology for my mistakes to anybody unknowingly during the course of the study.

TABLE OF CONTENTS

<i>TITLE PAGE</i>	i
<i>DECLARATION</i>	ii
<i>CERTIFICATE</i>	iii
<i>ABSTRACT</i>	vi
<i>ACKNOWLEDGEMENT</i>	ix
<i>LIST OF FIGURES</i>	xiv
<i>LIST OF TABLES</i>	xx
<i>NOTATION AND ABBREVIATIONS</i>	xxii
1 CHAPTER 1: INTRODUCTION	1
1.1 AIRCRAFT SYSTEM IDENTIFICATION	1
1.2 AIRCRAFT CONTROLLER DESIGN	4
1.3 AIRCRAFT NAVIGATION SYSTEM	5
1.4 RESEARCH MOTIVATION	5
1.5 RESEARCH OBJECTIVES AND METHODOLOGY	6
1.6 CHAPTER SCHEME	8
2 CHAPTER 2: LITERATURE REVIEW	10
2.1 PARAMETER ESTIMATION	10
2.2 AIRCRAFT CONTROLLER DESIGN	15
2.3 AIRCRAFT NAVIGATION SYSTEM	17
3 CHAPTER 3: AIRCRAFT SPECIFICATIONS	22
3.1 AIRCRAFT	22
3.2 HANSA-III AIRCRAFT	27
4 CHAPTER 4: AIRCRAFT SYSTEM IDENTIFICATION	31
4.1 FLIGHT DATA GENERATION	35
4.2 DATA COMPATIBILITY CHECK	42
4.3 AERODYNAMIC MODELLING- HANSA-III AIRCRAFT	50
4.4 METHODOLOGY OF PARAMETER ESTIMATION	52
4.5 VALIDATION	59

5	CHAPTER 5: AIRCRAFT CONTROLLER DESIGN	63
	5.1 CONTROL SYSTEM	63
	5.2 AIRCRAFT STABILITY AND CONTROL SYSTEM	68
	5.2.1 AIRCRAFT STABILITY	68
	5.2.2 AIRCRAFT CONTROLS	70
	5.2.3 AIRCRAFT AXES & REFERENCE SYSTEM	71
	5.2.4 REFERENCE FRAMES	72
	5.2.5 LONGITUDINAL STABILITY	73
	5.3 LONGITUDINAL EQUATION IN WIND AXIS	86
	5.4 PID TUNING METHODS	93
	5.4.1 CLOSED LOOP TECHNIQUES	94
	5.4.2 OPEN LOOP TECHNIQUES	104
	5.5 CLASSICAL CONTROL APPROACH	107
	5.5.1 PD COMPENSATED CONTROLLER USING RL TECHNIQUE	110
	5.5.2 UNCOMPENSATED FEEDBACK CONTROL SYSTEM	113
	5.5.3 DESIGN ALGORITHM OF PD COMPENSATED CONTROLLER	116
	5.6 MODERN CONTROL METHODS	126
	5.6.1 POLE PLACEMENT TECHNIQUE	127
	5.6.2 LINEAR QUADRATIC REGULATOR	134
	5.7 VALIDATION	141
6	CHAPTER 6: AIRCRAFT NAVIGATION SYSTEM	149
	6.1 DEAD RECKONING	151
	6.2 NEWTON DIFFERENCE	160
	6.3 VALIDATION	164
7	CHAPTER 7: CONCLUSION AND FUTURE WORK	170
8	CHAPTER 8: REFERENCES	173
	APPENDIX	
	APPENDIX A: CURRICULUM VITEA	183
	APPENDIX B: MATLAB CODES	187
	APPENDIX C: EQUATION OF MOTION	191

APPENDIX D: GAIN AND CO-ORDINATE ESTIMATION	198
APPENDIX E: PUBLICATIONS	232

LIST OF FIGURES

		Page No.
1.1	Concept of System Identification	2
1.2	Flowchart Representation of Methodology	7
3.1	Aircraft Classification	24
3.2	Classification of Airplane	27
3.3	Hansa-III Aircraft	28
4.1	Wing and Tail Contribution to the Pitching Moment of Hansa-III Aircraft	37
4.2	Flight Dataset Pre-processing HALM5	38
4.3	Flight Dataset Pre-processing HALD1	39
4.4	Flight Dataset Pre-processing HALP1	40
4.5	3211 Elevator Input, HALM1	41
4.6	3211 Elevator Input, HALM3	41
4.7	3211 Elevator Input, HALM5	41
4.8	Doublet Elevator Input, HALD1	41
4.9	Pulse Elevator Input, HALP1	41
4.10	The measured and computed response of motion variables ($\theta, a_z, \alpha, q, V, \delta_e$) pertaining to Multi-step HALM5 Input form	47
4.11	The measured and computed response of motion variables ($\theta, a_z, \alpha, q, V, \delta_e$) pertaining to Doublet HAALD1 Input form.	48
4.12	The measured and computed response of motion variables ($\theta, a_z, \alpha, q, V, \delta_e$) pertaining to Pulse HALP1 Input form.	49
4.13	Output Error Method	53
4.14	showing convergence of HALM5 Input in terms of Aerodynamic Derivatives ($C_{Lq}, C_{L\alpha}, C_{L0}, C_{D0}, C_{D\alpha}, C_{D\delta_e}, C_{mq}, C_{m0}, C_{m\alpha}, C_{m\delta_e}$)	54
4.15	showing convergence of HALD1 Input in terms of Aerodynamic Derivatives ($C_{Lq}, C_{L\alpha}, C_{L0}, C_{D0}, C_{D\alpha}, C_{D\delta_e}, C_{mq}, C_{m0}, C_{m\alpha}, C_{m\delta_e}$)	55

4.16	showing convergence of HALP1 Input in terms of Aerodynamic Derivatives ($C_{Lq}, C_{L\alpha}, C_{L0}, C_{D0}, C_{D\alpha}, C_{D\delta e}, C_{mq}, C_{m0}, C_{m\alpha}, C_{m\delta e}$)	56
4.17	The measured and computed results obtained from ML: HALM5	57
4.18	The measured and computed results obtained from ML: HALD1	58
4.19	Parameter estimation from HALM4 and validation using HALD1	60
4.20	Compared Result of Wind-Tunnel, Dataset M-3, and MLH35 in term of Graphical representation	61
5.1	Open-loop Control System	64
5.2	Closed-loop Control System	65
5.3	Time-Variant Vs Time- Invariant	66
5.4	Linear Time-Variant Control system	67
5.5	Non- Linear Time-Variant Control system	67
5.6	Stable, Unstable, and Neutral System	69
5.7	Aircraft Controls	70
5.8	Stability Axes System	72
5.9	Wing and Tail contribution of Hansa-III Aircraft	73
5.10	Short period Frequency and Damping ratio	85
5.11	Estimation of Variables α, β, V from Wind-axis	87
5.12	Open-loop Control System of Hansa-III	91
5.13	Open-loop Step Response of Hansa-III	92
5.14	Closed-loop Control System of Hansa-III	92
5.15	Closed-loop Step Response of Hansa-III	93
5.16	Simulink block diagram of estimating K_u and T_u	95
5.17(1-4)	Estimation of K_u, T_u , Step response and Simulink block diagram of PID Controller: ZN	97
5.18	Simulink block diagram of PI Controller: ZN	97
5.19	Step response of aircraft dynamics with PI Controller: ZN	98
5.20	Simulink block diagram of PD Controller: ZN	98
5.21	Step response of aircraft dynamics with PD Controller: ZN	99
5.22	Step response and Simulink Block diagram of PID Controller: MZN	100
5.23	Simulink block diagram of PID Controller: TL	101

5.24	Simulink block diagram of PI Controller: TL	101
5.25	Step response of aircraft dynamics with PID and PI Controller: TL	102
5.26	Step response and Simulink block diagram of PID Controller: AH	104
5.27	Root-locus Plot of Uncompensated Controller	108
5.28	Bode-Plot of Uncompensated Controller	110
5.29	Schematic Diagram of PID Controller	111
5.30	Flowchart to design aircraft Pitch Controller	112
5.31	Uncompensated Feedback Control System	113
5.32	Step response of Uncompensated Feedback Control System	114
5.33	Root-Locus and Bode-Plot of Uncompensated Feedback Control System	115
5.34	Location of Closed Dominant Pole	117
5.35	Determination of Damping Ratio	117
5.36	Root-Locus of PD Compensated Controller	118
5.37	Pitch Attitude Control System	120
5.38	Pitch angle Verses Step Input	121
5.39	Pitch Angle Step Response	122
5.40	Root-Locus Plot compensated Controller	122
5.41	Bode-Plot compensated Controller	123
5.42 (1-3)	Compensator Diagram	124
5.43	Bar Pictorial Representation with and without Controller in Time-Domain	125
5.44	Bar Pictorial Representation with and without Controller in Frequency-Domain	126
5.45	Feedback Control Design	127
5.46	Pole Placement	128
5.47	Step Response using pole placement without scaling effect	132
5.48	Closed-Loop Step Response using pole placement with scaling effect	133
5.49	Flowchart of Linear Quadratic Regulator	135
5.50	Closed Loop Step Response using LQR Controller	139

5.51	Result of Hansa-III with general aviation Airplane using MZN	142
5.52	Result of Hansa-III with general aviation Airplane using ZN	143
5.53	Result of Hansa-III with general aviation Airplane using TL	143
5.54	Result of Hansa-III with general aviation Airplane using AH	144
5.55	Simulink block diagram of Attitude Controller of Hansa-III	145
5.56	LQR Result of Hansa-III with general aviation Airplane: Validation	147
6.1	Dead Reckoning	151
6.2	Flowchart of Dead Reckoning	153
6.3	RoadMap for geodetic co-ordinate Estimation	154
6.4	NED Coordinate System	155
6.5	Forecast of Acceleration in X, Z, and Heading angle	157
6.6	Geographical co-ordinates at Initial Phase of Flight test, IIT Kanpur	158
6.7	Forecasted Value of X, Y Aircraft Coordinates using DR	159
6.8	Forecasted Value of Longitude, Latitude in degrees using DR	160
6.9	Forecasted Value of X, Y Aircraft Coordinates using Newton-Difference Method	161
6.10	Comparison of Forecasted Value of X Position of aircraft using DR and Newton-Difference Method	162
6.11	Comparison of Forecasted Value of Y Position of aircraft using DR and Newton-Difference Method	163
6.12	Comparison of Forecasted Value of Longitude, latitude of aircraft using DR and Newton-Difference Method	163
6.13	Forecasted Value of Longitude using Exponential Smoothing Technique	165
6.14	Forecasted Value of Latitude using Exponential Smoothing Technique	166
6.15	Forecasted Value of Longitude, Latitude in degrees using Exponential Smoothing Technique	166
6.16	Graphical Representation of Longitude, Latitude using (D.R, ES, ND)	168
C. 1	Components of gravitational force in body axis	196

D.1	Comparison of Proportional gain value of Multi-step Input datasets	202
D.2	Comparison of Integral gain value of Multi-step Input datasets	202
D.3	Comparison of Derivative gain value of Multi-step Input datasets	203
D.4	Comparison of Proportional gain value of Pulse Input datasets	203
D.5	Comparison of Integral gain value of Pulse Input datasets	204
D.6	Comparison of Derivative gain value of Pulse Input datasets	204
D.7	Comparison of Proportional gain value of Doublet Input datasets	205
D.8	Comparison of Integral gain gain value of Doublet Input datasets	205
D.9	Comparison of Derivative gain value of Doublet Input datasets	206
D.10	Comparison of Proportional gain value of Multi-step, Doublet, and Pulse input datasets	206
D.11	Comparison of Integral gain value of Multi-step, Doublet, and Pulse input datasets	207
D.12	Comparison of Derivative gain value of Multi-step, Doublet, and Pulse input datasets	207
D.13	Comparison of Proportional gain value of Multi-step, Doublet, and Pulse input datasets of PD Controller	208
D.14	Comparison of Integral gain value of Multi-step, Doublet, and Pulse input datasets of PD Controller	208
D.15	Comparison of Proportional Integral gain value of Multi-step, Doublet, and Pulse input datasets of PD Controller	209
D.16	Step response of Multi-step Input Dataset H0-H12 using Ziegler Nicholas tuning technique	211
D.17	Step response of Doublet, and Pulse Input Dataset D1, HP1, and HP2 using Ziegler Nicholas tuning technique	212
D.18	Step response of Multi-step Input Dataset H0-H12 using Modified Ziegler Nicholas tuning technique	214
D.19	Step response of Multi-step Input Dataset H0-H12 using Modified Ziegler Nicholas tuning technique	215
D.20	Step response of Multi-step Input Dataset H0-H12 using Tyreus-Luyben tuning technique	217

D.21	Step response of Doublet, Pulse Input Dataset HD1, HP1, and HP2 using Tyreus-Luyben tuning technique	218
D.22	Step response of Multi-step Input Dataset H0-H12 using Astrum-Hagglund tuning technique	220
D.23	Step response of Doublet, Pulse Input Dataset HD1, HP1, and HP2 using Astrum- Hagglund tuning technique	221
D.24	Step response of Multi-step Input Dataset H0-H12 using Ziegler Nicholas tuning technique of PI Controller	223
D.25	Step response of Doublet, Pulse Input Dataset HD1, HP1, and HP2 using Astrum- Hagglund tuning technique	224
D.26	Step response of Multi-step Input Dataset H0-H12 using Tyreus-Luyben tuning technique of PI Controller	226
D.27	Step response of Doublet, Pulse Input Dataset HD1, HP1, and HP2 using Astrum- Hagglund tuning technique	227
D.28	Step response of Multi-step Input Dataset H0-H12 using Ziegler Nicholas tuning technique of PD Controller	229
D.29	Step response of Doublet, Pulse Input Dataset D1, P1, and P2 using Ziegler Nicholas tuning technique	230

LIST OF TABLES

		Page No.
3.1	Comparison of Aircraft	27
3.2	Geometrical and Aerodynamic Parameters	29
3.3	Power Plant Specifications of Hansa-III	29
3.4	Specification of Control Surface deflection and C.G Range of Hansa-III	30
4.1	Estimation of Scale factor and bias factor	50
4.2	Parameter Estimation Using ML Method for Longitudinal case: Multi-step, Doublet, and Pulse Inputs	59
4.3	Compared Result of Longitudinal Derivatives of Wind-Tunnel, Dataset M-3, and MLH35 [4]	61
5.1	Geometrical and Aerodynamic Parameter of Hansa-III	74
5.2	Estimation of Non-dimensional derivatives using Analytical Method	84
5.3	Estimation of short-Period Damping ratio and frequency	84
5.4	Classical PID Tuning Parameters : ZN	97
5.5	Classical PID, PD, PI Tuning Parameters Value : ZN	99
5.6	Classical PID Tuning Parameters : MZN	100
5.7	Classical PID Tuning Parameters: TL	101
5.8	Classical PID, PI Tuning Parameters Value : TL	102
5.9	Classical PID Tuning Parameters: AH	103
5.10	Classical PID Tuning Parameters : Open-loop ZN	105
5.11	Classical PID Tuning Parameters : CHR	105
5.12	Classical PID Tuning Parameters : Cohen-Coon	106
5.13	Hansa-III Pitch Attitude Characteristics	125
5.14	Time domain Performance characteristics using Pole-Placement Technique	134
5.15	Time domain Performance characteristics using LQR	140
5.16	Result Validation of PID Tuning Techniques with General aviation Airplane	142

5.17	Time Domain Characteristics with and without Controller of Hansa-III	145
5.18	Comparison of Time domain characteristics	146
5.19	LQR Result Validation of Time domain characteristics with General Aviation Airplane	146
6.1	Conversion XY Co-ordinate to Latitude and Longitude	159
6.2	Estimation of Percentage Error	164
6.3	Comparison of values of Longitude, Latitude using Exponential Smoothing, Newton Difference Method, and Dead Reckoning Technique	168
D.3	Estimation of Cartesian Coordinates Using Flight Data	231

NOTATION AND ABBREVIATIONS

Notation

a_x, a_y, a_z	Linear accelerations along x, y, z body axes (m/s^2)
ϵ	Downwash
C_Y	Side force Coefficient
E	Error
g	acceleration due to gravity
H	Angular Momentum
J	Cost Function
K_β	Scale Factor
L, M, N	Pitching, rolling, and Yawing moment
M	Net Moment
m	Mass of aircraft (kg)
p, q, r	roll, pitch, yaw rates ($rad-s^{-1}$)
R	Measurement co-variance Matrix
T	Thrust
u, v, w	Longitudinal, lateral, and vertical airspeed
V	Airspeed (m/s)
X, Y, Z	Force acting toward flow direction, toward right wing, and underneath through it
Θ	vector of unknown parameters
α	angle of attack
β	slide slip angle

Q	Dynamic Pressure
Δ	Bias
$\delta_a, \delta_e, \delta_r$	aileron, elevator, rudder deflection angle
ζ	Time delay
ρ	Air density
Φ, θ, ψ	angle of roll, pitch and yaw (degree)
$\dot{p}, \dot{q}, \dot{r}$	Rate of roll, pitch, and yaw rate
X_E, Y_E, Z_E	Force acting toward Geographical North, Geographical East, and centre of the earth
X_w, Y_w, Z_w	Force acting relative to velocity vector, toward right wing, and underneath through it
u_o, v_o, w_o	Perturbed velocity along X, Y, and Z
$\Delta u, \Delta v, \Delta w$	Small perturbations along X, Y, and Z
M_q	Non-dimensional variation of pitching moment with pitch rate
$M_{\dot{\alpha}}$	Non-dimensional variation of pitching moment with change in angle of attack
Z_{α}	Non-dimensional variation of Z force with angle of attack
M_{α}	Non-dimensional variation of pitching moment with angle of attack
$w_{n_{sp}}$	Frequency of short period
ξ_{sp}	Damping ratio of short period
ξ_p	Frequency of Phugoid Motion
w_{n_p}	Damping ratio of Phugoid Motion
\bar{C}	mean aerodynamic chord
I_{XX}, I_{YY}, I_{ZZ}	Moment of Inertia about x, y, z axes
I_{XY}, I_{XZ}, I_{YZ}	Products of inertia in the XY, XZ and YZ plane, respectively, kg-m ²

V_H Tail Volume ratio

Abbreviations

ACH	Attitude Control System
AH	Astrum Haglund
ANN	Artificial Neural Network
AOA	Angle of attack
ASCG	Measured from center of gravity to accelerometer
CFD	Computational Fluid Dynamics
CG	Center of gravity
CS	Control System
DC	Direct Current
DLR	Deutsche Forschungsanstalt für Luft- und Raumfahrt (German Aerospace Centre)
DR	Dead Reckoning
EKF	Extended Kalman Filter
ES	Exponential Smoothing
FFT	Fast Fourier Transformation
FOPID	Fractional Order PID Controller
FPR	Flight Path Reconstruction
FSFC	Full state feedback Controller
GLONASS	Global Navigation Satellite System
GN	Gauss Newton
GPS	Global Positioning System
IMU	Inertial Measurement Unit
INS	Inertial Navigation System
LM	Levenberg Marquardt
LP	Long Period
LQR	Linear Quadratic Regulator
LS	Least Square

MAC	Mean Aerodynamic chord
ML	Maximum Likelihood
MZN	Modified Ziegler Nicholas
NAL	National Aerospace Laboratory
NBCG	Measured from center of gravity of aircraft to nose-boom
ND	Newton Difference
NGN	Neural Gauss Newton
NLI	Non-Linear Invariant
NLO	Non-linear Observer
OAT	Outside Air Temperature
PID	Proportional, Integral, Derivative
QDR	Quadrotor Dead Reckoning
RCTA	Research cum trainer aircraft
SP	Short Period
TF	Transfer Function
TL	Tyreus- Luyben
UAV	Unmanned Aerial Vehicle
XKF	Exogeneous Kalman Filter
ZN	Ziegler Nicholas

Subscripts

$\alpha, \beta, \dot{\alpha}, \dot{\beta}$	With respect to $\alpha, \beta, \dot{\alpha} \frac{b}{2V_\infty}, \dot{\beta} \frac{b}{2V_\infty}$
∞	Freestream
f	Fuselage
M	Mach number
m	Measured variables
p, q, r	With respect to $p \frac{b}{2V_\infty}, q \frac{b}{2V_\infty}, r \frac{b}{2V_\infty}$
ss	Steady-state
t	Horizontal tail
w	Wing

Superscript

- Derivative with respect to time
- ~ Variable in frequency domain

Longitudinal Stability and Control Derivatives

C_{D_0}	Coefficient of drag force at zero angle of attack
C_{D_α}	Change in Coefficient of drag force with change in angle of attack
$C_{D_{\delta e}}$	Change in Coefficient of drag force with change in elevator deflection angle
C_{L_α}	Change in Coefficient of lift force with change in angle of attack
C_{L_0}	Coefficient of lift force at zero angle of attack
C_{L_q}	Change in Coefficient of lift force with change in pitch rate
$C_{L_{\delta e}}$	Change in Coefficient of lift force with change in elevator deflection angle
C_{m_0}	Coefficient of pitching moment at zero angle of attack
C_{m_α}	Change in Coefficient of pitching moment with change in angle of attack
C_{m_q}	Change in Coefficient of pitching moment with change in pitch rate
$C_{m_{\delta e}}$	Change in Coefficient of pitching moment with change in elevator deflection angle

$$C_{D\alpha} = \frac{\partial C_D}{\partial \alpha}$$

$$C_{D\delta_e} = \frac{\partial C_D}{\partial \delta_e}$$

$$C_{L\alpha} = \frac{\partial C_L}{\partial \alpha}$$

$$C_{Lq} = \frac{\partial C_L}{\partial (q\bar{c}/2u)}$$

$$C_{L\delta_e} = \frac{\partial C_L}{\partial \delta_e}$$

$$C_{m\delta_e} = \frac{\partial C_m}{\partial \delta_e}$$

$$C_{m\alpha} = \frac{\partial C_m}{\partial \alpha}$$

$$C_{mq} = \frac{\partial C_m}{\partial (q\bar{c}/2u)}$$

CHAPTER 1

INTRODUCTION

Control Systems are an integral part of modernization. Enormous applications of control systems surround us in day-to-day life such as traffic control systems, rocket fire, the Lift-off of a space shuttle to Earth's circle, and auto-guided vehicles transporting goods in aerospace assembly workspace glides along to reach their destination are some of the examples of an automatic control system. Based on these live examples, the research study aims to design, simulate, and develop the Control system and navigation of trainer aircraft Hansa-III based on a six degrees of freedom linear dynamic model using a maximum likelihood algorithm for estimating aerodynamic derivatives. Developing a mathematical model is a key parameter required for designing a control system. Aircraft system identification applies to engineering systems like aerospace vehicles to develop a mathematical model of the system. System identification was first defined by Zadeh stated, "Identification is a tool to identify systems on the basis of Inputs, outputs, and test conditions which is elaborately discussed in the next section(Roudbari & Saghafi, 2016)

1.1 AIRCRAFT SYSTEM IDENTIFICATION

The input-output model interface for developing the mathematical model in the existence of noise and disruptions is known as System Identification. In Layman's Understanding, System Identification is identifying parameters of the physical system subjected to observations to develop a mathematical model for the system.

General System Identification: The basic elements to define Identification problems include

- (a) Input to experiment behaviour of the physical system in the form of Maneuverers
- (b) Mathematical Model of the physical system
- (c) Responses in terms of Measurement
- (d) Methodology adopted to define system Identification

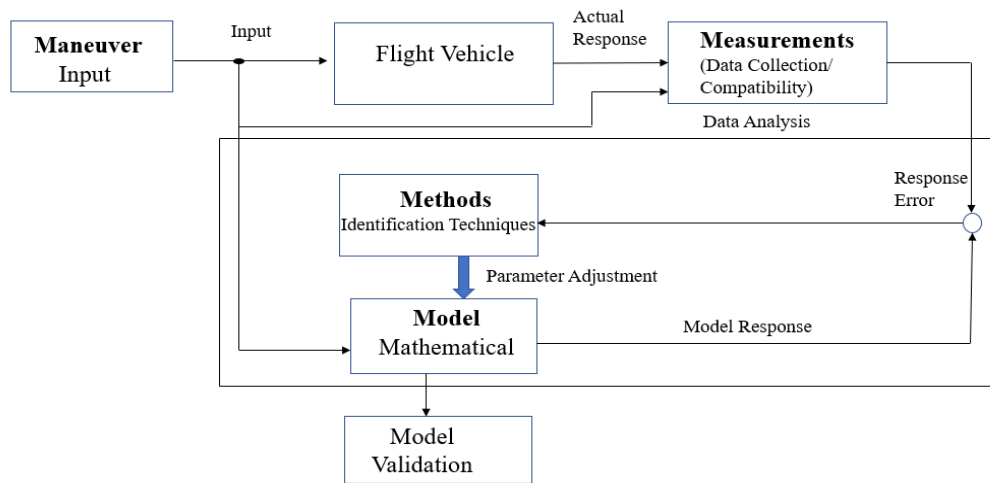


Fig 1.1: Concept of System Identification

The German Aerospace Centre (DLR) developed the Quad M by outlining five components that are essential to understanding System Identification as presented in Fig 1.1 (Hamel, 2019)(Hamel & Jategaonkar, 1996a)

Maneuverers: Control inputs are fed into system dynamics to experience the consequences despite output.

Measurement: High-quality sensors are used to evaluate the system's process and measurement noise, also known as a data compatibility check.

Model: It consists of mathematical equations based on the Newtonian law of motion. The Linear and non-linear models are used for flight vehicle system Identification.

Methodology: It is based on the Input/output interface and used for the time and frequency domain.

Validation: It defines testing, measuring, executing, and validating physical systems. It identifies whether the model meets desired expectations or not.

Approaches to System Identification

System Identification is classified on the basis of model class and model structure(Hoffer et al., 2013)

1. *The model class*

(i) Linear/ Non-linear (ii) Parametric/ Non-parametric

Linear Models are simpler and more flexible for stochastic dynamics as well as the convergence of the physical system is guaranteed whereas the Non-linear model requires enough computations with no guarantee of convergence. Linear approximation is helpful for robust control design as Linear models give continuous responses to system parameters and give a better understanding to predict complex system behaviour. The system modelling is improved by linearized approximation thus linear modelling is advisable. Recent technology advancements expedite the more often usage in parameter estimation areas such as designing controls and autopilots, handling fault-tolerant issues, expanding the v-n curve, monitoring system health, and contrasting wind tunnel test results with analytical techniques like CFD (Computational Fluid Dynamics).

Parametric Identification techniques include the least-square, maximum likelihood methodology to identify model parameters, referred to as black-box modelling(Leontaritis & Billings, 1985)(Jameson & Cooke, 2012a). Non-Parametric identification techniques include neural networks and genetic algorithms and they do not require postulates to assume a model structure. These models are used to gain knowledge of model complexity and model validation(Juang & Suzuki, 1986)

2. The model Structure

(i) Black box (ii) Grey box (iii) user-defined model

The Black-box model assumes an unknown system and model parameters don't have constraints. Grey-box model assumes that some of the system-related information is known and parameters have constraints. User-defined model is a generic user-defined model using an input/ output interface.

Vehicle categorization is correlated and captures one aspect of system identification at one time on the basis of model class and structure(Roudbari & Saghafi, 2016)(Hardier & Bucharles, 2010)(Tischler & Remple, 2006)

General Attributes of System Identification are

- (i) Cost-effective
- (ii) Self-governing System
- (iii) Elimination of Random/Systematic error

1.2 AIRCRAFT CONTROLLER DESIGN

In terms of multi-rotor drones, flying cars, and hybrid airships, aerospace technology is expanding rapidly. In the context of automatic control design, it has played a crucial role as a catalyst by encouraging the researcher's interest in areas such as reconnaissance missions, terrain surveillance, aerial photography, etc. An autopilot alleviates pilot tasks during innumerable flight regimes and handles

adverse weather conditions to provide stability. The controller design requires comprehensive expertise in control theory, parameter estimation (R. Kumar, 2012) (Harper & Cooper, 1986), and flying handling quality. An enormous PID tuning approach to optimize gain values of the controller such as Ziegler Nicholas, Astrom-Haglund, Modified Ziegler Nicholas, and Tyreus-Luyben are used to study time domain characteristics as discussed by (Deepa & Sudha, 2016)(JAISWAL & PRAKASH, 2022). Modern approaches such as Pole-Placement, and LQR to design the Pitch controller of Hansa-III aircraft are discussed elaborately in chapter 5 of the thesis.

1.3 AIRCRAFT NAVIGATION SYSTEM

The evolution of research in the discipline of Navigation is always captivating as it is applied to detect orientation, exact position, and velocity. The research study inspects the problem statement for aircraft positioning systems depending on inertial sensor measurement apportioned by Hansa-III. The dead Reckoning approach measures position once GPS is not functional as suggested by M. Jayachandran thus D.R. algorithm is accomplished within the aircraft display system which acquires position information, and attitude (Jayachandran et al., 2009). The numerous applications of Dead Reckoning are surveillance, mobile robots, marine navigation, aircraft navigation, and automotive navigation. Pure D.R. technique is cheaper, economical, and causes systematic error thus pure D.R. technique is not applied where accurate position, radio-signal-based navigation is required. INS is integrated with dead reckoning equipment to provide accurate, reliable navigation results.

1.4 RESEARCH MOTIVATION

An enormous amount of work in the area of parameter estimation using various methodologies like Output error method (OEM), Filter error method (FEM), and Equation error method (EEM) had been accomplished for Hansa-III aircraft but there is a clear research gap when it comes to design a controller to make the

system fully autonomous so that it can be utilized for training pilots, analysis of dynamic systems, research-oriented activities, fault-tolerant system, accidental investigation.

No research is carried out for Hansa-III in terms of navigation henceforth, the dead reckoning navigational technique will be implemented to study the attitude, and orientation of the system so that it can be used for surveillance in terrain-prone areas, aerial photography, monitoring of floods/droughts.

Designing an auto-controller, and integrating a novel navigational approach using parameter estimation of Hansa-III motivates to perpetrate research in this area.

1.5 RESEARCH OBJECTIVES AND METHODOLOGY

Research Objectives

1. Estimation of longitudinal stability and control derivatives from real flight data of Hansa-III aircraft using Output Error Method
2. Design of PID Controller for aircraft pitch control, analyzing stability and performance characteristics for hardware implementation
3. Integration of Dead Reckoning approach to estimate the expected position of Hansa-III Aircraft

Methodology:

The methodology proposed for this study is discussed in form of a flow-chart:

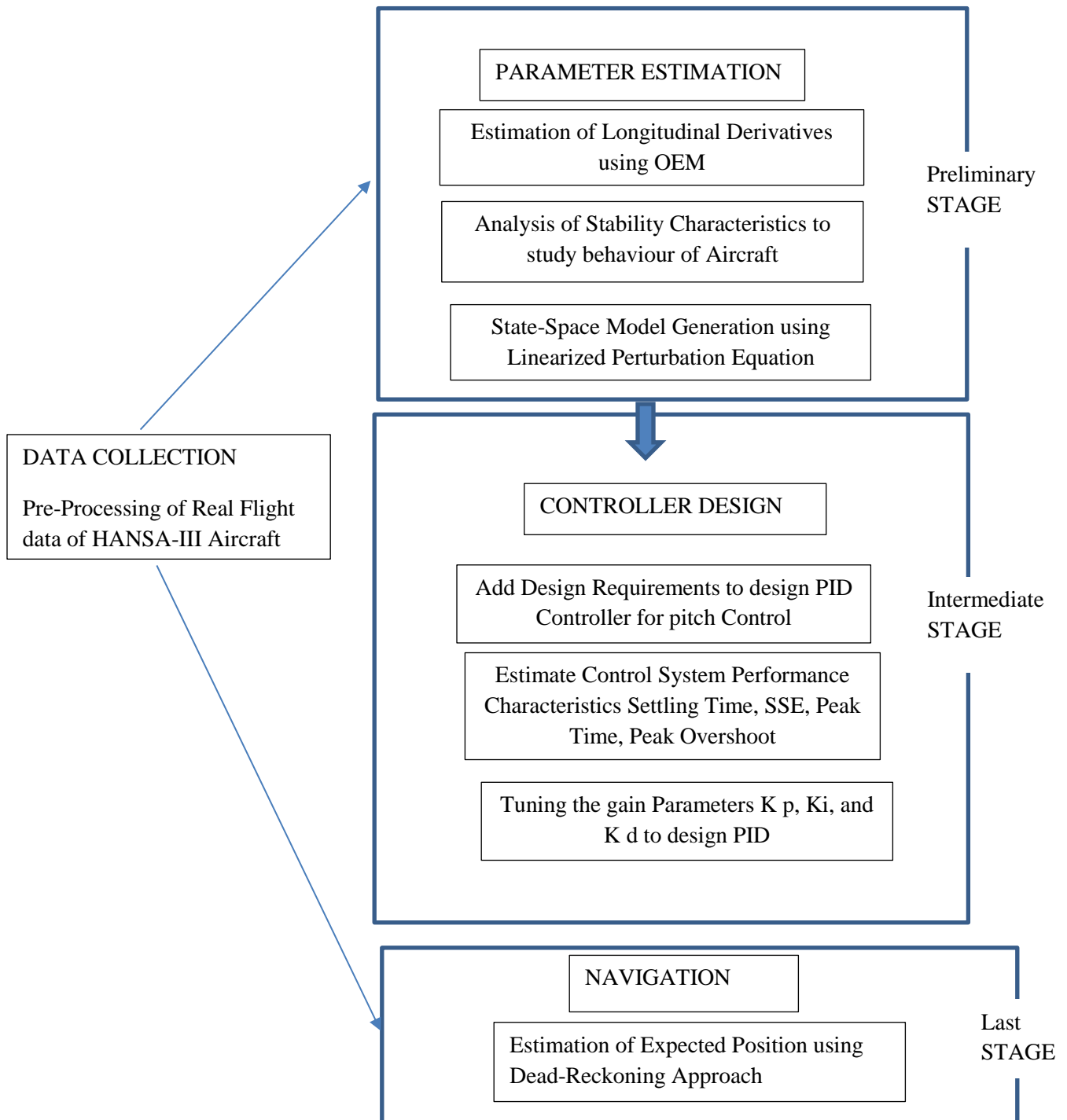


Fig 1.2 Flowchart Representation of Methodology

1.6 CHAPTER SCHEME

The thesis comprises Seven Chapters which are outlined as:

Chapter 1 The first chapter contains the overview of Aircraft parameter Estimation, Control Design Approaches, Aircraft Navigation System, research motivation, objectives, modelling tools, and research summary

Chapter 2 covers the literature survey of the attitude control system, aircraft system Identification, modelling, simulation, and dead reckoning method, design of the pitch control system.

Chapter 3 discusses the classification and categories of aircraft and a brief description of model specifications.

Chapter 4 discusses the procedure of Parameter Estimation, file processing, Data compatibility check, Mathematical modelling, and Maximum Likelihood Technique for the estimation of longitudinal derivative.

Chapter 5 briefly presents aircraft stability and control, automatic control system, Reference frame, Linearized equation of motion, state-space matrix representation for controller design, PID Controller Design, Tuning PID parameters using ZN, AH, MZN, TL techniques, Controller design using Root-Locus, pole-placement, LQR approach and comparing results using Simulation

Chapter 6 presents an estimation of navigational parameters (latitude, longitude, altitude) using Dead Reckoning, a Comparison of results using exponential smoothing, and the Newton-difference method.

Chapter 7 discusses the conclusion derived from the three objectives and a brief scope for future work is identified to extend the research study. Lastly, references in the form of the research paper, technical report, book, and chapters are referred to in the thesis.

SUMMARY:

In this chapter, we discussed the concepts of aircraft system Identification, aircraft controller design, and aircraft navigation system. Additionally, the research motivation for choosing the topic, research objectives, and methodology are also presented. The chapter scheme covers topics such as Introduction, Literature Review, Aircraft Model Specifications, Aircraft Parameter Estimation, Aircraft Controller Design, Aircraft Navigation System, conclusion, and scope for future work.

CHAPTER -2

LITERATURE SURVEY

System Identification is a scientific discipline to identify the model based on the Input/ output observations. Parameter Estimation is an extremely formidable, extensively applied example of system Identification that estimates the attributes of a dynamic system based on conceptualization consideration of the mathematical model (Hamel, 1979)(Iliff, 1989). The task of best estimate determination is known as parameter estimation. A lot of research has been conducted in the area of parameter estimation of Hansa-III. The current technological advancement reflects the gap between automation and to design attitude controller of Hansa-III. The research study aims to design a controller by implementing a statistical output error approach to estimate the expected position of Hansa-III. To intervene in the gap, the autonomous controller integrated with the dead Reckoning algorithm to estimate navigational parameters is designed.

The Literature is reviewed in three different sections a) Parameter Estimation, b) Controller Design, and c) Aircraft Navigation as Dead Reckoning

2.1 PARAMETER ESTIMATION

The task of best estimate determination is known as parameter estimation. The successful application is due to fine data processing handling capability, better-measuring techniques, and appropriate flight-test for adequate aerodynamic modelling (Hamel, 1979)(Klein, 1989)

Bryan discussed the adequacy of modelling forces and moments and validated the mathematical model. The author introduces aerodynamic modelling that includes the relationship of forces and moments about an axis respectively. The aerodynamic model is in the form of Taylor series expansion such as

$$C_j = \sum_j \frac{\partial C_j}{\partial \sigma} \sigma + \sum_j \frac{\partial C_j}{\partial u} u$$

Where j stands for rolling, pitching, and yawing moment (l, m, and n), X, Y, and Z forces in X, Y, and Z direction, σ as motion variables airspeed, angle of attack, side-slip angle, and u as control input(Bryan, 1911).

E. Seckel, J. Morris, and R. D. Finck stated aerodynamic parameters are estimated using three different approaches at the early stage of aircraft design such as wind-tunnel Testing Method, Flight test, and analytical method. Among all the three modes, the analytical method was the convenient process of estimating parameters but the accuracy is low to attain thus results obtained from the analytical need to be validated from wind-tunnel and flight tests [21]- [22]

Hamel, P. G., and Jategaonkar, R. V., discussed the theory and evolution of system Identification of various flight vehicles in chronological order. The author also determined the damping ratio and frequency from flight data as well as applications in the area of system Identification(Hamel & Jategaonkar, 1996b).

K.W. Iliff, Hamel, and Jategaonkar stated Maximum Likelihood has been successfully used to flight data for parameter estimation. The acknowledged standard approach for estimating an aircraft's stability and control derivatives uses ML with process noise and measurement noise. (Hamel & Jategaonkar, 1996a)(Iliff, 1989) (Jategaonkar, 2015)

Hamel, Jategaonkar, Maine and Iliff covered a broader aspect of output error as its applicability has been extended to the non-linear system. The most applicable

version of Maximum Likelihood: its advantages and properties are discussed elaborately(Hamel & Jategaonkar, 1996a)(Maine & Iliff, 1986) (Hamel, 1979)

Klein addressed linear regression for model determination, the applicability of ML in the frequency domain and time domain, and data compatibility. The parameter estimation techniques at different flying regimes, and unsteady, unstable aircraft conditions were also addressed by the author(Klein, 1989).

D. Kuehme, N. R. Alley, C. Phillips, B. Cogan, E. A. Morelli and J. A. Grauer discussed OEM, FEM, EEM, EKF, Regression analysis in the time domain for parametric identification as this methodology describes a correlation between flight test-bed data and linear model(Kuehme et al., 2014) used this technique to study longitudinal, lateral Stability, control, and damping coefficients of PTERA research aircraft using SI Toolbox SIDPAC. The disadvantages of the time domain led to the introduction of the concept of a frequency domain. FFT is a method for analysis that changes the domain from time to frequency as the convergence rate is faster, handles control design problems easily, robustness to noise (Morelli & Grauer, 2020)

R. Jategaonkar, states that there are three categories for parameter estimation: equation error method (EEM), output error method (OEM), and filter error technique (FEM)stated parameter estimation is categorized into three types: equation error method (EEM), output error method (OEM), filter error method (FEM) [8]. The equation error method defines a class as the Least square method which defines the cost function. Using the output error method, the error is reduced that occurs between the system output variable and the system predicted variable. (Jategaonkar, 2015)

Peyada et.al addressed parameter estimation methods in terms of process and measurement noise. Traditional methods: EEM cannot handle process and measurement noise, OEM handles measurement noise, and both process and measurement noise are handled by FEM from flight data. The research article also

uses GN and LM optimization techniques in estimating the parameters of Hansa-III(Peyada et al., 2008)

R. Kumar discussed the estimation of derivatives for highly maneuverable, unsteady, unstable aircraft at a high angle of attack. This motivates researchers to study in this field as special efforts are required to meet the challenges involved in non-linear model identification. The author successfully estimated the parameters of Hansa-III near stall region using Maximum Likelihood. This method is widely applicable in time-domain analysis to estimate derivatives using flight data of the vehicle. Maximum Likelihood is a widely used statistical technique to minimize the error and make the system dynamically stable. The author estimated the lateral-directional parameters of Hansa-III using a conventional approach such as Least-square, Maximum Likelihood, and Neural Technique as Neural Gauss-Newton. The background information of both approaches is discussed as well and variations of the effect of the type of control inputs are also highlighted in the article (Jategaonkar, 2015)(R. Kumar & Ghosh, 2014)

Grauer discussed the estimation of aerodynamic derivatives using the filter error method (FEM), of a non-linear aircraft model in consideration of turbulence effects. Results were simulated with NASA's generic aircraft Transport model. Time and frequency domain approaches were used to demonstrate the effectiveness of the approach. This paper explains how to solve real-time data compatibility problems. Data compatibility is a part of parameter estimation and is used to check data accuracy by making bias-free and error-free flight data(Grauer, 2015)

E. T. C. Kim explained that M.L.E.M was implemented to estimate **the** stability and control derivative of a 4-seater canard aircraft, firefly. This methodology has benefits that measure both process and measurement noise. Results from DATCOM and CFD were compared to those from a wind tunnel.(Kim et al., 2015)

C. Gottlicher, discussed optimal control methodology is operated for parameter estimation of the dynamic model utilizing Cost function 'J' that is derived by using

OEM. Estimated results are compared with the least square method to get the optimum result.(Göttlicher et al., 2016)

R. K Chauhan and S. Singh, reviewed the applicability and background information of various parameter estimation techniques such as OEM, FEM, EEM, and ANN. Techniques like Modified delta, delta, and ML were also successfully reviewed. Results are compared based on the critical review of the research work.(Chauhan & Singh, 2018)

S. Sadrela, R. Dhayalan et.al, discussed longitudinal, lateral-directional characteristics of CDRW-based UAV. The mathematical model of UAVs is formulated and a kinematic consistency check of real flight data is performed. Various techniques like Neural Gauss Newton (NGN), ML, and LS were implemented to obtain weak and strong derivatives of UAV(Saderla et al., 2019).

H.O. Verma and N.K. Peyada, estimated stability and control derivatives using the classical estimation approach ML, and LS. The author discussed ANN as an alternative approach to the stall condition of an aircraft. The efficacy of the Extreme learning machine method in terms of standard deviation such as Gauss Newton is validated with Maximum Likelihood(Verma & Peyada, 2021)

R. Jaiswal, O. Prakash, and S. Chaturvedi, “A Preliminary Study of Parameter Estimation for Fixed Wing Aircraft and High Endurability Parafoil Aerial Vehicle” 2022 discussed ML as the best tool to define output error method. This methodology is highly efficient when the sample size is large but inefficient in handling process noise. This statistical technique is not used for non-linear dynamic systems and noisy environmental interruptions (Jaiswal et al., 2020)(R. Kumar, 2012)

2.2 AIRCRAFT CONTROLLER DESIGN

The attitude control design requires a suitable controller to fulfil the required needs. The theory of modern control plays a vital role in the robust control system. This type of robust method such as Linear Quadratic Regulator deals with non-linearity and uncertainty without affecting system performance. The traditional control approach makes trade-offs amidst robustness and performance. Many research problems are solved using the same technique that results in optimal performance. A lot of research has already conducted to intervene in the gap between traditional and modern methodology.

E.H.J Pallet explained the principle of aircraft stability and control, fundamental of aerodynamics. The longitudinal motion modes, including long-period and short-period modes, are thoroughly described. (Pallett, 1954)

Jefferey D. Robinson discussed LQR Technique to locate poles precisely for an optimal solution. The author developed the LQR algorithm by minimizing the value of cost-function J and choosing Q , R scaler weighs wisely (Robinson, 1991)

R.C. Nelson discussed aircraft equation of motion. The author also reviewed the basic principle of aircraft stability and control along with auto-pilot design. For designing the pitch attitude control system, time and frequency domain design requirements were discussed. The comparative study of classical and modern control methods was also briefed (Nelson, 1989)

Krishnaswamy Srinivasan presented pole-placement and LQR technique for estimation of state-feedback gain matrix k . The state and observer estimation were explained thoroughly (Srinivasan, 2006)

Wahid. N, Hassan, et al proposed two methodologies PID and fuzzy logic PID to control aircraft Pitch angle. The mathematical model of aircraft is developed and implemented in the Simulink environment. The results were compared in the form

of time-domain characteristics and fuzzy PID proved to produce the best optimal solution(Wahid & Hassan, 2012).

Yibo Li, et al, discussed the LQR method for designing the control law of the Longitudinal stability Augmentation System of UAVs. The control law is designed using output feedback (Yibo Li, Chao Chen, n.d.)

Mohammad Shahrokhi and Alireza Zomorodi, present a comparative assessment of various open-loop and closed-loop tuning methods. The techniques are analyzed for Single Input Single Output Systems to get the optimized value of gains K_P , K_I , and K_D (Mohammad Shahrokhi and Alireza Zomorodi, 2005)

Amir Torabi, et al, compared performances of classical and modern control approaches for aircraft pitch attitude control systems. The performances of fuzzy logic, PID, and LQR Controllers were compared to get an optimal solution (Torabi et al., 2021)

Khoi Niguen Dang, optimized the design of the attitude controller of the quad-rotor using a system Identification approach. LQR theory was used to design Linear quality servos to improve performance characteristics (Dang et al., 2015)

Deepa and Sudha discussed a mathematical model for pitch control of general aviation aircraft and designed a PID Controller by tuning PID parameters with Ziegler Nicholas, Modified Ziegler Nicholas, Tyreus-Luyben, and Astrum-Haglund approaches. Results in the form of Time-domain specifications of different tuning techniques are compared. ZN proved to be better in all terms and conditions(Deepa & Sudha, 2016)

Amlan Basu, et al, focus on designing PID and FOPID Controller using tuning techniques like Ziegler Nicholas, Astrum-Hagglund, Cohen-Coon, and CHR. The fundamental of each method is discussed and well explained in the form of a step response (Basu et al., 2016)

Tamayo used UAV as a platform that aims to study all three aircraft parameters such as system Identification, control, and navigation. Eigenvalues of the non-linear model are linearized using linearization theory to study dynamic performances(Basu et al., 2016)

Joao P. Hespanha, discussed state-space representation, state-feedback design, controllability, observability, and optimal control methods. This book aims to provide background information for modern design techniques(Jo & December, 2017)

Valderrama, designed an aircraft pitch controller to improve the stability and performance of UAVs. Ziegler Nicholas methodology was adopted to tune the PID controller. Various time domain performances to study the performance of the controller were discussed (Villarreal-Valderrama et al., 2019)

W. Ahmed designed a longitudinal autopilot for altitude and pitch control. He designed multi-loop configurations using eigen-structure Assignment (EA) and PID. The inner loop is configured by EA for stability and the PID Controller is used to design the outer loop for controlling altitude and pitch Control. (W. Ahmed, Z.Li, 2019)

M. Raja and Om Prakash discussed the satellite attitude control system. The PD-compensated controller to meet design specifications using the root-locus algorithm is constructed using the control system toolbox. Time-domain characteristic of the satellite is discussed elaborately (Raja & Prakash, 2020)

2.3 AIRCRAFT NAVIGATION SYSTEM

Aircraft Navigation System as Dead Reckoning

The theory investigates the problem statement related to parameter estimation for aircraft positioning systems based on Inertial sensor measurements provided by flight test of Hansa-III aircraft. In terrain-prone, steep places, some satellite-based

signal transmission techniques, such as (GNSS), cannot be used; as a result, the Dead Reckoning method is used to make precise future predictions.

Philips G Mattos discussed the implementation of an algorithm describing GPS and DR. The drift issues caused by unaided GPS, unaided DR, coupled GPS, and DR are explained. Integrated GPS (global positioning satellite) and DR (Dead Reckoning) sensors are used to track and navigate low-cost vehicles. Results for GPS, DR with a loosely coupled, and DR with a tight coupled were compared and discussed. Tightly coupled DR gives the best optimum result as compared with all three (G.Mattos, 1994)

Zeev Berman. et al, discussed future aspects of the aviation navigation systems such as the dead reckoning system. The author discussed background information on Dead Reckoning and Inertial sensors. Different configurations of aviation navigation systems are discussed. He presented an actual statistical model and varied wind vectors to match actual data. To quantify horizontal positional inaccuracy, the Dead Reckoning system, standalone inertial sensors, and inertial sensors integrated with the DR system were compared. (Berman, 1998)

M. Jayachandran, presented a dead-Reckoning approach using Inertial sensors for position estimation at the time GPS drops out. When GPS is not working, the method is useful for navigation. A Navigational algorithm is implemented within the display system of aircraft that receives information about attitude, and position (Jayachandran et al., 2009)

G. S. Reddy presented various advanced navigational systems varying from satellite to archaic forms for the application of aircraft. This study investigates various navigation systems to enhance system's accuracy as the accuracy range for the type of military application is the major concern of systems. The research concentrates on a gyro-based inertial navigation system to increase the system's accuracy. Integration of the INS-GPS-GLONASS system is applied for combat aircraft, ships, and long-range missiles (Reddy & Saraswat, 2013)

Lorenzo, experimented with the dead reckoning of UAV using XKF (Exogeneous Kalman filter) and NLO (Non-linear observer) IMU sensors such as (acceleration, rate gyros, an inclinometer); and altimeter; the camera is used. Position, velocity, and altitude are used as observed states. XKF gives the best optimum result as compared with NLO. The result of calculated velocity comprises a bias effect. Biases of various sensors such as accelerometers, gyroscopes, and optical flow velocity are also estimated up till the availability of GNSS (Fusini et al., 2017)

Parinaz Kasebzadeh covered broader aspects of parameter estimation for applications of mobile positioning. The navigational parameters such as position using the PDR of mobile robots were estimated. The PDR algorithm was designed to get more accurate gait parameters which will improve the accuracy of the position estimate. The Pedestrian Dead Reckoning algorithm is developed for the mobile position. Various cases of positioning algorithms are discussed and the drawbacks are mitigated using a model-based sensor fusion technique (Kasebzadeh, 2017)

T. Mahmoud discussed the benefits as well as drawbacks of integrating the INS system with GPS. The specification of the system varies in accuracy, reliability, update rate, budget, size, and mass. The study investigates the performance of INS/GPS systems and different algorithms. INS is integrated with dead reckoning equipment to provide accurate, reliable navigation results. This study investigates the performances of loose couple INS/ GPS, tightly coupled INS/GPS, and INS using SIMULINK. Tightly coupled INS/GPS gives better performance than loosely coupled integration (Mahmoud & Trilaksono, 2018)

Pedro Paulo Liborio Lima do Nascimento, discussed the alternative procedure of estimating navigation coordinates once GPS systems are inaccurate, unavailable in tunnels, dense and terrain-prone areas. The author integrated the dead reckoning algorithm with a GDOP (Geometric Dilution of precision) based positioning solution. The simulated results in term of root mean square error are compared to

stand-alone GPS, GPS +DR. The error was reduced from 97%- 98% to 83%-88%(Do Nascimento et al., 2018)

I.K. A. Shurin, The research used quadrotors for applications both indoors and outdoors such as surveillance, mapping, and transportation. The fusion of accurate navigation systems such as INS/GNSS is required to accomplish the task. Environmental Constraints lead to drift in time in the navigation solution thus pedestrian dead reckoning is mitigated in pure Inertial Navigation. It enables the quadrotor to estimate the distance from peak to peak. The simulated result shows the accuracy of the navigation solution while comparing INS and QDR approaches. QDR navigation solution is bounded while the INS solution diverges (Shurin & Klein, 2020)

Piotr Lichota presents an aircraft controller design procedure for tracking aircraft trajectory. The study used Maximum Likelihood and Extended Kalman filter estimation techniques to identify parameters and obtain a mathematical model of a non-linear transport aircraft model. The Linear Quadratic Regulator approach is used to design a controller for accurate aircraft tracking trajectory. It is found that tracking error is proportional to wind velocity in the presence of wind proportional to turbulence intensity in the presence of turbulence and admissible for small-moderate disturbances (Lichota et al., 2020)

Omri Asraf, Firas Shama, and Itzik Klein, the study suggested PDR Net, a deep-learning version of pedestrian dead reckoning that can be used for user positioning. In the study, distance regression and changing heading angles are used to identify smartphone locations. Indoor navigation is a good application for the PDR technique. Experimental Results display proposed methodology outperforms the traditional one (Asraf et al., 2022)

SUMMARY

This chapter entrusts a literature survey on Parameter Estimation, Controller design, and Navigation. Based on the study, it was observed that the M.L technique is applied to the flight data in the time-domain for the estimation of parameters. It is the standard approach for the estimation of derivatives of an aircraft and has capability of handling measurement noise too. Once the ML technique is applied to estimate the parameters, the methodology adopted to design attitude controller on the basis of the research study is LQR. This robust method deals with optimal problems by concentrating on design requirements without sacrificing its performance. Some surveys in term of aircraft navigation system observed signal transmission methods such as GNSS is not able to forecast future information at the time of signal loss thus Dead Reckoning methodology can be used for future prediction.

CHAPTER- 3

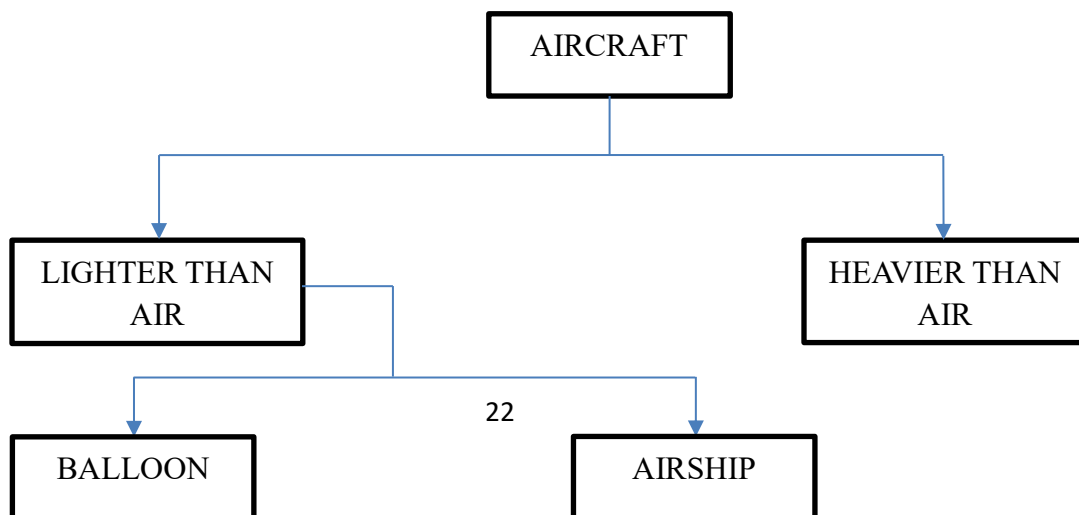
AIRCRAFT SPECIFICATIONS

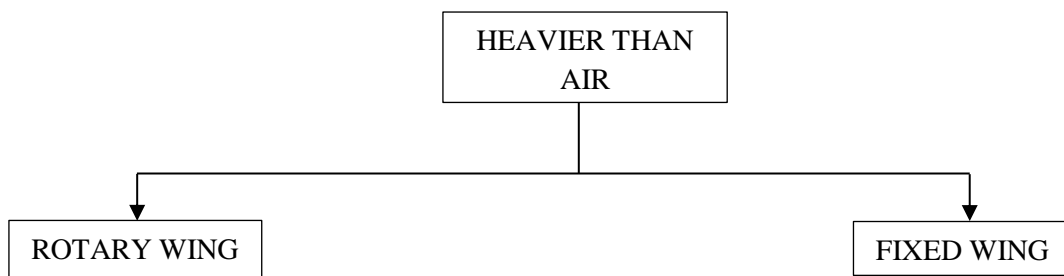
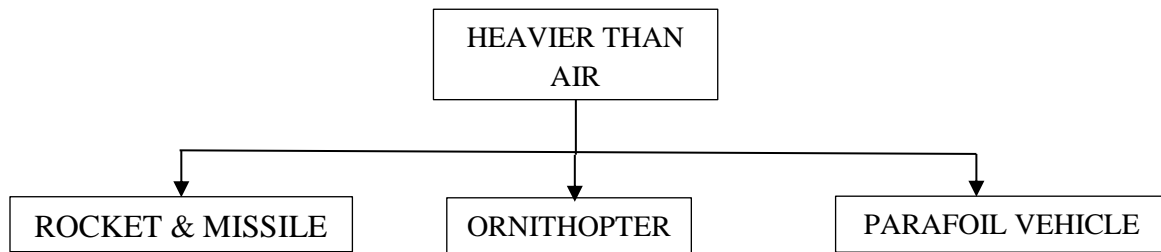
The study addresses the classification of aircraft as lighter than air/ heavier than air machines. The stratification of the aeroplane as Military, Commercial, Transport, and Trainer is discussed as a research study focalized on the research cum trainer aircraft- Hansa-III. It is a fully composite, low-wing configuration, tricycle landing gear, and two-seater aircraft. The drawing as shown in Figure 3.3 illustrates the characteristics of the model concerned. The general features and specifications are mentioned in the below section

3.1 AIRCRAFT

The generic term “Aircraft” includes all man-made machines flying in the air for example kites, parachutes, helicopters, aero-planes, rockets, missiles, airships, gliders, auto-gyro, hybrid aerial vehicles, etc. An aeroplane is an aircraft but the reverse of it is not always the same. Fixed wing heavier than aerial machines includes an aero-plane which stands for vehicles that fly in the air and are propelled forward by jet engines to produce thrust. Aircraft are broadly classified as displayed in Figure 3.1:

CLASSIFICATION







Helicopter



Aeroplane

Fig 3.1 Aircraft Classification(Devalla & Prakash, 2014)(R. Kumar & Ghosh, 2015)(Kornienko & Well, 2003)(Heredia & Ollero, 2009)(Ramesh et al., 2020)(SPACE India, 1988)

Lighter than Air:

A man-made vehicle that flies in the air and produces thrust on its own to move forward without an engine falls under this class. The aerodynamic force (lift) is always greater than its weight which helps this class of vehicles to fly in the air. These systems include balloons, dirigibles, and blimps, often used for surveillance, monitoring natural calamities, and advertisement as shown in Figure 3.1

Balloons:

Montgolfier brothers were the first individuals who succeeded in placing the man-made object “Balloon” in the air in 1782 (SABHARWAL, 2003). It consists inflated bag with a gondola attached by ropes. It is difficult to control the flight as it moves in the wind direction.

Airship:

Controlled balloons with non-rigid structures often referred to as dirigibles consist of a gondola and an inflated bag with an engine and propeller. Horizontal tail fins with movable rudder are attached in dirigibles termed airship which is used for movement in upward, downward, left, and right direction. Henry Gifford's airship on 24 September 1852 was the first airship 144 feet long, with a diameter of 39 (SABHARWAL, 2003). feet flew in the air. Rigid airships called zeppelins include a framework of steel and aluminium with a long cylinder of the nose and pointed tail. The first ever-built, biggest hydrogen-filled airship 'Hidenberg' is 803 feet long, 135 feet in diameter with a space of 70 passengers (SABHARWAL, 2003). These machines are often used for surveillance, and advertisement due to excellent endurance, and durability.

Blimps:

Non-rigid small airships fall in this class of vehicle. Blimps are used for advertisement and submarine patrols.

Heavier than Air:

Machines that fly in the air and are propelled forward by jet engines to produce thrust falls under this category. It comprises ornithopters, rockets and missiles, parafoil aerial vehicles, multi-copters, and airplanes as referred to in Fig 3.1

Missile:

Missiles are heavy-range guided weapons that possess the capability of self-ignition for damage on the selected target.

Ornithopter:

The hovering of insects and birds inspired to generate the concept of a flapping machine termed an Ornithopter. Flapping flight has two classes-

bird and Insect(Ansari et al., 2006). Bird is useful for indoor application and too fast in forward flight whereas insects have light wing structure approximately 1% of the insect's weight proves to be viable for the production of MAV(Ellington, 1984). Flapping wing micro aerial vehicles have agile behaviour, small size, broad v-n curve, and promising characteristics at low Reynolds(Caetano et al., 2013)

PAV:

PAV is the category of parachute UAV having characteristics of high endurance, robustness, and safety during system damage. It contains a non-rigid wing structure termed parafoil depends on wind gusts for manoeuvring.

Helicopter:

Rotary wing aircraft derive lift from rotary blades termed rotorcraft. The helicopter has a set of blades known as main rotor blades and tail rotor blades move opposite to each other to maintain stability.

Aero-plane:

Fixed wing, heavier than aerial machines includes an aero-plane which stands for vehicles that fly in the air and are propelled forward by jet engines to produce thrust. Based on type, an aero-plane is categorized into (i) Military (ii) Transport/cargo (iii) Commercial (iv)Trainer, and many more as shown in Figure 3.2. Military aircraft are designed to protect the nation from an enemy. It may be fixed or rotary. These combat aircraft are purposefully designed to enable aerial warfare. Cargo-type aircraft are commercially designed for the transportation of goods. Commercial aircraft come under civil aircraft used for the transportation of passengers or multiple loads of cargo.

Research cum trainer aircraft is used for study as well as for research

purposes. These types of aircraft are also used for flight training. One of the examples of Indian research aircraft is Hansa.

Various Categories of aircraft are compared on the basis of their features discussed in above section is displayed in Table 3.1

S. No.	Factors	Airship	UAV	Rotorcraft	Fixed Wing Aircraft
1	Design	Simple	Moderate	Complex	Complex
2	Stability	Stable	Highly Stable	Less Stable	Stable
3	Manoeuvrability	Less	Moderate	Highly	Moderate
4	Control	Simple	Simple	Complex	Complex
5	Auto-Controller	Primitive	Advanced	Advanced	Advanced
6	Flight Data Test Time	High	High	Less	Moderate

Table 3.1: Comparison of Aircraft

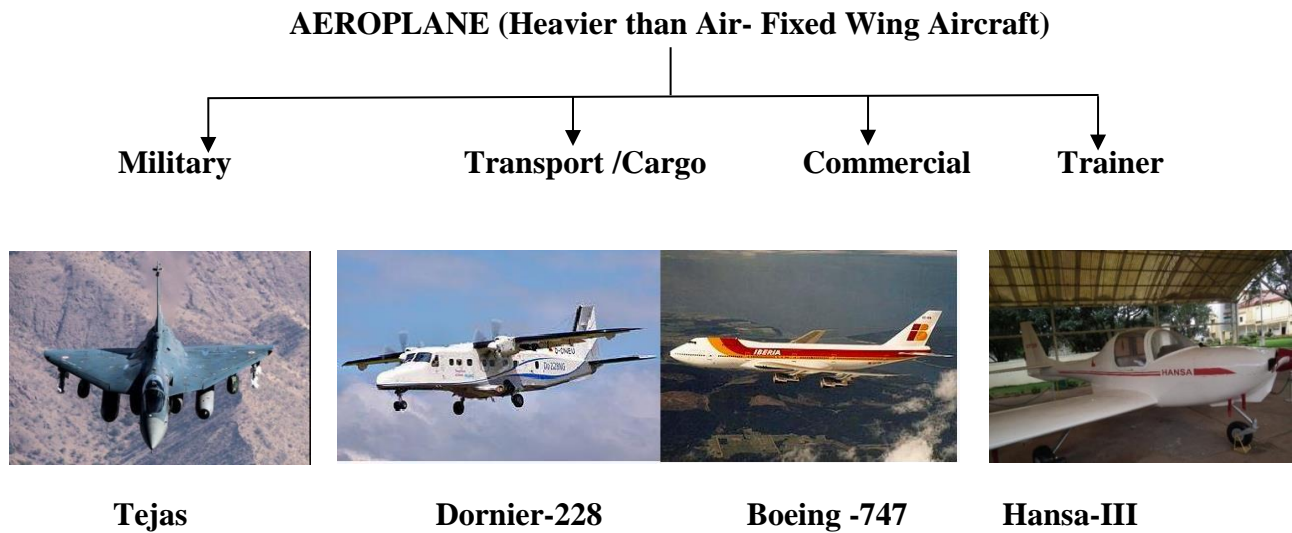


Fig 3.2 Classification of Airplane (*Timeline of HAL Tejas, n.d.*)(*Dornier-228, n.d.*)(*Boeing-747, n.d.*)(*NAL Hansa, 2000*)

3.2 HANSA-III AIRCRAFT

Hansa-III is a research cum trainer, two-seater aircraft manufactured by NAL, India, and useful for research purposes. Three designs were developed

by NAL in which Hansa-II was built as a prototype and Hansa-III was finalized for production.

This aircraft fully satisfies my problem statement so I chose this particular aircraft for my study. To fetch the flight data, multi-variant sensors are instrumented in the aircraft for flight data acquisition. The aircraft structure is fully composite having a low wing configuration with a tricycle landing gear arrangement. It consists of a Rotax-914 F3 engine coupled with a Hoffmann propeller(R. Kumar, 2012). Hansa-III has already covered more than 4000 flying hours.



Fig 3.3.Hansa-III aircraft (Jaiswal et al., 2020)

Geometrical Parameters	Value	Geometrical Parameters	Value
Wing		Horizontal Tail	
Planform area (S)	12.47(m ²)	Planform area (S_t)	2.04(m ²)
Aspect ratio (A)	8.8	Aspect ratio (A)	6.35
MAC (\bar{c})	1.21(m)	MAC (\bar{c})	0.59(m)
Root Chord (c_r)	1.3(m)	Root Chord (c_r)	0.78(m)
Tip Chord (c_t)	0.8	Tip Chord (c_t)	0.354(m)
Taper ratio (Λ)	6(deg)	Taper ratio (Λ)	0.454
Aircraft		Aerodynamic Derivatives	
Aircraft span (b)	10.47(m)	$(C_{L_{\alpha,w}})_{ss}$	4.5

Mass (m)	750(kg)	$(C_{L_{\alpha_t}})_{ss}$	1.48
Velocity (V)	36(m/s)	$(C_{m_{\alpha_f}})_{ss}$	0.3
Moment of Inertia I_Y	907(kg-m ²)	$(C_{L_{\alpha_t} \frac{d\epsilon}{d\alpha}})_{ss}$	0.22
Moment arm (l_t)	3.624(m)		
Density (ρ)	0.96(kg/m ³)		
Moment of Inertia I_X	925(kg-m ²)		

Table 3.2: Geometrical and Aerodynamic Parameters of Hansa-III (R. Kumar, 2012)

POWER PLANT SPECIFICATIONS

Number of engines	One
Make	Bombardier Rotax 914 F3
Engine limits Max. continuous power Engine max. power	100 BHP @ 5500 rpm (Propeller rpm 2265) 115% @ 5800 rpm (5 min) (Propeller rpm 2385)
Idle RPM	1400 rpm (Propeller rpm 580)
Manifold pressure	38.4in Hg at 115% power (max. 5 min)
Acceleration	Max. 5 secs. at -0.5g
Rating, full throttle at sea level pressure altitude	100 BHP, Max, continuous @ 5500 RPM (Propeller rpm 2265) 115 BHP @ 5800 rpm (Propeller rpm 2385) contingency power for max. 5 min.
Max. Oil Temp.	Max. 130°C Min. 50°C
Max. Oil pressure	7 bar
Fuel grade	AV Gas 100 LL
Oil specification	Castrol Syntrol, non-detergent, fully synthetic engine oil
Coolant	SERVOKOOL
Propeller Limit	Hoffmann makes HO-V 352F() 170 FQ+3 Max. propeller RPM never exceeds 2700 RPM
Altitude (Max Operating)	10,000 feet

Table 3.3: Power Plant Specifications of Hansa-III (NAL, 2000)

CONTROL SURFACE MOVEMENT

Rudder	30° left, 30° right; -1-2°
Wing flaps	20° for landing 1° 20° for take-off 1°
Elevator	30° up, 25° down; +2°
Elevator trim tab	22° up, 33° down; A2°
Aileron	20° up, 20° down; +2°
Forward limit	21.94 % of MAC aft of wing MAC LE
Aft. Limit	27.47 % of MAC aft of wing MAC LE

Table 3.4: Specification of Control Surface deflection and C.G Range of Hansa-III(NAL, 2000)

SUMMARY

This chapter represents a brief model description in terms of geometrical, aerodynamic parameters, power plant, and control surface specifications so that it can be useful for deducing the state-space representation of the model.

CHAPTER- 4

AIRCRAFT SYSTEM IDENTIFICATION

A flying machine's motion in the atmosphere is characterized by flight dynamics. The vehicular attitude and the resultant flight path are decided by the vehicle responding to aerodynamics, gravitational, propulsive, and control forces acting upon it. The domain of flight dynamics is sectioned into features such as stability and control, Performance, Navigation, and guidance. System Identification is a part of flight dynamics that creates a mathematical model of a physical system based on measurements.

System Identification is defined as “*Identification is the process of determining a system's initial and final states using input and output from another system that belongs to the same class as the system being tested.*”(Zadeh, 1962)

The random observations in the course of measurement and process noise are distorted due to sensors, and external disturbances. Boeing-737 Max disaster represents failure of stability Augmentation system(Sgobba, 2019). Reforming the system for innovation, and providing certification to a new computer-based system leads malfunctioning of MCAS (Maneuvering characteristic Augmentation system) resulting in a catastrophic crash that took 346 lives(Psas et al., 2014). Tools are needed to address fatalities due to faulty sensors, flight handling characteristics at high AOA, and fault-tolerant control systems. Wind tunnel testing, modelling and Simulation predict aircraft dynamics to design controllers but are limited to small- scale models therefore System Identification

approach should be used to handle imperfections (Jameson & Cooke, 2012b). Handling of imperfect measurements is simplified by evaluating the parameters of the system using statistical techniques. In the past years, system Identification has expanded its growth due to its application in designing controllers, health monitoring, and analysis of dynamic systems, making systems fully autonomous, and fault-tolerant. System Identification is applied to study the time-variant tracking behavior of vehicle subsystems in real time to update system modeling by parameter estimation in continuous intervals to detect sensor fault, and system failure (Tang et al., 2009a) (Melody et al., 2000) (Hardier et al., 2016). Real-time LS is applied in the area of Robotics, aerospace and automotive (Ljung & Gunnarsson, 1990) (Hardier, 2015)

Aircraft parameter estimation is the best illustration of system identification methodology. The process of determining the best estimates that occur in the dynamic model to represent the physical system is the methodology of parameter estimation. System Identification is a statistical investigation that handles estimating the value of derivatives based on measured experimental data. Designing autopilots and controllers, expanding the flight envelope, comparing the results of analytical techniques like CFD with wind tunnel tests, simulation, dynamic analysis, evaluating flying characteristics, confirming aircraft performance, and accident investigation are some of the major applications. Development of mathematical models for the physical systems subjected to imperfect observation or measurement. This phenomenon is termed as system identification.

Bryan intuited the conception of aerodynamic modelling, which relates forces and moments as a function of translational and rotational motion variables respectively. The analytical methodology is the foremost technique of parameter Estimation at the initial phase of aircraft design as the accuracy level is low thus Flight and Wind-Tunnel test is required. The observational/ experimental method provides a strong

hold to attain the desired result as compared to the analytical. Some of the traditional methods for linear systems in the frequency/ time domain are FFT, ML, and LS(Bryan, 1911).

The values acquired through wind tunnel testing require validation from flight test data as it is difficult to obtain the value of power effects, and propulsive effects at different flight conditions.

The advancement of Flying Vehicular System Identification and its application in chronological order is discussed by Hamel and Jategaonkar(Hamel & Jategaonkar, 1996a). Miliken first tried to use the static and dynamic parameters from actual flight data in 1947(Milliken W.F.Jr, 2003)

The three categories of traditional parameter estimation techniques are as follows as suggested by Ravindra Jategaonkar(Jategaonkar, 2015): (i) EEM, (ii) OEM, (iii) FEM. Least square also known as regression analysis defines a category of Equation error method in which the flight dynamic model of the physical system is not known. The least-square accounts for process noise, not measurement noise. Non-linear/ Ordinary LS methodology was introduced by Shinbrot and Greenberg(Shinbrot, 1951)(Greenberg, 1951). The performance capability of this methodology is robustly determined by data quality. The cost function is in the form of an Input-Output equation defined directly in the Equation-error Method. In the case of the output error method (OEM), the model parameters are altered consecutively for error minimization between the system output and response of the predicted model. This method has the potential to solve non-linear optimization problems too. Its application for parameter estimation makes use of flight data and needs the postulation of accurate flight dynamic formulation. This process assumes that process noise is imperceptible and handles measurement noise along with process noise. This is the most applicable time-domain method for aircraft parameter estimation. One of the most efficient OEMs is the Maximum Likelihood intuited by Fischer is inapplicable to the non-linear system as handling a non-linear model structure is practically difficult. The FEM faces difficulty in extending it

through multiple experiments by treating the process noise distribution matrix independently for every maneuver as proposed by the researcher (Iliff, 1989) [23]It does not guarantee the correct postulate of the model. This methodology has the capability of handling process and measurement noise and is also extended to the non-linear system as proposed by Jategoankar (Jategaonkar, 2015) thus FEM is applied for unique cases only as the majority of parameter estimation problems are solved by the Output error method or Least-square method. Since the last three decades, the method of maximum likelihood has been used successfully for parameter estimates utilizing flight data. This statistical technique minimizes error and makes the system dynamically stable as proposed by Rakesh Kumar(R. Kumar, 2012).ML is the best tool to define output error method. This methodology is highly efficient when the sample size is large but inefficient in handling process noise thus process noise is assumed to be negligible and measurements taken by sensors are corrupted by measurement noise. This statistical technique is not used for non-linear dynamic systems and noisy environmental interruptions. Accuracy is measured in terms of Cramer-Rao bounds in this method.

Numerous subjects related to estimating aircraft parameters include linear and stepwise regression, characteristics, and applicability of statistical techniques, like maximum likelihood as explained by Klien (Klien & Morelli, 2006). The research work in the area of parameter estimation in different flying regimes at high AOA for unstable aircraft is also addressed by Klein. Estimating unsteady aerodynamics on a lifting surfaces involves several techniques which are complex for a purpose of estimating parameters(Morino, 1974)(Robert, n.d.). Queizo.et.al discussed the vortex system to consider the downwash effect for swept, and tapered wing(Queijo et al., 1978). The unsteady aerodynamic effects is modelled in longitudinal/ lateral equations for estimating aerodynamic derivatives(Queijo et al., 1979)(Raisinghani & Ghosh, n.d.)(Wells, W. R., Banda, S. S., and Quam, 1979)(Singh & IIT Kanpur, n.d.).

A wider level of fidelity for non-linear systems like aircraft, rotary-wing aircraft, missiles, and UAVs makes this technique unique and novel on the other side ANN faces difficulty in estimating parameters at higher AOA. System Id is applied to study the time-variant tracking behaviour of vehicle subsystems in real time to update system modelling by parameter estimation in the continuous interval (Tang et al., 2009b)(Hardier, 2015)(Ljung & Gunnarsson, 1990)to detect sensor fault and system failure. Real-time LS is applied in the areas of Robotics, aerospace, and automotive(Jategaonkar, 2015)(Tischler & Remple, 2006)(Zadeh, 1962)

General System Identification: The Quad-M in system Identification defines Maneuverers, Models, Measurement, and Methodology which is discussed elaborately in the below section

- (a) Input to experiment behaviour of the physical system in the form of Maneuverers
- (b) Mathematical Model of the physical system
- (c) Responses in terms of Measurement
- (d) Methodology adopted to define system Identification

4.1 FLIGHT DATA GENERATION

The Flight test of Instrumented Research cum Trainer Aircraft Hansa-III was regulated at the flight Lab of IIT Kanpur and flight data was collected operating data acquisition system(R. Kumar, 2012)

Symbolic Representation to define Real Flight data :

During flight testing, numerous longitudinal flight data sets were acquired. Using the eight data sets, longitudinal aerodynamic characteristics were estimated making use of Maximum likelihood.

The Terminology HA resembles ‘Hansa-III’, L is Longitudinal, and numerals ‘1-8’ define the number of data sets such as HAL1, HAL2, HAL3

For longitudinal, the letter(s) accompanied by ‘L’ such as ‘M’ correspond to multi-step, ‘D’ as a doublet, and ‘P’ as pulse elevator control inputs.

Flight Data Generation:

Hansa-III is a research cum trainer, two-seater type aircraft manufactured by NAL, India, and useful for research purposes. Three designs were developed by NAL in which Hansa-II was built as a prototype and Hansa-III was finalized for production. This aircraft fully satisfies my problem statement so I chose this particular aircraft for my study. To fetch the flight data, multi-variant sensors are instrumented in the aircraft for flight data acquisition. The aircraft structure is fully composite having a low wing configuration with a tricycle landing gear arrangement. It consists of a Rotax-914 F3 engine coupled with a Hoffmann propeller (NAL, 2000). A Flight test is carried out to record an enormous amount of longitudinal flight data for evaluating longitudinal parameters using the Maximum likelihood method (Jategaonkar, 2015). The flight tests at different altitudes such as (4000ft, 6000ft, and 8000ft) at 1200 N thrust were conducted. Elevator control inputs such as multistep, doublet, and pulse were accustomed for generating flight data at low AOA. The raw data is computed in the form of velocity (V), rates (p, q, r), pitch angle (θ), yaw angle (ψ), roll angle (ϕ), deflection angles ($\delta_e, \delta_a, \delta_r$) accelerations (a_x, a_y, a_z), α , and β for locating the sensors position. An accelerometer reading measures accelerations in the body axes that are in close proximity to the C.G. The deflections by control surfaces δ_e are measured through a potentiometer. The Gyroscope measures the angular rates (p, q, r) and ($\dot{p}, \dot{q}, \dot{r}$) are calculated from angular rates numerical differentiation (p, q, r). OAT gauze measures the temperature. Some calibration factors and correction factors are recommended while sensor measurement so that they can be incorporated into the mathematical modeling of aircraft.

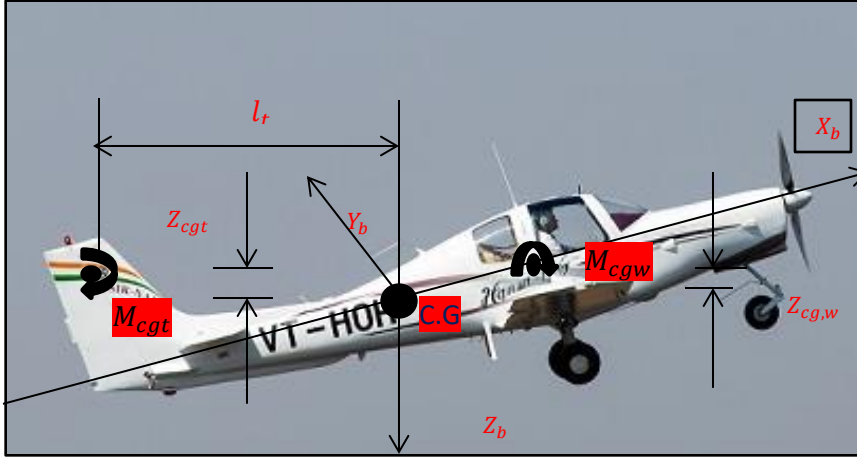


Fig 4.1 Wing and Tail Contribution to the Pitching Moment of Hansa-III

Flight Data at Low Angle of Attack

In terms of voltage (3-2-1-1) multi-step, doublet, and pulse input types, the raw flight data was recorded. The raw data was converted using the relevant calibration chart into the corresponding motion and control variables. Figures 4.5-4.9 presented below show five data sets of longitudinal multistep 3211 Input form (HALM1, HALM2, HALM3, HALM4, and HALM5), one dataset (HALD1) and two datasets (HALP1, HALP2) were generated using the elevator as input. Figure 4.2 discusses below mentioned (δ_e) elevator deflection angle, (α) angle of attack, (θ) pitch angle, (q) pitch rate, (V) velocity, (a_x) acceleration along the x-axis and (a_z) acceleration along the z-axis in the graphical representation.

About the trim state, the elevator deflects by (± 2 to ± 6 degrees). The X-axis and Z-axis linear accelerations (a_x , a_z) at trim conditions are 1 ms^{-2} and -10 ms^{-2} , The α_{trim} varies from 2-10 deg and the perturbation speed is 56m/s. The state variables α , θ , β , ψ , δ_e , ϕ in degree a_x , a_y , a_z are in m/s^2 p , q , r in degree/s, and V in m/s.

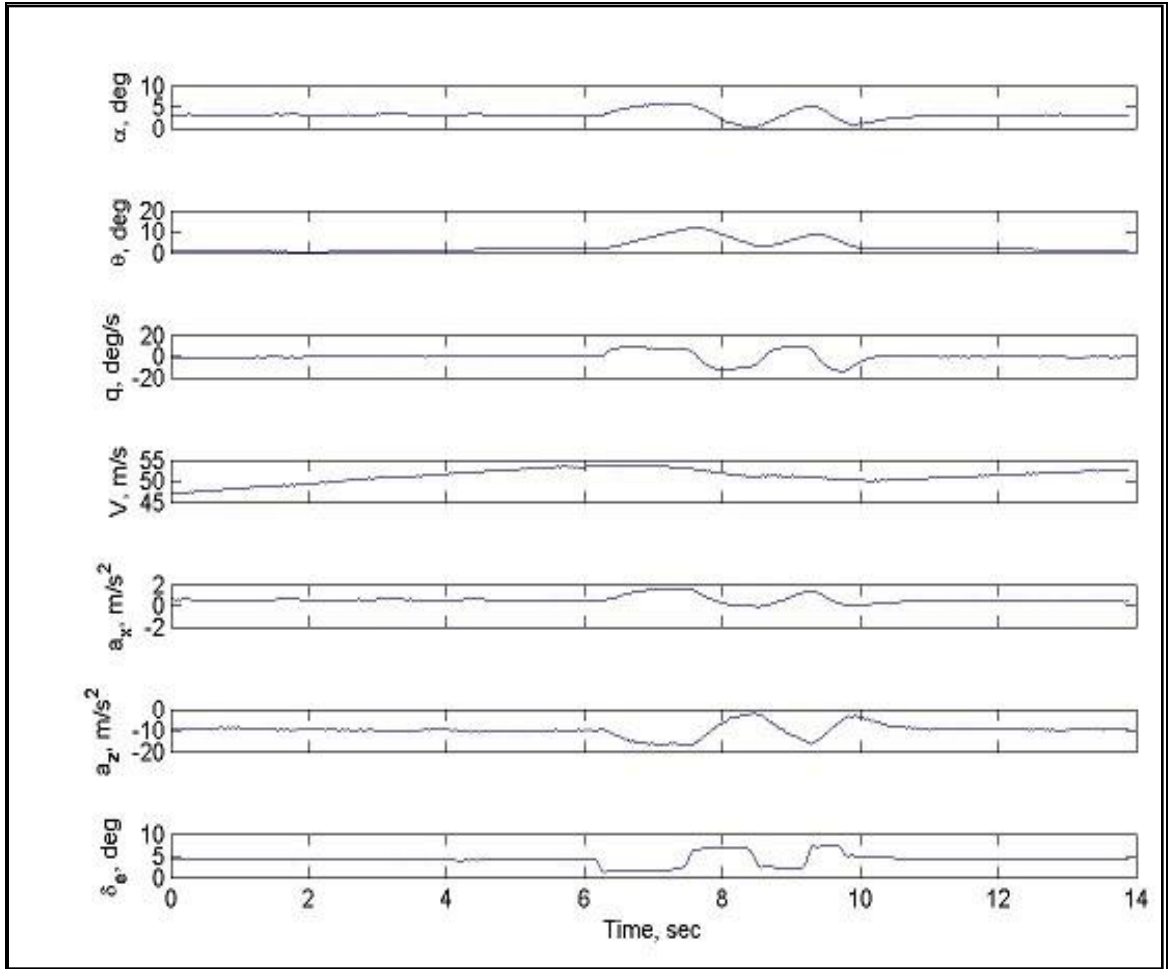


Fig 4.2 Flight Dataset Pre-processing HALM5

Figure 4.2 shows the processed longitudinal flight data about HALM5 input form including motion variables (α) angle of attack in degrees, (θ) pitch angle in degrees, (q) pitch rate in degree/s, (V) velocity in m/s, (a_x) acceleration along the x-axis and (a_z) acceleration along the z-axis in m/s^2

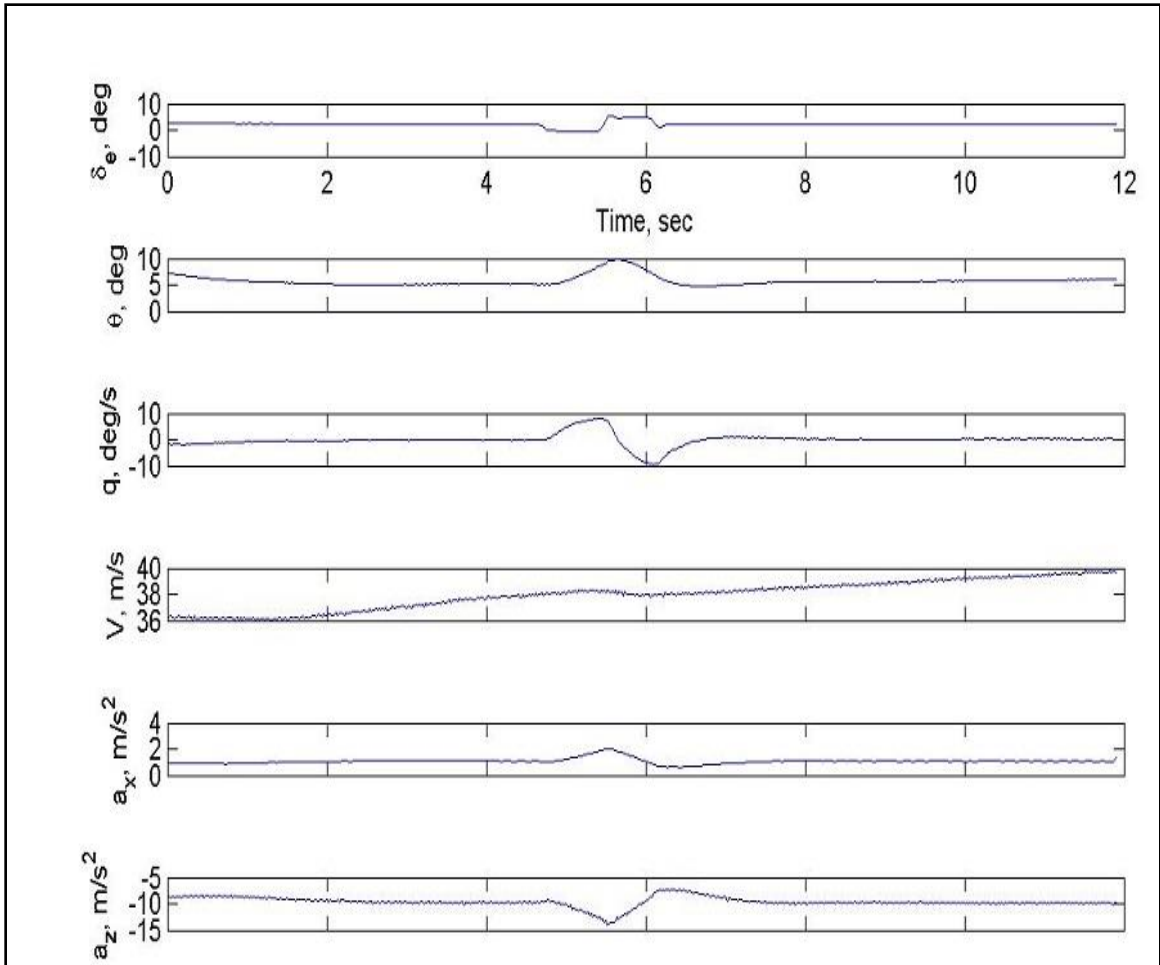


Fig 4.3 Flight Dataset Pre-processing, HALD1

Figure 4.3 shows the processed longitudinal flight data about doublet HALD1 input form including motion variables (α) angle of attack in degrees, (θ) pitch angle in degrees, (q) pitch rate in degree/s, (V) velocity in m/s, (a_x) acceleration along the x-axis and (a_z) acceleration along the z-axis in m/s^2

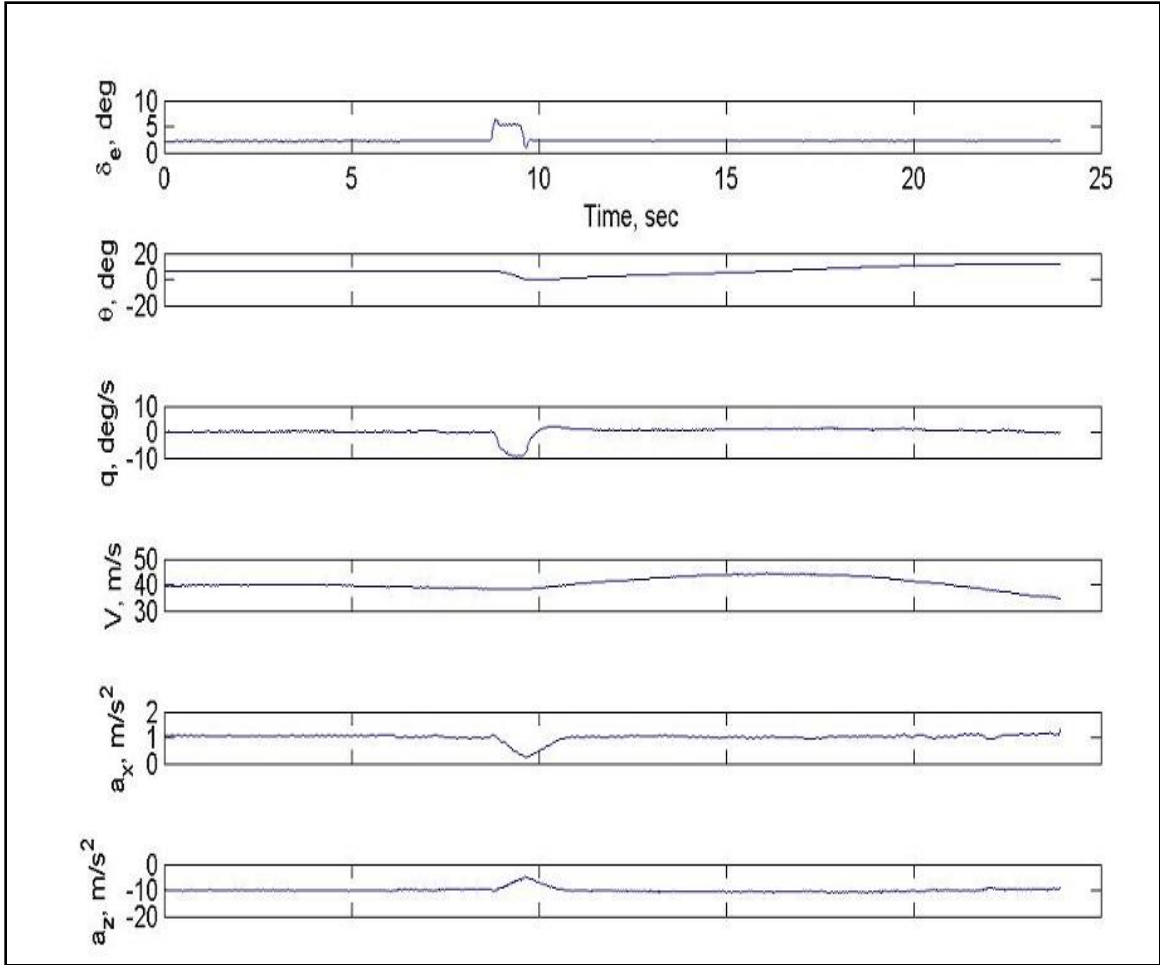


Fig 4.4 Flight Dataset Pre-processing, HALP1

Figure 4.4 shows the processed longitudinal flight data about the Pulse HALP1 input form including motion variables (α) angle of attack in degrees, (θ) pitch angle in degrees, (q) pitch rate in degree/s, (V) velocity in m/s, (a_x) acceleration along the x-axis and (a_z) acceleration along the z-axis in m/s^2

The three variations of Elevator Control Input: Multi-step (3-2-1-1), Doublet, and Pulse are presented in this chapter. The pilot executes these three elevator forms by deflecting the elevator from its trim state to acquire longitudinal data.

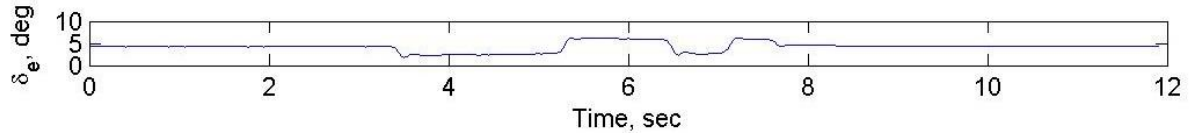


Fig 4.5 3211 Elevator Input, HALM1

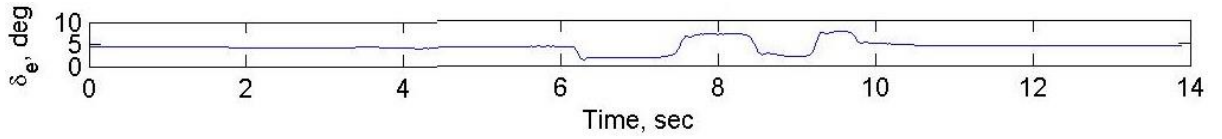


Fig 4.6 3211 Elevator Input, HALM3

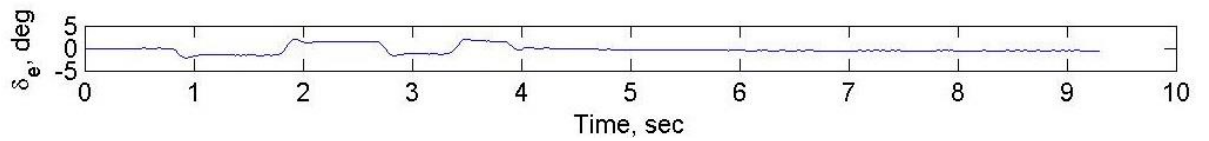


Fig 4.7 3211 Elevator Input, HALM5

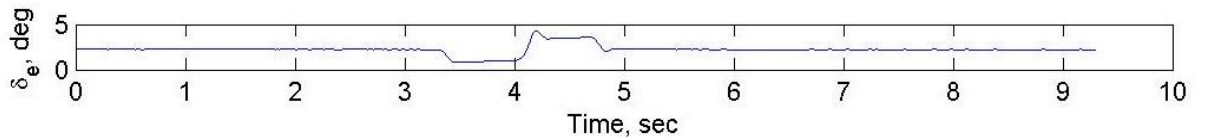


Fig 4.8 Doublet Elevator Input, HALD1

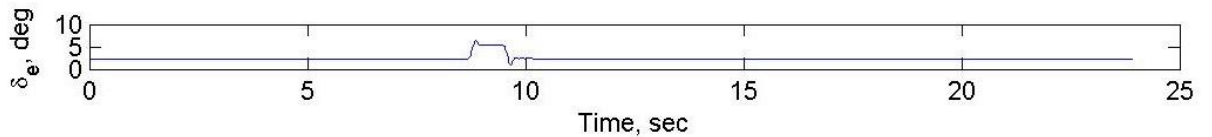


Fig 4.9 Pulse Elevator Input, HALP1

Figures 4.5 - 4.9 present different forms of elevator control input at the low and moderate angles of attack to generate longitudinal datasets.

4.2 DATA COMPATIBILITY CHECK

Sensors that detect accelerations, locations, and rates related to the translational and rotational motion of the C.G. and additionally orientation/ magnitude of the velocity of the relative air are part of the instrumentation on Research Cum trainer aircraft. To verify that the measurements are mutually consistent, kinematic relationships between the attributes are used. The analysis is termed data compatibility analysis (Klien & Morelli, 2006)

Data compatibility analysis demonstrates that the kinematic relations satisfy the sensor measurements if the measurements are perfect. Practically, Sensor Measurement includes a systematic error, as well as random errors thus these equations, serve as tools for calibrating the instrumentation errors as well as correcting the measured data from the sensors to estimate systematic errors. Accuracy and consistency is prerequisite for modelling the structure and parameter estimation. Consequently, these measurements are applied to rigid aircraft that are checked for compatibility. Processed flight data include systematic and random error which requires to be removed.

The chapter covered data compatibility checks for the Hansa-III flight data. The systematic errors includes zero shift biases, scale factors, and time shifts that make data incompatible to be used. In the context of the parameter Estimation of an aircraft, an enormous variable is measured and recorded during testing. therefore, a data compatibility check must be carried out before parameter estimation.

The goal of flight path reconstruction (FPR), also known as data compatibility check, was to confirm that the measurements used to identify the model were accurate and consistent. Data Compatibility is first introduced by

Gerlachin in 1966, for flight path reconstruction. All biases are measured and initial conditions were evaluated by Mulder 1975(Klien & Morelli, 2006)

Mathematical Model

The six DOF model consists of kinematic equations, recorded angular rates, and measured accelerations.

- 1) Determination of systematic error that includes zero shifts, scale factors, and time delays.
- 2) Generation of aircraft states such as velocity components, which implies state estimation.

The bias and scale factor present in the measured state variable using the Maximum Likelihood MATLAB Code (Jategaonkar, 2015). The following equations used for reconstructing the dynamics of RCTA Aircraft are mentioned in the below section

Kinematic Equations

These equations are sets of translational, rotational, and navigation equations on body-fixed axis.

Translational Equations

$$\dot{u} = -q w + r v - g \sin \theta + a_x \quad 4.1$$

$$\dot{v} = -r u + p w + g \sin \theta \cos \varphi + a_y \quad 4.2$$

$$\dot{w} = -p v + q u + g \sin \theta \cos \varphi + a_z \quad 4.3$$

Rotational Equations

$$\dot{\varphi} = p + q \sin \varphi \tan \theta + r \cos \varphi \tan \theta \quad 4.4$$

$$\dot{\theta} = q \cos \varphi - r \sin \theta \quad 4.5$$

$$\dot{\psi} = q \sin \varphi \sec \theta + r \cos \varphi \sec \theta \quad 4.6$$

Navigational Equations

$$\begin{aligned} \dot{x}_E = & u \cos \psi \cos \theta + v (\cos \psi \sin \theta \sin \varphi - \sin \psi \cos \varphi) & 4.7 \\ & + w (\cos \psi \sin \theta \cos \varphi + \sin \psi \sin \varphi) \end{aligned}$$

$$\begin{aligned} \dot{y}_E = & u \sin \psi \cos \theta + v (\sin \psi \sin \theta \sin \varphi + \cos \psi \cos \varphi) + w (\sin \psi \sin \theta & 4.8 \\ & \cos \varphi - \cos \psi \sin \varphi) \end{aligned}$$

$$\dot{h} = u \sin \theta - v \cos \theta \sin \varphi - w \cos \theta \cos \varphi \quad 4.9$$

The above equations are nonlinear, coupled differential equations. The equations contain (u, v, w) , (ψ, θ, φ) , (x_E, y_E, h) , (p, q, r) , and (a_x, a_y, a_z) as state variables that can be evaluated using measured angular rates, and linear accelerations. Based on an estimation of the above state variables, utilizing the equations provided below, it is simple to deduce other variables as well.

$$V = \sqrt{u^2 + v^2 + w^2} \quad 4.10$$

$$\alpha = \tan^{-1}\left(\frac{w}{u}\right) \quad 4.11$$

$$\beta = \sin^{-1}\left(\frac{v}{V}\right) \quad 4.12$$

$$\bar{q} = \frac{1}{2} \rho V^2 \quad 4.13$$

Since the effects of flight under given operating conditions are not easy to test in a laboratory thus calibration is essential for error elimination from flight data. Let us consider the sensor model equation in terms of biases, time delay, scale factor, and measured variable 'y_m' as

$$y_m(t) = k_y y(t - \zeta) + \Delta y \quad 4.14$$

Where k stands for scale factor, Δ is bias effect and ζ the time delay. Ideally, the value of scale-factor must come unity. The bias factor (Δ), and time-delay (ζ) should be negligible. It is assumed to be a constant instrumentation error.

The linear accelerations calibrated at COG are estimated from acceleration ($a_{x_m}^{AS}$, $a_{y_m}^{AS}$, $a_{z_m}^{AS}$) by using a navigational sensor, accelerometer, and X, Y, Z in equation (4.15-4.17) refers to the position of accelerometer (R. Kumar, 2012)

$$a_{xCG} = a_{x_m} + (q^2 + r^2) X + (p q - r) Y - (p r + q) Z - \Delta a_x \quad 4.15$$

$$a_{yCG} = a_{y_m} - (p q + r) X + (p^2 + r^2) Y - (q r - p) Z - \Delta a_y \quad 4.16$$

$$a_{zCG} = a_{z_m} - (p r - q) X - (q r - p) Y + (p^2 + q^2) Z - \Delta a_z \quad 4.17$$

Where subscript m refers to measured quantities. X_{ASCG} , Y_{ASCG} , and Z_{ASCG} as accelerometer positions to COG. The bias measurement a_x^{CG} , a_y^{CG} , a_z^{CG} indicated by Δa_x , Δa_y and Δa_z . The rates p , q , and r stand for $p_m - \Delta p$, $q_m - \Delta q$ and $r_m - \Delta r$ acquired from measured rates (p_m , q_m and r_m) correcting biases (Δp , Δq , and Δr). The state equations (4.18-4.24) incorporate the bias term as given below. Refer Appendix C

$$\dot{u} = - (q_m - \Delta q) w + (r_m - \Delta r) v - g \sin \theta + a_x^{CG} \quad 4.18$$

$$\dot{v} = - (r_m - \Delta r) u + (p_m - \Delta p) w + g \cos \theta \sin \varphi + a_y^{CG} \quad 4.19$$

$$\dot{w} = - (p_m - \Delta p) v + (q_m - \Delta q) u + g \cos \theta \cos \varphi + a_z^{CG} \quad 4.20$$

$$\dot{\varphi} = (p_m - \Delta p) + (q_m - \Delta q) \sin \varphi \tan \theta + (r_m - \Delta r) \cos \varphi \tan \theta \quad 4.21$$

$$\dot{\theta} = (q_m - \Delta q) \cos \varphi - (r_m - \Delta r) \sin \varphi \quad 4.22$$

$$\dot{\psi} = (q_m - \Delta q) \sin \varphi \sec \theta + (r_m - \Delta r) \cos \varphi \sec \theta \quad 4.23$$

$$\dot{h} = u \sin \theta - v \cos \theta \sin \varphi - w \cos \theta \cos \varphi \quad 4.24$$

The sideslip angle and the angle of attack at nose-boom modelled in term of scale factor and bias is given below where variables k_α and k_β stands for scale factors, $\Delta \alpha_{NB}$ and $\Delta \beta_{NB}$ as biases for α , and β .

$$V_m = \sqrt{u^2 + v^2 + w^2} \quad 4.25$$

$$\alpha_{NB, m} = K_\alpha \tan^{-1} (w_{NB}/u_{NB}) + \Delta \alpha_{NB} \quad 4.26$$

$$\beta_{NB, m} = K_\beta \sin^{-1} \left(\frac{v_{NB}}{(u_{NB}^2 + v_{NB}^2 + w_{NB}^2)^{1/2}} \right) + \Delta \beta_{NB} \quad 4.27$$

$$\varphi_m = \varphi \quad 4.28$$

$$\psi_m = \psi \quad 4.29$$

$$h_m = h \quad 4.30$$

The x_{NBCG} , y_{NBCG} , and z_{NBCG} stand for offset distances taken from COG in the below equation, and at the aircraft nose-boom the velocity components are given by

$$U_{NB} = u - (r_m - \Delta r) y_{NBCG} + (q_m - \Delta q) z_{NBCG} \quad 4.31$$

$$V_{NB} = v - (p_m - \Delta p) z_{NBCG} + (r_m - \Delta r) x_{NBCG} \quad 4.32$$

$$W_{NB} = w - (q_m - \Delta q) x_{NBCG} + (p_m - \Delta p) y_{NBCG} \quad 4.33$$

Compatibility Factors Calculation Using Longitudinal Actual Flight Data

Flight path Reconstruction using ML Matlab code was taken on real processed data at a low-moderate angle of attack applying observations equation (Jategaonkar, 2015)

Figure 4.10 - 4.12 displays the input variables α , θ , β , q , a_z and V measured and estimated responses.

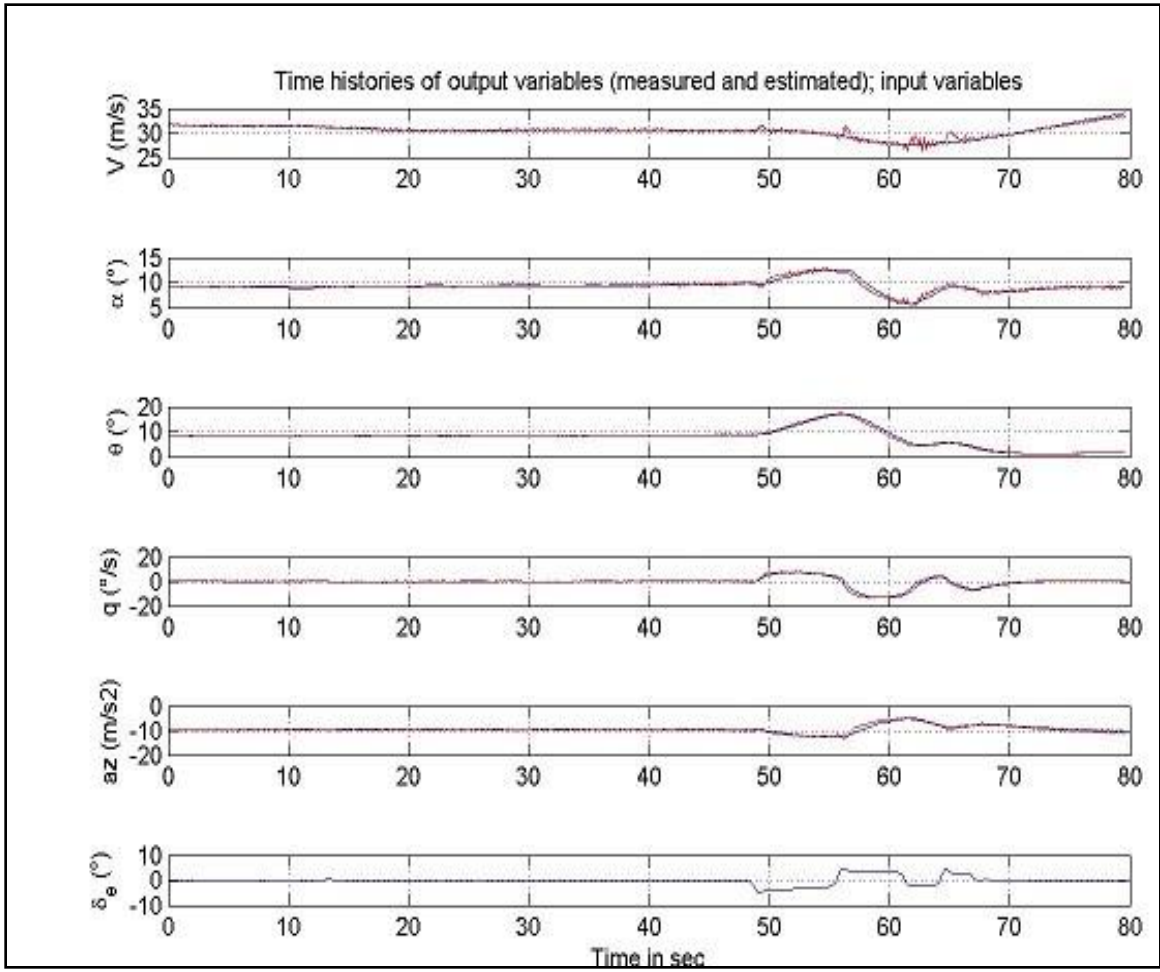


Figure 4.10 displays measured and estimated responses of longitudinal motion variables (θ , a_z , α , q , V , δ_e) obtained from FPR for multistep HALM5 Input form

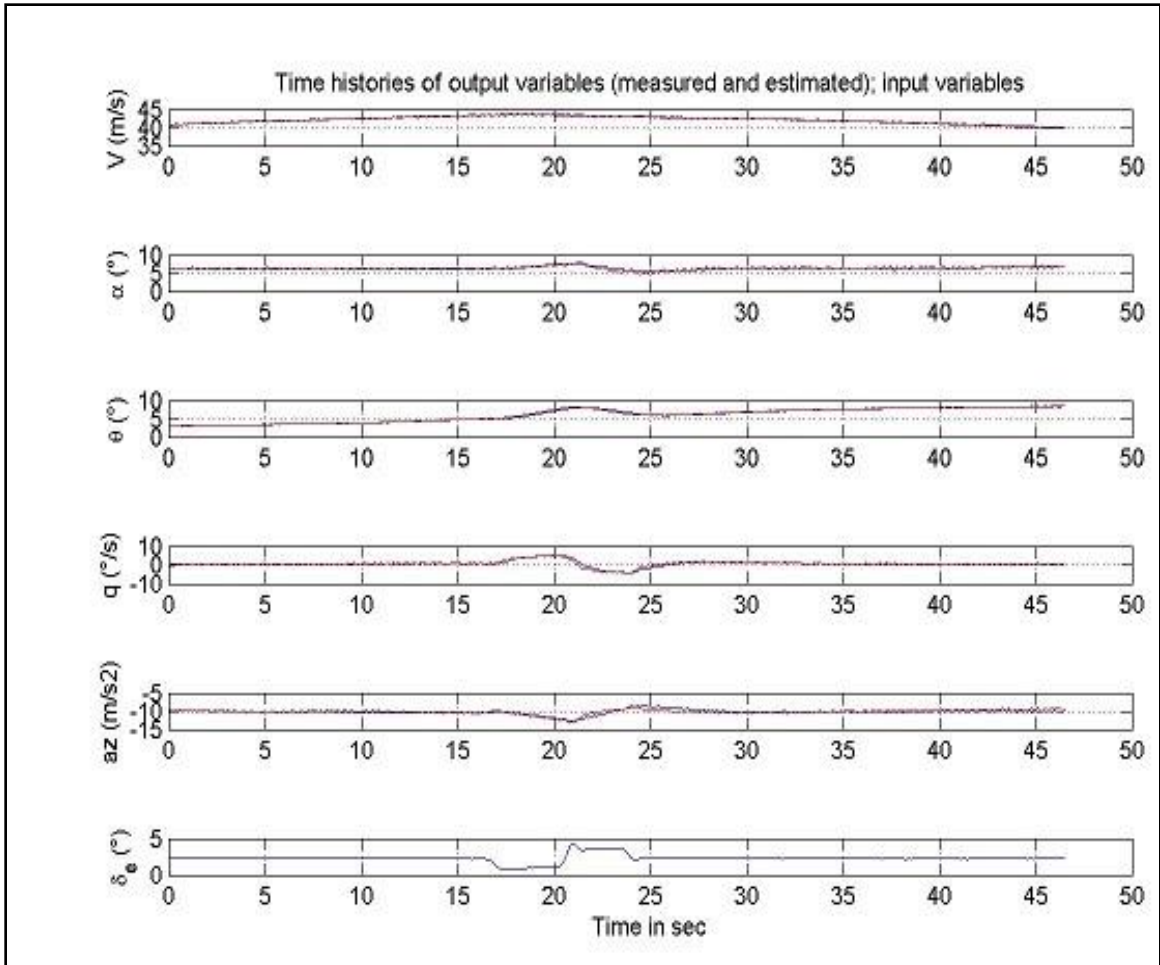


Figure 4.11 displays measured and estimated responses of longitudinal motion variables (θ , a_z , α , q , V , δ_e) obtained from FPR for doublet HALD1 Input form.

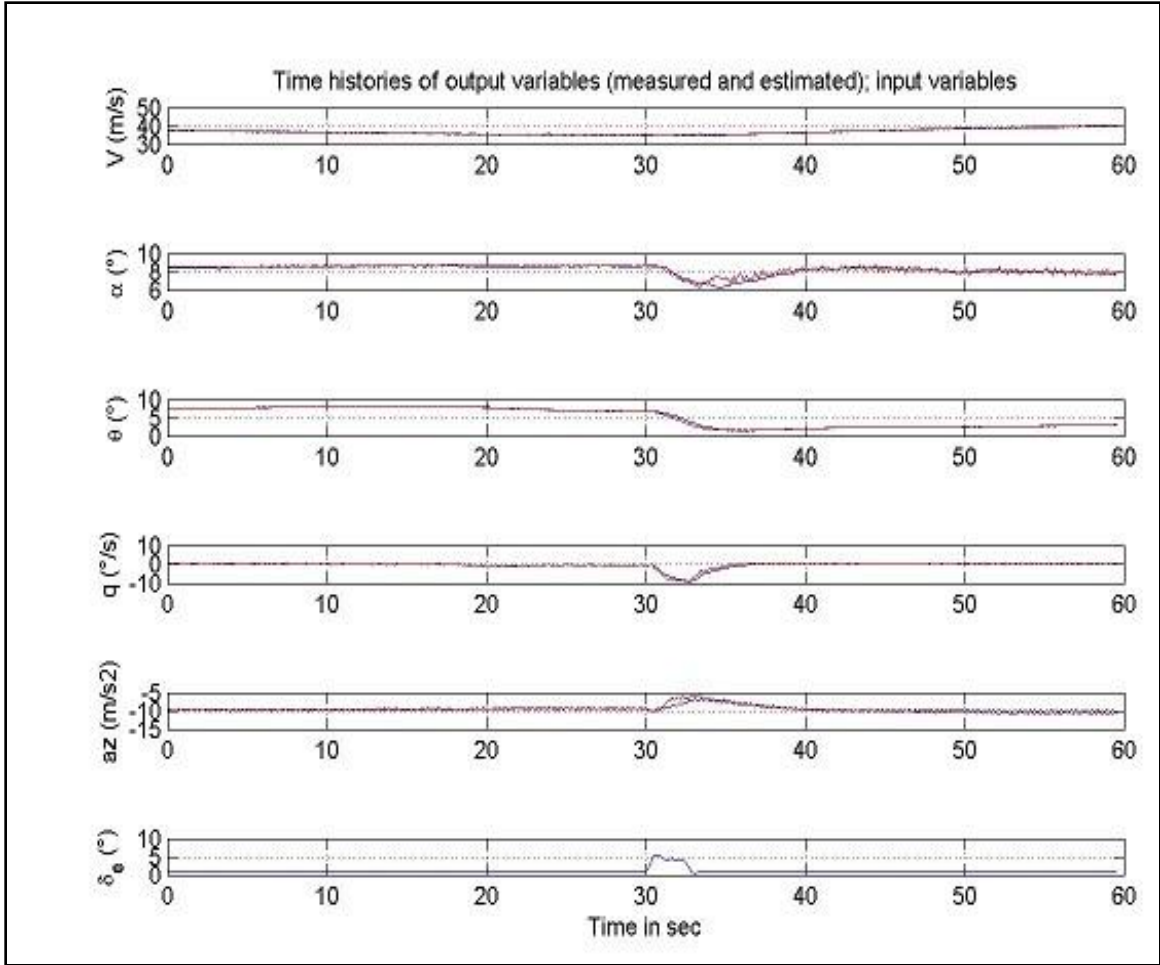


Figure 4.12 displays measured and estimated responses of longitudinal motion variables (θ , a_z , α , q , V , δ_e) obtained from FPR for pulse HALP1 Input form.

It is remarked from the above figures that estimated responses compliment well with given measured responses. It is found that the desired control input is enforced so fast that velocity variation is slightly low which mismatches the estimated response with the measured one.

The estimation of scale factors using the Maximum Likelihood method to check data compatibility is represented below (R. Kumar, 2012)

$$\Theta = [\Delta p \Delta q \Delta r \Delta a_x \Delta a_y \Delta a_z \Delta \alpha \Delta \kappa]^T \quad 4.34$$

The unknown vector represents bias and scale factor for the reconstruction of longitudinal dynamics of RCTA aircraft. The ML technique is used for the estimation of compatibility factors. The level of parameter accuracy is evaluated by the Cramer-Rao bounds.

Table 4.1 presented in the below section shows the values of bias, and scale factor ($\Delta \kappa_\alpha$) in the form of $\Delta p \Delta q \Delta r \Delta a_x \Delta a_y \Delta a_z \Delta \alpha \Delta \kappa_\alpha$ for all data-sets. It has been noted that the scale factor value is nearly one and bias is assumed to be negligible. The deviation in the values of these factors is due to interference effects produced by the propeller or atmospheric turbulence thus slight deviation in these factors is assumed during flight test.

S. No	Data	Δa_x	Δa_y	Δa_z	Δp	Δq	Δr	K_α	$\Delta \alpha$
1	HALM1	0.412	-0.218	-0.59	0.0019	-0.00075	-0.0059	0.93	0.045
2	HALM2	0.238	-0.235	-0.297	0.0015	-0.0015	-0.0058	0.85	0.045
3	HALM3	0.089	0.086	-0.012	-0.0004	-0.0009	0.0037	1.01	0.039
4	HALM4	0.137	-0.115	-0.286	-0.0001	-0.0015	-0.0021	0.91	0.143
5	HALM5	-0.35	-0.087	-0.178	-0.000048	-0.0029	-0.0004	0.7	0.02
6	HALD3	0.814	0.116	-0.454	-0.000005	0.00001	-0.0035	0.89	0.194
7	HALP1	1.01	0.15	-0.09	0.000003	0.00002	0.00001	0.87	0.073
8	HALP2	0.11	0.135	0.0151	-0.0003	-0.0007	0.002	0.92	0.075

Table 4.1: Estimation of Scale factor and bias factor

Table 4.1 shows the scale and bias factor of different data sets and it is observed that data set HALM3 of multi-step elevator input has the value of scale factor is 1.01 which illustrates its relevancy from other datasets.

4.3 AERODYNAMIC MODELING OF HANSA-III AIRCRAFT

Equations of motion are used to create the mathematical model of the Hansa-III aircraft. The aerodynamic forces and moments will be estimated using this. The

flight test was carried on at different manoeuvres of the elevator such as multi-step, doublet, and pulse input. It is mostly found that longitudinal motion predominantly excites short-period mode rather than phugoid thus short- period equations are used to estimate longitudinal parameters. These equations are a set of state equations, observation equations, and equations of motion (refer to Appendix C)

Governing Longitudinal Equation in Wind Axis in short-period mode (Peyada et al., 2008) (Jategaonkar, 2015)

Force Equation

$$\dot{V} = -\left\{\frac{\bar{q}.s}{m}\right\} C_D + g \sin(\alpha - \theta) + \left\{\frac{T}{m}\right\} \cos \alpha \quad 4.35$$

$$\dot{\alpha} = -\left\{\frac{\bar{q}.s}{m.v}\right\} C_L + q + \frac{g}{V} \cos(\alpha - \theta) - \left\{\frac{T}{m.v}\right\} \sin \alpha \quad 4.36$$

$$\dot{\theta} = q \quad 4.37$$

Moment Equation

$$\dot{q} = \left(\frac{\bar{q}.s.c}{I_y}\right) \cdot C_m + \left\{\frac{T}{I_{yy}}\right\} l_{tz} \quad 4.38$$

To analyse the aircraft dynamics, the aircraft is modelled in terms of mathematical equations as aerodynamic stability and control derivatives shown below

$$C_L = \left\{ C_{L_0} + C_{L_\alpha} \cdot \alpha + C_{L_q} \cdot \frac{q\bar{c}}{2U_1} + C_{L_{\delta_e}} \cdot \delta_e \right\} \quad 4.39$$

$$C_D = \left\{ C_{D_0} + C_{D_\alpha} \cdot \alpha + C_{D_q} \cdot \frac{q\bar{c}}{2U_1} + C_{D_{\delta_e}} \cdot \delta_e \right\} \quad 4.40$$

$$C_m = \left\{ C_{m_0} + C_{m_\alpha} \cdot \alpha + C_{m_q} \cdot \frac{q\bar{c}}{2U_1} + C_{m_{\delta_e}} \cdot \delta_e \right\} \quad 4.41$$

Assumptions:

Thrust setting angle = 0; Flight path γ = constant at cruise state; flight velocity is constant as elevator control input excites short-period dynamics(JAISWAL & PRAKASH, 2022)

Simplified longitudinal state equation to estimate non-dimensional derivatives as longitudinal stability and control predominantly excite short-period mode

$$\dot{\alpha} = -\left\{\frac{\bar{q} \cdot s}{m \cdot v}\right\} C_L + q \quad 4.42$$

$$\dot{\theta} = q \quad 4.43$$

$$\dot{q} = \left(\frac{\bar{q} \cdot s \cdot c}{I_y}\right) \cdot C_m \quad 4.44$$

Simplifying set of equations

$$\dot{\alpha} = q - \frac{\rho V S_w}{2m} \{C_{L_0} + C_{L_\alpha} \cdot \alpha + C_{L_q} \cdot \frac{q \bar{c}}{2U_1} + C_{L_{\delta_e}} \cdot \delta_e\} \quad 4.45$$

$$\dot{\theta} = q \quad 4.46$$

$$\dot{q} = \frac{\rho V^2 S_w \bar{c}}{2I_y} \{C_{m_0} + C_{m_\alpha} \cdot \alpha + C_{m_q} \cdot \frac{q \bar{c}}{2U_1} + C_{m_{\delta_e}} \cdot \delta_e\} \quad 4.47$$

The parameter vector (Θ) determines the value of non-dimensional longitudinal derivatives which is given as (R. Kumar, 2012)

$$\Theta = [C_{L_0} \ C_{L_\alpha} \ C_{L_q} \ C_{L_{\delta_e}} \ C_{D_0} \ C_{D_\alpha} \ C_{D_{\delta_e}} \ C_{m_0} \ C_{m_\alpha} \ C_{m_q} \ C_{m_{\delta_e}}]^T \quad 4.48$$

4.4 METHODOLOGY OF PARAMETER ESTIMATION

Maximum Likelihood

Maximum likelihood is generally applicable for estimating longitudinal

derivatives of dynamic models utilizing actual flight data. M.L estimators are reliable, effective, efficient, and used for covariance matrices with no state noise. It is formulated by minimizing Cost function ‘J’ which is the difference between measured and estimated response as expressed in equation(Jategaonkar, 2015)(R. Kumar, 2012) (Jaiswal et al., 2020)

$$J(\Theta, R) = L(z|\Theta, R) = \frac{1}{2} \sum_{k=1}^N [z(tk) - y(tk)]^T R^{-1} [z(tk) - y(tk)] + N/2 \ln |\det(R)| + Nn_y/2 \ln(2\pi) \quad 4.49$$

$$\ln |\det(R)| + Nn_y/2 \ln(2\pi)$$

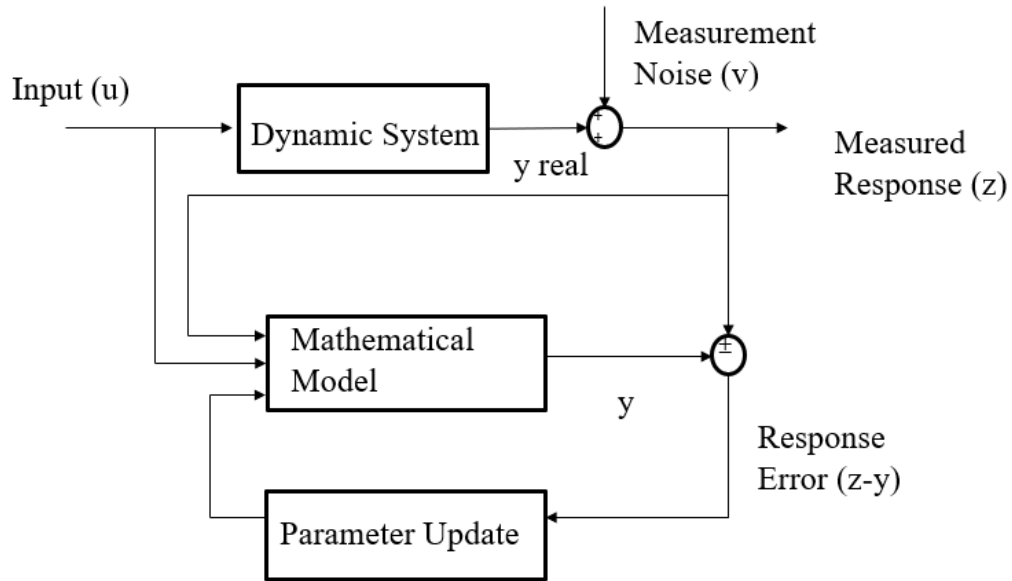


Figure 4.13 Output Error Method

Properties of Maximum likelihood function(Jategaonkar, 2015):

1. Asymptotically unbiased is a characteristic property of maximum likelihood

estimates $\lim_{n \rightarrow \infty} E(\Theta_{ML}) = \Theta$

2. The novel feature of maximum likelihood estimates is that they are asymptotically consistent.
3. The estimates ML have the virtue of being asymptotically efficient with respect to the statistical precision bounds known as Cramer Rao bounds.

PARAMETER ESTIMATION

The longitudinal derivatives were estimated using the compatible flight data corresponding to various control inputs, including multi-step [3211], doublet, and pulse using the ML code (Jategaonkar, 2015)

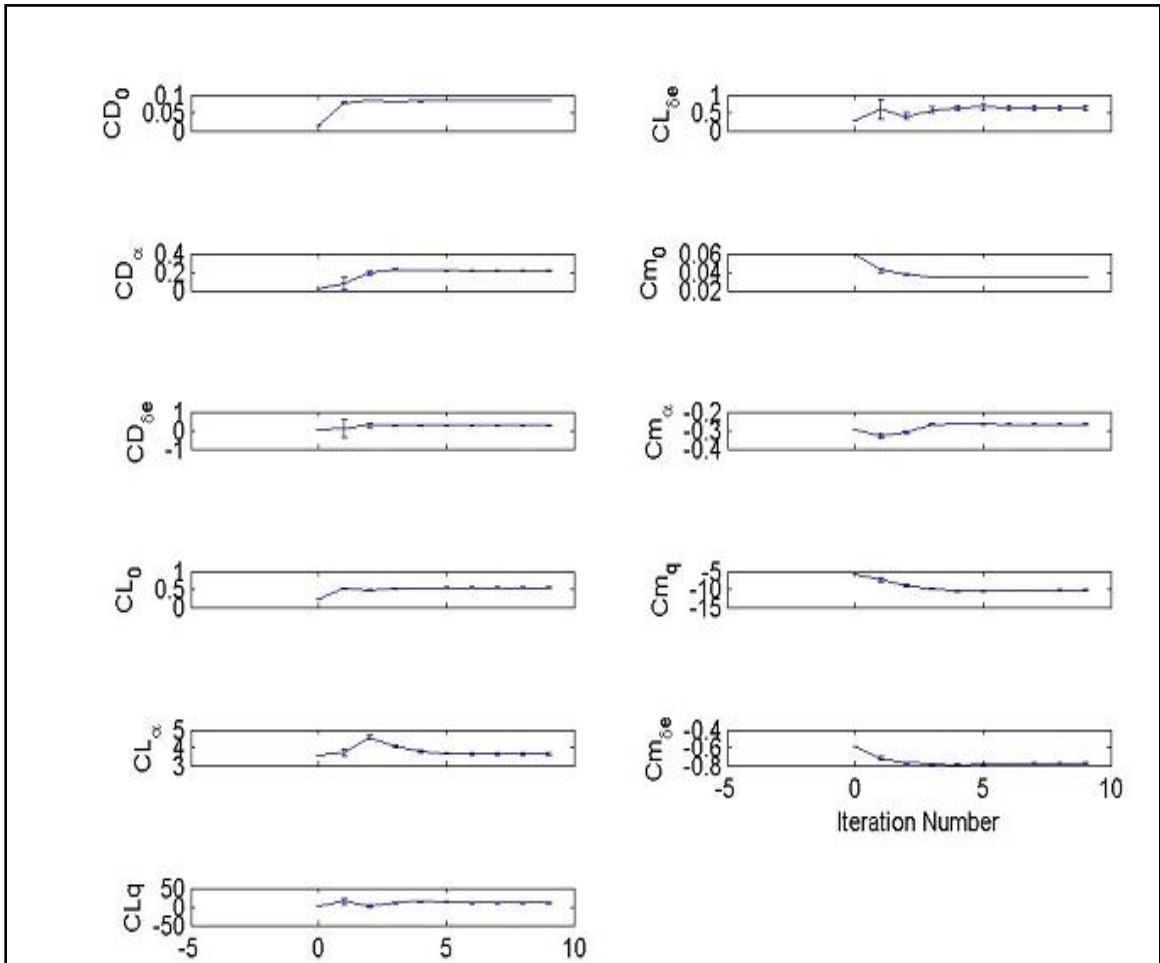


Fig 4.14 shows the convergence of HALM5 Multi-step Input in terms of Aerodynamic Derivatives (C_{Lq} , $C_{L\alpha}$, C_{L_0} , C_{D_0} , $C_{D\alpha}$, $C_{D\delta e}$, C_{m_q} , C_{m_0} , C_{m_α} , $C_{m_{\delta e}}$)

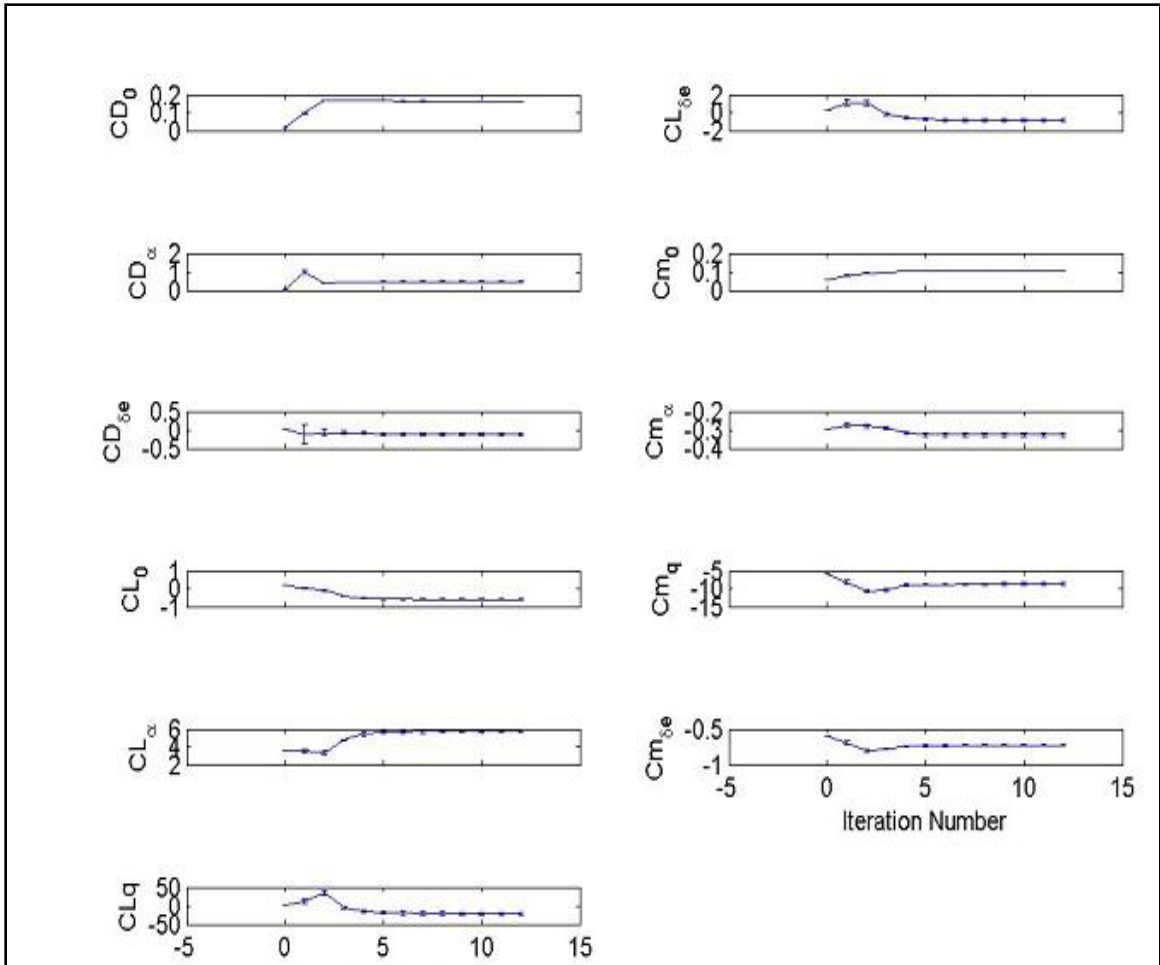


Fig 4.15 shows the convergence of HALD1 Doublet Input in terms of Aerodynamic Derivatives (C_{Lq} , $C_{L\alpha}$, C_{L0} , C_{D0} , $C_{D\alpha}$, $C_{D\delta e}$, $C_{m q}$, C_{m_0} , $C_{m\alpha}$, $C_{m\delta e}$)

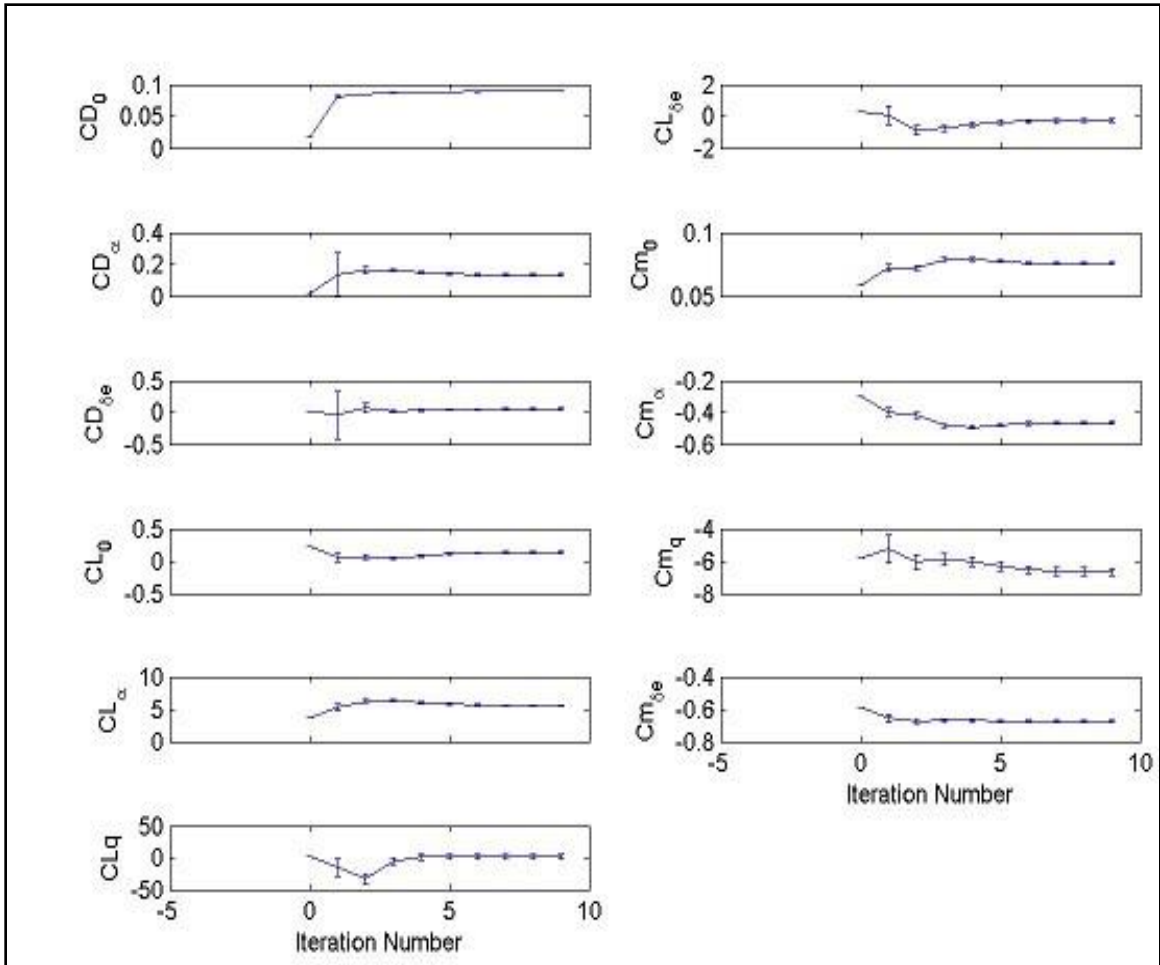


Fig 4.16 shows the convergence of HALP1 Pulse Input in terms of Aerodynamic Derivatives (C_{Lq} , $C_{L\alpha}$, C_{L0} , C_{D0} , $C_{D\alpha}$, $C_{D\delta e}$, C_{mq} , C_{m0} , $C_{m\alpha}$, $C_{m\delta e}$)

Figures presented in the above section show the estimated response of derivatives (C_{Lq} , $C_{L\alpha}$, C_{L0} , C_{D0} , $C_{D\alpha}$, $C_{D\delta e}$, C_{mq} , C_{m0} , $C_{m\alpha}$, $C_{m\delta e}$) The ML technique is applied to eight data- sets of elevator input as a multi-step, doublet, and Pulse for parameter estimation.

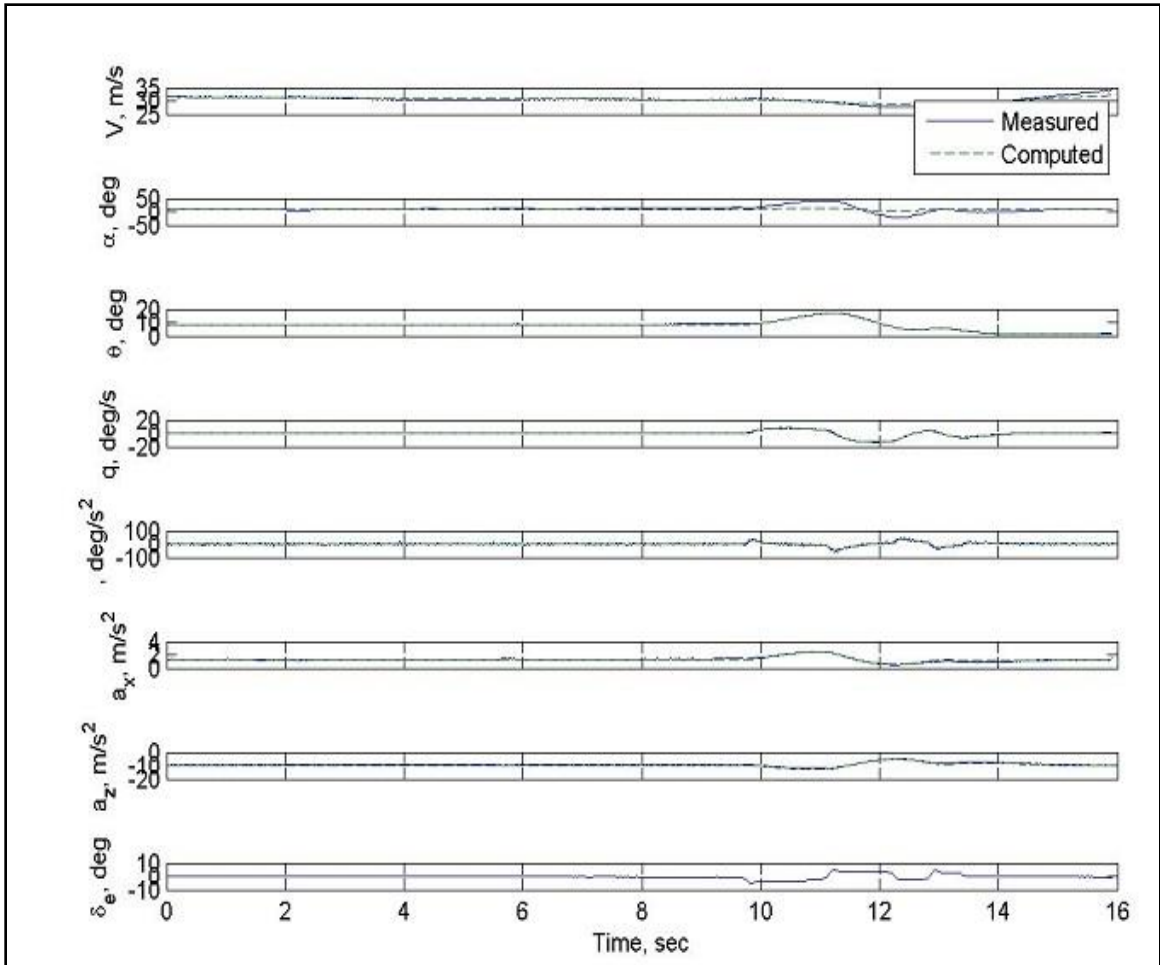


Fig 4.17 The measured and computed results obtained from ML: HALM5

Figures 4.17 presented in the above section measure the estimated and measured response of variables (α , θ , q , a_x , and a_z) through the X, Z body axis in the act of parameter estimation. The data sets' responses HALM5 show a strong correlation between the estimated and measured motion variables

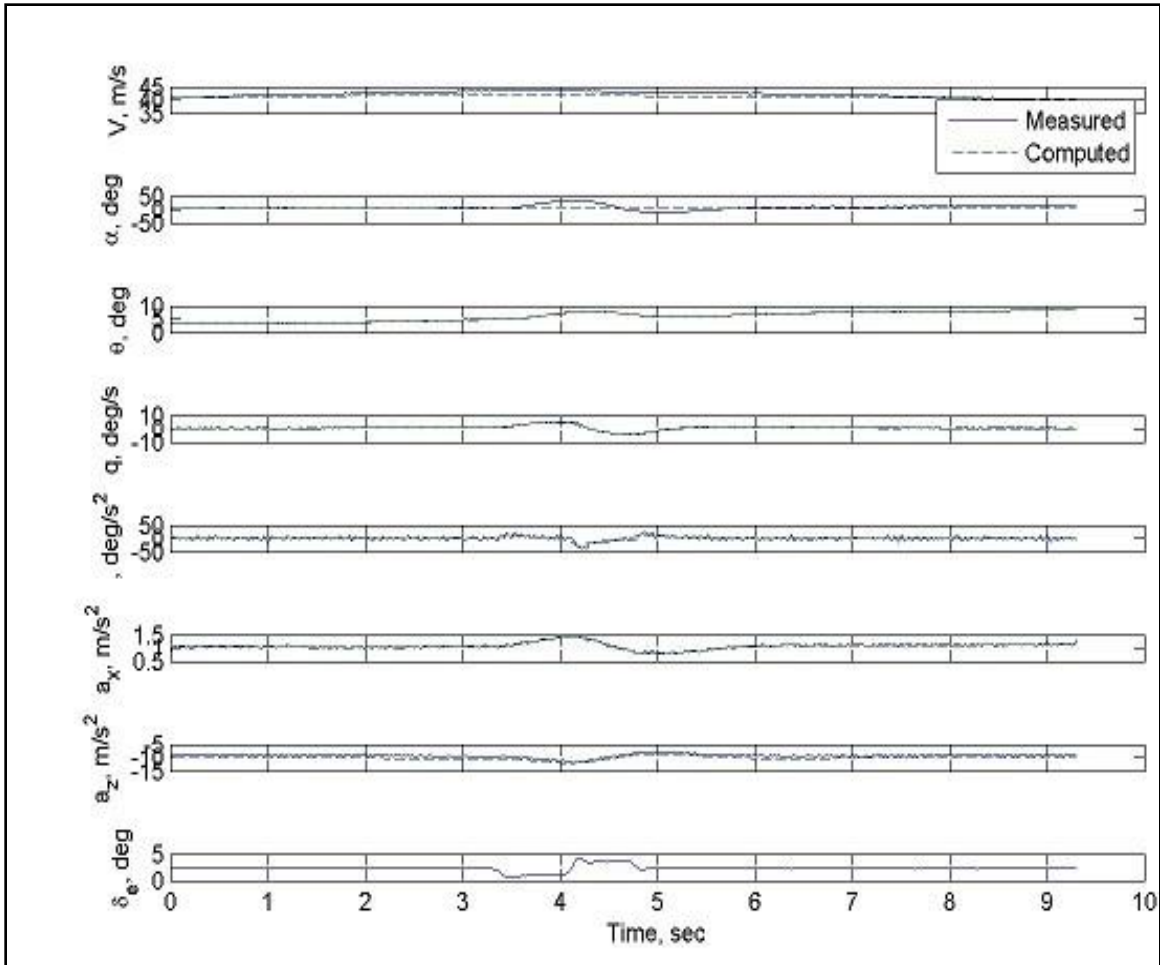


Fig 4.18 The measured and computed results obtained from ML: HALD1

Figure 4.18 presented in the above section measure the estimated and measured response of variables (α , θ , q , a_x , and a_z) through the X, Z body axis in the act of parameter estimation. The data sets' responses HALD1 show a strong correlation between the estimated and measured motion variables.

Table 4.2 presents the numeric value of parameters estimated through the ML method. It is observed from the tabulated data that the value of parameters is accurate and close to wind tunnel values.

Data	C_{D_0}	C_{D_α}	$C_{D_{\delta e}}$	C_{L_0}	C_{L_α}	$C_{L_{\delta e}}$	C_{m_0}	C_{m_α}	$C_{m_{\delta e}}$	C_{m_q}
W.T	0.035	0.086	0.026	0.354	4.97	0.26	0.052	-0.4596	-1.008	
HALM1	0.059	0.263	0.165	0.037	5.964	0.194	0.078	-0.407	-0.734	-8.57
HALM2	0.053	0.216	0.136	0.0842	5.69	0.184	0.076	-0.429	-0.711	-8.11
HALM3	0.0588	0.093	0.058	-0.18	3.94	0.5367	0.071	-0.35	-0.851	-11.1
HALM4	0.145	0.408	0.202	0.1141	6.16	0.27	0.0918	-0.6437	-0.909	-6.77
HALM5	0.0408	0.0282	0.0473	0.2254	6.4592	0.0196	0.0787	-0.4259	-	-
HALD1	0.2178	0.344	-0.577	-0.44	3.75	-2.027	0.183	-6.67	-0.51	-0.642
HALP1	0.164	0.463	-0.128	-0.606	5.78	-0.818	0.103	-8.67	-0.33	-0.728

Table 4.2: ML-based parameter estimation technique for the longitudinal case: Multi- step, Doublet, and Pulse Inputs

Table 4.2 exhibit that obtained values of aerodynamic derivatives using ML is reasonably accurate. The value of C_{L_α} , C_{m_q} , C_{m_0} , $C_{m_{\delta e}}$, C_{m_α} , C_{D_0} , is seen to approach wind tunnel values for most data sets and shows a slight variation in parameters such as C_{L_0} , C_{D_α} . The variance in the value from the wind tunnel is ignored since the weak parameters $C_{L_{\delta e}}$, C_{L_q} , and $C_{D_{\delta e}}$, have a minimal impact compared to the strong ones. It is also found that rare techniques are available to determine the accurate value of the weak parameters due to the unavailability of proper flight data or elevator input is not able to follow the desired variation. Additionally, one observation is noticed that there is a maximum deviation in the values from the Wind Tunnel result in the case of pulse Input as compared to Multi-step and Doublet. The Multi-step is more consistent as compared to different elevator Inputs. The results depicted in tabulated form provide information to the researcher about the Control Input types respectively.

4.5 VALIDATION

Model Validation is a proof-match exercise that is carried out by making use of the flight dataset HALM4 corresponds to the doublet input HALD1. The response was estimated by resolving six degrees of freedom Equations of motion. It is noticed

that the estimated response from HALM4 is close to the measured response of HALD1 and validates the result.

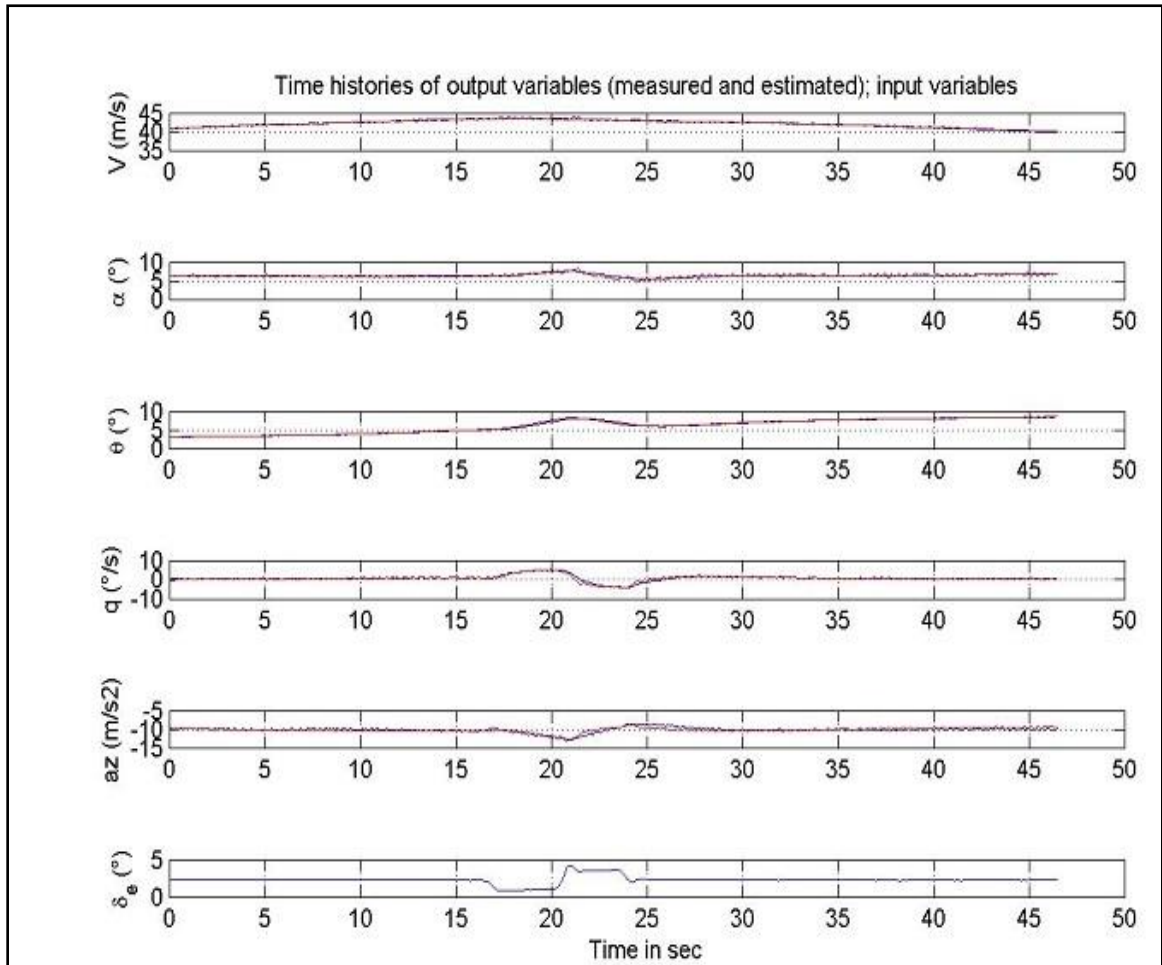


Fig.4.19 Parameter estimation from HALM4 and validation using HALD1

The results are also validated with the results that came from wind tunnel results as well as a reference paper. The results of strong derivatives are validated as they predominantly influence the stability and control of the system. MLH35 is the data set referred from the research paper as presented in Table 4.3 (R. Kumar, 2012)

Data	C_{L_0}	C_{L_α}	$C_{L_{\delta e}}$	C_{m_0}	C_{m_α}	$C_{m_{\delta e}}$	C_{m_q}
W.T	0.354	4.97	0.26	0.052	-0.4596	-1.008	
MLH35	0.092	5.409	0.282	0.073	-0.395	-0.719	-9.406
HALM1	0.037	5.964	0.194	0.078	-0.407	-0.734	-8.57
HALM2	0.0842	5.69	0.184	0.076	-0.429	-0.711	-8.11
HALM3	-0.18	3.94	0.5367	0.071	-0.35	-0.851	-11.1
HALM4	0.1141	6.16	0.27	0.0918	-0.6437	-0.909	-6.77
HALM5	0.2254	6.4592	0.0196	0.0787	-0.4259	-0.8665	-11.612

Table 4.3: Compared Results of Longitudinal Derivatives of Wind-Tunnel, Multi-step Datasets, and MLH35 (R. Kumar, 2012)

The bar pictorial representation of Longitudinal Derivatives of Hansa-III is compared with the results of Wind-Tunnel, Dataset HALM5, and MLH35 (R. Kumar, 2012) in Fig 4.20

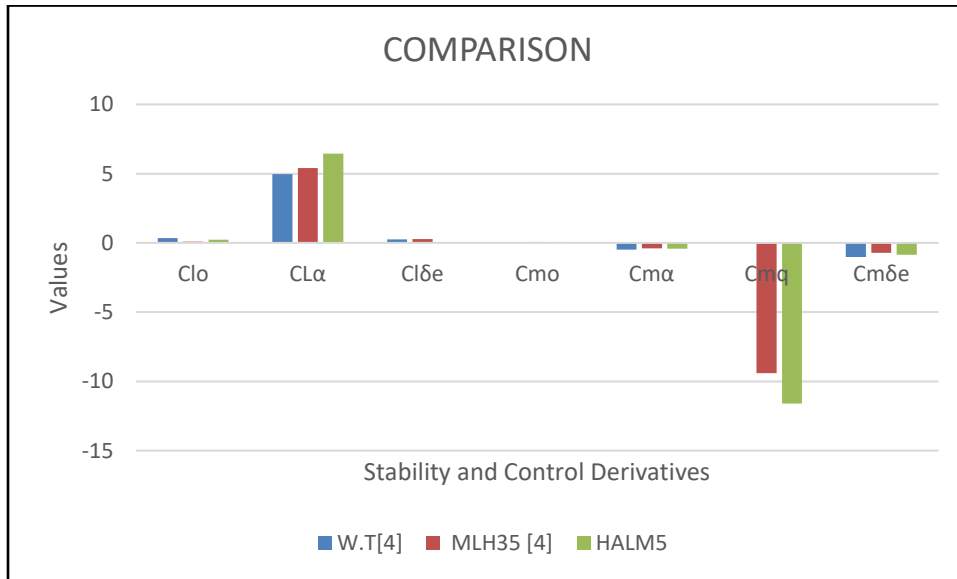


Fig 4.20 Compared Results of Wind-Tunnel, Dataset HALM5, and MLH35[10] in term of Graphical representation.

The result of multiple data sets is compared in the form of bar representation and the dataset HALM5 shows minimum variation with wind tunnel result as presented

in Table 4.3 thus the values of coefficients of HALM5 are utilized to calculate the transfer function of the pitch controller for execution of the second objective.

SUMMARY:

In this chapter, a flight test of Hansa-III was conducted for file processing. The Data Compatibility is checked for processed flight data to ensure measurements used in the model are error-free. Once the FPR is ensured then the equations of motion in the wind axis were used to formulate the aircraft mathematical model (refer to section 5.3) and longitudinal aerodynamic derivatives were estimated using ML Code (Jategaonkar, 2015). Model Validation is exercised once the parameters are estimated. Different datasets were used for designing the controller using different approaches as discussed in Appendix D1,D2.

CHAPTER -5

AIRCRAFT CONTROLLER DESIGN

This chapter addresses the introduction of aircraft stability, dynamics & automatic control. Hence, developing the expression of deriving six DOF equations of motion, linearized longitudinal perturbation equations, and longitudinal equations of motion in wind axes, the axes system is reviewed. Classical control theory and modern control theory is applied to design control system. To apply traditional, classical theory to design a control system, it is important to understand the concept of transfer function whereas, the concept of state-space formulation of system from governing equations is important for modern control methods. Both approaches are important to design control systems. The chapter discussed open-loop / closed-loop PID tuning techniques to the PID controller's gain parameters. The pitch controller is designed using Root-locus, Pole-placement, and Linear quadratic regulator methods for optimal results. Simulated Results of traditional, classical, and modern control methods are compared in this chapter.

5.1 CONTROL SYSTEM

Advanced level of control systems involved in all engineering disciplines such as aerospace automation, missile guidance, and control systems, robotics engineering, automotive, and space science. Hence it is necessary to be familiar with the basics of the control system. This chapter focuses on control system analysis both in the time and frequency domain as well a glimpse of an aircraft control system is introduced with a clear explanation.

A system comprises the number of components assigned to perform a specific task. The system is described as a control system since the input controls the output variable in it.

Classification:

1. Open-Loop and Closed-Loop Control System

Open-loop:

A system where measured output is independent of controlled activity. It consists of a system, controller, Input, and output signals for example:

1. Electric bulb
2. Stepper motor
3. Switching ON Fan

Advantages:

1. Simpler
2. Economical to operate.
3. A less complex system reduced maintenance cost
4. Highly Stable

Dis-Advantages:

1. Less accurate and reliable.
2. Calibration is required from time to time



Fig 5.1 Open-loop Control System

Closed-loop:

A system where controlled action depends on measured output is additionally known as a feedback control system. It consists of a system, controller, Input, output, feedback, and actuators for example:

1. An autopilot controller
2. Speed control of DC Motor
3. Missile/ Rocket Launcher system

Advantages:

1. High accuracy than open-loop systems.
2. Recalibration is not required
3. Automation Facility
4. Robustness

Dis-Advantages:

1. More Complex system increases maintenance cost
2. Less stable than the open-loop control system

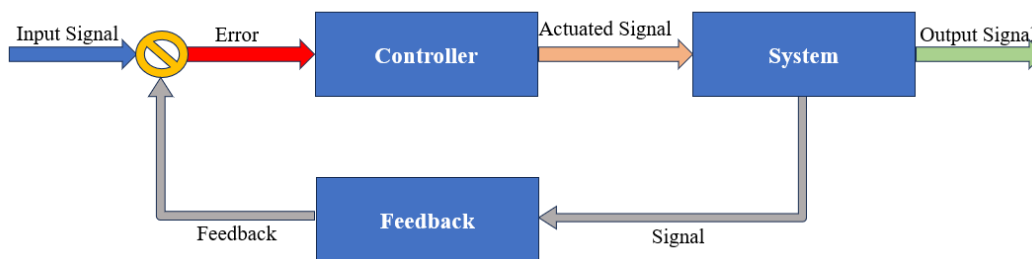


Fig 5.2 Closed-loop control system

2. Linear and non-linear Control Systems

Linear Control Systems:

A linear system is defined as a system in which variables have an exponent one for example $y = 3 * x$

Non- Linear Control Systems

A non-linear system is defined as a system in which variables have an exponent other than one for example $x^2 + y^2 = 6$

3. Time variant and Time in variant Control systems

Time variant control system:

Parameters of the control system vary with time and can be defined as the time-variant control system

Time In-variant control system:

The Parameters of the control system do not vary with time and can be defined as a time-invariant control system.

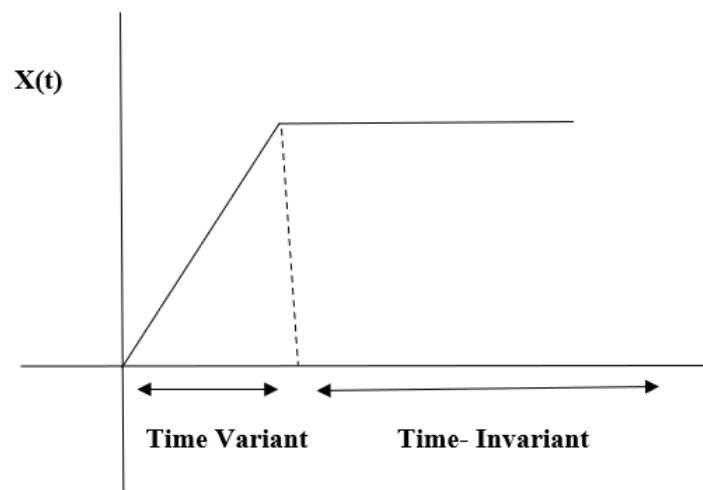


Fig 5.3 Time-Variant Vs Time- Invariant

4. Linear Time Variant and Non-linear Time Variant control system

Linear Time Variant control system:

The combination of linear systems with time-variant are the systems in which variables have an exponent of one and are time dependent.

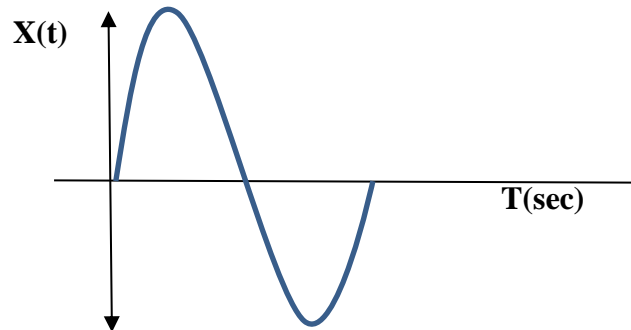


Fig 5.4 Linear Time Variant control system

Non-Linear Time Variant control system:

The combination of non-linear systems with time-variant are the systems in which variables have an exponent other than one and are time-dependent.

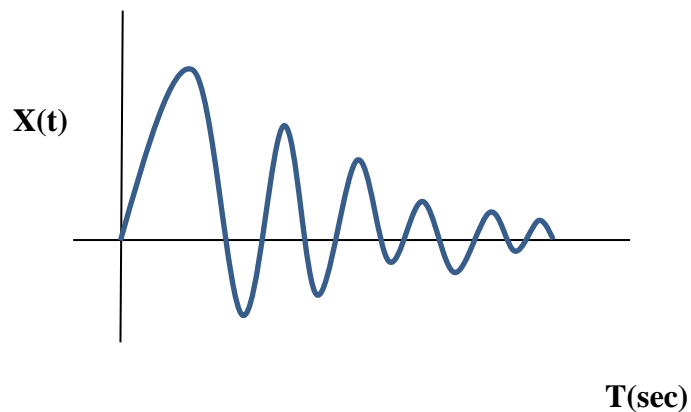


Fig 5.5 Non-Linear Time Variant control system

5. SISO and MIMO Control system

Single Input Single Output (SISO): The control system consists of one Input and one output for example speed controller of the fan.

Multiple Input Multiple Output (MIMO): The control system consists of multiple Input and multiple output parameters for example aircraft controller design, and auto-controller of the space vehicle.

To design an accurate control system for our research objective closed-loop, linear, time-invariant, SISO control system is elaborately discussed in sections 1,2,3,4 and 5

5.2 AIRCRAFT STABILITY AND CONTROL SYSTEM

5.2.1 AIRCRAFT STABILITY

Stability is the characteristic of the equilibrium state being stable. In physical terms, the net moment and resultant forces about the centre of gravity must be zero to satisfy stability conditions.

It is classified as static stability and dynamic stability

Static: Stability is the ability of a system to resume equilibrium even after being moved from its initial state. An example to discuss types of static stability is illustrated in the below section

Positive Static Stability

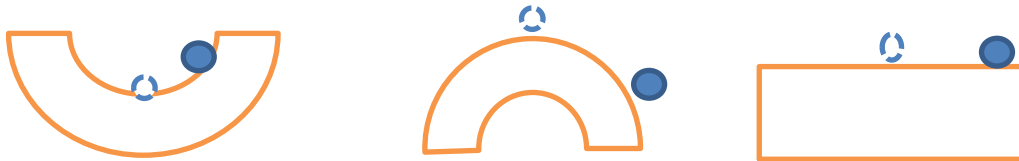
If the system is displaced from its initial state and restored to its original state such that forces and moments tend the system to attain an equilibrium point is referred to as a stable system as seen in Fig 5.6

Negative Static Stability

If the system is displaced from its initial state and tries to go away from its original state such that forces and moments tend the system to move away from the equilibrium point is referred to as an unstable system

Neutral Static Stability

The equilibrium point of the system is independent of displacing from the original state and is referred to as a neutrally stable system.



(i) Stable System

(ii) Unstable System

(iii) Neutral System

Fig 5.6 Stable, Unstable, and Neutral System

Dynamic: The response and behaviour of the motion of the system while displaced from its original state is termed dynamic stability.

Positive Dynamic Stability

If the system is displaced from its initial state and oscillations dampen the system towards the equilibrium point is termed a dynamically stable system

Negative Dynamic Stability

If the system is displaced from the initial state and amplitude of the oscillations rises and the system has negative damping then the system will never approach towards trim state thus referred to as a dynamically Unstable system

Neutral Dynamic Stability

If the system is displaced from its initial state and the amplitude of the oscillations never damps or remains constant termed a neutrally dynamically stable system

5.2.2 AIRCRAFT CONTROLS

Elevator:

The control surfaces are hinged to the trailing edge of the horizontal tail. These are found in pairs and provide longitudinal stability to an aircraft mentioned in Fig 5.7 Pitch control is attained by changing the aircraft lift by deflecting the flapped portion of the horizontal tail entitled as the elevator.

Ailerons:

The control surfaces are hinged to the trailing edge of an aircraft wing tip. These are found in pairs and provide lateral stability to an aircraft. They are performed in a synchronized manner as one aileron is raised and the other is lowered known as the aircraft's rolling motion.

Rudder:

The control surfaces are hinged to the trailing edge of the vertical tail and provide directional stability to an aircraft. Yaw control is attained by deflecting the flapped portion of the vertical tail termed as rudder. It turns the aircraft in the left and right direction similar to the rudder of a boat.



Fig 5.7 Aircraft Controls

5.2.3 AIRCRAFT AXES AND REFERENCE SYSTEM

Aircraft controls can be acknowledged by defining an axes coordinate system as the aircraft is free to rotate about 3 axes which are mutually perpendicular to each other as mentioned in Fig 5.8 and the pilot can handle and control the motion about axes in all directions hence the axes system is defined as

Longitudinal Axis:

Lateral stability about longitudinal axes is a key feature of these axes. Ailerons are lateral control that provides rolling motion to an aircraft that moves one wing down and the other wing up.

Lateral Axis:

Longitudinal stability about lateral axes is a key feature of these axes. Elevators are longitudinal control that provides pitching motion to an aircraft that moves the aircraft nose in an up-and-down direction.

Vertical Axis:

Directional stability about vertical axes is a key feature of these axes. Rudders are directional control that provides Yawing motion to an aircraft which moves the aircraft to the left and right.

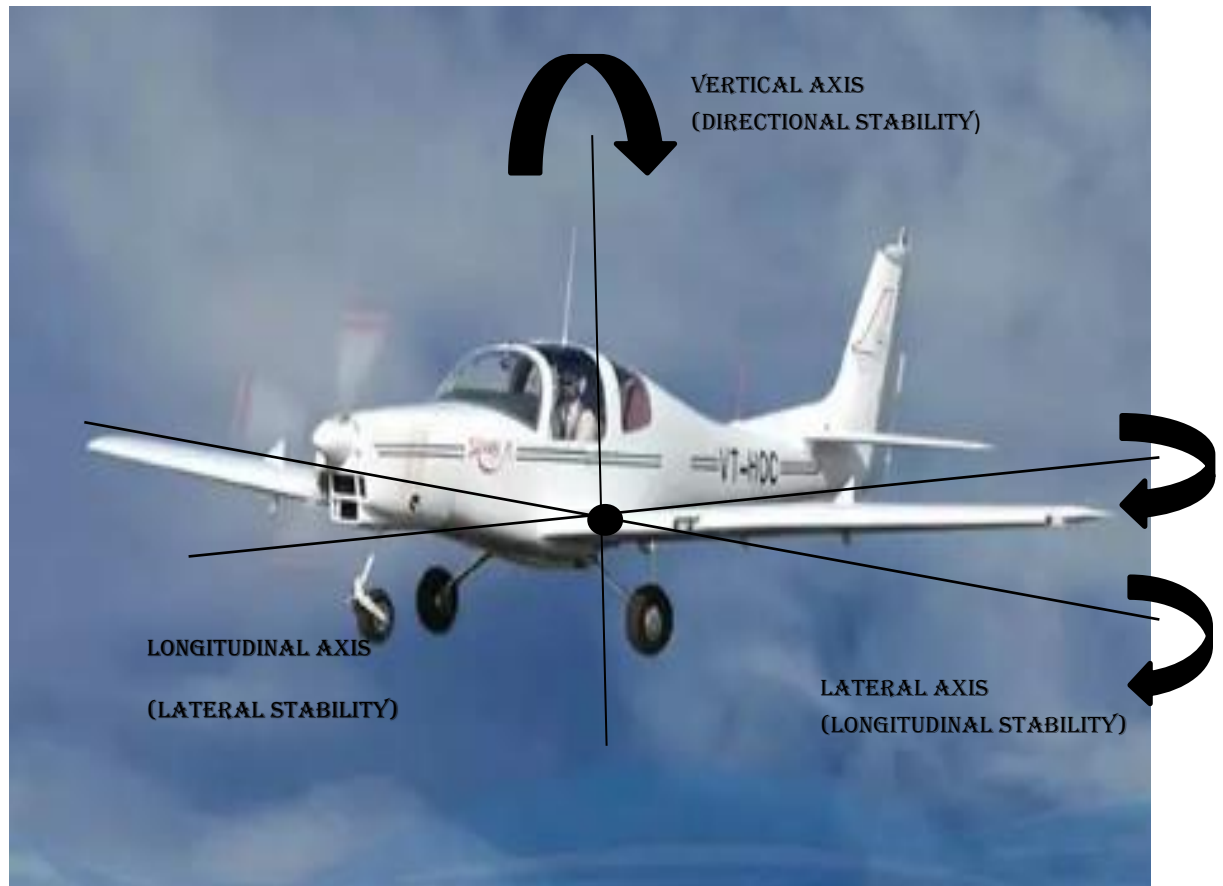


Fig 5.8 Stability Axes System

5.2.4 REFERENCE FRAMES

Inertial Axes: A frame of reference that is having constant velocity or remains stationary. All of Newton's laws are applied in this frame of reference.

Earth Axes: A frame of reference in which the origin is located on the earth's surface. X_E points towards the geographical north, Y_E points towards the geographical east, and Z_E points towards the centre of the earth.

Body Axes: A frame of reference in which the origin is located on the aircraft's centre of gravity, with the X pointing towards the aircraft nose and the Y axes pointing towards the right wing and the Z axis passing beneath through it.

Wind Axes: A frame of reference in which the origin is situated on the aircraft's centre of gravity, with X_w axes pointing forward relative to the velocity vector, Y_w axes pointing towards the right wing, and Z axes underneath through it.

Stability Axes: This axes system is defined for aircraft stability and fixed with aircraft. X-axes point forward toward the flow direction. Y-axes point towards the right wing, and Z-axes underneath through it.

Based on the Axes control system, Aircraft stability is classified into three types as

1. Longitudinal Stability
2. Lateral Stability
3. Directional Stability

5.2.5 LONGITUDINAL STABILITY

The synonym term “pitch stability” is the tendency of an aircraft to attain a trim state about the lateral axis. Longitudinal Stability provides pitching motion by moving the aircraft nose in upward and downward directions. Elevators are control surfaces that contribute longitudinal motion of an aircraft.

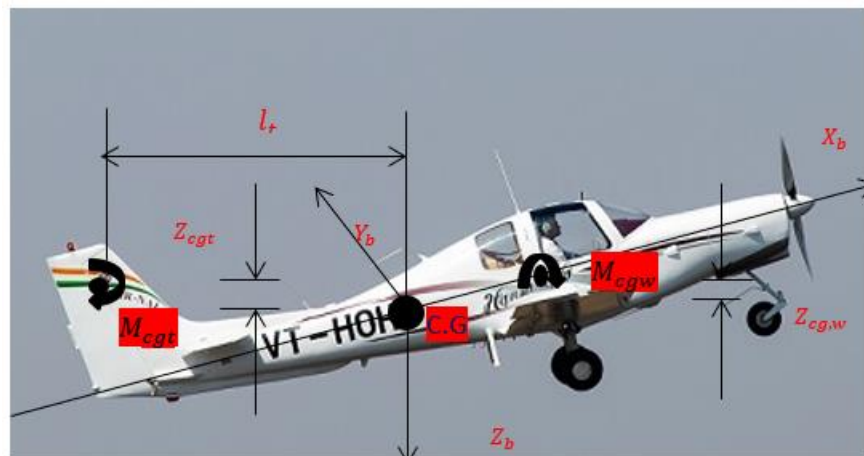


Fig 5.9 Wing and tail Contribution of Hansa-III Aircraft

Geometrical Parameters	Value	Geometrical Parameters	Value
Wing		Horizontal Tail	
Planform area (S)	12.47(m ²)	Planform area (S _t)	2.04(m ²)
Aspect ratio (A)	8.8	Aspect ratio (A)	6.35
MAC (\bar{c})	1.21(m)	MAC (\bar{c})	0.59(m)
Root Chord (c _r)	1.3(m)	Root Chord (c _r)	0.78(m)
Tip Chord (c _t)	0.8	Tip Chord (c _t)	0.354(m)
Taper ratio (Λ)	6(deg)	Taper ratio (Λ)	0.454
Aircraft		Aerodynamic Derivatives	
Aircraft span (b)	10.47(m)	(C _{Lα,w}) _{ss}	4.5
Mass (m)	750(kg)	(C _{Lαt}) _{ss}	1.48
Velocity (V)	36(m/s)	(C _{mα,f}) _{ss}	0.3
Moment of Inertia (I _Y)	907(kg-m ²)	(C _{Lαt} $\frac{d\epsilon}{d\alpha}$) _{ss}	0.22
Moment arm (l _t)	3.624(m)		
Density (ρ)	0.96(kg/m ³)		
Moment of Inertia (I _X)	925(kg-m ²)		

Table 5.1 Geometrical and Aerodynamic Parameters (R. Kumar, 2012)

Analytical Calculation to estimate Longitudinal Stability

The pitch stiffness C_{m_α} is the deciding factor in to state longitudinal stability of the system which is estimated by referring to fig 5.9 and Table 5.1

The permissible range of C.G: Forward C.G position is 21.94% of MAC and aft C.G Position is 27.47% of MAC as MAC of the wing is 1.21m (NAL, 2000)

Forward C.G position= 0.26

Aft C.G Position= 0.332

$$C.G = (0.26+0.332)/2 = 0.296$$

The Aerodynamic centre lies at the quarter chord point for a symmetrical airfoil as MAC is 1.21 m hence $X_{ac} = 0.3025$

$$V_H = \frac{l_t \times S_t}{S \times \bar{c}} = \frac{3.624 \times 2.04}{12.47 \times 1.21} = 0.489$$

$$\eta = \frac{Q_t}{Q_w} < 1 \text{ (Assume tail efficiency factor as unity)}$$

The wing's pitching moment coefficient

$$\begin{aligned} C_{m_{\alpha,w}} &= C_{L_{\alpha,w}}(X_{cg} - X_{ac})/MAC \\ &= 4.5(0.296-0.3025)/1.21 = -0.207 \end{aligned}$$

The coefficient of the horizontal tail's pitching moment

$$\begin{aligned} C_{m_{\alpha,t}} &= -C_{L_{\alpha,t}} \eta V_H \left(1 - \frac{d\epsilon}{d\alpha}\right) \\ &= -1.48 \times 1 \times 0.489 + 0.489 \times 0.22 = -0.6155 \end{aligned}$$

The coefficient of the fuselage pitching moment

$$C_{m_{\alpha,f}} = 0.3$$

By combining the contributions from the airplane's wings, fuselage, and tail, the total pitching moment may be calculated as (Nelson, 1998)

$$\begin{aligned} C_{m_{\alpha}} &= C_{L_{\alpha,w}}(X_{cg} - X_{ac})/MAC + C_{m_{\alpha,f}} - C_{L_{\alpha,t}} \eta V_H \left(1 - \frac{d\epsilon}{d\alpha}\right) \\ &= 4.5(0.296-0.3025)/1.21 + 0.3 + 0.22 \times 0.489 - 1.48 \times 1 \times 0.489 = -0.345 \end{aligned}$$

The contributing factor determining aircraft static stability is $C_{m_{\alpha}} < 0$ to attain longitudinal stability.

The Stick-Fixed neutral point(Nelson, 1998)

$$\begin{aligned} \bar{X}_{np} &= X_{ac} - C_{m_{\alpha,f}}/C_{L_{\alpha,w}} + C_{L_{\alpha,t}} \eta V_H \left(1 - \frac{d\epsilon}{d\alpha}\right) \\ &= 0.3025 + 0.089 = 0.3915 \end{aligned}$$

$$\text{Stick-fixed Static Margin} = \bar{X}_{np} - \bar{X}_{cg} = 0.3915 - 0.296 = 0.095$$

The Positive value of the Static Margin illustrates that the system is longitudinally statically stable thus control system can be designed to attain the research objective

Longitudinal modes of motion:

Frederick W. Lanchester, Aerodnetics, develops the fundamental concept of longitudinal dynamic stability(Nelson, 1989).In the early stages of his study, Lanchester noticed the motions of a glider during flying. He conducted various experiments with gliders and discovered that all flying machines possess oscillatory motions while disturbed from the original equilibrium state. Two oscillatory modes are long-period and short-period.

Long Period mode

This oscillatory mode is lightly damped and its motion occurs at a constant angle of attack. As its name, this mode has a long period also termed phugoid

Short Period mode

This oscillatory mode is heavily damped and its motion occurs at a constant speed. As its name, this mode has a short period.

Longitudinal Dynamics is characterised by damping ratio & frequency of short period and long period. Before deducing the expression of longitudinal modes, the equation of motion must be linearized by applying the small disturbance theory as explained below.

Linearized Perturbation equation using small-disturbance theory

This theory solves complex engineering application-based problems by linearizing force and moment equations to reduce system complexity. This theory applies to steady-state flight conditions and is inapplicable for stalled flights. It is assumed

that all state variables are replaced with a summation of steady-state value and perturbation.

$$u = u_0 + \Delta u \quad X = X_0 + \Delta X$$

$$v = v_0 + \Delta v \quad Y = Y_0 + \Delta Y$$

$$w = w_0 + \Delta w \quad Z = Z_0 + \Delta Z$$

$$p = p_0 + \Delta p \quad L = L_0 + \Delta L$$

$$q = q_0 + \Delta q \quad M = M_0 + \Delta M$$

$$r = r_0 + \Delta r \quad N = N_0 + \Delta N$$

$$\delta = \delta_0 + \Delta \delta$$

Assumptions:

1. It is assumed that X- axes lie along the aeroplane velocity vector.
2. Considering reference conditions as symmetric.
3. It is assumed that forces in the force equation include propulsive force and thrust force is assumed to be constant. Thrust force is produced due to the propulsion system of an aircraft and creates a moment if not lies through the airplane's Centre of gravity assumed to be constant.

X-axes force equation can be rewritten as;

$$X_0 + \Delta X - mg \sin(\theta_0 + \Delta \theta) = m \left[\frac{d}{dt} (u_0 + \Delta u) + (q_0 + \Delta q)(w_0 + \Delta w) - (r_0 + \Delta r)(v_0 + \Delta v) \right] \quad 5.1$$

Assuming $w_0 = v_0 = q_0 = r_0 = p_0 = \phi_0 = \theta_0$ for X axes, the equation reduces to

$$X_0 + \Delta X - mg \sin(\theta_0 + \Delta \theta) = m \Delta \dot{u} \quad 5.2$$

As per trigonometric identity; $\text{Sin}(\theta_0 + \Delta\theta) = \text{Sin}\theta_0\text{Cos}\Delta\theta + \text{Cos}\theta_0\text{Sin}\Delta\theta$

For Smaller angles $\text{Sin}\Delta\theta = \Delta\theta$; $\text{Cos}\Delta\theta = 1$

Substituting all trigonometric relations in the above equation to obtain force equation in reduced form $\text{Sin}(\theta_0 + \Delta\theta) = \text{Sin}\theta_0 + \Delta\theta\text{Cos}\theta_0$

Thus, $X_0 + \Delta X - mg(\text{Sin}\theta_0 + \Delta\theta\text{Cos}\theta_0) = m\Delta\dot{u}$

If perturbations are set equal to zero; then reference steady-state conditions are depicted as $X_0 - mg\text{Sin}\theta_0 = 0$

Finalized X force equation can be written as: $\Delta X - mg(\text{Sin}\theta_0 + \Delta\theta\text{Cos}\theta_0) = m\Delta\dot{u}$

ΔX as Δ in resultant forces in X-direction and if X is a function of u, w, δ_e, δ_T then

ΔX is represented as $\Delta X = \frac{\partial X}{\partial u} \Delta u + \frac{\partial X}{\partial w} \Delta w + \frac{\partial X}{\partial \delta_e} \Delta \delta_e + \frac{\partial X}{\partial \delta_T} \Delta \delta_T$

$\frac{\partial X}{\partial u}, \frac{\partial X}{\partial w}$ terms are known as stability derivatives $\frac{\partial X}{\partial \delta_e}, \frac{\partial X}{\partial \delta_T}$ as Control derivatives where δ_e is elevator input, and δ_T is throttle input.

Substituting the value of ΔX relation from the above equation to obtain the equation as

$$\frac{\partial X}{\partial u} \Delta u + \frac{\partial X}{\partial w} \Delta w + \frac{\partial X}{\partial \delta_e} \Delta \delta_e + \frac{\partial X}{\partial \delta_T} \Delta \delta_T - mg \Delta \theta \text{Cos}\theta_0 = m\Delta\dot{u} \quad 5.3$$

Now re-arranging above equation to deduce the X direction force equation as

$$\left(m \frac{d}{dt} - \frac{\partial X}{\partial u}\right) \Delta u - \left(\frac{\partial X}{\partial w}\right) \Delta w + (mg \text{Cos}\theta_0) \Delta \theta = \frac{\partial X}{\partial \delta_e} \Delta \delta_e + \frac{\partial X}{\partial \delta_T} \Delta \delta_T \quad 5.4$$

Dividing the above equation by 'm' to get a simplified expression as $\left(\frac{d}{dt} - \frac{\partial X}{\partial u}\right) \Delta u - \left(\frac{\partial X}{\partial w}\right) \Delta w + (g \text{Cos}\theta_0) \Delta \theta = \frac{\partial X}{\partial \delta_e} \Delta \delta_e + \frac{\partial X}{\partial \delta_T} \Delta \delta_T$ where X_u, X_w are aerodynamic derivatives.

The set of linearized perturbation equations of motion in the X direction is expressed as:

$$\left(\frac{d}{dt} - X_u\right)\Delta u - X_w\Delta w + (g \cos\theta_0)\Delta\theta_0 = X_{\delta_e}\Delta\delta_e + X_{\delta_T}\Delta\delta_T \quad 5.5$$

Linearized Longitudinal perturbation force and moment equation can be expressed as (Nelson, 1989):

$$\left(\frac{d}{dt} - X_u\right)\Delta u - X_w\Delta w + (g \cos\theta_0)\Delta\theta_0 = X_{\delta_e}\Delta\delta_e + X_{\delta_T}\Delta\delta_T \quad 5.6$$

$$-Z_u\Delta u + [(1 - Z_w)\frac{d}{dt} - Z_w]\Delta w - [(u_0 + Z_q)\frac{d}{dt} - (g \sin\theta_0)]\Delta\theta = \quad 5.7$$

$$Z_{\delta_e}\Delta\delta_e + Z_{\delta_T}\Delta\delta_T$$

$$-M_u\Delta u - (M_w\frac{d}{dt} + M_w)\Delta w + \left(\frac{d^2}{dt^2} - M_q\frac{d}{dt}\right)\Delta\theta = M_{\delta_e}\Delta\delta_e + \quad 5.8$$

$$M_{\delta_T}\Delta\delta_T$$

$$Z_{\dot{w}} = -C_{z\dot{\alpha}} \frac{c}{2u_0} \frac{QS}{u_0 m} \quad 5.9$$

$$Z_u = -C_{zq} \frac{c}{2u_0} \frac{QS}{m} \quad 5.10$$

$C_{z\dot{\alpha}}$, C_{zq} is Z force non-dimensional components contribute pitching motion very little so neglected Z_q and $Z_{\dot{w}}$ effects hence rewriting sets of longitudinal equations in state-space form

Where x is a state vector, A as a state matrix, u refers to the control vector and B is the control matrix. Comparing state-space form with generalized state-space equation yields

$$\begin{bmatrix} \Delta\dot{u} \\ \Delta\dot{w} \\ \Delta\dot{q} \\ \Delta\dot{\theta} \end{bmatrix} = \begin{bmatrix} X_u & X_w & 0 & -g \\ Z_u & Z_w & u_0 & 0 \\ M_u + M_w Z_u & M_w + M_w Z_w & M_q + M_w u_0 & 0 \\ 0 & 0 & 1 & 0 \end{bmatrix} \begin{bmatrix} \Delta u \\ \Delta w \\ \Delta q \\ \Delta\theta \end{bmatrix} +$$

$$\begin{bmatrix} X_{\delta_e} & X_{\delta_T} \\ Z_{\delta_e} & Z_{\delta_T} \\ M_{\delta_e} + M_w Z_{\delta_e} & M_{\delta_T} + M_w Z_{\delta_T} \\ 0 & 0 \end{bmatrix} \begin{bmatrix} \Delta\delta_e \\ \Delta\delta_T \end{bmatrix} \quad 5.11$$

$$\dot{X} = Ax + Bu$$

Long-Period Approximation

Approximating longitudinal state-space equation to the long-period mode by assuming $\Delta\alpha$ as zero and neglecting pitching moment equation to deduce expression of long-period mode.

The characteristics of long-period mode are changes in altitude, pitch altitude, and motion occurring at constant " α "

$$\Delta\alpha = \frac{\Delta w}{u_0}, \quad \Delta\alpha = 0 \text{ signifies } \Delta w = 0$$

The simplified state equation is reduced by applying assumptions such as (Nelson, 1998):

$$\begin{bmatrix} \Delta\dot{u} \\ \Delta\dot{\theta} \end{bmatrix} = \begin{bmatrix} X_{u\pm} & -g \\ \frac{-Z_u}{u_0} & 0 \end{bmatrix} \begin{bmatrix} \Delta u \\ \Delta\theta \end{bmatrix} \quad 5.12$$

The eigenvalues of matrix A can be solved by $|\lambda I - A|=0$

$$\lambda^2 - X_u \lambda - \frac{Z_u g}{u_0} = 0 \quad 5.13$$

$$\lambda_{lp} = [X_u \pm \sqrt{X_u^2 + 4 \frac{Z_u g}{u_0}}] / 2 \quad 5.14$$

The physical systems are modelled by the second-order differential equation. To illustrate aircraft dynamic motion let us consider the mechanical system comprised

of mass, spring, and damper system. The non-homogeneous second-order differential equation of the physical system can be explained as:

$$m \frac{d^2x}{dt^2} + c \frac{dx}{dt} + kx = F(t) ; \frac{d^2x}{dt^2} + \frac{c}{m} \frac{dx}{dt} + \frac{k}{m} x = \frac{F(t)}{m} \quad 5.15$$

Where $F(t)$ is the forced force function. If the driving force is zero, then the system response is termed a free response and vice versa referred to as a forced response. The differential equation's solution can be expressed in writing by substituting as $x = Ae^{\lambda t}$ in the above equation

$$\lambda^2 Ae^{\lambda t} + \frac{c}{m} \lambda Ae^{\lambda t} + \frac{k}{m} Ae^{\lambda t} = 0 \text{ or } \lambda^2 + \frac{c}{m} \lambda + \frac{k}{m} = 0 \text{ or } \lambda^2 + 2\xi\omega_n\lambda + \omega_n^2 = 0$$

The above phrase refers to the roots of the characteristic equation as

$$\lambda_{1,2} = -\frac{c}{2m} \pm \sqrt{\left(\frac{c}{2m}\right)^2 - \frac{k}{m}}$$

Comparing the above equation with characteristic equation of long-period mode yields a damping factor and natural frequency as

$$\omega_{nlp} = \sqrt{-\frac{Z_u g}{u_0}} \quad 5.16$$

$$\xi_{lp} = -\frac{X_u}{2\omega_{nlp}} \quad 5.17$$

Short-period Approximation

Short-period motion is heavily damped and characterized by assuming $\Delta u = 0$ and leaving the X-force equation. The change in AOA and the motion that continues for several seconds at a constant speed are the hallmarks of short-period mode.

The simplified state equation is reduced by applying assumptions such as (Nelson, 1998):

$$\begin{bmatrix} \Delta \dot{w} \\ \Delta \dot{q} \end{bmatrix} = \begin{bmatrix} Z_w & u_0 \\ M_w + M_{\dot{w}} Z_w & M_q + M_{\dot{w}} u_0 \end{bmatrix} \begin{bmatrix} \Delta w \\ \Delta q \end{bmatrix} \quad 5.18$$

In terms of AOA using the expression, $\Delta \alpha = \frac{\Delta w}{u_0}$ the equation can be rewritten as

$$\begin{bmatrix} \Delta \dot{\alpha} \\ \Delta \dot{q} \end{bmatrix} = \begin{bmatrix} \frac{Z_\alpha}{u_0} & 1 \\ M_\alpha + M_{\dot{\alpha}} \frac{Z_\alpha}{u_0} & M_q + M_{\dot{\alpha}} \end{bmatrix} \begin{bmatrix} \Delta \alpha \\ \Delta q \end{bmatrix} \quad 5.19$$

The eigenvalues of the above state equation are estimated by using the expression $|\lambda I - A| = 0$

The characteristic equation of the above expression can be written as

$$\lambda^2 - \left(M_q + M_{\dot{\alpha}} + \frac{Z_\alpha}{u_0} \right) \lambda + M_q \frac{Z_\alpha}{u_0} - M_\alpha = 0 \quad 5.20$$

The roots of the above characteristic equation are:

$$\lambda_{sp} = \left[\left(M_q + M_{\dot{\alpha}} + \frac{Z_\alpha}{u_0} \right) \pm \left[\left(M_q + M_{\dot{\alpha}} + \frac{Z_\alpha}{u_0} \right)^2 - 4 \left(M_q \frac{Z_\alpha}{u_0} - M_\alpha \right) \right]^{\frac{1}{2}} \right] / 2 \quad 5.21$$

The characteristic equation and the above equation being compared of short-period mode yields a damping factor and natural frequency as (Nelson, 1998)

$$\omega_{nsp} = \left[\left(M_q \frac{Z_\alpha}{u_0} - M_\alpha \right) \right]^{1/2} \quad 5.22$$

$$\xi_{sp} = - \left[M_q + M_{\dot{\alpha}} + \frac{Z_\alpha}{u_0} \right] / (2\omega_{nsp}) \quad 5.23$$

The flight control designer handles the flying quality of aeroplane by estimating short- and long-period damping and frequency of Hansa-III by referring to Table 5

$$V_H = \frac{l_t \times S_t}{S \times \bar{c}} = \frac{3.624 \times 2.04}{12.47 \times 1.21} = 0.489$$

$$\eta = \frac{Q_t}{Q_w} < 1 \text{ (Assume tail efficiency factor as unity)}$$

$$C_{m_{\dot{\alpha}}} = -2C_{L_{\alpha t}} \eta V_H \frac{l_t}{\bar{c}} \frac{d\epsilon}{d\alpha} = \frac{-0.7797}{1.21} = -0.644$$

$$M_{\alpha} = u_0 C_{m_{\alpha}} \frac{QS\bar{c}}{u_0 I_{yy}} = -4.379/s \quad u_0 = 36.244\text{m/s}; C_{m_{\alpha}} = -0.4259$$

$$M_q = C_{m_q} \frac{\bar{c}}{2u_0} \frac{QS\bar{c}}{I_{yy}} = \frac{-144.47}{72.48} = -1.99/s$$

$$M_{\dot{\alpha}} = C_{m_{\dot{\alpha}}} \frac{QS\bar{c}}{I_{yy}} \frac{\bar{c}}{2u_0} = -0.1105/s$$

$$C_{Z_{\alpha}} = -[(C_{L_{\alpha}} + C_{D_0})] = -6.4908$$

$$Z_{\alpha} = C_{Z_{\alpha}} \frac{QS}{m} = -68.040$$

Estimating un-damped natural frequency and damping ratio of Short-period and long-period mode by substituting values of non-dimensional stability and control derivatives from the above equations

Short-period Approximations

$$w_{n_{sp}} = \sqrt{\frac{Z_{\alpha} M_q}{u_0} - M_{\alpha}} = \sqrt{\frac{(-68.040 \times -1.99)}{36.244} - (-4.379)} = \sqrt{\frac{135.399}{36.244}} = 2.84 \text{ rad/s}$$

$$f_{n_{sp}} = \frac{2.84}{6.28} = 0.45/s$$

$$\xi_{sp} = -\frac{(M_q + M_{\dot{\alpha}} + \frac{Z_{\alpha}}{u_0})}{2w_{n_{sp}}} = \frac{3.9975}{5.68} = 0.70$$

Long-period Approximations

$$w_{n_p} = \sqrt{\frac{-Z_u g}{u_0}}$$

$$\xi_p = \frac{-X_u}{2w_{n_p}}$$

$$X_u = \frac{-[C_{D_u} + 2C_{D_0}]QS}{mu_0} = \frac{[-3C_{D_0}]QS}{mu_0} = \frac{0.1224 \times 630.47 \times 12.47}{27,183} = -0.0354/s \quad C_{D_u} \text{ is}$$

neglected at low flight speed; subsonic a/c

$$Z_u = \frac{C_{Z_u} QS}{mu_0} = \frac{[\{-\frac{M^2}{1-M^2}\} C_{L_0} - 2C_{L_0}]QS}{mu_0} = \frac{[-2C_{L_0}]QS}{mu_0} = \frac{-0.458 \times 630.47 \times 12.47}{27,183} = -0.1303/s ;$$

Mach is neglected at subsonic flight

$$w_{n_p} = \sqrt{\frac{-Z_u g}{u_0}} = \sqrt{\frac{1.2782}{36.244}} = 0.1877 \text{ rad/s}$$

$$\xi_p = \frac{-X_u}{2w_{np}} = \frac{-(-0.0354)}{2 \times 0.1877} = 0.0942$$

$$\lambda_{1,2} = -\xi_p w_{np} \pm i w_{np} \sqrt{1 - \xi_p^2}$$

$$\lambda_{1,2} = -0.0176 \pm i0.186$$

Non- dimensional Derivative	Value	Non- dimensional Derivative	Value
M_α (s ⁻²)	-4.379	X_u (s ⁻¹)	-0.0354
M_q (s ⁻¹)	-1.99	Z_u (s ⁻¹)	-0.1303
$M_{\dot{\alpha}}$ (s ⁻¹)	-0.1105	$C_{m_{\dot{\alpha}}}$	-0.644
ξ_p	0.0942	w_{np} (rad/s)	0.1877
ξ_{sp}	0.70	w_{nsp} (rad/s)	0.45

Table 5.2: Estimation of Non-dimensional derivatives using Analytical Method

Non-dimensional Derivatives of different elevator control Inputs Multistep, doublet, and Pulse estimated using the Maximum likelihood algorithm and results were validated with analytical calculations derived in the above section as discussed in Table 5.3

Input Signals	Cmo	Cm α	Cmq	CL0	Cd0	CL α	M α	Mq	Z α	M α dot	Xu	Zu	ω_{sp}	D.R sp
M1	0.08	-0.41	-8.57	0.04	0.06	5.96	-4.19	-1.46	-63.13	-0.11	-0.05	-0.02	2.59	0.64
M2	0.08	-0.43	-8.11	0.08	0.05	5.69	-4.41	-1.38	-60.19	-0.11	-0.05	-0.05	2.59	0.61
M3	0.07	-0.35	11.10	-0.18	0.06	3.94	-3.60	1.89	-41.91	-0.11	-0.05	0.10	1.19	-0.26
M4	0.09	-0.64	-6.77	0.11	0.15	6.16	-6.62	-1.16	-66.08	-0.11	-0.13	-0.07	2.95	0.52
M5	0.08	-0.43	-11.61	0.23	0.04	6.46	-4.38	-1.98	-68.13	-0.11	-0.04	-0.13	2.85	0.70
D1	0.18	-0.51	-6.67	-0.44	0.22	3.75	-5.24	-1.14	-41.59	-0.11	-0.19	0.25	2.56	0.47
P1	0.10	-0.33	-8.67	-0.61	0.16	5.78	-3.39	-1.48	-62.30	-0.11	-0.14	0.35	2.44	0.68
P2	0.03	-0.27	-10.00	0.55	0.08	3.65	-2.78	-1.71	-39.13	-0.11	-0.07	-0.32	2.15	0.67

Table 5.3: Estimation of short-Period Damping ratio and frequency

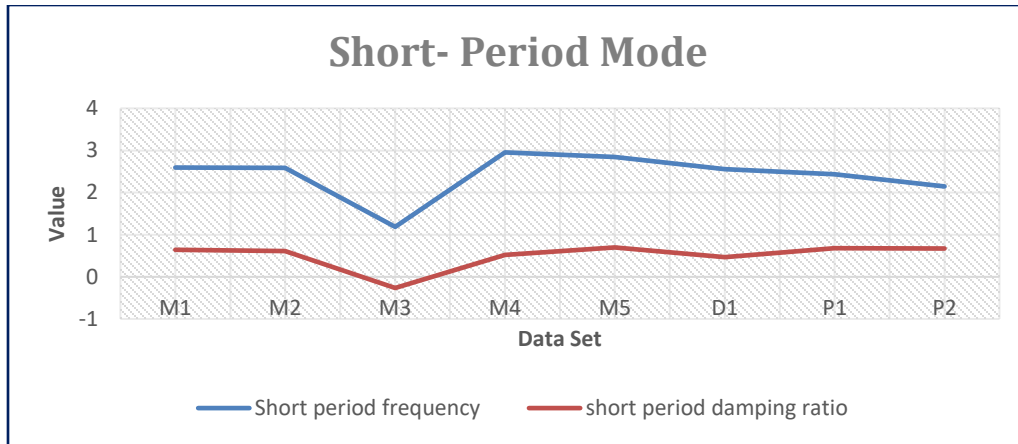


Fig 5.10 Short-period Frequency and Damping ratio

The short period frequency and damping ratio of different elevator inputs M1, M2, M3, M4, M5, D1, P1, and P2 is reflected in figure 5.10 and table 5.3 for assessment of flying handling quality. As the dynamic quality of the aircraft is closely related to its ability to fly, it is a difficult task for a flight control designer to create a controller with good dynamic properties (JAISWAL & PRAKASH, 2022) [ref]. When investigating pilot handling, the damping and frequency of both short- and long-term periods are crucial.

Lateral Stability

Aircraft Lateral stability also referred to as ‘roll stability’ is the tendency of an aircraft to attain a trim state about the longitudinal axis. Lateral Stability provides rolling motion by moving aircraft in forward and rearward directions. Ailerons are control surfaces that contribute lateral motion of an aircraft.

Directional Stability

The synonym term ‘Yaw stability’ is the tendency of an aircraft to attain a trim state about the normal axis. Directional Stability provides yawing motion by moving aircraft in the left and right directions. Rudders are control surfaces that contribute directional motion of an aircraft.

Lateral- Directional modes of motion:

Spiral divergence

It is a phenomenon that occurs when an aircraft is directionally stable but laterally unstable. This instability produces spiralling motion have characteristics of slowly convergent and divergent states. This spiral is sometimes difficult to handle if preventive measures are not taken at the right time by the pilot.

Dutch-roll mode

It is a coupled phenomenon of lateral-directional motion that combines the characteristics of rolling, yawing, and side-slipping. The lightly damped oscillations have low frequency with a period of 3-15sec. Iceskater is the perfect example to resemble its features.

Rolling mode

Directional divergence is a synonym for roll mode. This motion has characteristics of high convergence with low frequency. An ever-increasing sideslip angle should be avoided if disturbed from equilibrium. This instability mode is avoided by designing a proper vertical tail surface.

5.3 LONGITUDINAL EQUATION IN WIND AXIS

Derivation to establish state-space linearized longitudinal perturbation equation to estimate the aircraft transfer function(Klien & Morelli, 2006) (Jaiswal et al., 2020)

Aircraft sensors like pitot tube measure airspeed V rather than body-axes velocities u , v , and w . In the same manner, sensors attached in aircraft measure the angle of attack, and sideslip angle thus it is identified that non-dimensional aerodynamic coefficients are characterized as α, β, V having a relationship as:

$$\alpha = \tan^{-1} \frac{w}{u} \quad 5.24$$

$$\beta = \sin^{-1} \frac{v}{V} \quad 5.25$$

Where airspeed is denoted as $V = \sqrt{u^2 + v^2 + w^2}$

$$v = V \sin \beta \quad 5.26$$

$$w = V \sin \alpha \cos \beta \quad 5.27$$



Fig 5.11 Estimation of Variables α, β, V from Wind-axis

Referring to the figure 5.11 in terms of α, β, V as

$$u = V \cos \alpha \cos \beta \quad 5.28$$

Differentiating equation, a and b to get a simplified equation as (Klien & Morelli, 2006):

$$\dot{V} = \frac{1}{V} (u\dot{u} + v\dot{v} + w\dot{w}) \quad 5.29$$

$$\dot{\alpha} = \left(\frac{u\dot{w} - w\dot{u}}{u^2 + w^2} \right) \quad 5.30$$

$$\dot{\beta} = \frac{(u^2 + w^2)\dot{v} - v(u\dot{u} + w\dot{w})}{V^2 \sqrt{u^2 + w^2}} \quad 5.31$$

Rewriting longitudinal force equation in wind axes by substituting values of $\dot{u}, \dot{v}, \dot{w}$ from Appendix C 5.55- 5.57 and u, v, w from the above equations into above 5.29-5.31 to get expression in terms of α, β, V

$$\dot{V} = - \left\{ \frac{\bar{q} \cdot s}{m} \right\} C_D + g (\cos\phi \cos\theta \sin\alpha \cos\beta + \sin\phi \cos\theta \sin\beta - \sin\theta \cos\alpha \cos\beta) + \left\{ \frac{T}{m} \right\} \cos\alpha \cos\beta \quad 5.32$$

$$\dot{\alpha} = - \left\{ \frac{\bar{q} \cdot s}{m \cdot V \cos\beta} \right\} C_L + q + \frac{g}{V \cos\beta} (\cos\phi \cos\theta \cos\alpha + \sin\theta \sin\alpha) - \left\{ \frac{T}{m \cdot V \cos\beta} \right\} \sin\alpha - \tan\beta (p \cos\alpha + r \sin\alpha) \quad 5.33$$

Assuming $\beta=\phi=0$ for longitudinal motion and using trigonometric identities Sin(A-B), and Cos(A-B) as:

Force Equation(Klien & Morelli, 2006)

$$\dot{V} = - \left\{ \frac{\bar{q} \cdot s}{m} \right\} C_D + g \sin(\alpha - \theta) + \left\{ \frac{T}{m} \right\} \cos\alpha \quad 5.34$$

$$\dot{\alpha} = - \left\{ \frac{\bar{q} \cdot s}{m \cdot v} \right\} C_L + q + \frac{g}{v} \cos(\alpha - \theta) - \left\{ \frac{T}{m \cdot v} \right\} \sin\alpha \quad 5.35$$

$$\dot{\theta} = q \quad 5.36$$

Moment Equation(Klien & Morelli, 2006)

$$\dot{q} = \left(\frac{\bar{q} \cdot s \cdot c}{I_y} \right) \cdot C_m + \left\{ \frac{T}{I_{yy}} \right\} l_{tz} \quad 5.37$$

To analyse the aircraft dynamics, the aircraft is modelled in terms of mathematical equations as aerodynamic stability and control derivatives shown below(Nelson, 1998)

$$C_L = \{ C_{L_0} + C_{L_\alpha} \cdot \alpha + C_{L_q} \cdot \frac{q \bar{c}}{2U_1} + C_{L_{\delta_e}} \cdot \delta_e \} \quad 5.38$$

$$C_D = \left\{ C_{D_0} + C_{D_\alpha} \cdot \alpha + C_{D_q} \cdot \frac{q\bar{c}}{2U_1} + C_{D_{\delta_e}} \cdot \delta_e \right\} \quad 5.39$$

$$C_m = \left\{ C_{m_0} + C_{m_\alpha} \cdot \alpha + C_{m_q} \cdot \frac{q\bar{c}}{2U_1} + C_{m_{\delta_e}} \cdot \delta_e \right\} \quad 5.40$$

Assumption: thrust setting angle = 0, Flight path $\gamma = \text{constant}$ at cruise state, flight velocity = constant for short period mode

$$\dot{\alpha} = - \left\{ \frac{\bar{q} \cdot S}{m \cdot v} \right\} C_L + q \quad 5.41$$

$$\dot{\theta} = q \quad 5.42$$

$$\dot{q} = \left(\frac{\bar{q} \cdot S \cdot c}{I_y} \right) \cdot C_m \quad 5.43$$

Simplifying set of equations

$$\dot{\alpha} = q - \frac{\rho V S_w}{2m} \left\{ C_{L_0} + C_{L_\alpha} \cdot \alpha + C_{L_q} \cdot \frac{q\bar{c}}{2U_1} + C_{L_{\delta_e}} \cdot \delta_e \right\} \quad 5.44$$

$$\dot{\theta} = q \quad 5.45$$

$$\dot{q} = \frac{\rho V^2 S_w \bar{c}}{2I_y} \left\{ C_{m_0} + C_{m_\alpha} \cdot \alpha + C_{m_q} \cdot \frac{q\bar{c}}{2U_1} + C_{m_{\delta_e}} \cdot \delta_e \right\} \quad 5.46$$

Substituting values of S_w , \bar{c} , V , ρ , I_y & m from Table 5

$$\dot{\alpha} = q - \frac{0.96 \times 36 \times 12.47}{2 \times 750} \left[C_{L_0} + C_{L_\alpha} \cdot \alpha + C_{L_q} \cdot \frac{q(1.211)}{2 \times 36} + C_{L_{\delta_e}} \cdot \delta_e \right]$$

$$\dot{\theta} = q$$

$$\dot{q} = \frac{0.96 \times (36)^2 \times 12.47 \times 1.21}{2 \times 907} \left\{ C_{m_0} + C_{m_\alpha} \cdot \alpha + C_{m_q} \cdot \frac{q(1.211)}{2 \times 36} + C_{m_{\delta_e}} \cdot \delta_e \right\}$$

Substituting values of derivatives of S & C from ML method using multistep HALM5 Input (Refer Chapter 4, Table 4.3)

$$\dot{\alpha} = q - 0.0646 - 1.851 \cdot \alpha - 0.1793 \cdot q + 0.00562 \cdot \delta_e$$

$$\dot{\theta} = q$$

$$\dot{q} = 0.806 - 4.403 \cdot \alpha - 2.01 \cdot q - 8.95 \cdot \delta_e$$

Solving equation:

$$\dot{\alpha} = 0.8207 \cdot q - 1.851 \cdot \alpha + 0.00562 \cdot \delta_e - 0.0646 \quad 5.47$$

$$\dot{q} = -2.01 \cdot q - 4.403 \cdot \alpha - 8.95 \cdot \delta_e + 0.806 \quad 5.48$$

$$\dot{\theta} = q \quad 5.49$$

Generalized State equation in Matrix form may be written:

$$\dot{x} = A x + B u \quad 5.50$$

$$y = C x + D u \quad 5.51$$

To define A(plant matrix), B(control matrix), C(output matrix), and D(null matrix) as they are reflected in the above equation are compared with state space matrix form as A, B, C,& D.

$$\begin{bmatrix} \dot{\alpha} \\ \dot{q} \\ \dot{\theta} \end{bmatrix} = \begin{bmatrix} -1.851 & 0.8207 & 0 \\ -4.403 & -2.01 & 0 \\ 0 & 1 & 0 \end{bmatrix} \begin{bmatrix} \alpha \\ q \\ \theta \end{bmatrix} + \begin{bmatrix} -0.0056 & -8.95 \\ -0.0646 & -0.806 \\ 0 & 0 \end{bmatrix} [\delta] \quad 5.52$$

$$[\theta] = [0 \quad 0 \quad 1] \begin{bmatrix} \alpha \\ q \\ \theta \end{bmatrix} + [0][\delta] \quad 5.53$$

The transfer function is required to construct a PID Controller. The transfer function of short period mode can be represented by using the formulae discussed below

$$\text{T.F} = \left| \frac{C \text{ Adj}(Is-A)B}{Is-A} \right| + D$$

The following is a representation of the transfer function for the elevator deflection angle from the pitch angle: $G(s)$

$$G(s) = \frac{\theta(s)}{\delta(s)} = \frac{-\{8.95s+16.5313\}}{s^3+3.861s^2+7.33141s} \quad 5.54$$

Open loop Transfer function

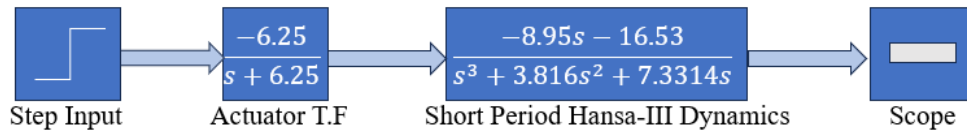


Fig.5.12 Open Loop Control system of Hansa-III

The Open loop CS as illustrated in Fig.5.12 is independent of response in an action of control. The following is a representation of the estimated transfer function for the pitch angle to the elevator deflection angle $G3(s)$

$$G3(s) = \frac{\theta(s)}{\delta(s)} = \frac{-\{8.95s+16.5313\}}{s^3+3.861s^2+7.33141s} \quad 5.55$$

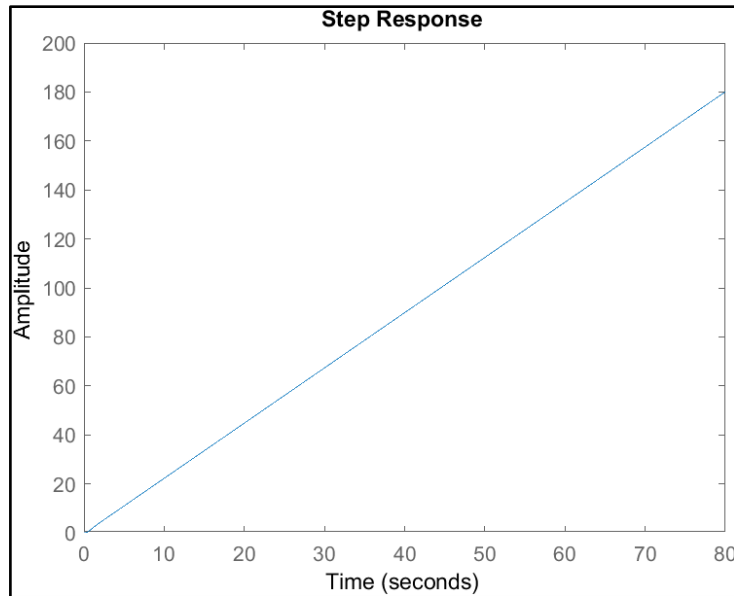


Fig.5.13 Open Loop Step Response of Hansa-III

The amplitude of the step response as displayed in Figure 5.13 of Open-loop CS is undamped which justifies to design of the controller in Closed-loop.

Closed loop Transfer function

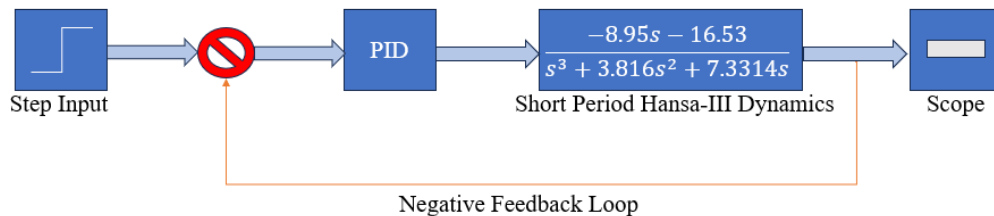


Fig. 5.14 Closed Loop Control system of Hansa-III

The controller of closed-loop CS displayed in Fig 5.14 depends on the output response termed feedback control system. The transfer function $G4(s)$ is the output response of the input fed to the control system

$$G4(s) = \frac{\theta(s)}{\delta(s)} = \frac{\{55.94s+103.3\}}{s^4+10.07s^3+31.18+101.8s+103.3} \quad 5.56$$

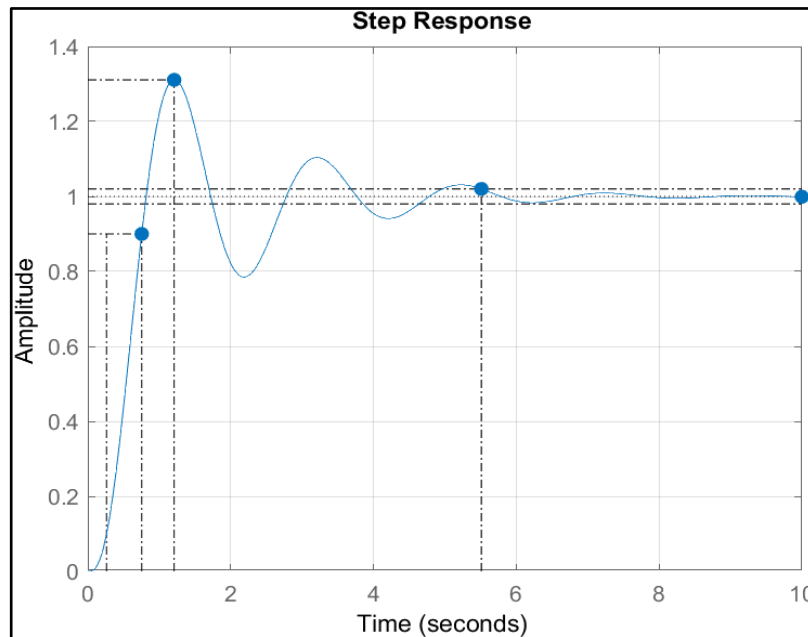


Fig. 5.15 Closed-loop Step- response of Hansa-III

The amplitude of the step response as displayed in Figure 5.15 of Closed-loop CS is damped and does not satisfy design requirements.

5.4 PID TUNING METHODS

PID Controller

PID stands for proportional, Integral, and derivative. This controller boosts the system's stability and reduces steady-state error. It is used in modern industry as an automatic process control for the flight control system. The three terms P, I, and D effectively control the system dynamics by calculating the error between the measured value and the desired value. The gain of these three parameters is tuned as per the system design requirements. The feedback control system uses a PID controller to precisely regulate the intended output. (Nelson, 1989)

$$u(t) = K_P e(t) + K_I \int e(t)dt + K_D \frac{d}{dt}e(t) \quad 5.57$$

Taking Laplace transformation of the above equation and reducing it to

$$U(s) = [K_P + \frac{K_I}{s} + K_D s] E(s) \quad 5.58$$

The transfer function of the PID Controller $G_{PID} = \frac{U(s)}{E(s)} = K_P + \frac{K_I}{s} + K_D s$
 $= [\frac{K_P s + K_I + K_D s^2}{s}]$

PID tuning methods are used to compare the performance characteristics of the controller. Based on the control system response in terms of settling time, steady state error, percent overshoot, gain value and rise time the desirable methodology is adopted. These methods are listed into two categories

1. Closed Loop Tuning Method

Closed-loop tuning methods are used when the control system is run in a closed loop and the controller is tuned automatically. Some closed-loop methods are: Ziegler Nicholas (ZN), Modified Ziegler Nicholas(MZN), Tyreus – Luyben(TL), Astrom – Hagglund (AH) (Mohammad Shahrokhi and Alireza Zomorodi, 2005)

2. Open Loop Tuning Method

Open-loop tuning technique is used when the control system is run in an open loop and the controller is tuned manually. Open-loop Ziegler Nicholas, CHR, Cohen and Coon, and Fertik are a few examples of open-loop techniques. (Mohammad Shahrokhi and Alireza Zomorodi, 2005)

5.4.1 CLOSED LOOP TECHNIQUES

1. Ziegler Nicholas

This trial and error technique was first put forward by Ziegler and Nicholas in 1942 for tuning gains of the PID Controllers. This approach was also used to tune PID Controller of a quadrotor helicopter for attitude determination(He & Zhao, 2014). Both open-loop and closed-loop control systems can make use of it and apply it

when the mathematical model is unavailable(V. Kumar & Patra, 2016). This method determines gain by considering two parameters such as ultimate gain (K_u) and (T_u) as the period of oscillation at K_u . Process modelling is not required for this technique. Some consequences of ZN are time-consuming due to several iterations while estimating ultimate gain, and in-applicability for an open-loop unstable process. This tuning technique shows smooth transient behaviour. The block diagram shown in Figure 5.16 is used to estimate the gain parameters of PID while adopting various tuning techniques discussed in Table 5.4 using the software SIMULINK and algorithm (refer Appendix B 1). The steps followed to determine the value of K_u and T_u is stated below:

Step 1. Initializing K_I and K_D to be zero and the iterating numeric value of K_P to attain marginal stability curve in Scope

Step 2. Estimating the value of K_u and T_u from neutrally stable curve as displayed in the figure 5.17 (1-2)

Step 3. The gain of K_p becomes K_u when the system achieves neutral oscillation and T_u reflects the time- period of oscillations between one cycle occurring at an ultimate gain.

Step 4. The gain value for this research study is estimated are $K_u = 1.3400$, $T_u(s) = 1.5040$ s

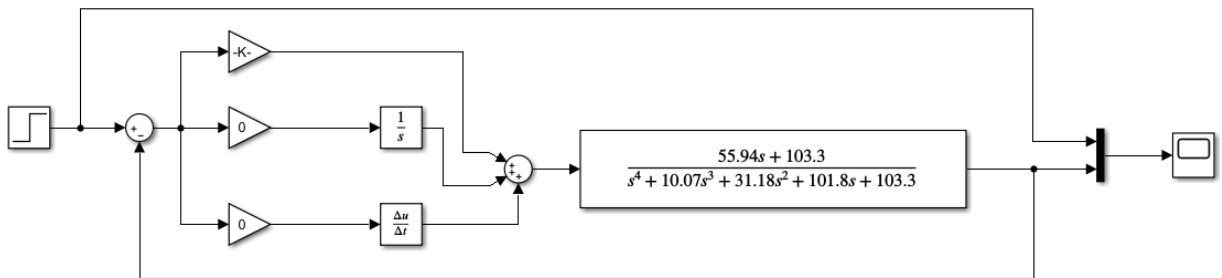
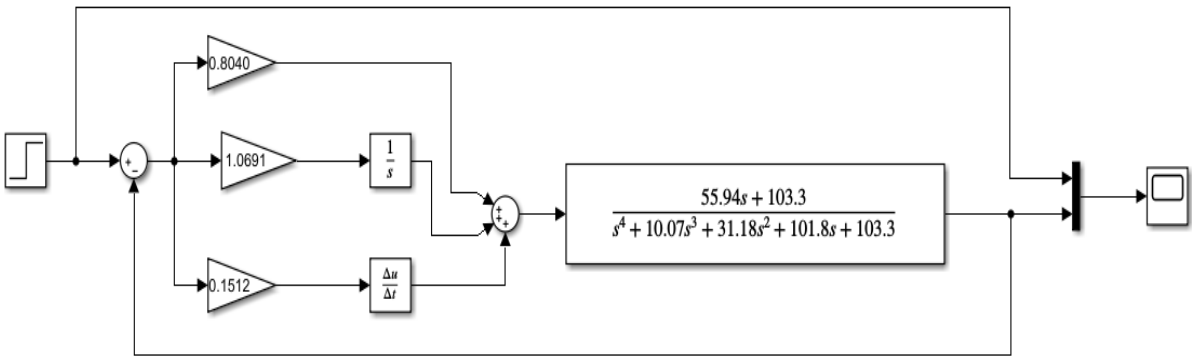
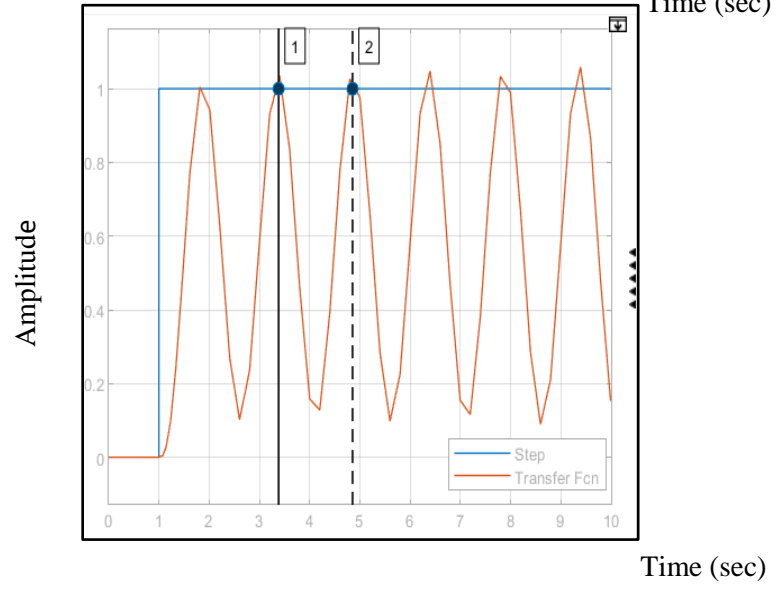
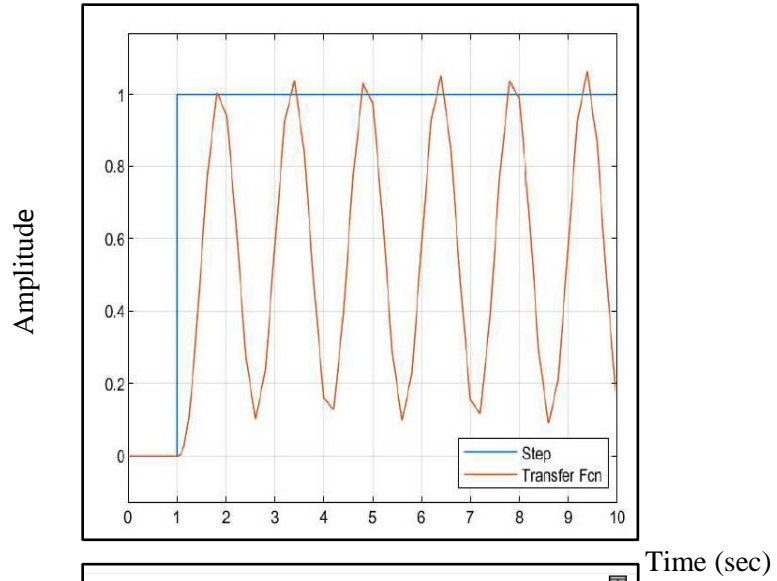


Fig 5.16 Simulink block diagram of estimating K_u and T_u



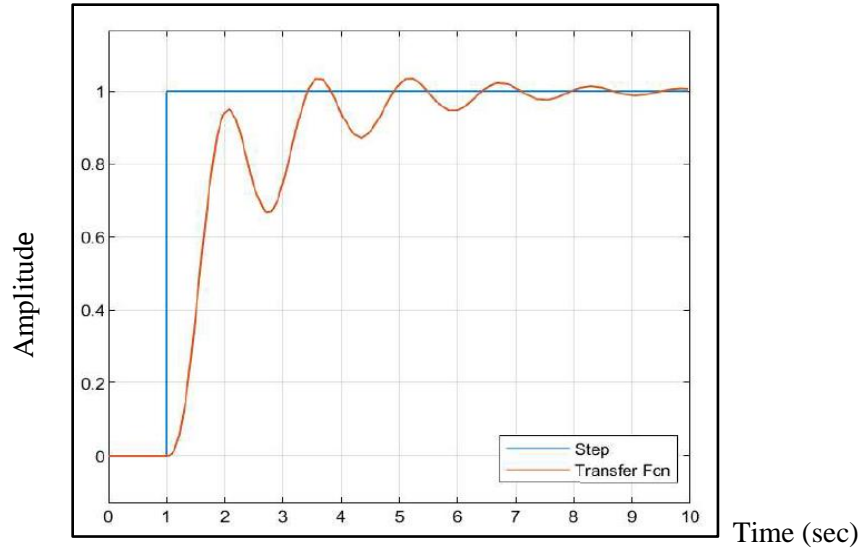


Fig 5.17(1-4) Estimation of K_u , T_u , Step response and Simulink Block diagram of PID Controller: ZN

The step response in Fig 5.17(1-4) shows decayed oscillatory motion having damped amplitude signifies the stability of the pitch controller.

SNo	Methods	K_P	K_I	K_D
1.	PID	$0.6K_u$	$(0.6K_u)\left(\frac{2}{T_u}\right)$	$(0.6K_u)(T_u/8)$
2.	PD	$0.8K_u$	-	$0.1 * K_u * T_u$
3.	PI	$0.45K_u$	$(0.45K_u)\left(\frac{1}{0.83T_u}\right)$	-

Table 5.4 Classical PID Tuning Parameters: ZN(Deepa & Sudha, 2016)

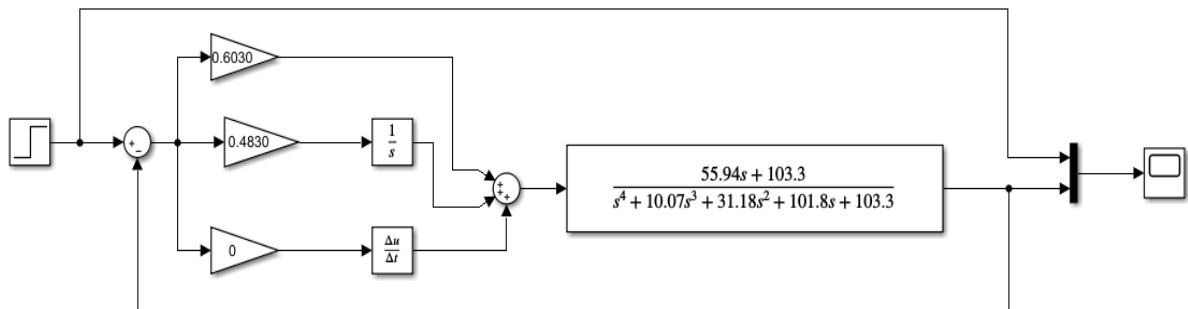


Fig 5.18 Simulink block diagram of PI Controller: ZN

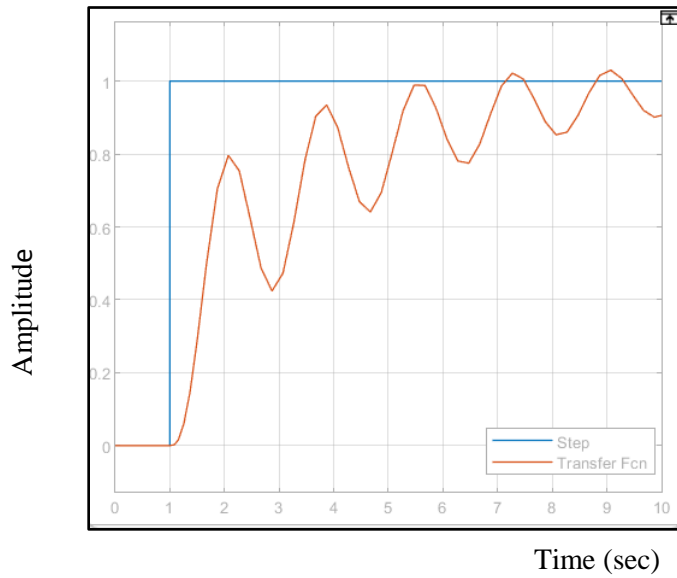


Fig 5.19 Step response of aircraft dynamics with PI Controller: ZN

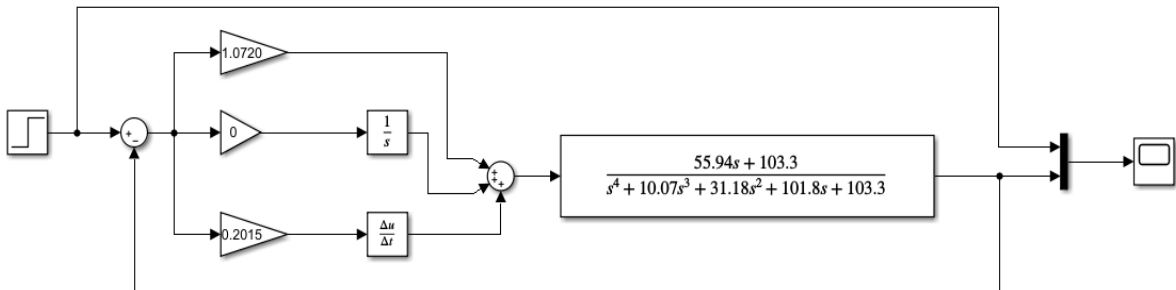


Fig 5.20 Simulink block diagram of PD Controller

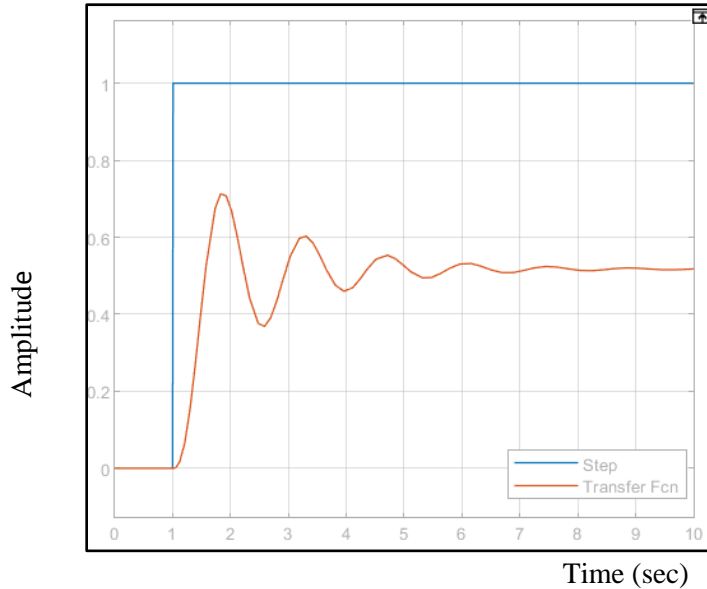


Fig 5.21 Step response of aircraft dynamics with PD Controller

S.No	Controller	K_P	K_I	K_D
1.	Classic PID	0.8040	1.0691	0.1512
2.	PD	0.2015	-	1.0720
3.	PI	0.6030	48.117	-

Table 5.5 Classical PID, PD, PI Tuning Parameters Value: ZN

The gain parameters of PID, PD and PI while adopting ZN are discussed in Table 5.5 using Table 5.4 to illustrate the type of controller such as PID, PI, and PD have high K_I gain value that affects overall system performance &

The gain parameters of PID presented in Table 6 illustrate that all types of controller have high value of K_I which overall affects the system performance and leads to a responsive steady-state system.

2. Modified Ziegler Nicholas

This method is utilised when it is difficult to quantify oscillation caused by a 1/4 decay ratio for some loops' and when set point changes for significant overshoots cannot be measured properly. This tuning technique shows smooth transient behaviour. The gain values k_P, k_I, k_D using modified Ziegler Nicholas setting is shown below (Basu et al., 2016) (Deepa & Sudha, 2016). The step response

illustrating aircraft dynamics are shown in Fig 5.22 using an algorithm (refer to Appendix B2)

SNo	Methods	K_P	K_I	K_D
1.	PID	$00.33K_u$	$0.5T_u$	$0.33T_u$
		0.4422	0.7520	0.4963

Table 5.6 Classical PID Tuning Parameters: MZN

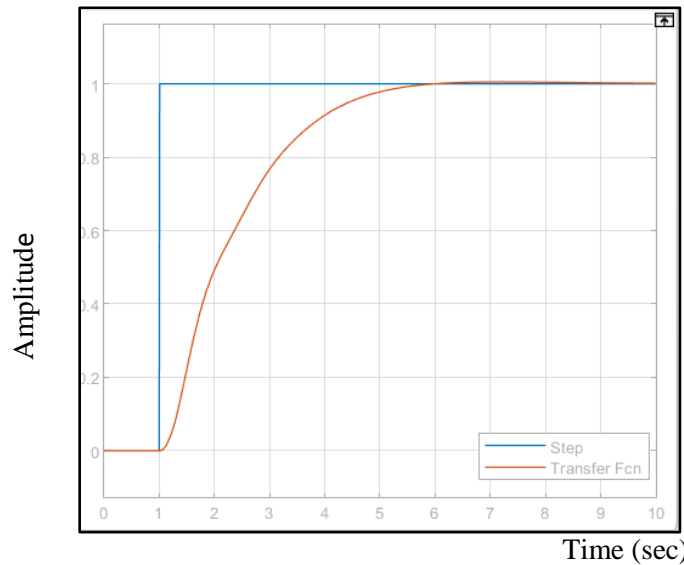
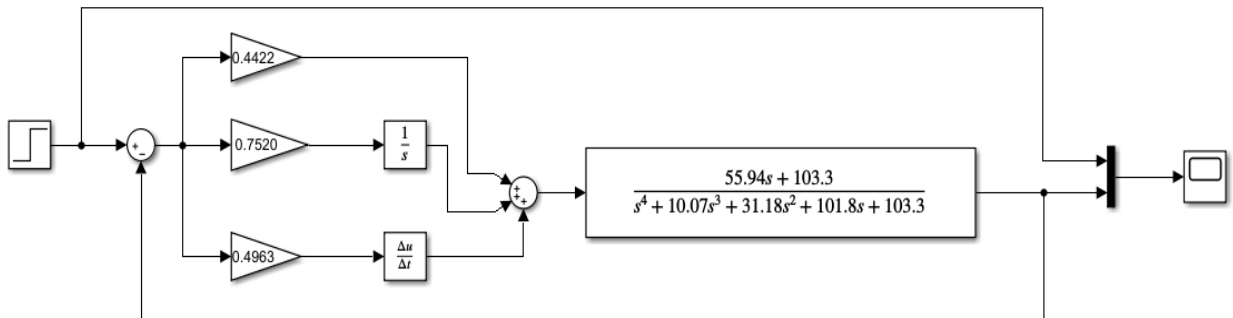


Fig 5.22 Step response and Simulink Block diagram of PID Controller using MZN

Figure 5.22-unit step response depicts an aperiodic, non-oscillatory motion of the pitch controller that is both highly stable and responsive in steady state.

3. Tyreus Luyben

This technique is similar to Ziegler Nicholas and operates for PID and PI Controllers. The gain values k_p, k_I, k_D is different for this controller setting and mentioned below. It is time-consuming and attains marginal stability. This tuning technique shows smooth transient behaviour. The two characteristics of ultimate gain and the time-period is calculated using the same procedure as discussed in Ziegler Nicholas (Basu et al., 2016)(Deepa & Sudha, 2016). The step response illustrating aircraft dynamics is shown in Fig. 5.25 using algorithm (refer to Appendix B3)

S No	Methods	K_P	K_I	K_D
1.	PID	$K_u/3.2$	$(2.2T_u)$	$T_u/6.3$
2.	PI	$K_u/3.2$	$(2.2T_u)$	—

Table 5.7 Classical PID Tuning Parameters: TL

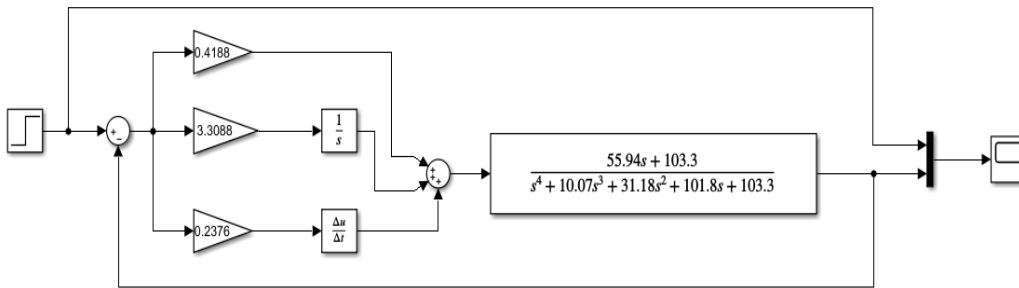


Fig 5.23 Simulink Block diagram of PID Controller using TL

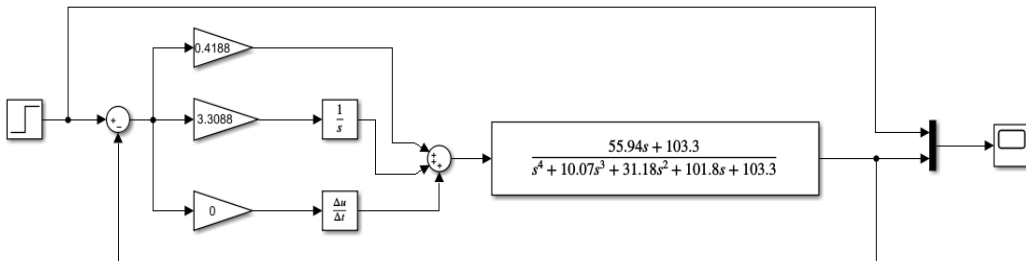


Fig 5.24 Simulink Block diagram of PI Controller using TL

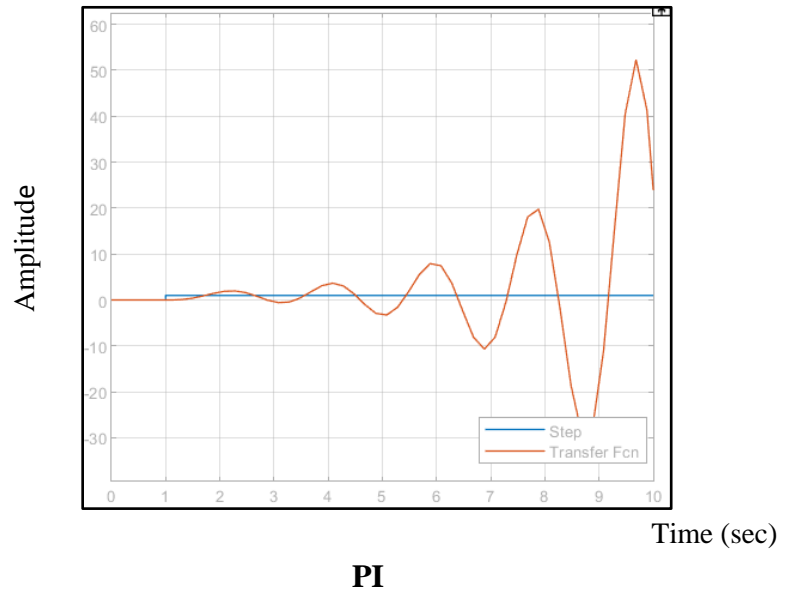
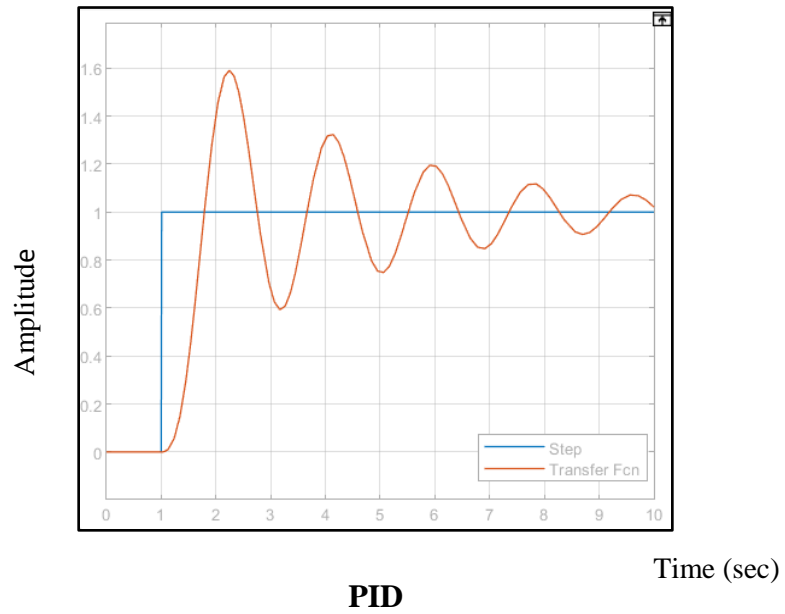


Fig 5.25 Step response of PID and PI Controller using TL

S.No	Methods	K_P	K_I	K_D
1.	PID	0.4188	0.2376	3.3088
2.	PI	0.4188	3.3088	0

Table 5.8 Classical PID, PI Tuning Parameters Value: TL

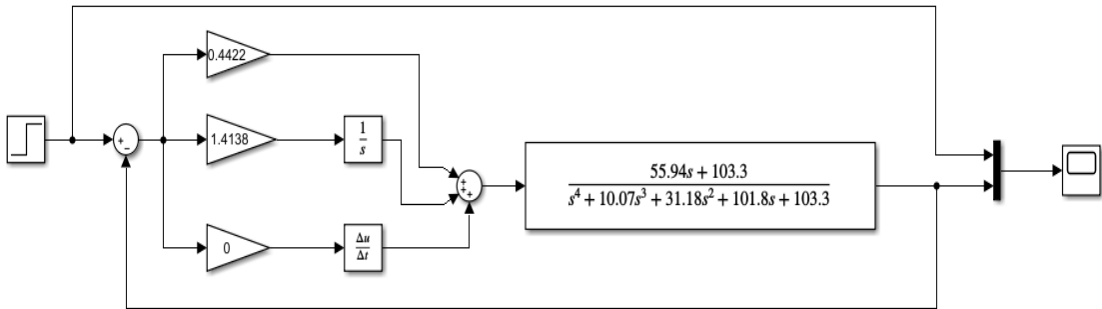
As discussed in Table 5.8, the unit step response in Fig. 12 illustrates an oscillatory motion of the pitch controller with a high amount of proportional gain, which causes the entire system to create constant steady state error and system sensitivity is reduced.

4. Astrum-Haglund

This technique is initiated by Astrum-Haglund and uses non-linear feedback. The gain values k_P, k_I, k_D is different for this controller setting and are mentioned below. The two characteristics such as ultimate gain and the Time-period are calculated from limit cycle oscillation. This tuning technique shows oscillatory transient behaviour and does not involve a derivative filter (Basu et al., 2016)(Deepa & Sudha, 2016). The step response illustrating aircraft dynamics is shown in Fig 5.26 using an algorithm (Refer to Appendix B4)

S.No	K_P	K_I	K_D
1.	$0.32K_{pu}$	$0.94T_u$	0
2.	0.4422	1.4138	0

Table 5.9 Classical PID Tuning Parameters: AH



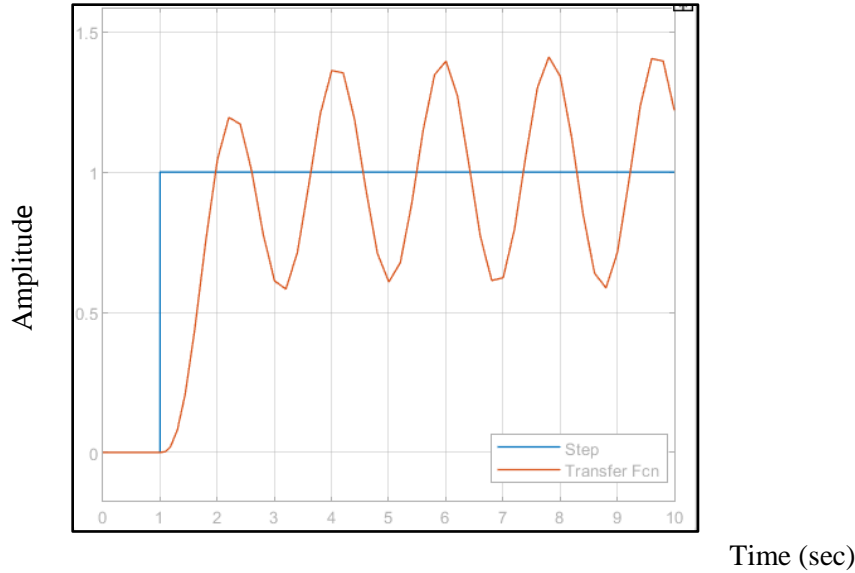


Fig 5.26 Step response and Simulink Block diagram of PID Controller: AH

The oscillatory motion in Fig.5.26 with the un-damped amplitude of the pitch controller indicates system instability in the unit step response. Table 5.9's PID gain parameters provide as an excellent example of steady-state performance.

In a similar pattern, all PID Closed-loop tuning approaches are applied to Multistep, Doublet, and Pulse Input datasets for gain optimization and results are compared using tabular and graphical representation in Appendix D1, D2.

5.4.2 OPEN-LOOP TECHNIQUE

1. Open-loop Ziegler Nicholas

This method is similar to Ziegler Nicholas but the dynamics of the plant are modelled by the dead time model plus the first-order model given by expression (Basu et al., 2016)

$$G_m(s) = \frac{k_m e^{-ds}}{\Omega_m s + 1} \quad 5.59$$

Where Ω_m is dead time model, and k_m is the model gain. The gain parameters k_P, k_I, k_D is obtained by using Table 5.10

SNo	Methods	K_P	K_I	K_D
1.	PID	$\frac{1.2 \Omega_{pn}}{k_m d}$	$2d$	$0.5d$
2.	P	$\frac{1 \Omega_m}{k_m d}$	-	-
3.	PI	$\frac{0.9 \Omega_m}{k_m d}$	$\frac{d}{0.3}$	-

Table 5.10 Classical PID Tuning Parameters: Open-loop ZN (Mohammad Shahrokhi and Alireza Zomorodi, 2005)

2. CHR Method

With the 20% overshoot and no overshoot options offered by this CHR (Chien, Hrones, and Reswch) technique provides the fastest response. This methodology is a modification of the Open-loop ZN technique (Mohammad Shahrokhi and Alireza Zomorodi, 2005) (Ahn et al., 2009). The parameters obtained using the dead time model plus the first-order model are shown in Table 5.11

SNo	Methods	K_P	K_I	K_D
1.	PID	$\frac{0.95 \Omega_m}{k_m d}$	$2.4d$	$0.42d$
2.	P	$\frac{0.3 \Omega_m}{k_m d}$	-	-
3.	PI	$\frac{0.6 \Omega_m}{k_m d}$	$4d$	-

Table 5.11 Classical PID Tuning Parameters : CHR (Mohammad Shahrokhi and Alireza Zomorodi, 2005)

3. Cohen-coon Method

This technique involves process reaction curve as the first step and secondly estimating parameters by approximating the dead time model plus first-order model using the following relationship [ref] (Mohammad Shahrokhi and Alireza Zomorodi, 2005)

$$\Omega_m = \frac{3}{2} (t_2 - t_1) \quad 5.60$$

$$d_m = \Omega_2 - \Omega_m \quad 5.61$$

Where t_1, t_2 = time at $\Delta c = 0.283\Delta c_s$, $\Delta c = 0.632\Delta c_s$, and C is plant output.

Once Ω_m, d_m , and k_m is known then tuning parameters are estimated using the dead time model plus the first order model is shown in Table 5.12

SNo	Methods	K_P	K_I	K_D
1.	PID	$\frac{1}{k_m} \frac{\Omega_m}{d} \left(\frac{4}{3} + \frac{d}{4\Omega_m} \right)$	$d \frac{32 + 6d/\Omega_m}{13 + 8d/\Omega_m}$	$d \frac{4}{11 + 2d/\Omega_m}$
2.	P	$\frac{1}{k_m} \frac{\Omega_m}{d} \left(1 + \frac{d}{3\Omega_m} \right)$	-	-
3.	PI	$\frac{1}{k_m} \frac{\Omega_m}{d} \left(\frac{9}{10} + \frac{d}{12\Omega_m} \right)$	$d \frac{30 + 3dm/\Omega_m}{9 + 20dm/\Omega_m}$	-
4.	PD	$\frac{1}{k_m} \frac{\Omega_m}{d} \left(\frac{5}{4} + \frac{d}{6\Omega_m} \right)$		$d \frac{6 - 2d/\Omega_m}{22 + 3d/\Omega_m}$

Table 5.12 Classical PID Tuning Parameters: Cohen - Coon (Mohammad Shahrokhi and Alireza Zomorodi, 2005)

4. Fertick Method

This technique is used in open-loop and uses the dead time model plus first-order model for the model using expression

$$G_m(s) = \frac{ke^{-ds}}{\Omega s + 1} \quad 5.62$$

$$\alpha_F = \frac{d}{d+\Omega} = \frac{T_d}{T_{ps}} \quad 5.63$$

Where α_F is fertick controllability, $T_d = d, T_{ps} = d + \Omega$. PID Controller is not applicable for plant whose $\alpha_F > 0.5$

5.5 CLASSICAL CONTROL APPROACH

Root Locus

The methodology to design flight control laws includes classical and modern control theory. In the past few decades, the FCS flight control system has been designed by making use of the root locus (Time- domain technique), or frequency domain technique. One of the best classical control techniques is the root locus introduced by W.R. Evan in 1948(Stojiljković et al., 2009) (Nelson, 1989). This methodology is simple, handy, and has system transparency as engineers can identify the gaps and modify them as per design requirements. It is also applied to design pitch attitude CS of F-104A aircraft(Stojiljković et al., 2009). The dynamics of the physical system are visible while operating. It is a graphical representation to analyse control systems. The necessary points to be noted while defining the stability of closed-loop systems are:

1. The closed-loop poles must be located in the left half of the complex plane.
2. The wider the gap of closed-loop poles from imaginary axes more system stability.

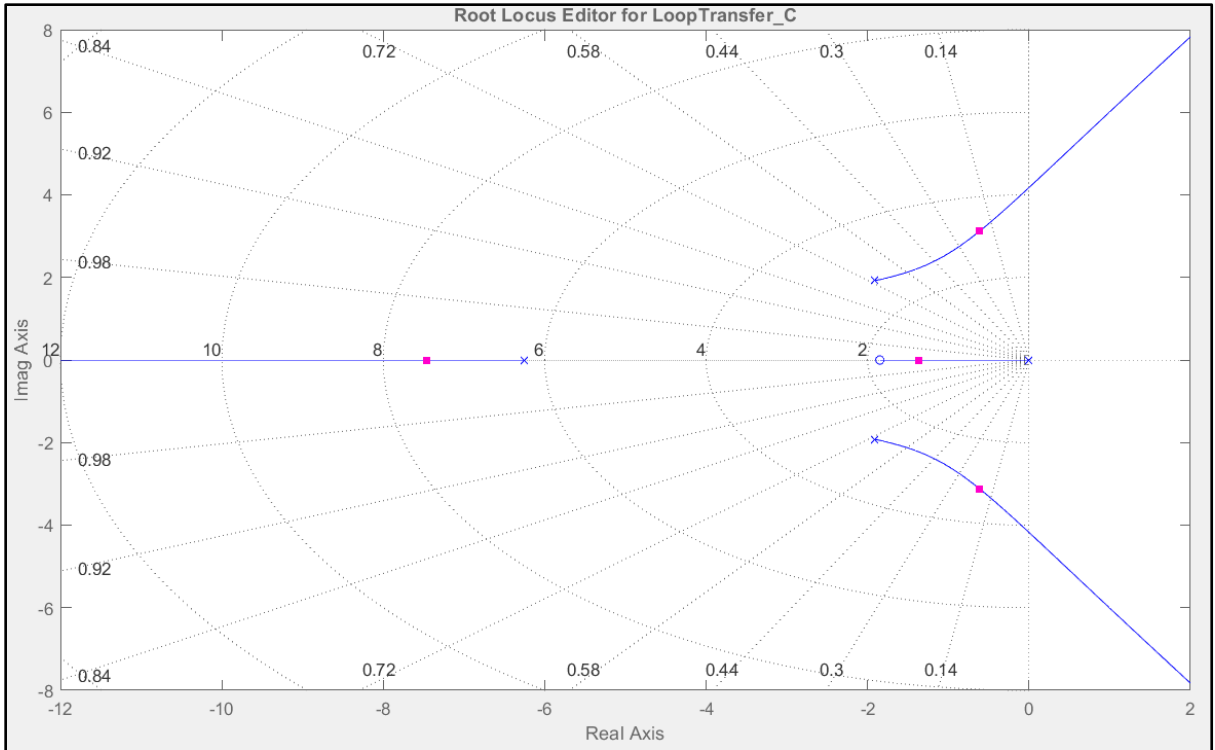


Fig 5.27 Root-Locus of Uncompensated Controller

As per the figure, the poles and zeroes lie at the left half of the complex plane which suggests the system stability is calculated using closed-loop TF G3

$$G3 = \frac{55.94s + 103.3}{s^4 + 10.07s^3 + 31.18s^2 + 45.82s}$$

Control system Toolbox is used to model, analyse, and design control systems in the time and frequency domain. The Root locus is viewed and the controller structure is manipulated in this toolbox. This toolbox is used to adjust the location of poles to attain desired system performance by varying system parameters in real-time. This technique also depicts system stability by having knowledge of pole location and estimating the natural frequency (w_n), and damping ratio (ζ) of the system. At a similar time, the bode plot, Nyquist plot, step response, gain, and phase margin are also viewed to modify the controller structure. Classical methods are limited to SISO systems while modern control theory has the scope of MIMO

system designs thus modern approaches are also covered in this study in the next section.

Bode Plot

This graphical method is introduced by the bode for stability analysis in the frequency domain. It contains two plots such as magnitude as well as phase plots which are plotted with logarithm values of frequency to give system information thus termed logarithm plots. Magnitude in decibels and phase angle in the degree of the LTI system are plotted for frequency.

Gain Margin: The gain at which the system stabilizes. It occurs at ω_{pc} (phase cross-over frequency) which is defined as frequency at -180° phase angle. If the magnitude in decibels of $G(j\omega)$ at ω_{pc} is positive then the gain margin will be negative and vice-versa. G.M= Gain at -180° phase.

Phase Margin: The phase angle at which the system becomes stable. It occurs at ω_{gc} (gain cross-over frequency) It is characterized as the frequency at zero decibel gain. If the phase in degrees ϕ_{gc} is positive than -180° then the phase margin will be negative and vice-versa.

$$P.M = 180^\circ + \text{Phase at } 0\text{db}$$

The stability criterion is determined by estimating the Gain Margin and phase margin from the Bode Plot. The system will be stable if the Gain Margin and Phase Margin are both bigger than zero.; If the gain margin is infinite and the phase never crosses -180° then too system attains stability.

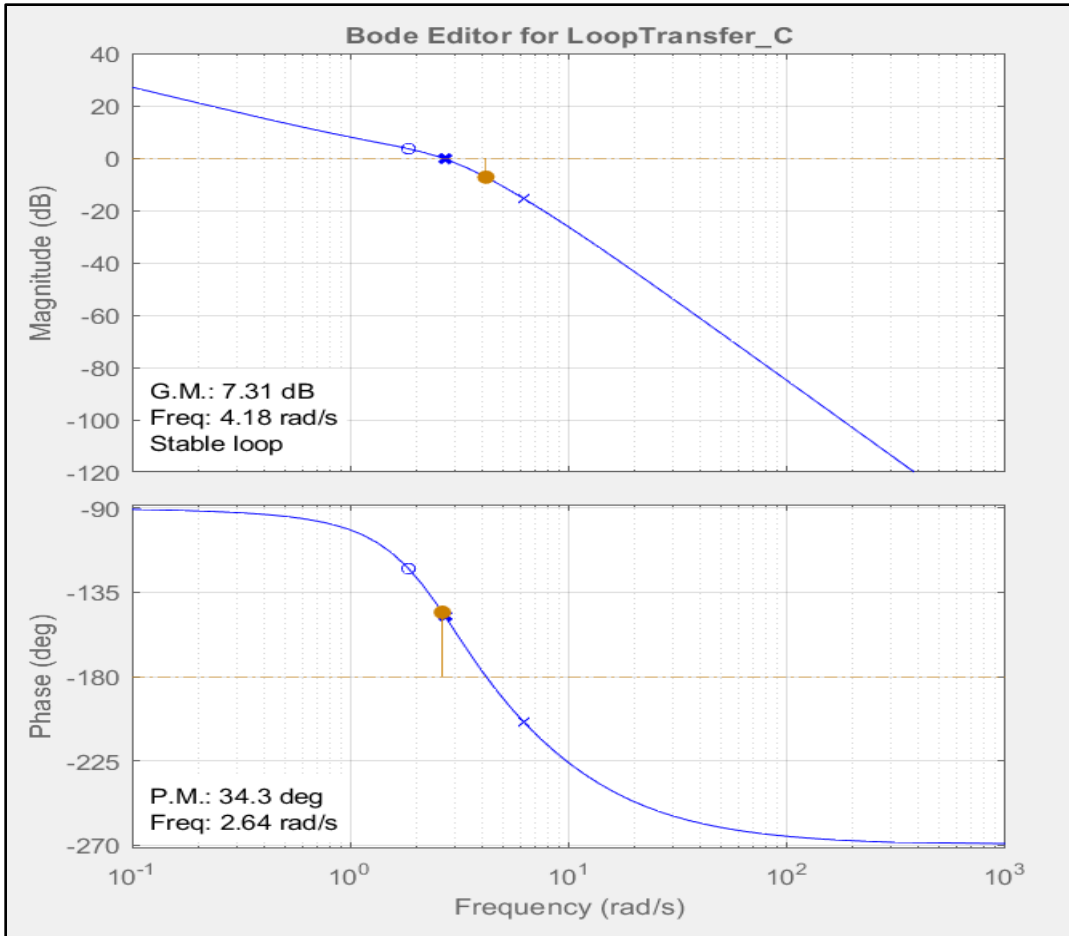


Fig 5.28 Bode-Plot of Uncompensated Controller

As per Figure 5.28, the value of the Gain margin and phase margin is positive which is calculated using closed-loop TF G_3 as discussed in the above section concludes the system stability.

5.5.1 PD COMPENSATED CONTROLLER USING ROOT LOCUS TECHNIQUE

Derivative Controller

This controller produces an output that is derivative of the error signal. This controller improves system stability

The transfer function of the derivative Controller $G_D = \frac{U(s)}{E(s)} = K_D s$

Integral Controller

The output of this controller is integral to the error signal. This will raise the system's type number which decreases steady state error but stability is decreased.

The transfer function of the Integral Controller $G_I = \frac{U(s)}{E(s)} = \frac{K_I}{s}$

PD Controller

PD stands for proportional, and derivative. The derivative filter is used for transient response analysis. The two terms proportional, and derivative effectively control the plant dynamics by producing output which is the combination of output P and D Controller. The system's stability will be improved by this combination without having an impact on steady-state error.

The transfer function of the PD Controller $G_{PD} = \frac{U(s)}{E(s)} = K_P + K_D s = K_P (1 + \frac{K_D}{K_P} s)$

where $\frac{K_D}{K_P}$ denotes T_D .

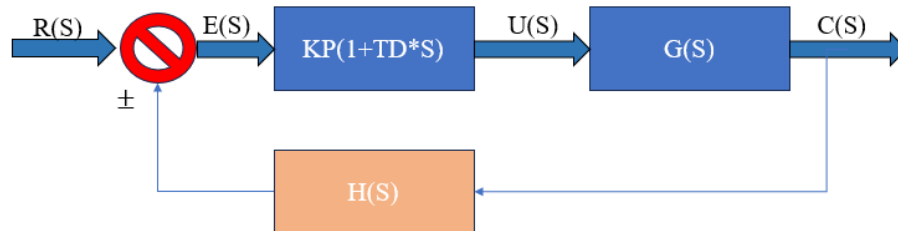


Fig 5.29 Schematic Diagram of PID Controller

METHODOLOGY

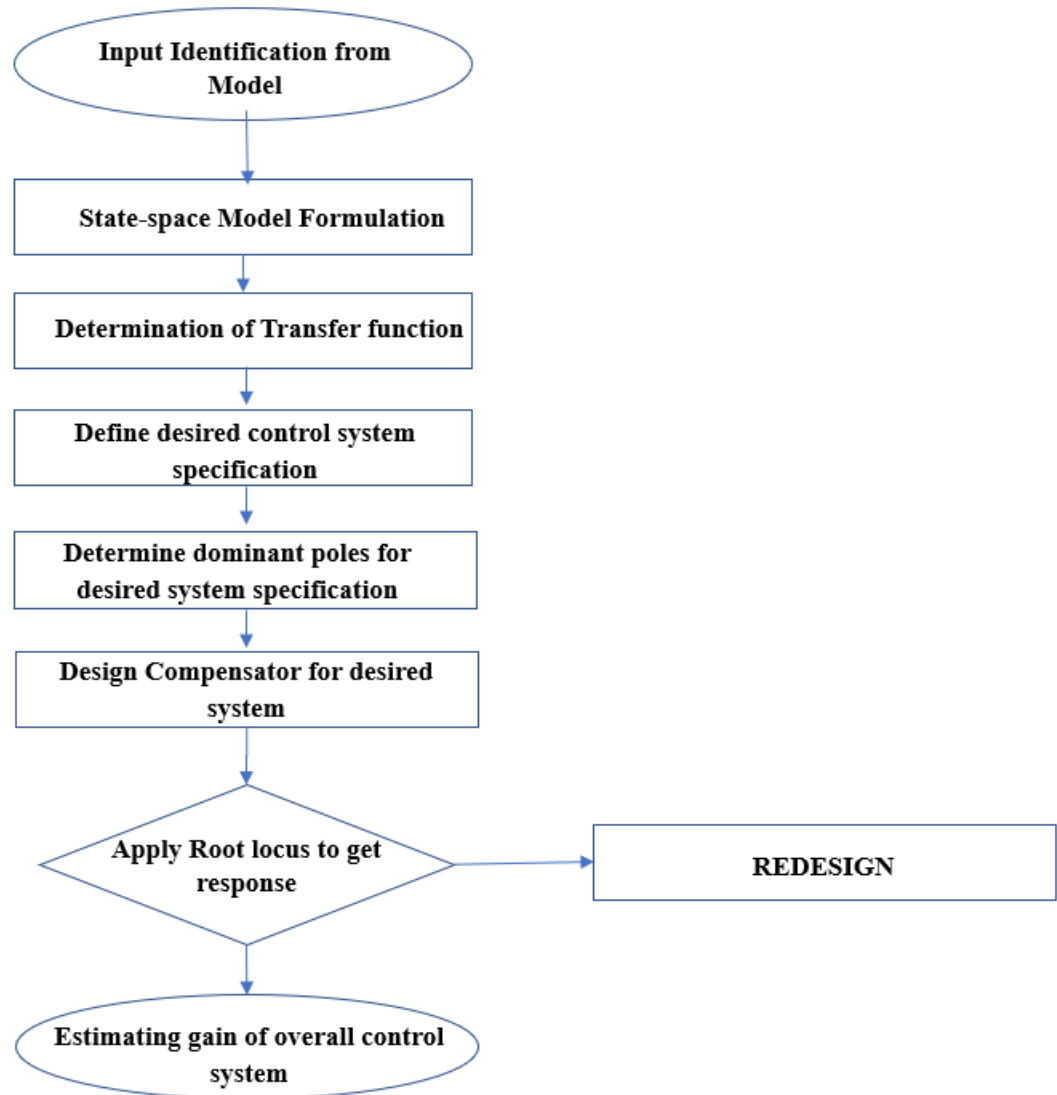


Fig 5.30 Flowchart to design aircraft Pitch Controller

Control System Design Specification

1. Settling Time < 10sec
2. Peak Overshoot < 20%
3. Steady State Error < 1%
4. Rise Time < 2sec
5. Gain Margin > 6Db

6. Phase Margin $>45^\circ$

5.5.2 UNCOMPENSATED FEEDBACK CONTROL SYSTEM

STEP1: Dynamics of an uncompensated feedback control system are analysed in MATLAB using the control system toolbox. The architecture used while designing the compensator is reflected in Fig 5.31

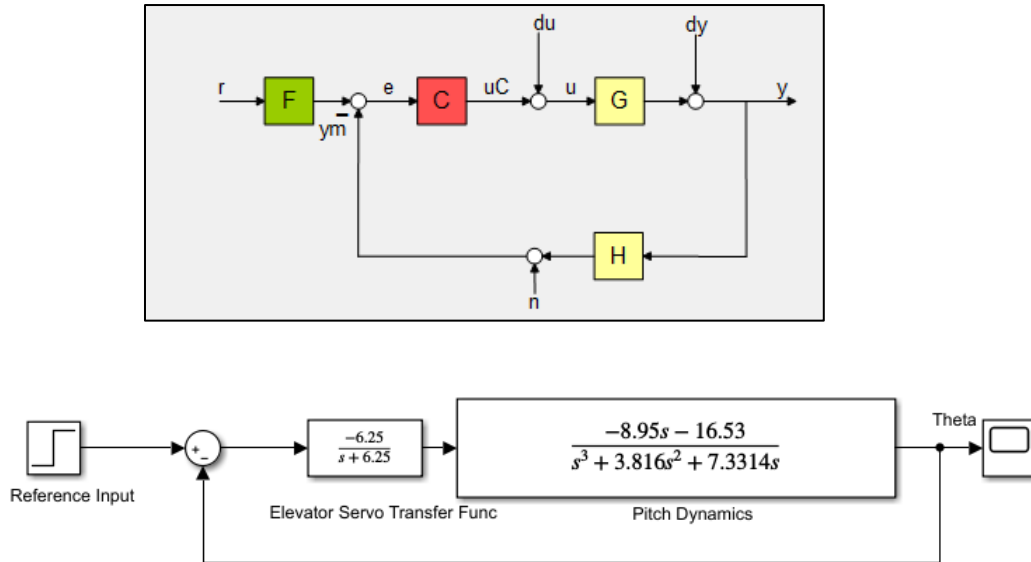


Fig 5.31 Uncompensated Feedback Control System

The uncompensated feedback control system includes elevator servomotor, Hansa-III pitch dynamics, reference input signal, and scope

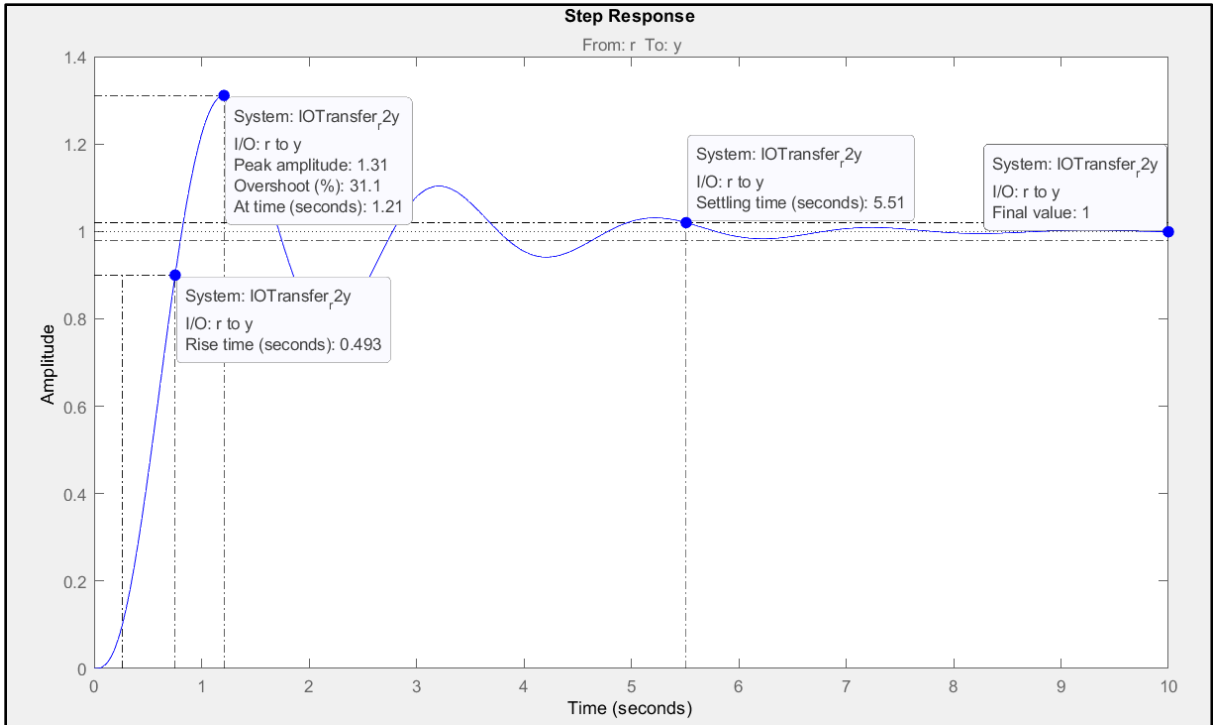


Fig 5.32 Step- Response of Uncompensated Feedback Control System

The uncompensated controller's step response as shown in above figure 5.32 explains the damping of the uncompensated pitch attitude system overshoots with 31.1% of amplitude 1.31. (It is required to drop down the value of overshoot by 20% as per design requirements). The oscillations damped gradually with the settling time of 5.51 seconds and experienced zero steady-state error which illustrates that the Integral controller is not required so a PD controller is designed.

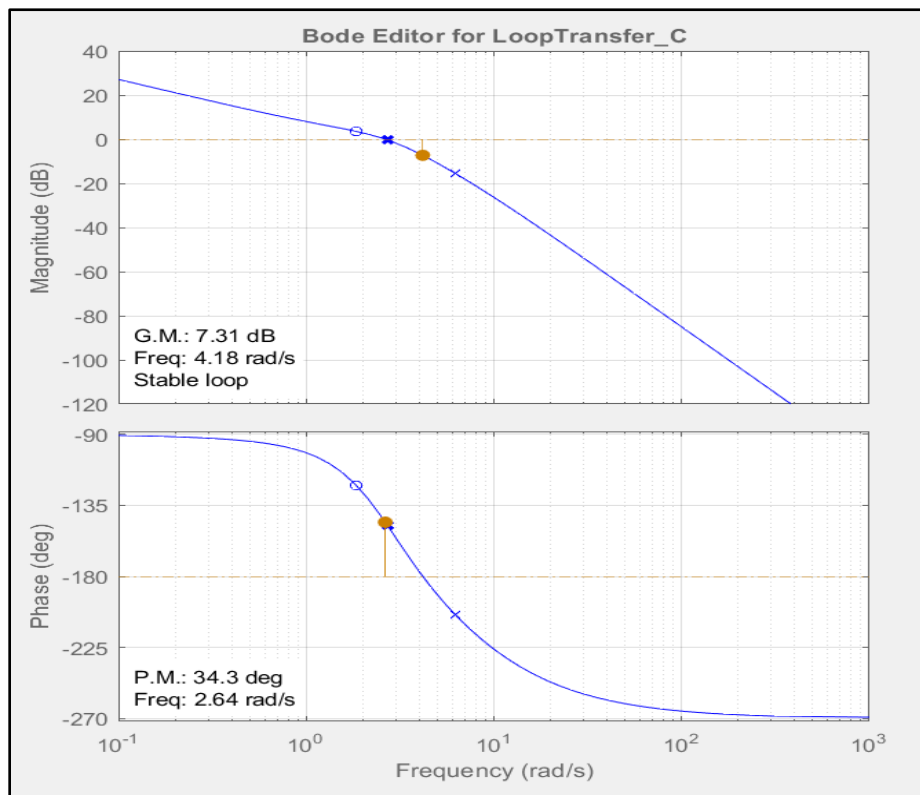
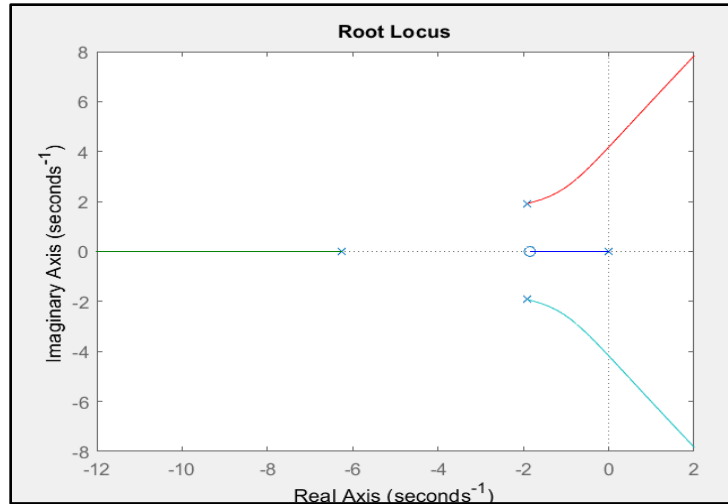


Fig 5.33 Root-Locus and Bode-Plot of Uncompensated Feedback Control System

The root-locus and bode-plot in fig 5.33 depicts the zeroes and poles of the control system whereas positive value of the phase margin in the bode plot signifies the system stability

5.5.3 DESIGN ALGORITHM OF PD COMPENSATED CONTROLLER

1. Define desired control system design specification
2. Determine dominant poles for desired design specification.
3. Design Compensator for the controller
4. Estimate the gain of the control system
5. Validate the result through SIMULINK software.

STEP 1: Control System Design Specification

1. Settling Time < 10sec
2. Peak Overshoot < 20%
3. Steady State Error < 1%
4. Rise Time < 2sec

STEP 2: Determination of Closed Dominant Pole

Figure 5.34 below displays the uncompensated controller's root locus which states that damping $\zeta = 0.456$ at 20% overshoot thus by visualizing the above figure the closed dominant pole is located at $-3.74+7.3i$ and the gain of the system is 1

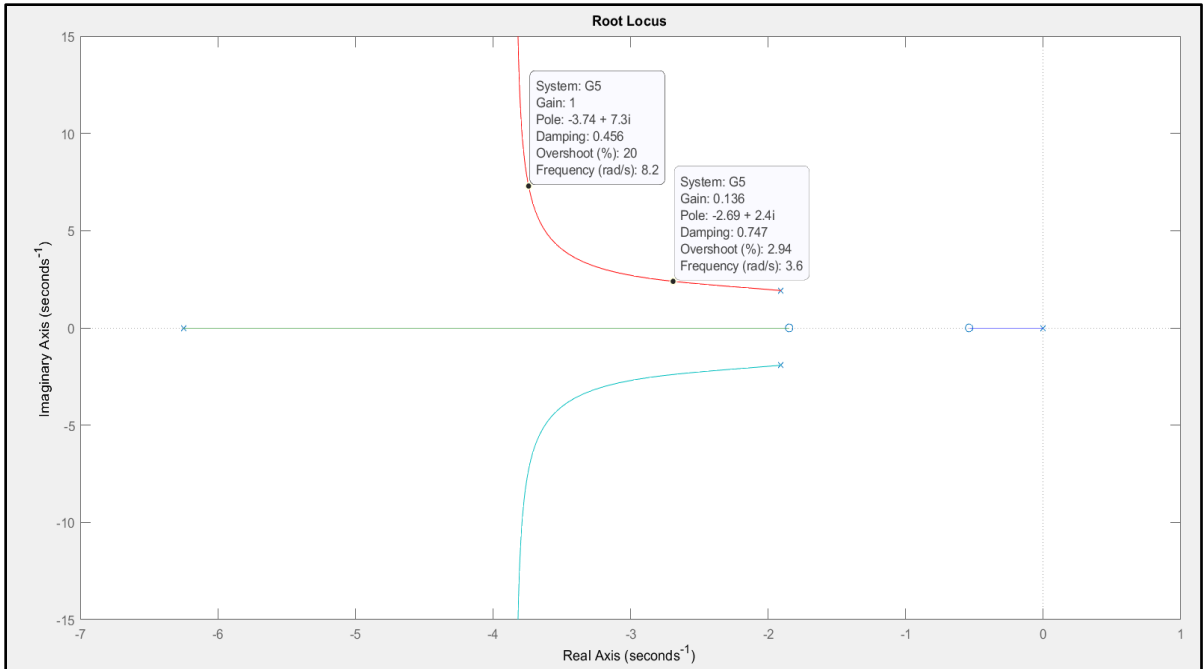


Fig 5.34 Location of Closed Dominant Pole

As per design specifications, settling time $T_s < 10$ sec as $\zeta \omega_n = \frac{4}{T_s}$ thus $\zeta \omega_n = 0.4$.

The damping ratio of SP mode is calculated by relationship as $\Theta = \cos^{-1} \zeta$. Consider ζ as 0.456 from the above figure as satisfying the design requirements. The estimated angle is found to be 62.87°

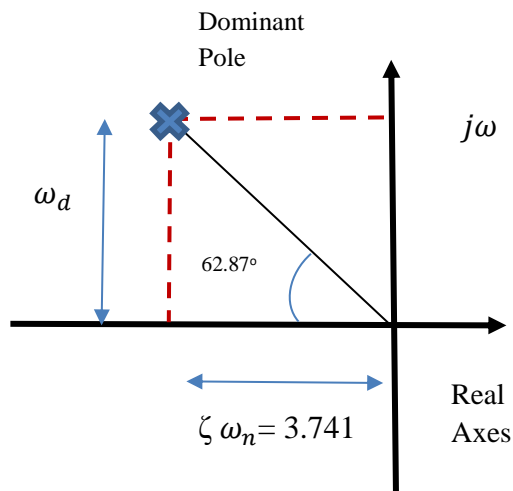


Fig 5.35 Determination of Damping Ratio

$\tan(62.87^\circ) = \frac{7.3}{\zeta \omega_n}$ thus $\zeta \omega_n = \frac{7.3}{1.951} = 3.741$ as per the given figure 5.35, the closed dominant poles from origin to s-plane is $-3.741 \pm 7.3j$ which validates the point reflected in the above figure.

STEP 3: Design of PD Compensated Controller

The controller has two complex poles, two real poles, and one zero as shown below

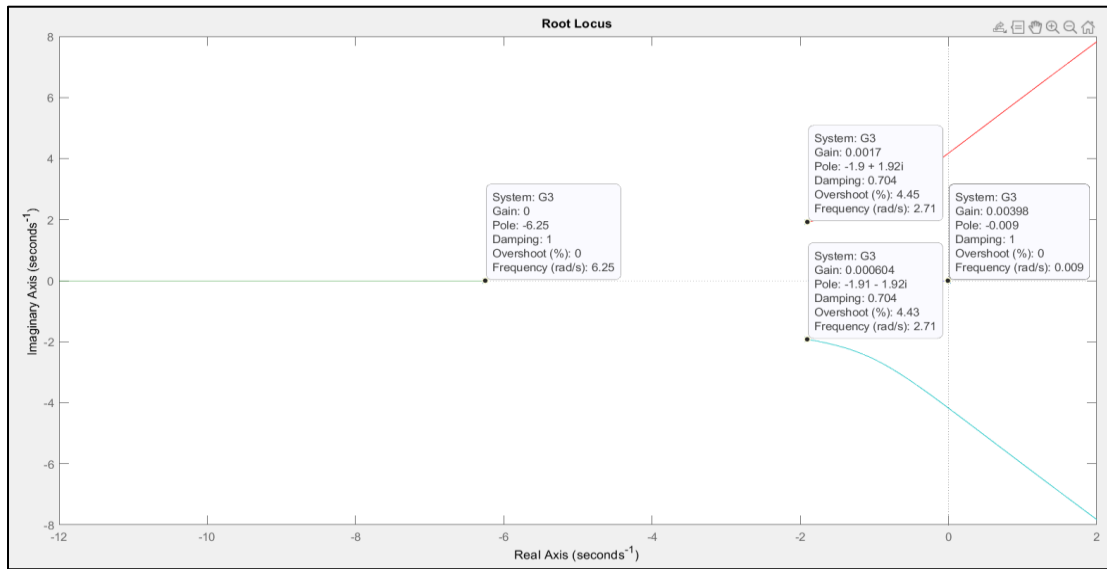


Fig 5.36 Root-Locus of PD Compensated Controller

The compensator can be designed by applying the root locus algorithm which is estimated by calculating angles from complex poles which is given by $A = 180^\circ - (\text{Summation of angles made by complex dominant pole to other poles}) + (\text{Summation of angles made by complex pole to other zeros})$

As reflected below Figure 5.36; the controller has two poles and one zero in Real axes thus A is estimated using the following expression as $A = 180^\circ - (\text{Summation of angles made by complex dominant pole to other poles})$

$$A = 180^\circ - (\theta_1 + \theta_2 + \theta_3 + \theta_4) + \theta_5 \text{ (Nagoor Kani - Control System 5.64 Engineering-RBA (2013).Pdf, n.d.)}$$

$$\tan(\theta_1) = \frac{y_2 - y_1}{x_2 - x_1} = \frac{0 - 7.3}{0 - -3.74} = -1.95$$

$$\theta_1 = 180^\circ - \tan^{-1}(-1.95) = -62.87^\circ = 117.13^\circ$$

$$\tan(\theta_2) = \frac{y_2 - y_1}{x_2 - x_1} = \frac{0 - 7.3}{-6.25 - -3.74} = 2.9083$$

$$\theta_2 = 180^\circ - \tan^{-1}(2.9083) = 70.992^\circ$$

$$\text{Complex pole } (-1.91 + 1.92i)\theta_3 = 180^\circ - \tan^{-1}\frac{7.3-1.92}{3.74-1.91} = 108.791^\circ$$

$$\text{Complex pole } (-1.91 - 1.92i)\theta_4 = 180^\circ - \tan^{-1}\frac{7.3+1.92}{3.74-1.91} = 101.227^\circ$$

Summation of angles made by complex dominant pole to other poles

$$X = 180^\circ - (\theta_1 + \theta_2 + \theta_3 + \theta_4) \quad 5.65$$

$$A = 180^\circ - (117.13^\circ + 71^\circ + 108.791^\circ + 101.227^\circ)$$

Summation of angles made by complex dominant pole to other zeros

$$Y = \theta_5 \quad 5.66$$

$$\theta_5 = 180^\circ - \tan^{-1}(-3.8624) = 104.516^\circ$$

$$A = X + Y \quad 5.67$$

$$A = -113.627^\circ$$

Now the angle measured by PD Compensated zero Z_C as reflected in the figure 5.4.26 mentioned below is calculated using a trigonometric relationship

$$\tan(180^\circ - 113.627^\circ) = \frac{7.3}{3.74 - Z_C} \quad 5.68$$

$$2.285 = \frac{7.3}{3.74 - Z_C}$$

$$Z_C = 0.5453$$

STEP4: Gain Estimation

Thus, the value of compensated zero is given by Z_C as 0.5453. It is possible to write the transfer function of compensated zero as $K(S+0.5453)$ where K is the system's loop gain.

The transfer function of the PD Controller $G_{PD} = \frac{U(s)}{E(s)} = K_P + K_D S = K_P \left(1 + \frac{K_D}{K_P} S\right)$

where $\frac{K_D}{K_P}$ denotes T_D .

$$G_{PD} = \frac{U(s)}{E(s)} = K_P + K_D S = K_P \left(1 + \frac{K_D}{K_P} S\right) = 0.5453(1 + 1.8s) \quad 5.69$$

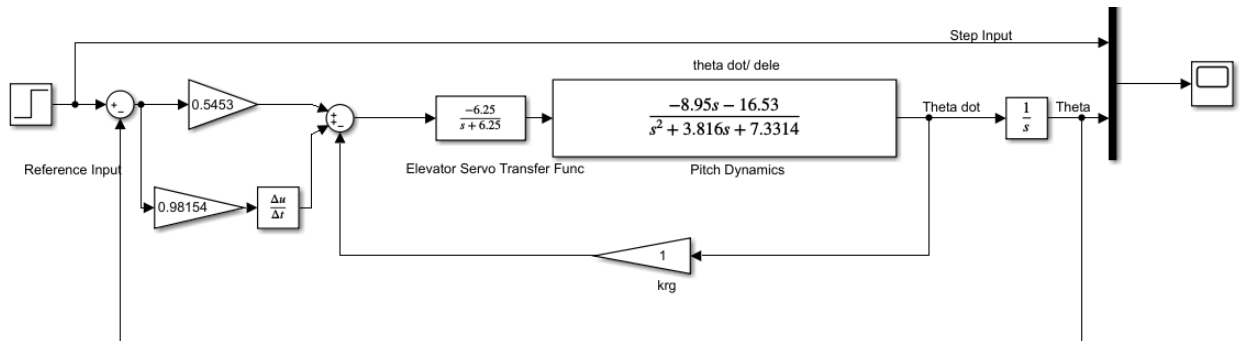


Fig 5.37 Pitch Attitude Control System

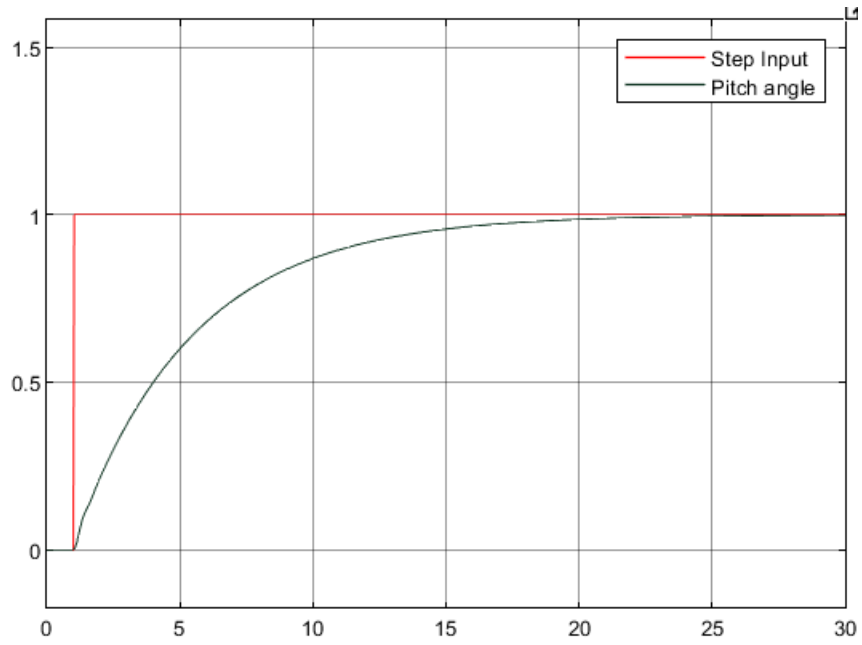
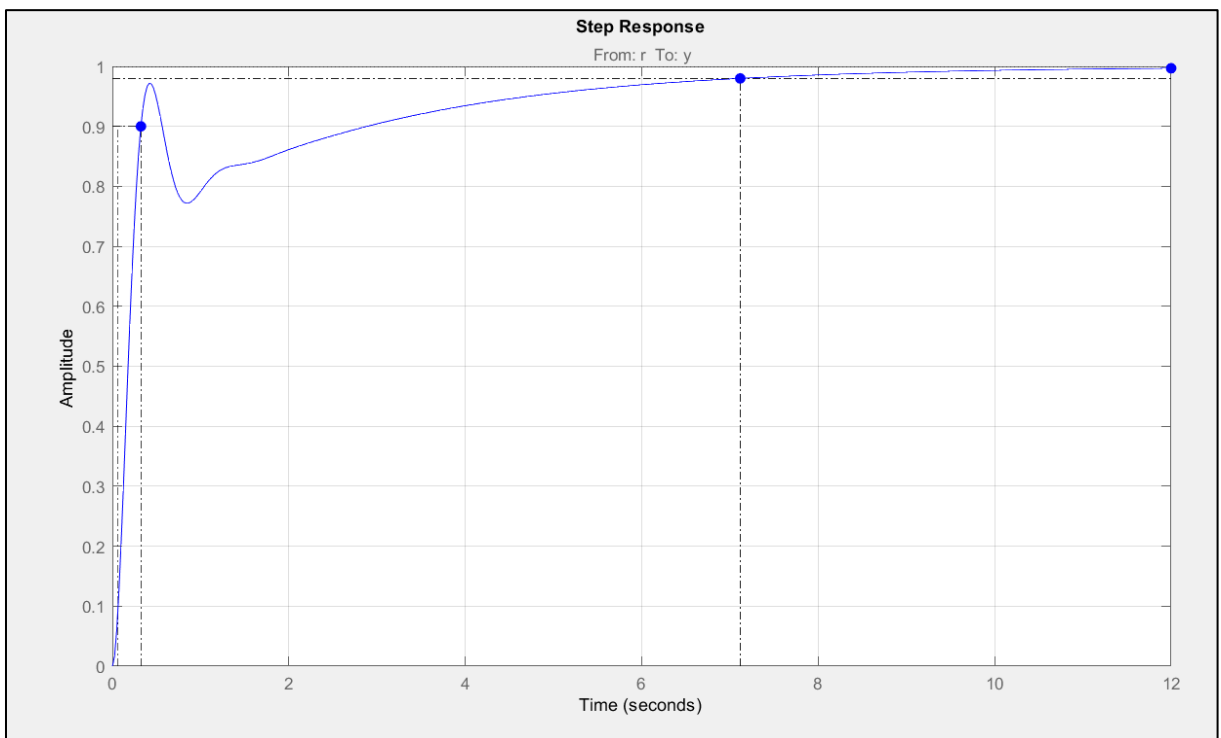


Fig 5.38 Pitch angle Verses Step Input



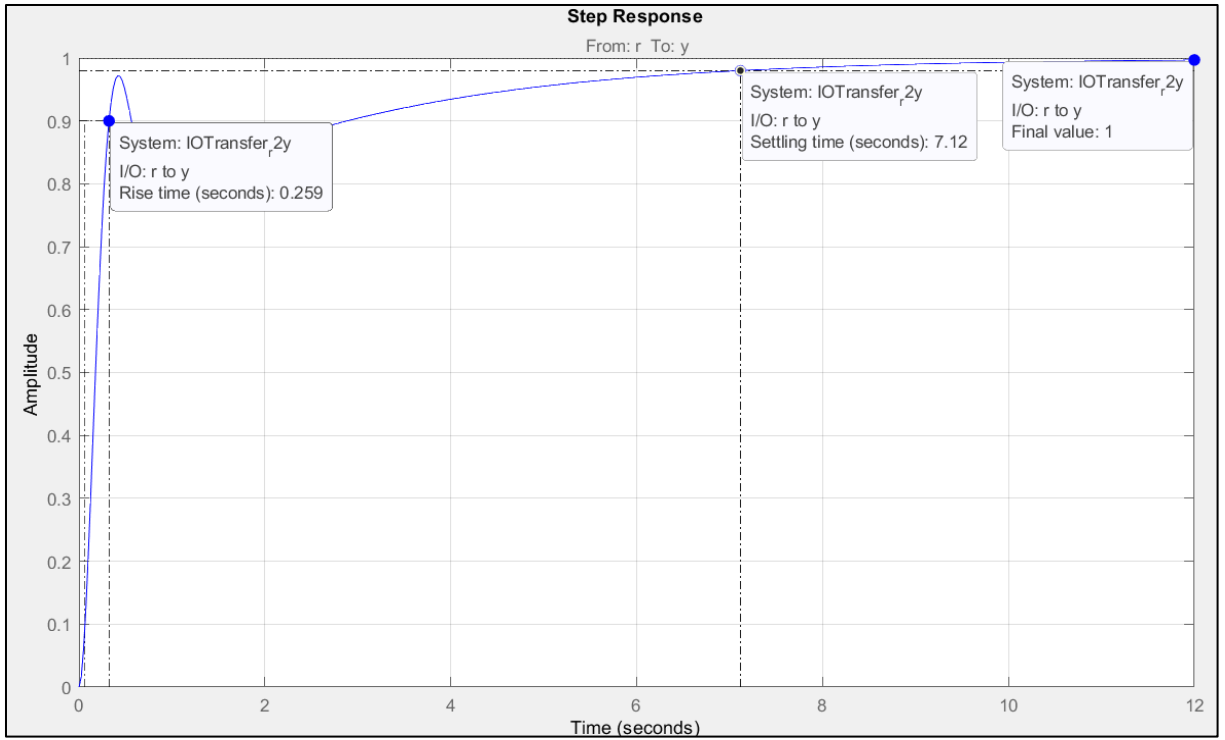


Fig 5.39 Step Response of the Pitch Angle

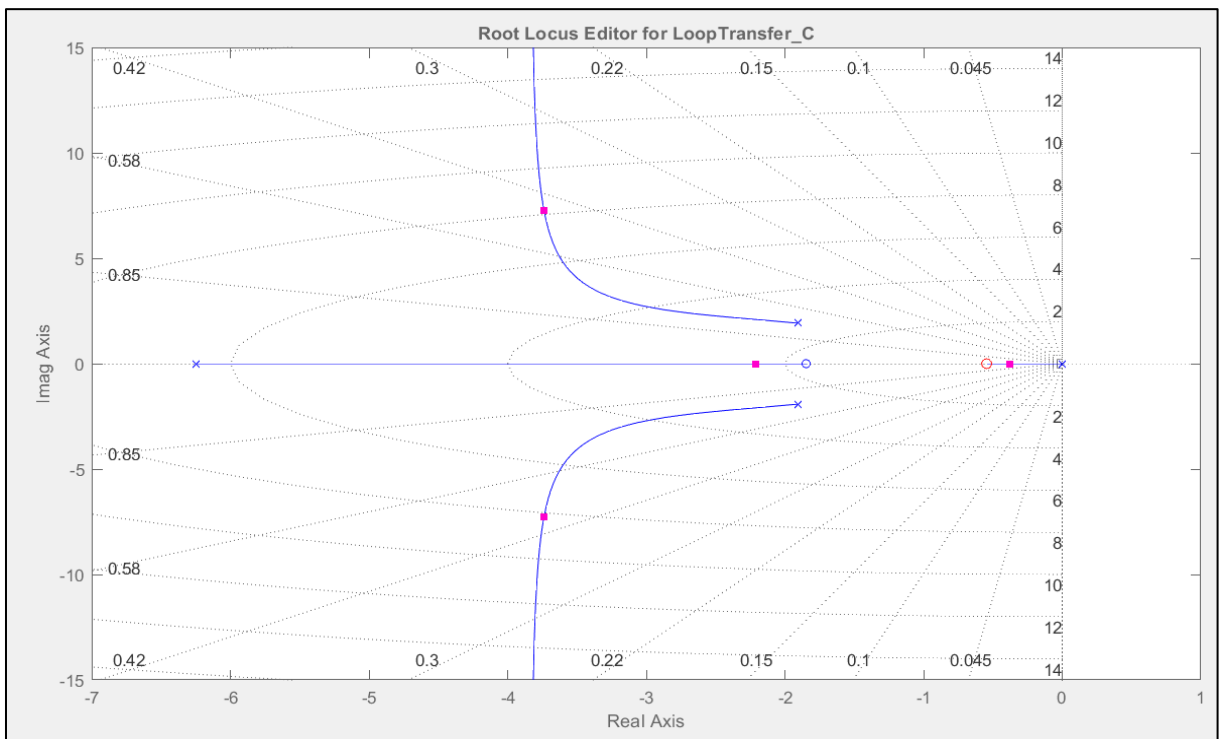


Fig 5.40 Root-Locus Plot compensated Controller

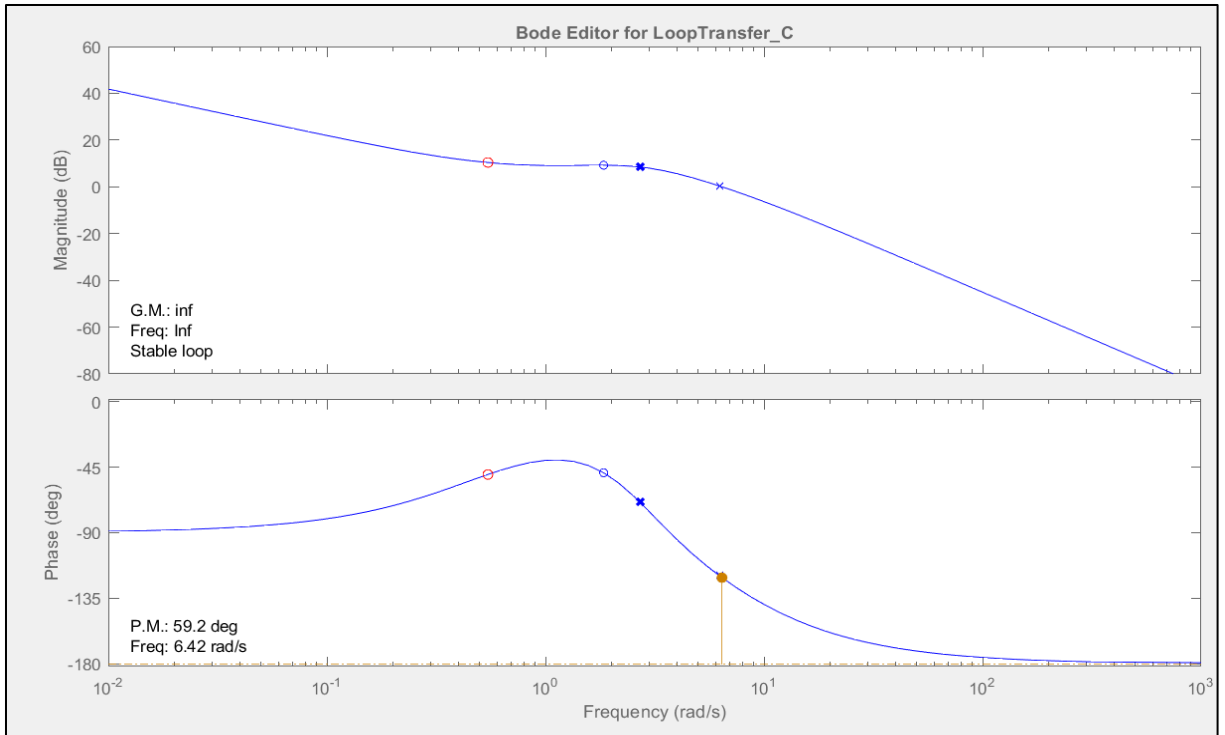
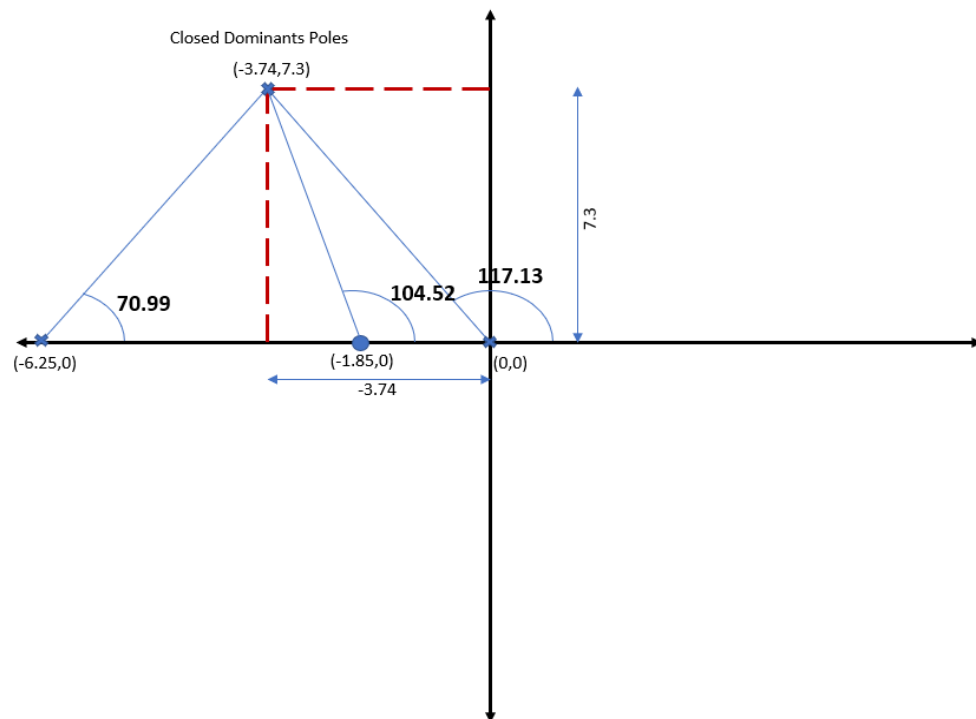


Fig 5.41 Bode Plot of compensated Controller



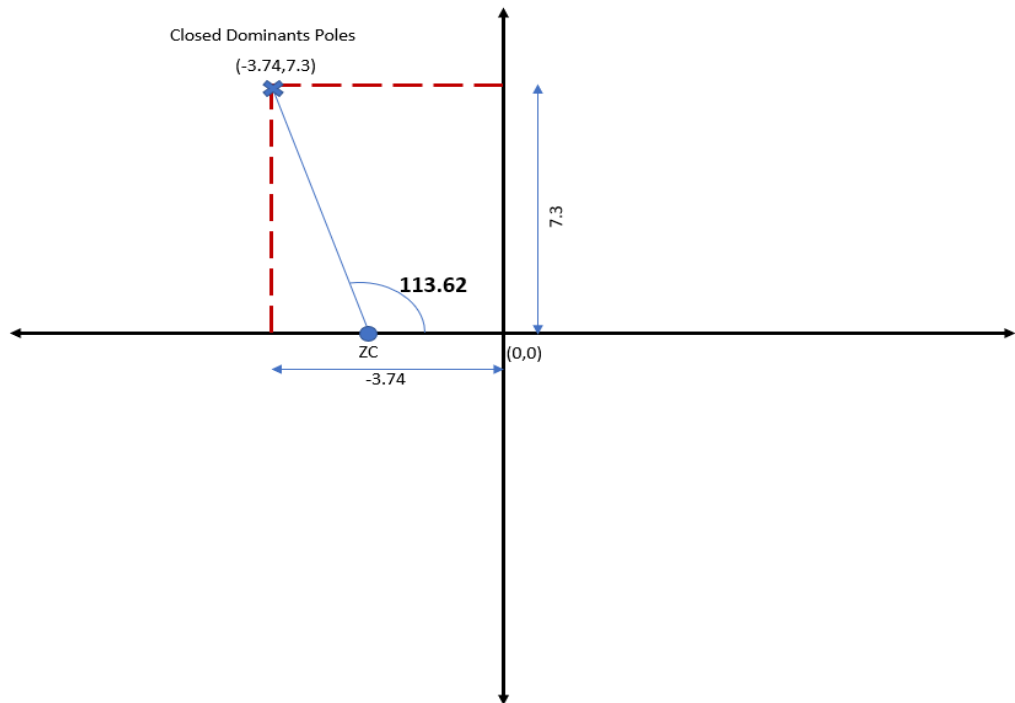
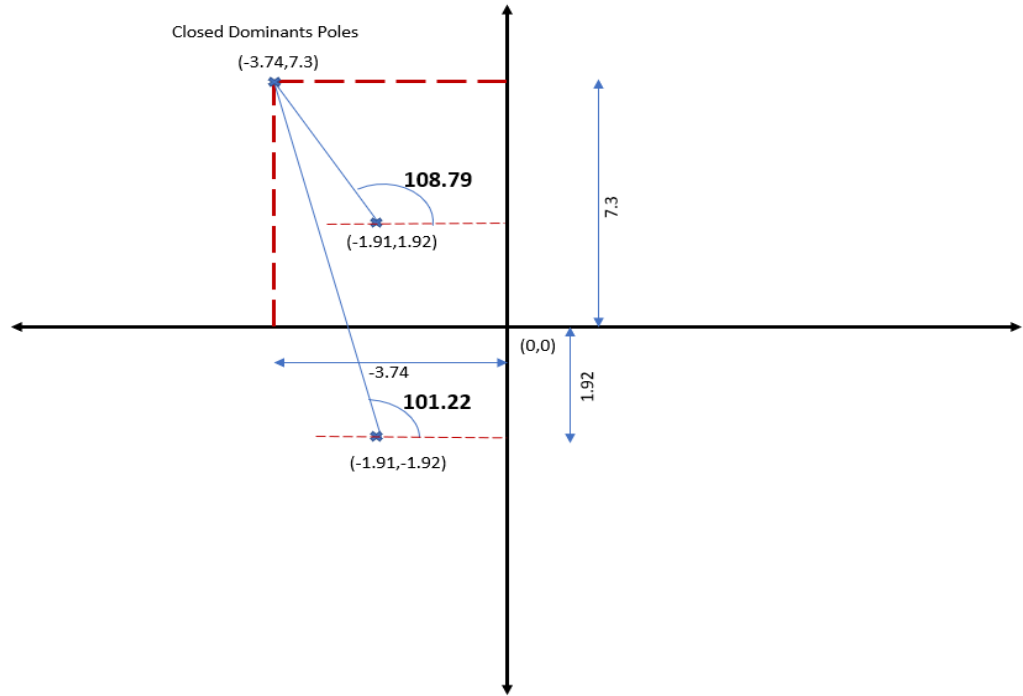


Fig 5.42(1-3): Compensator Diagram

The Time-domain characteristics with and without controller is displayed below in Tabulated and pictorial representation

S. No	Time Domain Characteristics	Without Controller	With Controller
1.	Settling Time<10sec	5.51	7.12
2.	Peak Overshoot<20%	31.1	0
3.	Steady State Error<1%	1	1
4.	Rise Time<2sec	0.493	0.259

S. No	Frequency Domain Characteristics	Without Controller	With Controller
1.	Gain Margin>6Db	7.31	∞
2.	Phase Margin>45°	34.3	59.2

Table 5.13 Hansa-III Pitch Attitude Characteristics

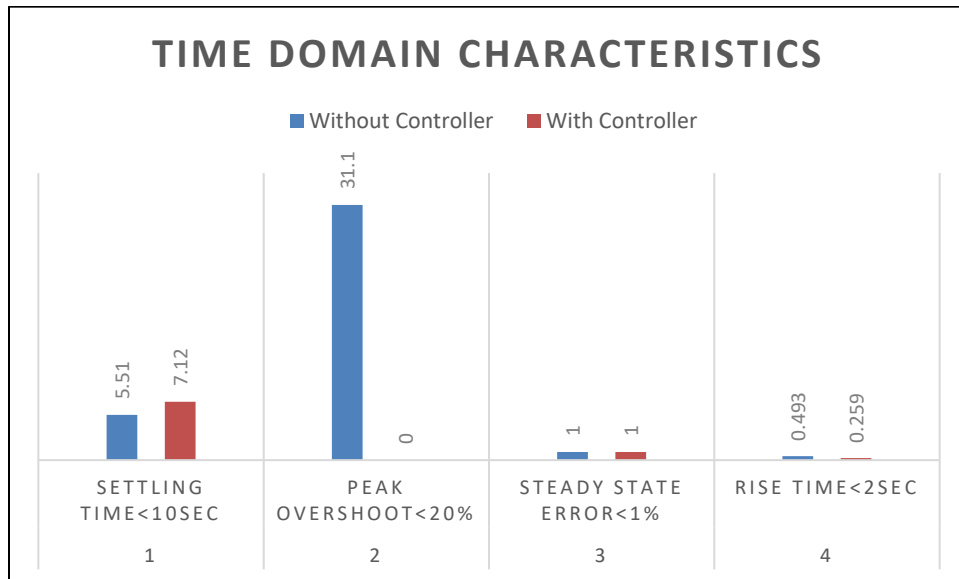


Fig 5.43 Bar Pictorial Representation with and without Controller in Time-Domain

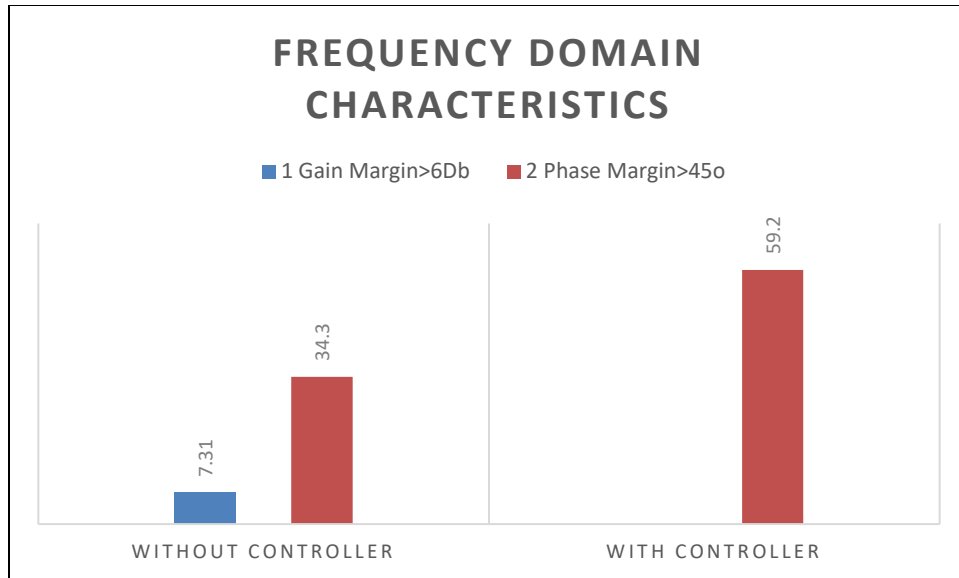


Fig 5.44 Bar Pictorial Representation with and without Controller in Frequency-Domain

All time-domain characteristics satisfying design requirements as displayed in Table 5.13. The stability criterion is determined by estimating Gain Margin and phase margin from Bode Plot. The system will be stable if the Gain Margin and Phase Margin are both bigger than zero.; If the gain margin is infinite and the phase never crosses -180° then too system attains stability. Table 5.13 and Figure 5.44 demonstrates that gain margin of the system with controller is infinite shows stable characteristics of Pitch attitude of RCT Aircraft.

5.6 MODERN CONTROL METHODS

Recent advancements in technology evolved novel approaches to design control systems termed modern control theory. Classical methods are limited to SISO systems while modern control theory has the scope of MIMO, time-variant, linear or non-linear systems. High-order systems are replaced by first-order differential equations to reduce system complexity. Optimization techniques are easily applicable to solve optimal control problems using this approach. A recent study on modern control theory had a significant impact on the aerospace sector(Nelson,

1989). Approaches such as guaranteed dominant pole placement, and LQR to design PID Controller of UAV(Debaleena et al., 2016). LQR and LQG Controller to study longitudinal and lateral flight dynamics is discussed and implemented for optimal estimation(Chrif & Kadda, 2014). Fuzzy PID Controller, Sliding mode controller, PID Controller to study pitch dynamics(Khalid et al., 2019)(Kisabo, 2012) as well as LQR and fuzzy logic to design aircraft roll, and yaw controllers are also discussed(Usta et al., 2011)(George, 2012). The Pitch attitude control system of F-4 fighter jet aircraft is designed using PID, fuzzy logic PID(BOSSERT DAVID E & KELLY, 2002). The two methodologies such as pole placement and LQR are proposed to estimate the gain matrix for designing the PID Controller of Hansa-III. The state feedback control system's block diagram is displayed in Figure 5.45

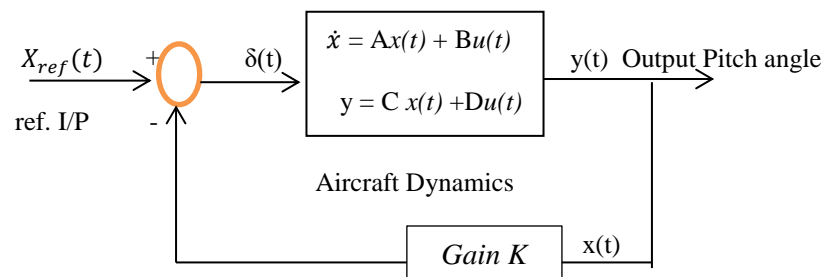


Fig 5.45 Feedback Control Design

5.6.1 POLE PLACEMENT TECHNIQUE

The Pole placement technique calculates the gain matrix to guarantee system stability. The Controller has to modify the A matrix to change system dynamics. The eigenvalue of A matrix indicates the system's poles whereas the location of poles dictates system stability thus desired pole location is an important feature of this technique satisfying all design requirements. The closed-loop dominant poles have faster system response as compared to other poles.

Generalized State equation in Matrix form may be written:

$$\dot{x} = A x + B u \quad 5.70$$

$$y = C x + D u \quad 5.71$$

To define A(plant matrix), B(control matrix), C(output matrix), and D(null matrix) as they are reflected in the above equation are compared with state space matrix form 5.27 as A, B, C,& D.

$$\begin{bmatrix} \dot{\alpha} \\ \dot{q} \\ \dot{\theta} \end{bmatrix} = \begin{bmatrix} -1.851 & 0.8207 & 0 \\ -4.403 & -2.01 & 0 \\ 0 & 1 & 0 \end{bmatrix} \begin{bmatrix} \alpha \\ q \\ \theta \end{bmatrix} + \begin{bmatrix} -0.00562 \\ -8.95 \\ 0 \end{bmatrix} [\delta] \quad 5.72$$

$$[\theta] = [0 \quad 0 \quad 1] \begin{bmatrix} \alpha \\ q \\ \theta \end{bmatrix} + [0][\delta] \quad 5.73$$

The open loop poles of matrix A are $0, -1.9305 \pm 1.8993i$

$$u = I.k_r - k * x$$

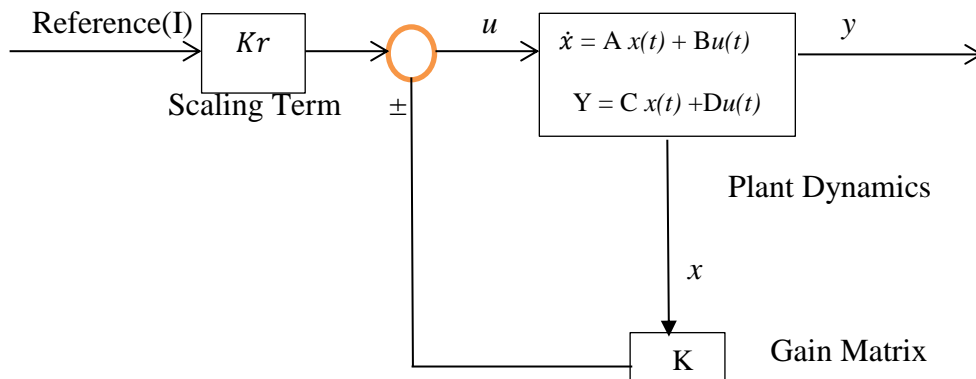


Fig 5.46 Pole Placement

The steps followed in the pole-placement technique are discussed as:

1. Check system state controllability
2. Choose closed-loop poles using the Butterworth methodology
3. Determine the Feedback gain matrix using Ackermann's theorem

STEP-I

If the states of the dynamic system affect the control input, controllability difficulties may arise. If the system state is unaffected then the system is uncontrollable. The sufficient condition for the system controllability test is the rank of the system is the same as the controllability matrix which is measured by $V = [B \ AB \ A^2*B]$ for third order system and in MATLAB scripted as $V = \text{ctrb}(A, B)$

$$V = \begin{bmatrix} 0.0056 & 7.3349 & -28.3611 \\ 8.9500 & -18.0142 & 3.9132 \\ 0 & 8.95 & -18.0142 \end{bmatrix}$$

The rank of $R1 = \text{rank}(V) = 3$

The system states controllable as the rank of V is of the same order as the system.

STEP-II

Closed-loop poles must lie at the desired location. All poles including dominant poles must lie at a specific location. It is required to avoid choosing closed-loop poles far away from open-loop poles. The value of closed-loop poles must not be highly negative as the system response will be too fast. The approach used in closed-loop pole selection employing the Butterworth polynomial equation for pole placement is dictated in equation 5.74 (Radhakant Padhi, n.d.)

Butterworth Polynomial equation can be rewritten as:

$$\left(\frac{s}{w_o}\right) = (-1)^{\frac{n+1}{2n}} \left[\frac{e^{j(2k+1)\pi}}{-1} \right]^{\frac{n+1}{2n}} \quad 5.74$$

where $k = 0, 1, 2, \dots$ so on

w_o = natural frequency

n = system order which states number of closed-loop poles

As per trigonometric identity:

$$e^{j(2k+1)\pi} = \cos(2k+1)\pi + j\sin(2k+1)\pi \quad 5.75$$

$$= \cos n(2k+1)\pi + j\sin(2k+1)\pi$$

As matrix A is of order three thus substituting n=3 in the above equation

$$\frac{n+1}{2n} = \frac{2}{3} \quad s = w_0 [\cos(2k+1)2\pi/3 + j\sin(2k+1)2\pi/3]$$

Case I:

$$K=0; w_0 = 2.7$$

$$S_1 = w_0 [\cos 2\pi/3 + j\sin 2\pi/3] = (-1/2 + j\sqrt{3}/2) * 2.7 = -1.35 + 2.338j$$

Case II:

$$K=1; w_0 = 2.7$$

$$S_2 = w_0 [\cos 2\pi + j\sin 2\pi] = -2.7$$

Case III:

$$K=2; w_0 = 2.7$$

$$S_3 = w_0 [\cos 10\pi/3 + j\sin 10\pi/3] = (-1/2 - j\sqrt{3}/2) * 2.7 = -1.35 - 2.338j$$

Case IV:

$$K=3; w_0 = 2.7$$

$$S_4 = w_0 [\cos 14\pi/3 + j\sin 14\pi/3] = (-1/2 + j\sqrt{3}/2) * 2.7 = -1.35 + 2.338j$$

Case V:

$$K=4; w_0 = 2.7$$

$$S_5 = w_0 [\cos 6\pi + j\sin 6\pi] = -2.7$$

Case VI:

$$K=5; w_0 = 2.7$$

$$S_6 = w_0 [\cos 22\pi/3 + j\sin 22\pi/3] = (-1/2 - j\sqrt{3}/2) * 2.7 = -1.35 - 2.338j$$

Desired closed-loop pole roots S_1, S_2, S_3 are $-1.35 \pm 2.338j, -1.3$

STEP III

The feedback gain matrix ‘K’ using the pole-placement technique is estimated using Ackermann’s method. The algorithm to estimate the gain matrix is presented in Appendix B5. This method solves the pole placement problem while designing the control system for time-invariant systems represented by the equation as(Nelson, 1998)(Radhakant PadhiDepartment of Aerospace Engineering, n.d.)

$$u(t) = -kx(t) \tag{5.76}$$

The modified system equation is expressed as $\dot{x} = (A - Bk)x$; let us define $A^* = A - Bk$ since the Cayley-Hamilton theorem states that A^* satisfies own characteristic equation thus

$$\phi(A^*) = A^{*n} + \alpha_1 A^{*(n-1)} + \dots - \alpha_{n-1} A^* + \alpha_n \tag{5.77}$$

PadhiDepartment of Aerospace Engineering, n.d.)

Consider trigonometric Identities as $I=I$; $A^* = A - Bk$; $A^{*2} = (A - Bk)^2$; $A^{*3} = (A - Bk)^3$

The system is states controllable as explained in step I thus pre-multiplying both sides of the equation by the inverse of the controllability matrix (Radhakant PadhiDepartment of Aerospace Engineering, n.d.)

$$C^{-1}\phi(A^*) = \begin{bmatrix} \alpha_2 k + \alpha_1 k A^* + k A^{*2} \\ \alpha_1 k + k A^* \\ k \end{bmatrix} \tag{5.78}$$

Now pre-multiplying both sides of the equation by $[0 \ 0 \ 1]$ matrix to obtain Ackermann’s equation

$$[0 \ 0 \ 1] \begin{bmatrix} \alpha_2 k + \alpha_1 k A^* + k A^{*2} \\ \alpha_1 k + k A^* \\ k \end{bmatrix} = [0 \ 0 \ \dots \ 1] C^{-1} \phi(A^*) = \tag{5.79}$$

$$k = [0 \ 0 \ \dots \ 1] C^{-1} \phi(A^*) \tag{5.80}$$

Where k is the feedback vector, $\phi(A^*)$ is desired characteristic equation of matrix A , and C is the controllability matrix

$$\phi(A^*) = \det(SI - (A - BK)) \quad 5.81$$

The closed loop poles of matrix $\phi(A^*)$ are:

$$-1.3000 + 0.0000i$$

$$-1.3500 + 2.3380i$$

$$-1.3500 - 2.3380i$$

The gain K as shown in the figure 5.47 is also determined using MATLAB function as 'acker' thus Gain $K = \text{acker}(A, B, S)$; $K = [-0.2612 \quad 0.0157 \quad 0.5728]$

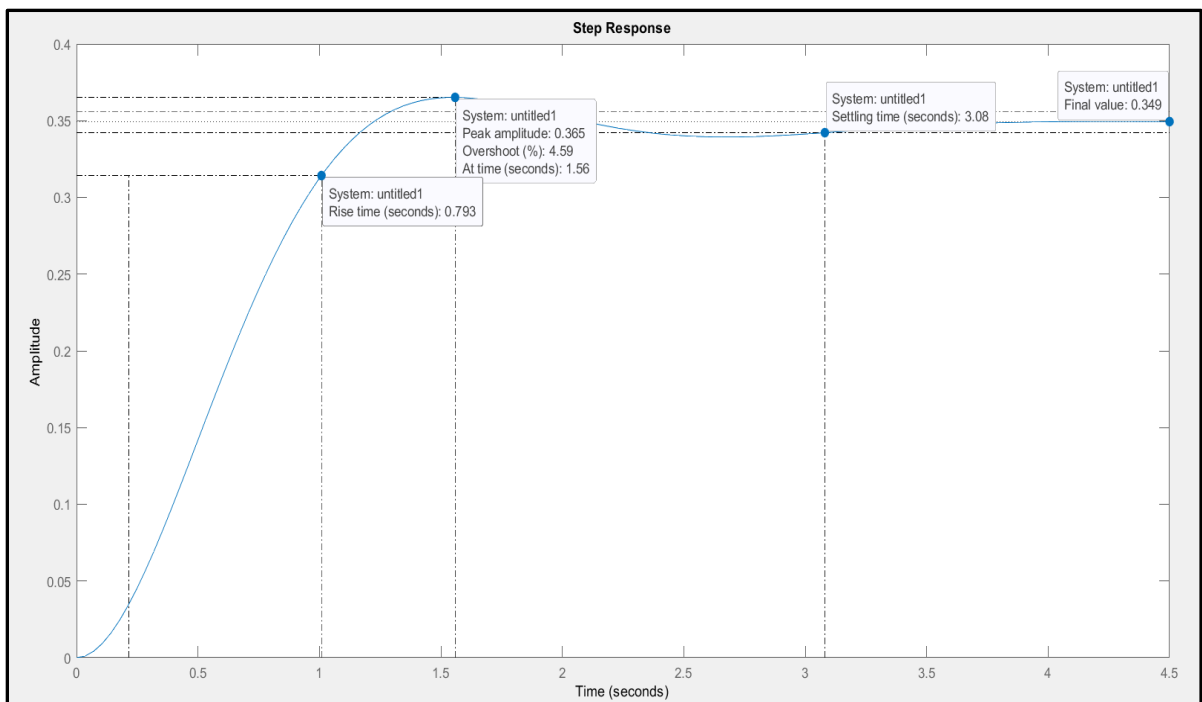


Fig 5.47 Step Response using pole placement without scaling effect

The scaling effect $\bar{N} = 0.5728$ compensates steady-state error to 0.01 of the system as shown in the above figure 5.47

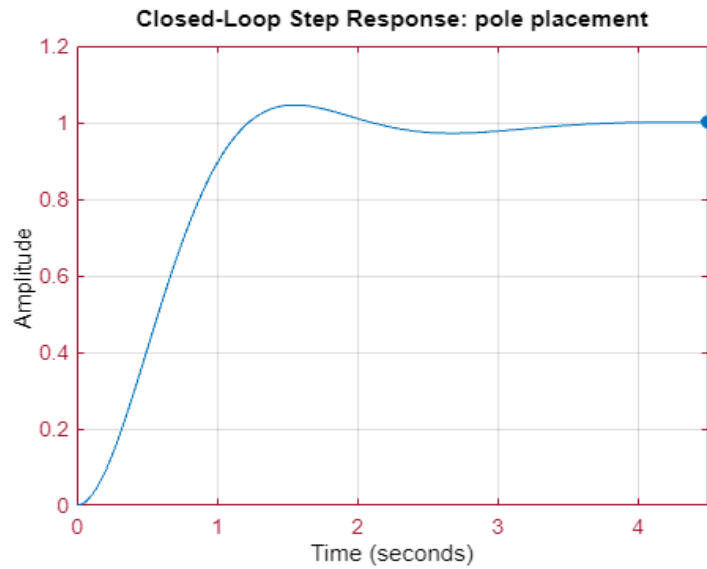
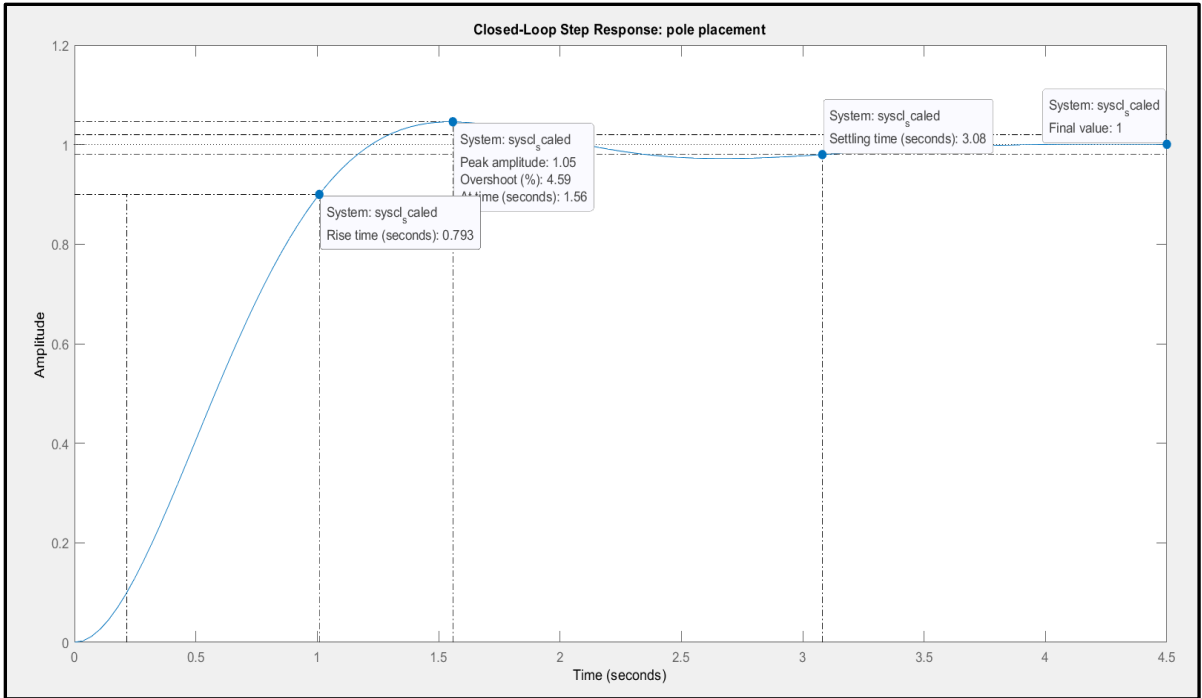


Fig 5.48 Closed-Loop Step Response using pole placement with scaling effect

The Time-domain characteristics with and without scaling effect is displayed below in Table 5.14

S.No	Closed loop Time-domain response	Design Specification	Pole-placement with Scaling effect	Pole-placement without Scaling effect
1.	Steady-state error	<1%	1	0.349
2.	Peak overshoot	<20%	4.59	4.59
3.	Settling Time (sec)	<10sec	3.08 s	3.08 s
4.	Rise Time (sec)	<5sec	0.793 s	0.793 s

Table 5.14 Time domain Performance characteristics using Pole-Placement Technique

The pitch angle response utilizing the pole assignment technique shown in Figure 5.47,5.48 depicts zero steady state error while compensating for steady state error from 0.349 to 0.01 with a scale factor $N = 0.5728$.

5.6.2 LINEAR QUADRATIC REGULATOR

The system performance in the time and frequency domain is measured in the form of settling time, rise time, peak time, Gain Margin, Phase Margin, and Bandwidth. Traditional methods cannot handle the problem of designing an aircraft attitude control system that requires pleasing design criteria. An advanced approach known as optimal control made it feasible to solve complex system problems. LQR is an optimal modern control approach that solves optimization problems by keeping the cost function minimal with subjected to a given set of constraints(Haddar et al., 2021). This method is comparable to pole placement since gain K is implemented similarly, as seen in Fig. 5.45, but gain K 's value is selected using a different process. By selecting closed-loop characteristics with the help of the cost function, optimal gain K is computed. (Wahid & Rahmat, 2010)(Ashraf et al., 2018)(JAISWAL & PRAKASH, 2022).

PROCEDURE TO SOLVE LQR PROBLEM

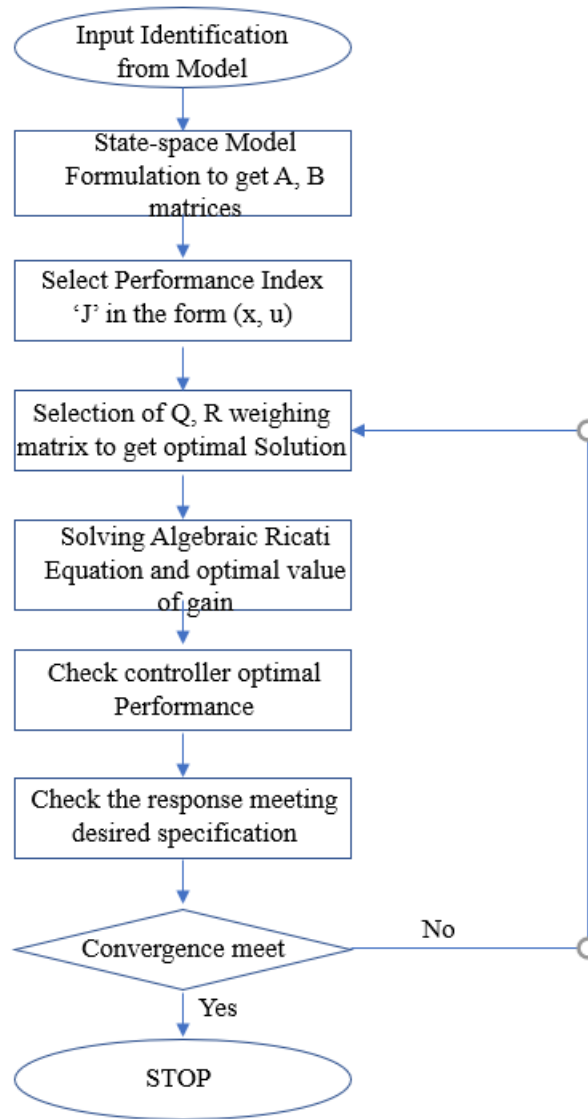
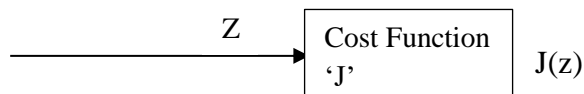


Fig 5.49 Flowchart of Linear Quadratic Regulator

The objective of this theory helps in satisfying all physical constraints and minimizes performance Index 'J'



$J(z)$ = Cost function that measures how much solution z costs. The set to solve optimization problem includes feasible sets $z = \{z_1, z_2, z_3, \dots, z_5\}$

$$J_3(z) = Q J_1(z) + R J_2(z)$$

The minimal value of the cost function gives an optimal solution. The performance Index can be rewritten as (Nelson, 1998):

$$J = \int_0^{\infty} \{x^T Q x + u^T R u\} dt \quad 5.82$$

Q , and R are known as scalar weights as well as the weighted squares of deviation of state from target and weighted square of control activity, x as a state vector, u as input vector. The Q term measures performance characteristic such as settling time (ST), rise time (RT), and peak time (PT) and the R term penalize actuator effort. The integrand function depicts the area under the curve. Q measures the convergence rate (Settling and Rise time), and R penalizes aggressive Input. The Q and R allow a trade-off between the rate of convergence and input activity.

Rise and Settling time implicit in $x^T Q x$ term. Damping ratio, overshoot, oscillations implicit on square functions. The positive and negative error is penalized using square functions. The peak value of the function is penalized using a square.

To penalize the negative values of the linear function, the states are squared and hence termed as a Linear quadratic function. These functions have a definite minimum value. The square is used because it leads to an easier analysis of the system.

Optimizing performance Index concerning parameters of state feedback and subject to given dynamics

$$\min J = \int_0^{\infty} \{x^T Q x + u^T R u\} dt \quad \longrightarrow \quad \dot{x} = Ax + Bu; u = -k x \quad \longrightarrow \quad \dot{x} = (A - Bk) x$$

whereas, $x(t) = n \times 1$ state vector, $Q = n \times n$ symmetric positive semi-definite matrix, $u(t) = m \times 1$ control vector, $R = m \times m$ symmetric positive semi-definite matrix as a result, J will be positive.

STEPS FOR K DETERMINATION

STEP 1: Formulate a linear state-space model to get Matrices A and B from plant dynamics

Generalized State equation in Matrix form is written as:

$$\dot{x} = Ax + Bu \quad 5.83$$

To define A(plant matrix), and B(control matrix), as they are reflected in the above equation are compared with state space matrix form

$$\begin{bmatrix} \dot{\alpha} \\ \dot{q} \\ \dot{\theta} \end{bmatrix} = \begin{bmatrix} -1.851 & 0.8207 & 0 \\ -4.403 & -2.01 & 0 \\ 0 & 1 & 0 \end{bmatrix} \begin{bmatrix} \alpha \\ q \\ \theta \end{bmatrix} + \begin{bmatrix} -0.00562 \\ -8.95 \\ 0 \end{bmatrix} [\delta] \quad 5.84$$

STEP 2: Choose weighing matrices Q, and R to get a minimal value of

performance Index for an optimal solution. Start with $Q = \begin{bmatrix} 1 & 0 & 0 \\ 0 & 1 & 0 \\ 0 & 0 & 1 \end{bmatrix}$, $R =$

$$\begin{bmatrix} 1 & 0 & 0 \\ 0 & 1 & 0 \\ 0 & 0 & 1 \end{bmatrix} \text{ and iterate as per design requirements.}$$

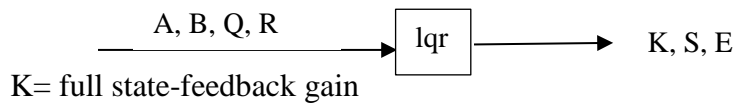
For SISO systems, R can be left at unity and Q33 weighs the most important state from the response of the system and leaves other weights at unity (Sushamshushekar Doddabasappa, 2019). Initializing $x = 400$, $Q = x * C^T * C$

$$C = [0 \quad 0 \quad 1] \quad Q = [0 \ 0 \ 0; 0 \ 0 \ 0; 0 \ 0 \ x] \quad R = [1]$$

STEP 3: Solve non-linear Algebraic Riccati Equation for determining matrix S which indicates the solution by using MATLAB function 'CARE'

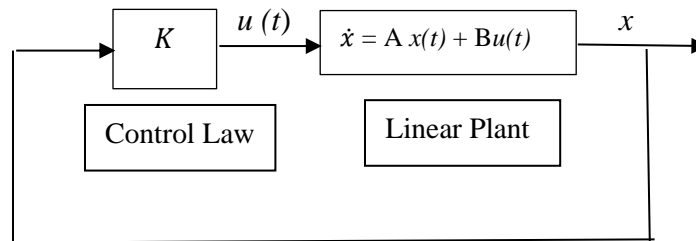
STEP 4: The optimal control law solves the algebraic Riccati equation for S as $A^T S + SA - SBR^{-1}B^T S + Q = 0$. The control law is stated as $u = -kx$ where $k = R^{-1}B^T S$ thus

determining gain by swapping all values for A, B, Q, R, and S. The Gain K is also obtained using lqr MATLAB function as $[K] = \text{lqr}(A, B, Q, R)$



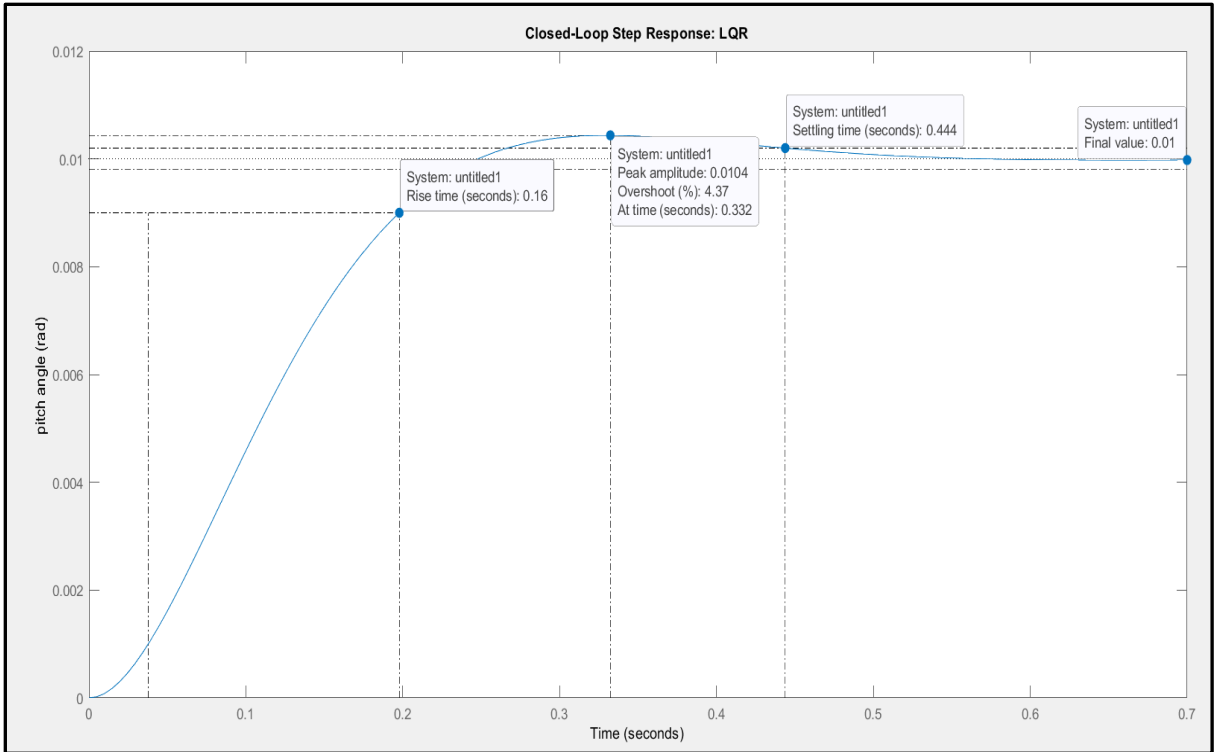
S= Ricati Matrix

E= eig (A-BK)



STEP 5: Choose the K solution that yields a stable system. The estimated value of optimal gain $K = [-0.4717 \ 1.88 \ 20.00]$ using algorithm discussed in Appendix B6

STEP 6: The closed-loop step response provides information on performance characteristics like settling time, peak time, SSE



To reduce steady-state error, a scale factor should be added to compensate for the error but for this controller design, the gain value is found to be unity which concludes that K itself stabilizes the system and steady-state error approaches 0.01 as per design requirement. Figure 5.50 displays the closed-loop step and pitch angle response using LQR controller.

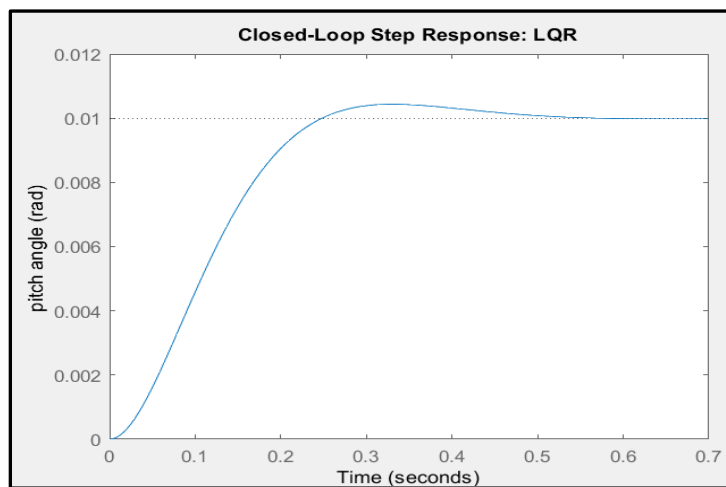


Fig 5.50 Closed Loop Step Response using LQR Controller

The Time-domain characteristics without scaling effect is displayed below in Table 5.15

S. No	Closed loop Time-domain response	Design Specification	LQR without Scaling effect
1.	Steady state error	<1%	1
2.	Peak overshoot	<20%	4.37
3.	Settling Time	<10sec	0.444 s
4.	Rise Time	<5sec	0.16 s

Table 5.15 Time domain characteristics using LQR

The pitch angle response utilizing LQR is shown in Fig.5.50, where the gain value is determined to be unity, concluding that K stabilizes the system by itself and that steady-state error approaches the design requirement of 0.01

Remark:

1. The optimal state feedback system is guaranteed to be stable if the system is fully controllable.
2. More the value of R, the lesser the the input activity but slow state behavior leads to poor performance thus system has poor controllability.
3. In a Controllable system, every coefficient of a closed-loop pole polynomial can be defined as desired closed-loop poles using state feedback
4. Optimal state feedback shows better performance than pole placement by enabling more systematic tuning/ trade-off between tracking and control activity.

5.7 VALIDATION

Controller Design is an Intermediate stage of the research study moreover, validation is a proof-match exercise that needs to be executed for result authentication. Results are validated in terms of time and frequency domain characteristics of classical and modern control methodologies for optimization of PID parameters of Hansa-III for pitch control

The outcomes of different varieties of the PID tuning method are analysed in the form of gain K_p , K_i , K_d . The gain K_p improves the accuracy of steady-state tracking, decreases system sensitivity, and creates a constant steady-state error. The gain K_d has a poor steady-state response but leads to system stability moreover K_i has a good steady-state response but leads to system instability. The Transfer function of the Pitch controller has two zeros in the numerator, one pole at the origin, and a denominator that makes the system highly stable.

The PID tuning techniques are applied and results are compared in the Tabulated and graphical figure presented below which concludes that modified ZN proclaims the finest result as Astrum -Hagglund did not have a derivative component that leads to system instability and the response is undamped oscillatory motion. The gain values using a technique such as ZN and MZN are compared and have a feature of stability and approach steady-state error frequently but MZN satisfies controller design requirements. The tuning approach TL manifests a larger value of K_d that increases aircraft stability despite that steady-state error is difficult to attain and thus unable to accomplish design requirements.

Method	General Aviation Airplane(Deepa & Sudha, 2016)	Hansa-III Aircraft
Modified ZN		
KP	0.6171	0.4422
KI	0.61	0.752
KD	0.406	0.4963
Ziegler Nicholas		
KP	1.122	0.804
KI	1.833	1.0691
KD	0.1711	0.1512
Tyresus- Luyben		
KP	0.8415	0.4188
KI	2.684	0.2376
KD	0.193	3.3088
Astrum- Hagglund		
KP	0.5984	0.4422
KI	0.94	1.4138
KD	0	0

Table 5.16 Result Validation of PID Tuning Techniques with general aviation airplane(Deepa & Sudha, 2016)

The results of different PID tuning Techniques in form of gain K_p , K_i , K_d is validated with general aviation airplane (Deepa & Sudha, 2016)

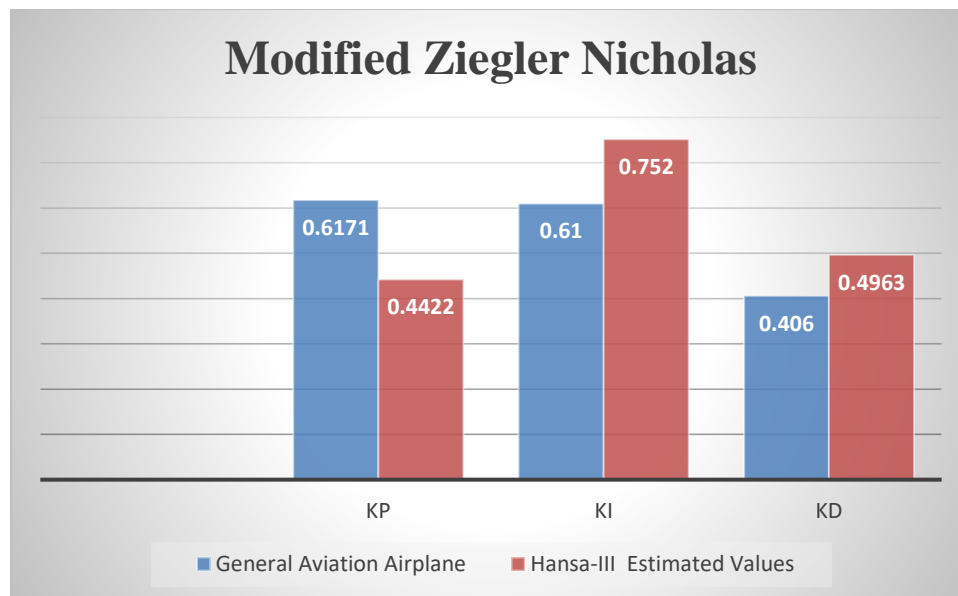


Fig 5.51 Result of Hansa-III with general aviation Airplane using MZN (Deepa & Sudha, 2016)

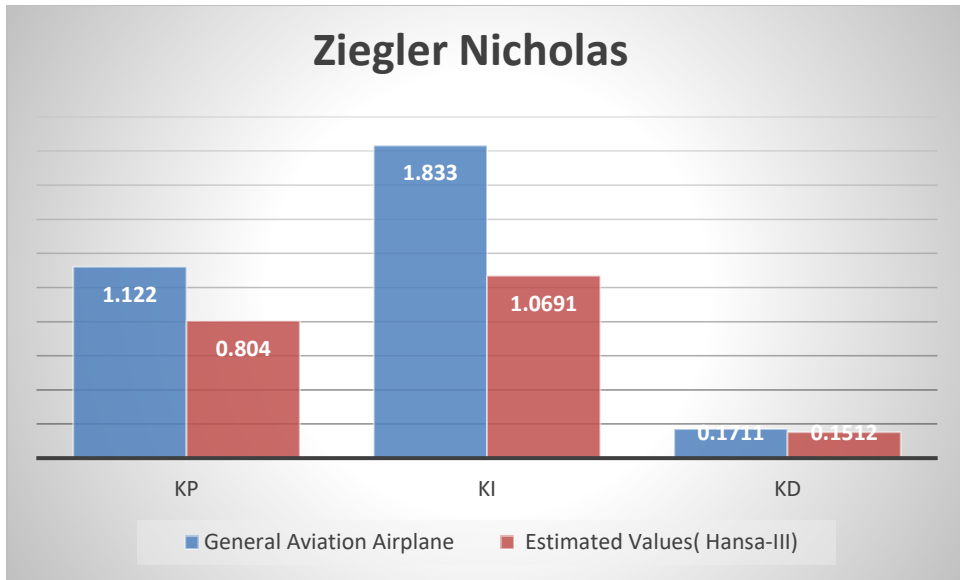


Fig 5.52 Result of Hansa-III with general aviation Airplane using ZN (Deepa & Sudha, 2016)

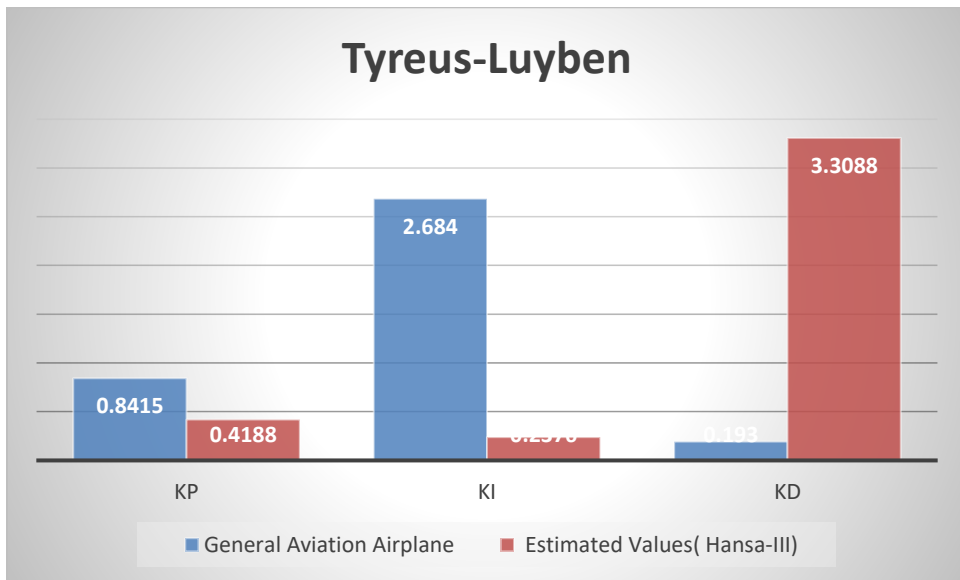


Fig 5.53 Result of Hansa-III with general aviation Airplane using TL (Deepa & Sudha, 2016)

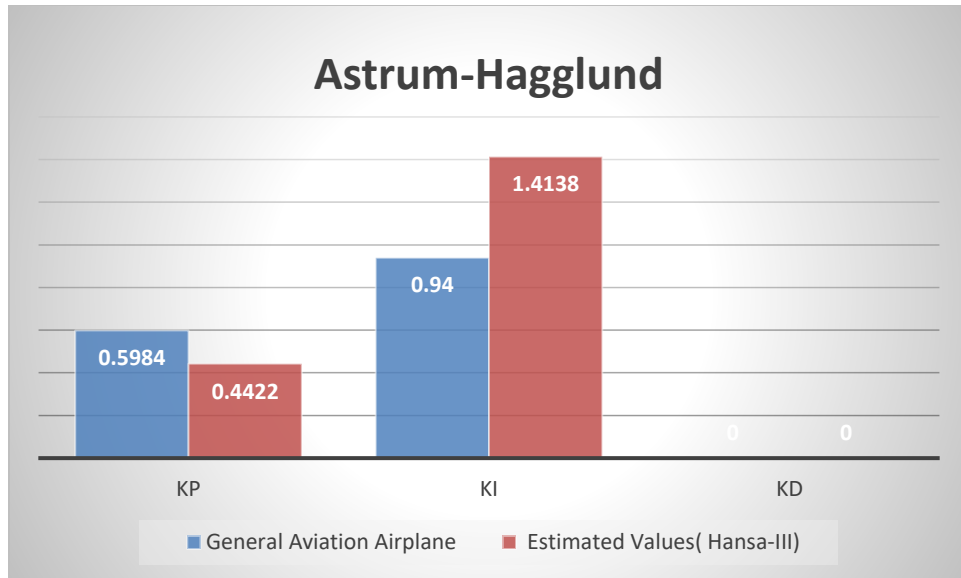


Fig 5.54 Result of Hansa-III with general aviation Airplane using AH (Deepa & Sudha, 2016)

- a) The second traditional approach to estimating gain values of K_p , K_i , and K_d is designing a compensator using a Root-locus Algorithm. The transfer function of compensated zero can be written as $K(S+0.5453)$ where K is the loop gain of the system which is briefly discussed in root-locus section. The compensated controller's transfer function is provided as

$$G_{PD} = \frac{U(s)}{E(s)} = K_p + K_D s = K_p \left(1 + \frac{K_D}{K_p} s\right) = 0.5453(1 + 1.8s)$$

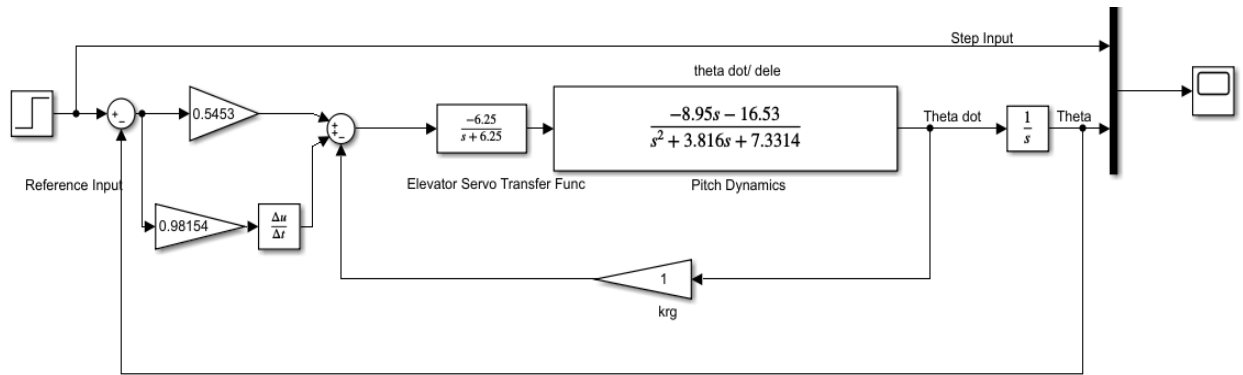


Fig 5.55 Simulink block diagram of Attitude Controller of Hansa-III

The Simulink block diagram of the Attitude Controller of Hansa-III is represented pictorially in Figure 5.55

The result in form of design specifications with and without the controller of Hansa-III is displayed in Table 5.17

S. No	Time Domain Characteristics	Without Controller	With Controller
1.	Settling Time<10sec	5.51 s	7.12 s
2.	Peak Overshoot<20%	31.1	0
3.	Steady State Error<1%	1	1
4.	Rise Time<2sec	0.493 s	0.259 s

Table 5.17 Time Domain Characteristics with & without Controller of Hansa-III

b) Modern control Techniques like pole placement and the linear quadratic regulator are used to estimate the gain matrix, and results are obtained in the form of Time-domain characteristics as displayed in Table 5.18 It is noted that the settling time is too fast for the LQR controller as compared to pole placement and LQR has an outstanding feature of approaching zero steady-state error.

S. No	Closed loop Time-domain response	Design Specification	Pole-placement without Scaling effect	LQR without Scaling effect
1.	Steady-state error	<1%	0.349	0.01
2.	Peak overshoot	<5%	4.59	0.332
3.	Settling Time	<5sec	3.08 s	0.44 s
4.	Rise Time	<2sec	0.793 s	0.16 s

Table5.18 Comparison of Time domain characteristics

The LQR Controller is chosen among traditional and modern approaches and the results obtained in the form of performance characteristics is validated with general aviation aeroplane (Wahid & Hassan, 2012)

S. No	Performance Characteristics	Hansa-III	General Aviation Airplane (Wahid & Hassan, 2012)
1.	Steady-state error	0.01	0.01
2.	Peak overshoot	0.332	4.35
3.	Settling Time	0.44 s	0.3655 s
4.	Rise Time	0.16 s	0.1335 s

Table5.19 LQR Result Validation of Time domain characteristics with General Aviation Airplane(Wahid & Hassan, 2012)

The performance characteristics of Hansa-III compared with General Aviation Airplane as shown below

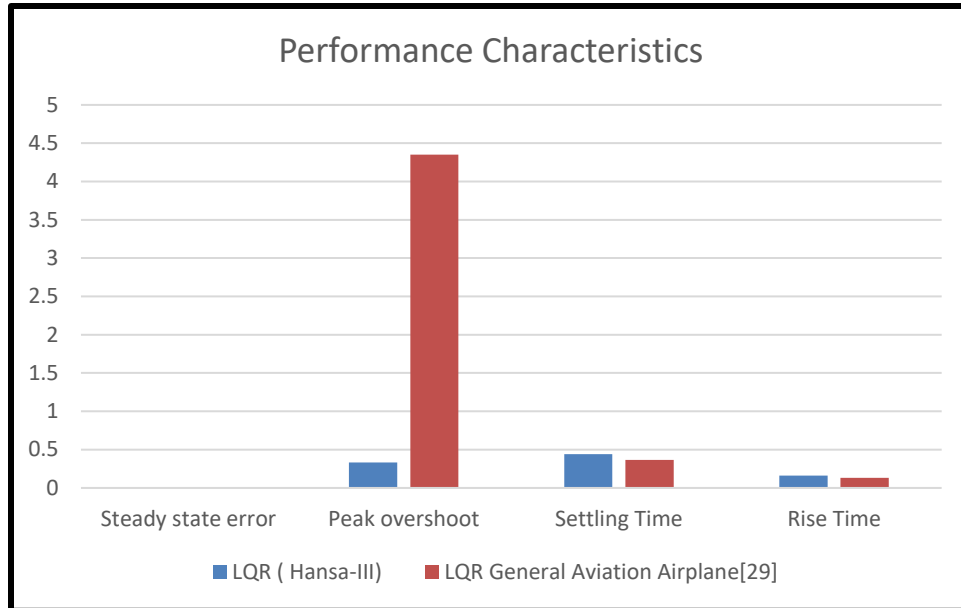


Fig 5.56 LQR Result of Hansa-III with general aviation Airplane (Wahid & Hassan, 2012)

SUMMARY

In this chapter, the basics of an automatic control systems, aircraft stability and Control systems, Aircraft axes systems, and reference frames for the formulation of longitudinal force and moment equations in wind axes were addressed. This chapter focuses on longitudinal stability, and longitudinal modes (short-period, Long-period) for assessing flying handling qualities in terms of damping ratio and frequency. The Longitudinal equations were used to formulate a state–space matrix representation to deduce the transfer function for solving pitch control problems. The gain parameters using different approaches such as closed-loop PID Tuning techniques: ZN, MZN, AH, and TL were used for gain estimation. PID Tuning approaches were also applied to different datasets Multistep, Doublet, and Pulse (refer Appendix D1, D2) for comparison of approaches.

Classical approaches such as Root-locus, and modern control approaches such as Pole-Placement, and LQR are discussed and results are compared for gain optimization. It is observed that the LQR Controller shows the best optimal result amidst classical and modern approaches. The FSFC (full state feedback controller) is designed and optimal control law for pitch control is developed.

CHAPTER -6

AIRCRAFT NAVIGATION SYSTEM

Research and Development in the field of Aircraft Navigation is always fascinating as it applies to finding the exact position, orientation, and velocity of aircraft. This study investigates the problem statements related to parameter estimation for aircraft positioning systems based on inertial sensor measurements provided by Hansa-III aircraft. Attitude and position can be resolved by an accelerometer and gyroscope. M. Jayachandran presented an approach to DR to measure aircraft position. When the GPS is not working, this procedure is useful for navigating. The Navigational algorithm is implemented within the display system of aircraft that receives information about attitude, and position (Jayachandran et al., 2009). Dead Reckoning is applied in numerous navigation applications such as aircraft navigation, automotive navigation, surveillance, mobile robots, and marine navigation. Zeev Berman discussed future aspects of aviation navigation systems as the Dead reckoning system. He presented an actual statistical model and varied wind vectors to match actual data. To measure the horizontal positioning error, he compared the dead reckoning system, standalone inertial sensors, and inertial sensors integrated with the DR system. (Berman, 1998). Parinaz estimated navigational parameters such as position using PDR (Pedestrian Dead Reckoning) of mobile robots. The PDR algorithm was designed to get more accurate gait parameters which will improve the accuracy of position estimates (Kasebzadeh, 2017). Philips integrated GPS and DR sensors to track and navigate low-cost vehicles. Results for GPS, tightly coupled DR, and loosely coupled DR are compared and explained. Tightly coupled DR gives the best optimum result as compared with all three. (G. Mattos,

1994)

Pure Dead Reckoning Technology is economical, cheaper and generate systematic inaccuracies, making it impractical to employ where a precise position-based radio-signal navigation system is needed. The study investigates the performances of tightly coupled INS/GPS, loose couple INS/ GPS, and INS using SIMULINK. Tightly coupled INS/GPS gives better performance than loosely coupled integration as proposed by T. Mahmoud(Mahmoud & Trilaksono, 2018). The DR approach is mitigated in a quad-rotor navigation system for better reliability and accuracy. It enables the quadrotor to estimate the distance from peak to peak. The simulated result shows the accuracy of the navigation solution while comparing INS and QDR approaches. QDR navigation solution is bounded while the INS solution diverges as proposed by A. Shurin (Shurin & Klein, 2020). Integration of the INS-GPS-GLONASS system to enhance systems accuracy is applied for combat aircraft, ships, and long-range missiles is discussed by G.S. Reddy (Reddy & Saraswat, 2013). Dead Reckoning approach is used in UAV as proposed by Lorenzo Fusini using XKF and NLO. IMU sensors such as (acceleration, rate gyros, inclinometer); altimeters; and cameras are used. Position, velocity, and altitude are used as observed states. XKF gives the best optimum result as compared with NLO(Fusini et al., 2017)

The selection of an accurate navigational coordinate estimation method is a big challenging issue for real-time navigation. Some methods like the GNSS Global Navigation satellite system are based on signal transmission through satellite but the challenge faced by these systems is loss of signal connectivity which is handled by using Dead reckoning(Kasebzadeh, 2017). Hansa-III, flight test is regulated and real flight data is gathered using a data acquisition system. Integration of the dead reckoning approach in Hansa-III aircraft is used for the estimation of latitude, longitude, and altitude (ϕ , θ , h) for future navigation prediction. Comparative assessment between dead reckoning and exponential smoothing is presented in tabulated and graphical form.

6.1 DEAD RECKONING

The Dead Reckoning methodology proposed for this study predicts the current location and velocity measurements by using previously determined locations over time elapsed on estimated speed. Pure Dead Reckoning is economical, and cheaper 8 Inertial measurement sensors including accelerometers, magnetometers, and gyroscopes are used for navigation through Dead Reckoning (Reddy & Saraswat, 2013). An accelerometer measures acceleration acting on the moving object to detect position whereas the magnetometer provides information about the direction and estimates magnetic induction. The gyroscope sensor measures the orientation and assesses the angular velocity (p, q, r) of an aircraft and provides position information, and orientation.

As per Figure 6.1, the absolute heading is measured by using sensors (gyroscope, digital compass). An odometer is used to measure the distance S_i .

The set of equations provides the DR solution

$$x_i = x_0 + \sum_{i=0}^{k-1} S_i \cos \theta_i \quad 6.1$$

$$y_i = y_0 + \sum_{i=0}^{k-1} S_i \sin \theta_i \quad 6.2$$

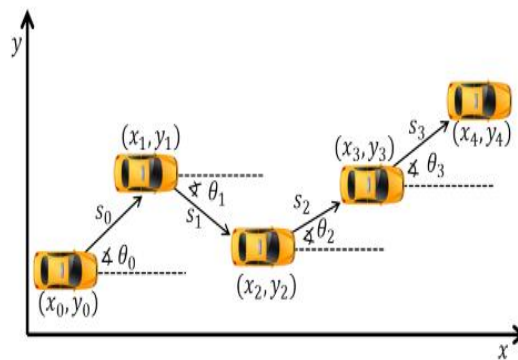


Fig 6.1 Dead Reckoning (Pedro Paulo Liborio Lima do Nascimento, Leandro Aparecido Villas, Bruno Yuji Lino Kimura, 2018)

The heading of the vehicle is the same as the INS heading as a heading is measured from the INS sensor thus $\theta_v = \theta_{INS}$

The NED coordinate system measures vehicle velocities in the North, East, and Down directions. $V_N = V_C \cos \theta$, $V_E = V_C \sin \theta$, $V_D = -\text{Altitude}$. The velocities are integrated to get the distance in the North, and East directions which state $S_E = V_E \Delta t$, $S_N = V_N \Delta t$ where Δt is the sampling time.

Dead Reckoning Algorithm

The approach used to get an accurate navigational parameter using the DR algorithm is explained through a flowchart discussed in Fig 6.2

Block 1 explains the NED North, East, and Down coordinate systems used to determine aircraft velocity in the NED direction.

Block 2 estimates V_N , V_E , V_D using expression as $V_N = V_C \cos \theta$, $V_E = V_C \sin \theta$, $V_D = -\text{Altitude}$

Block 3 estimates S_N , S_E , using expression as $S_E = V_E \Delta t$, $S_N = V_N \Delta t$ and X, Y, and Z coordinate is calculated as $X(K) = X(K-1) + S_E \cos \theta$, $Y(K) = Y(K-1) + S_N \sin \theta$, $Z = -h$

Block 4 depicts aircraft position in X, Y, and Z direction using expression as $X(K) = X(K-1) \pm \Delta X$, $Y(K) = Y(K-1) \pm \Delta Y$, $Z(K) = Z(K-1) \pm \Delta Z$

Block 5 predicts the value of heading, and altitude based on existing values to predict measurements.

Block 6 Aircraft position in X, Y, and Z direction from block 4 is converted to geodetic coordinates as latitude, longitude, and altitude for determination of geographical location.

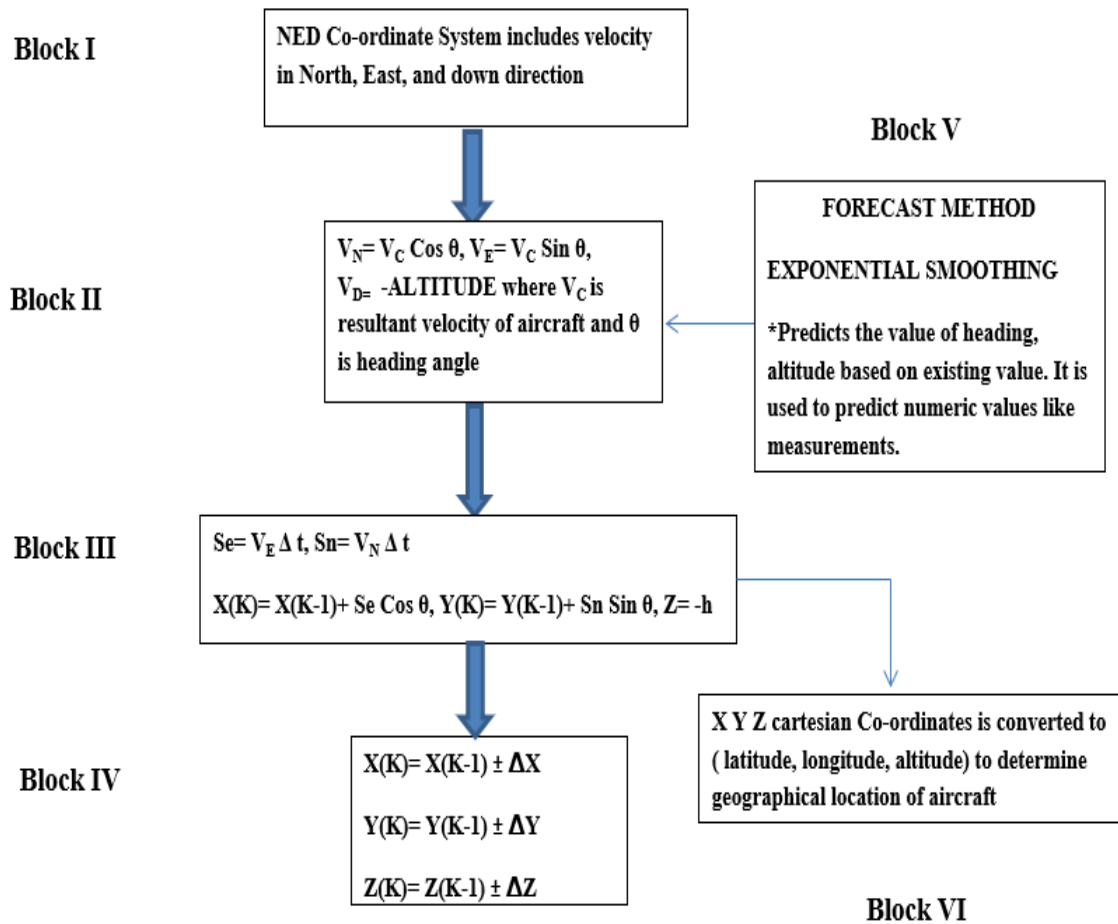


Fig 6.2 Flow chart of Dead Reckoning

ROAD MAP TO ESTIMATE GEODETIC CO-ORDINATES

The road map for geodetic co-ordinate Estimation is shown in Fig 6.3 followed by steps I, II, and III

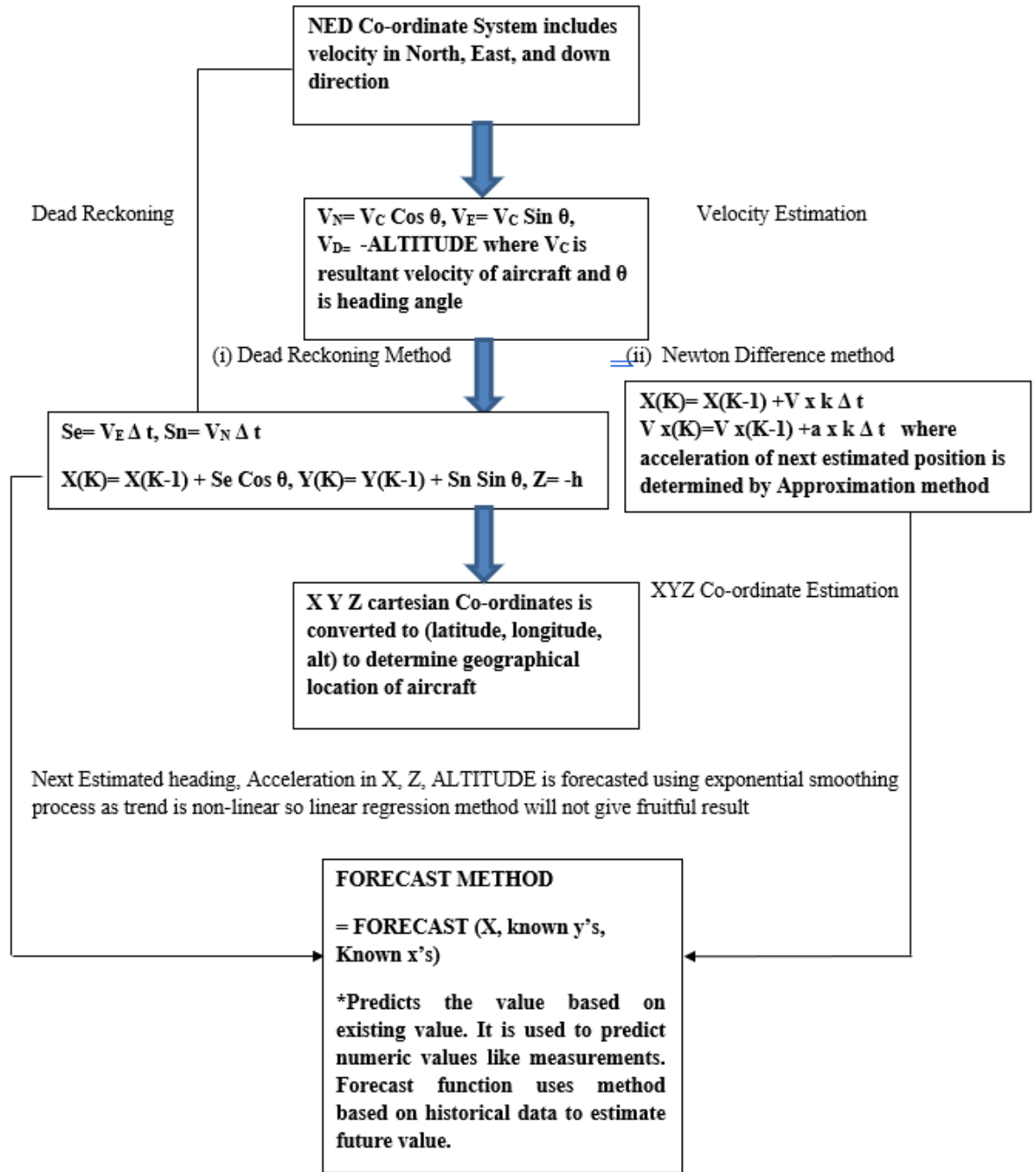


Fig 6.3 RoadMap for geodetic co-ordinate Estimation

STEP1: Heading angle is calculated using formulae $\text{ATAN2}(a_x, a_z)$ as shown in Figure 6.4 where the initial value of (a_x, a_z) is fetched from flight data refer to (Appendix D3) for forecast prediction.

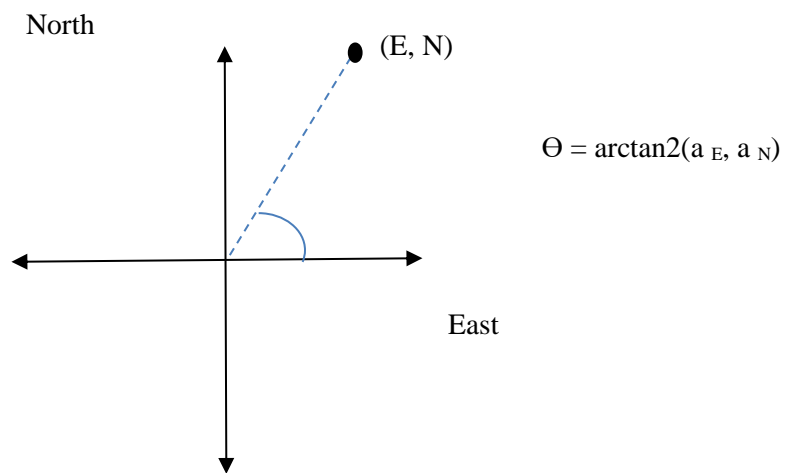
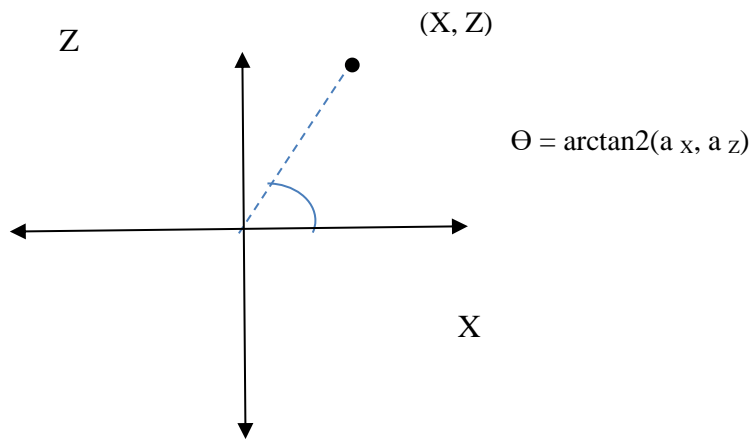
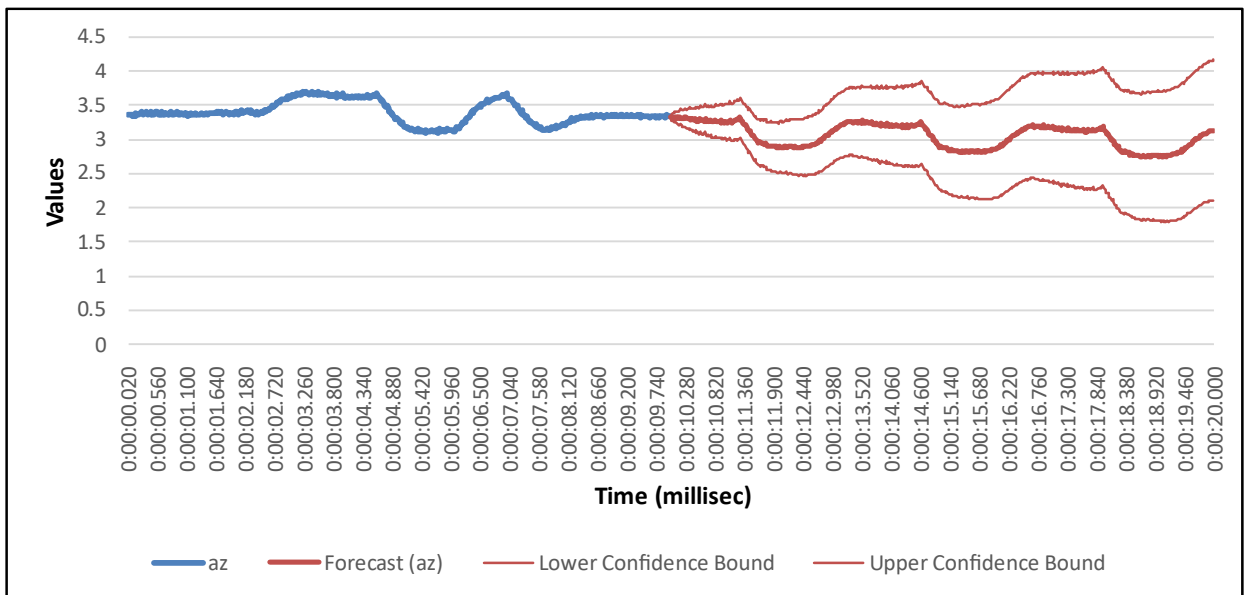
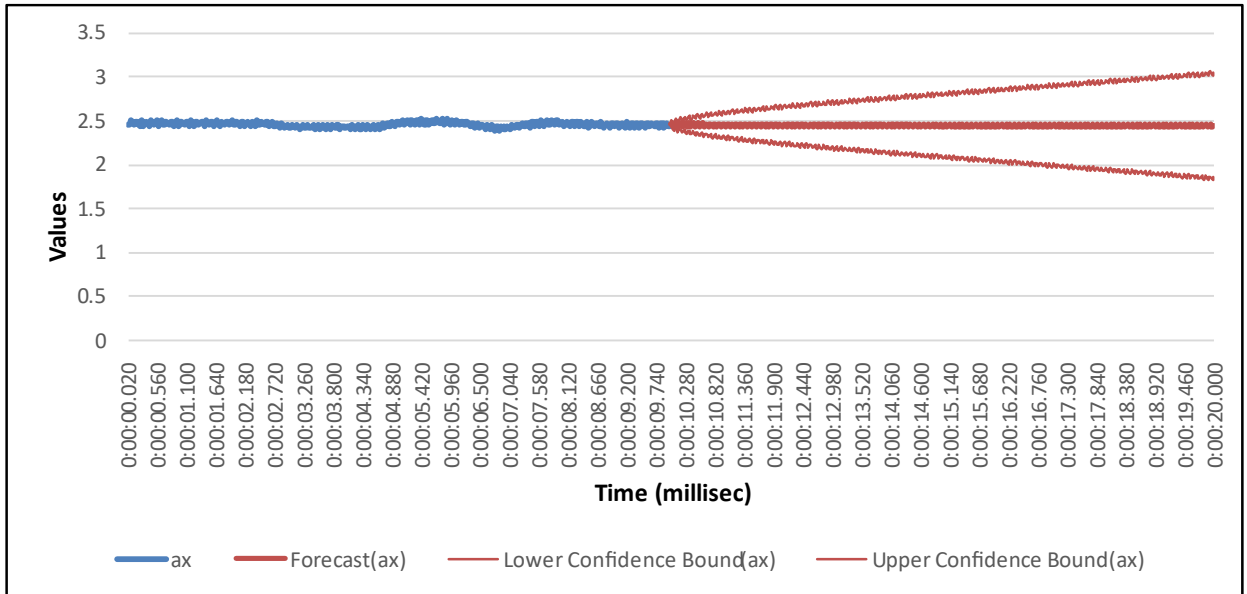


Fig 6.4 NED Coordinate System

A forecast sheet is used in Excel to predict the future value of the heading based on existing value. The flight test of Hansa-III aircraft with a time interval of 10 sec is gathered using a data acquisition system. X-axes resemble Time in (milli-sec) and Y-axes state the value of acceleration in the X-direction. The blue line in the below figure indicates real flight data and bold red line as forecast value and the light red line as lower and upper bounds of the ax.



X-axes resemble Time in (milli-sec) and Y-axes state the value of acceleration in the Z direction, the blue line in the above figure indicates real flight data and bold red line as forecast value, and the light red line as lower and upper bounds of az.

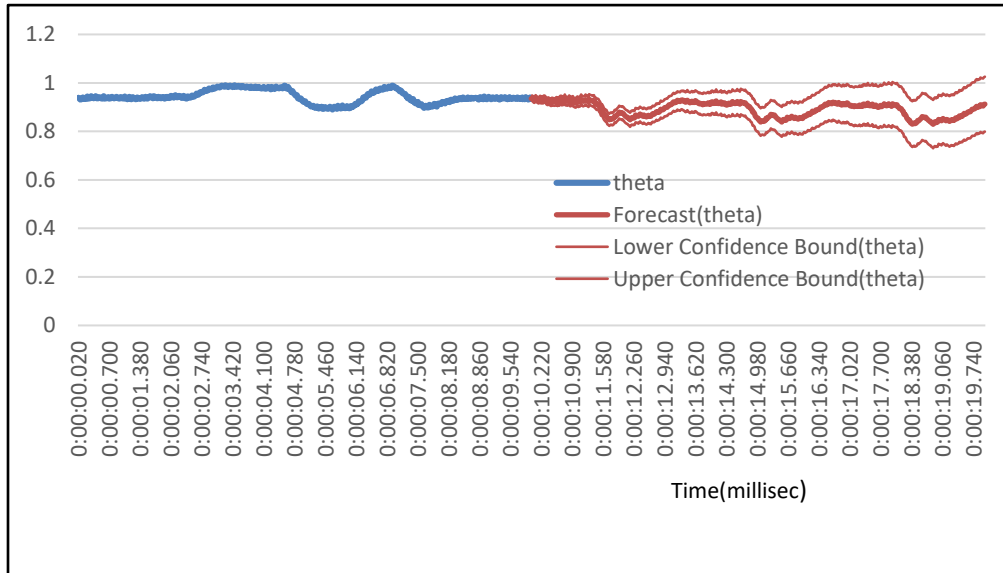


Fig 6.5 Forecast of Acceleration X, Z, and Heading angle

X-axes resemble Time in (milli-sec) and Y-axes state the value of the heading angle in radians where red lines in the curve depict the forecasted heading angle in Fig 6.5. The upper, and lower bounds explain the maximum, and minimum range of the heading angle.

STEP2: Dead Reckoning algorithm used to determine XYZ co-ordinates

$$V_N = V_C \cos \theta, S_N = V_N * \Delta t$$

$$V_E = V_C \sin \theta, S_E = V_E * \Delta t$$

$$V_D = -\text{Altitude}$$

$$X(K) = X(K-1) + S_e \cos \theta$$

$$Y(K) = Y(K-1) + S_n \sin \theta$$

$$Z = -h$$

$$X(K) = X(K-1) \pm \Delta X$$

$$Y(K) = Y(K-1) \pm \Delta Y$$

$$Z(K) = Z(K-1) \pm \Delta Z$$

STEP3: Conversion of X, Y, and Z Co-ordinate to geodetic Co-ordinate (Latitude, longitude, and Altitude) using MATLAB code is displayed in Table 6.1 (refer Appendix B7)

The file xyaS2 contains XYZ Cartesian co-ordinates of 10 sec as mentioned in the code

```
X=xyaS2(:1);  
Y=xyaS2(:2);  
Z=xyaS2(:3);  
X=X (:1);  
Y=Y (:1);  
Z=Z (:1);  
Origin = [80.232293, 26.518886,126.63];  
[Lat, Lon] =local2latlon (X, Y, Z, origin);  
zoom level=12;  
player = geoplayer (Lat (1), Lon (1), zoom Level);  
plot Route (player, Lat, Lon);
```

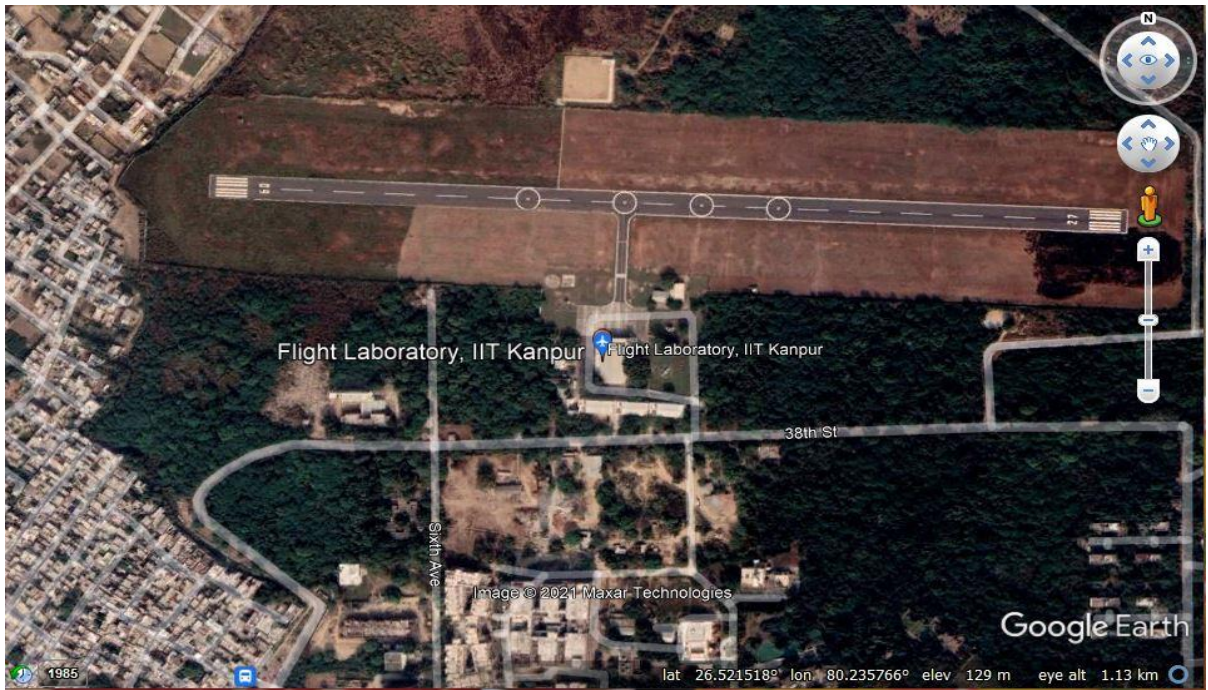


Fig 6.6 Geographical co-ordinates at Initial phase of Flight test, IIT Kanpur
(80.232293, 26.518886, 126.63)

The tabulated form and graphical representation in form of XY coordinate and longitude, latitude is displayed below

X(T)	Y(T)	LONGITUDE	LATITUDE
0.586526	0.318894	80.2323	26.5189
1.174282	0.636558	80.2323	26.5189
1.759109	0.957151	80.2323	26.5189
2.340916	1.280764	80.2323	26.519
2.92379	1.60331	80.2323	26.519
3.512289	1.920231	80.2323	26.519
4.095947	2.241993	80.2323	26.519
4.678165	2.565195	80.2323	26.519
5.257532	2.891248	80.2323	26.519
5.839366	3.214834	80.2323	26.5191

Table 6.1 Conversion XY coordinate to Latitude and Longitude

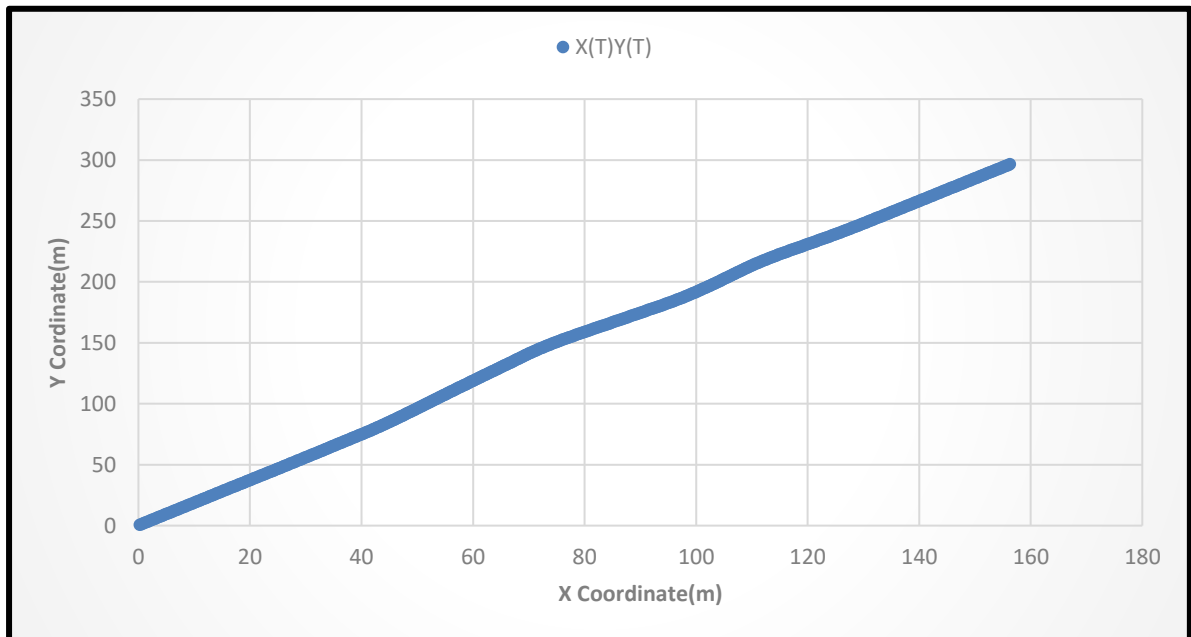


Fig 6.7 Forecasted Value of X, Y Aircraft Coordinates using DR

X-axes resemble X coordinates in (m) and Y axes state the value of Y coordinates in (m) in Fig 6.7. The blue line in the above figure indicates the XY

coordinate of the aircraft for the next 10 sec.

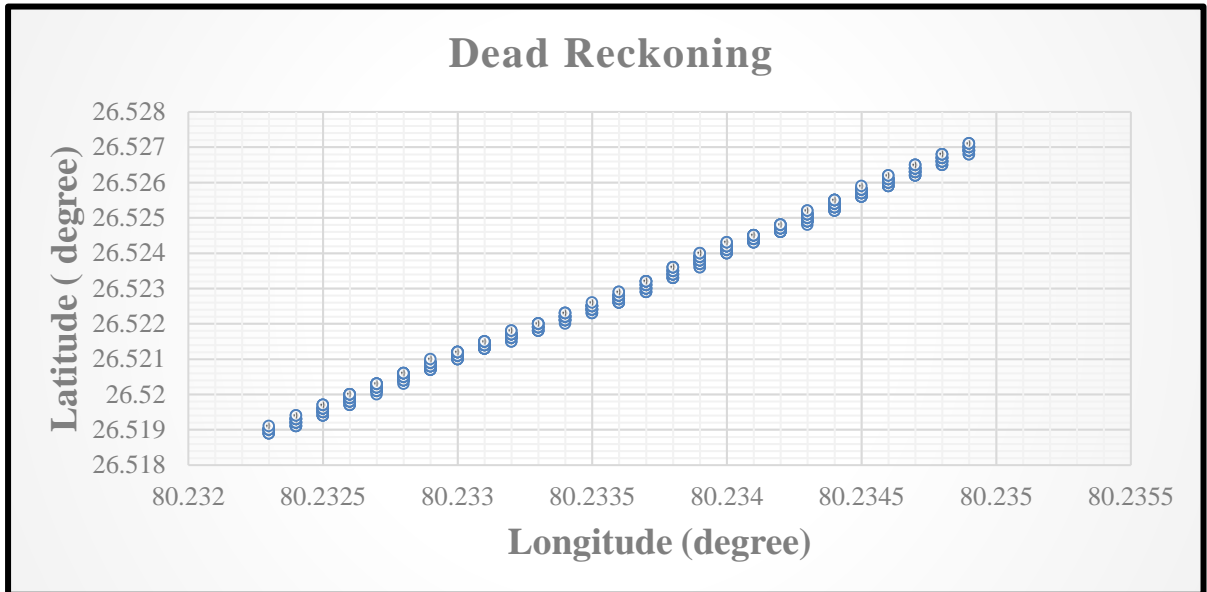


Fig 6.8 Forecasted Value of Longitude, Latitude in degrees using DR

Fig 6.8 axes resemble Longitude in (degrees) and Y axes state value of Latitude in (degrees). The blue line in the above figure indicates the aircraft position for the next 10 sec in form of (Longitude, Latitude)

6.2 NEWTON DIFFERENCE

This equation predicts the current location based on a previously determined equation in the discrete-time interval which is the concept of the dead reckoning approach.

The Inertial Measurement Unit includes an accelerometer that measures 3-axis translational a_x , a_y , a_z . The gyroscope measures 3-axis rotational p, q, and r values, and the air data sensor measures airspeed. Refer to Appendix D3. The acceleration of the object is the time rate of change of the body's momentum, according to Newton's second law of motion.

$$\frac{dV_x}{dt} = a_x, \quad \frac{V_x(t+\Delta t) - V_x(t)}{\Delta t} = a_x, \quad V_x(t+\Delta t) = V_x(t) + a_x \Delta t$$

$$X(K) = X(K-1) + V_x(k) * \Delta t \quad 6.3$$

$$V_x(K) = V_x(K-1) + a_x(k) * \Delta t \quad 6.4$$

$$z(K) = z(K-1) + V_z(k) * \Delta t \quad 6.5$$

$$V_z(K) = V_z(K-1) + a_z(k) * \Delta t \quad 6.6$$

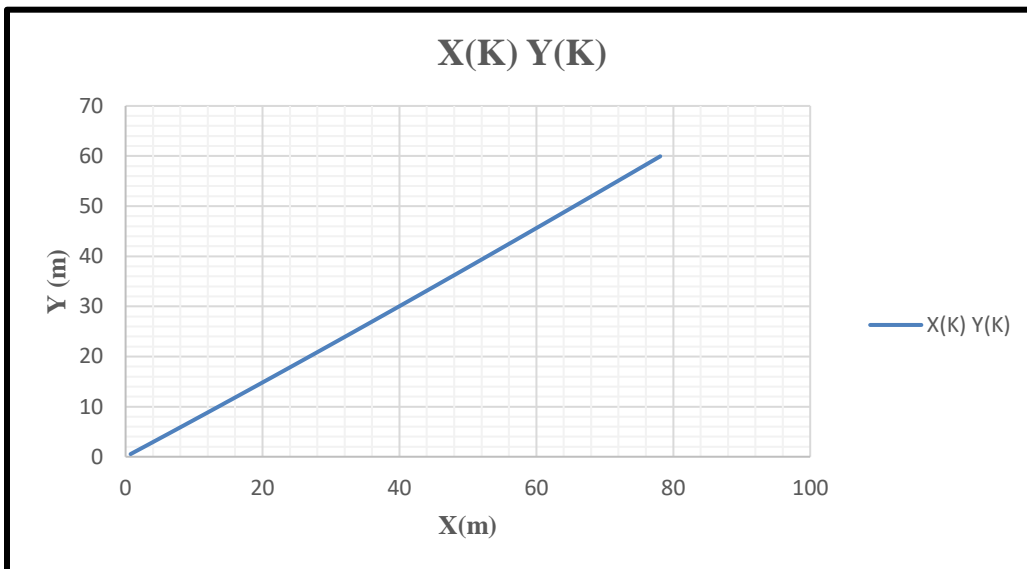


Fig 6.9 Forecasted Value of X, Y Aircraft coordinates using Newton-Difference Method

X-axes resemble X coordinates in (m) and Y-axes state the values of Y coordinates in (m). The blue line in figure 6.9 indicates XY coordinate of the

aircraft for the next 10 sec using newton-difference formulae

Comparison of Dead Reckoning and Difference formulae in terms of X, Y Coordinates

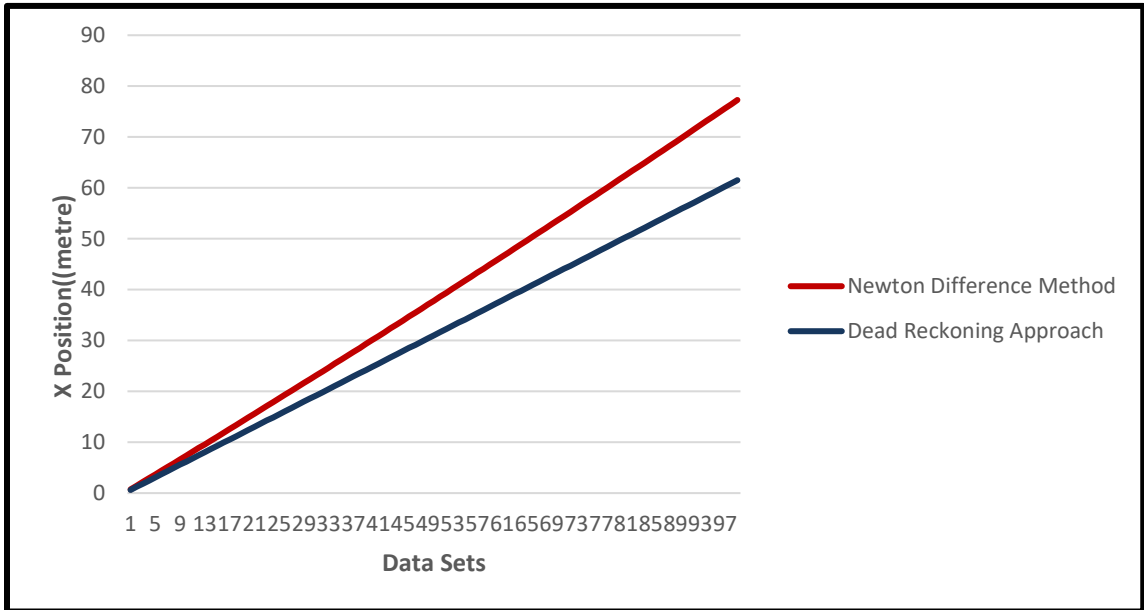


Fig 6.10 Comparison of Forecasted Value of X Position of aircraft using DR and Newton-Difference Method

X-axes resemble 100 datasets and Y-axes state value of X coordinates in (m). The blue line and red line in figure 6.10 indicate the X position of the aircraft for the next 10 seconds using the DR and Newton Difference method.

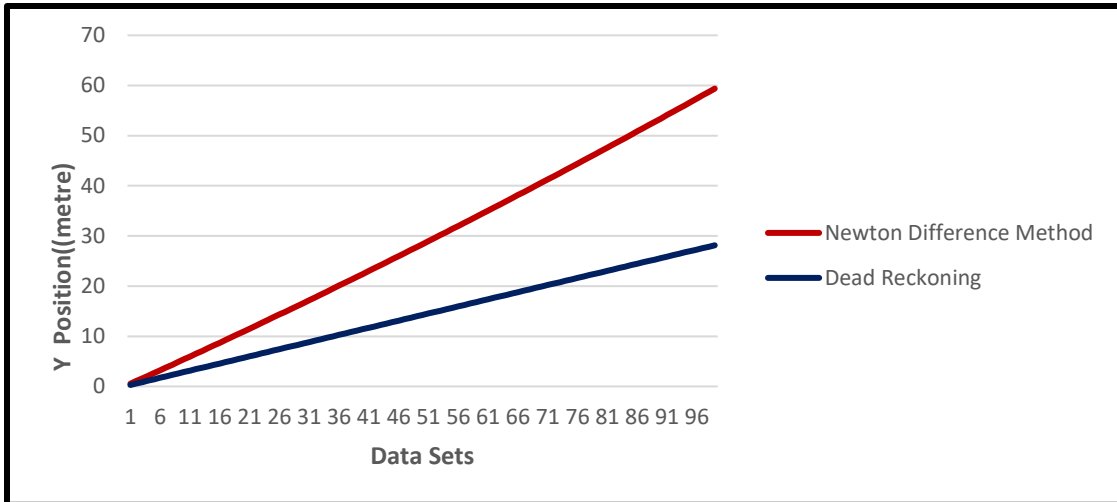


Fig 6.11 Comparison of Forecasted Value of Y Position of aircraft using DR and Newton-Difference Method

X-axes resemble 100 datasets and Y-axes state the values of Y coordinates in (m). The blue line and red line in above figure 6.11 indicate the Y position of the aircraft for the next 10 seconds using the DR and Newton Difference method

Aircraft Position Estimation

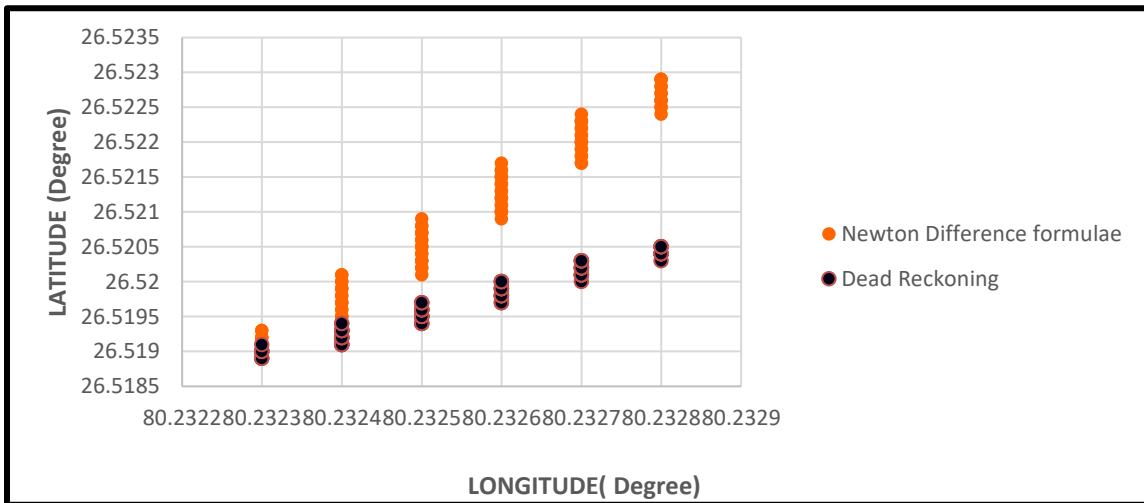


Fig 6.12 Comparison of Forecasted Value of Longitude, and Latitude of aircraft using DR and Newton-Difference Method

X-axes resemble Longitude in (degrees) and Y-axes state the value of Latitude in (degrees). The black line and orange line in above figure 6.12 indicate (the longitude and latitude) of the aircraft for the next 10 seconds using the DR and Newton Difference method.

LONGITUDE (N.D)	LATITUDE (N.D)	LONGITUDE (D.R)	LATITUDE (D.R)	%Error (LON)	%Error (LAT)
80.2323	26.519	80.2323	26.5189	0	-0.00038
80.2323	26.5193	80.2324	26.5191	0.000125	-0.00075
80.2324	26.5201	80.2325	26.5194	0.000125	-0.00264
80.2325	26.5208	80.2326	26.5197	0.000125	-0.00415
80.2326	26.5217	80.2327	26.52	0.000125	-0.00641
80.2328	26.5224	80.2327	26.5203	-0.00012	-0.00792

Table 6.2: Estimation of Percentage Error

It is found that there is a slight variation in the values of latitude but the values of longitude are quite similar for both techniques. The percentage error is quite small for longitude and latitude as shown in Table 6.2

6.3 VALIDATION

Statistical Technique in Time Series for validating the result using the Dead Reckoning approach is discussed below:

Exponential smoothing is used to study trend analysis of the non-linear irregular patterns of aircraft location. The Longitude of the next 5 sec is forecasted in the below section using exponential smoothing time series analysis. The exponential smoothing formulae

$$F_t = \alpha.M_{t-1} + (1 - \alpha)F_{t-1}$$

6.7

α is the smoothing constant which lies in the range $0 \leq \alpha \leq 1$; F_t is the forecasted value for time t ; F_{t-1} is the previous forecasted value for time $(t-1)$; M_{t-1} is the previously measured value of the physical quantity that needs to be forecasted at the time $(t-1)$. It is also expressed in term of Damping factor as $\zeta = 1 - \alpha$; $\zeta = 0.7$ as calculated by (JAISWAL & PRAKASH, 2022)

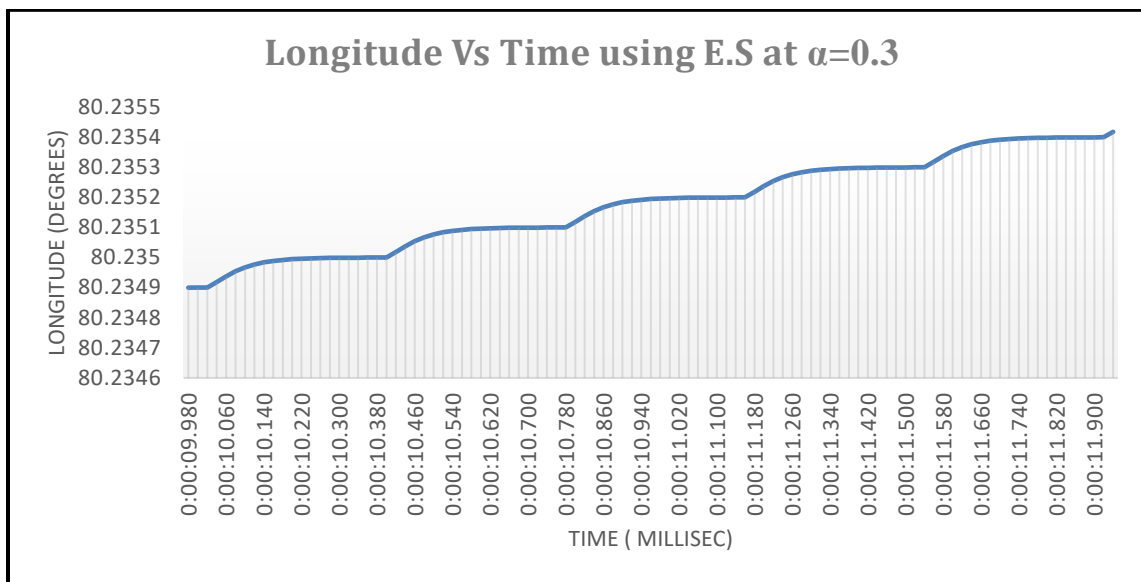


Fig 6.13: Forecasted Value of Longitude using Exponential Smoothing Technique

The Longitude of Fig 6.13 of the next 10 sec is forecasted in the above section using exponential smoothing time series analysis for $\alpha=0.3$

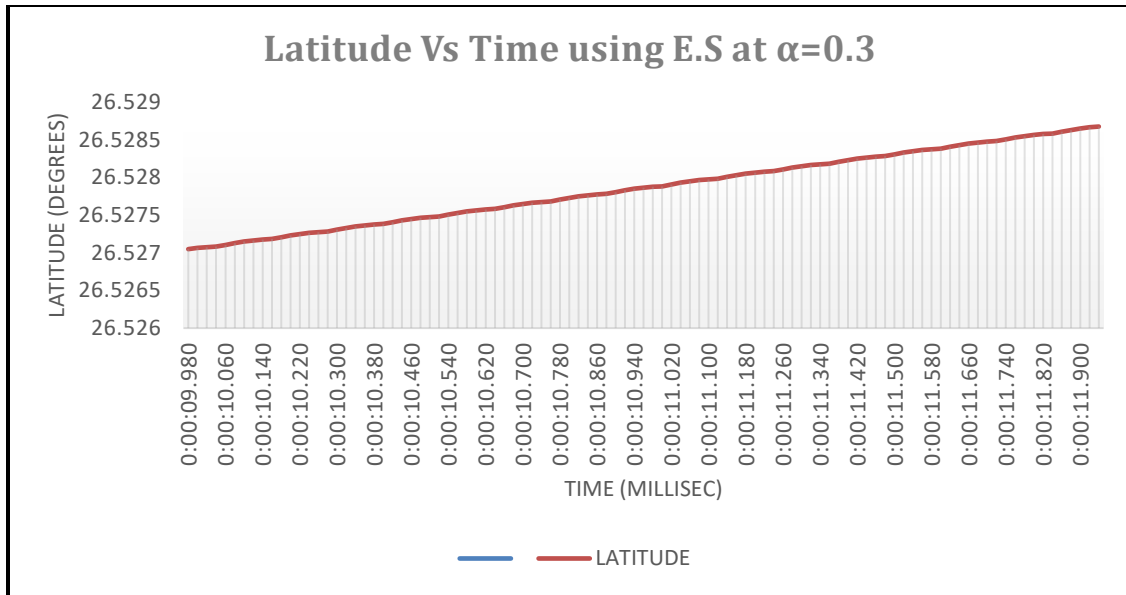


Fig 6.14 Forecasted Value of Latitude using Exponential Smoothing Technique

The Latitude of Fig 6.14 of the next 10 sec is forecasted in the above section using exponential smoothing time series analysis for $\alpha=0.3$

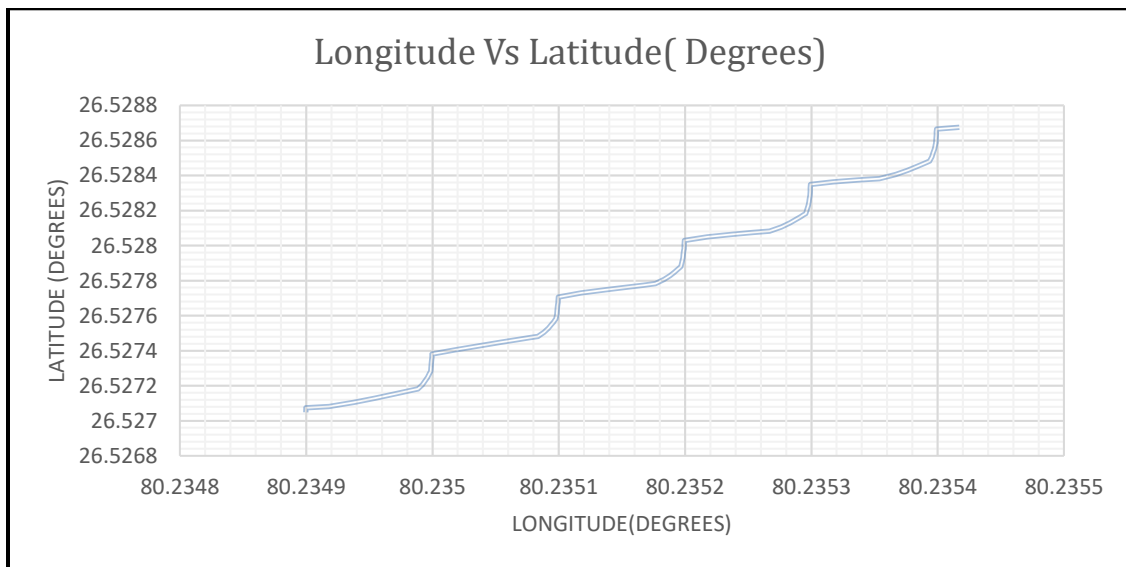


Fig 6.15 Forecasted Value of Longitude, Latitude in degrees using Exponential Smoothing Technique

The Longitude and Latitude of the next 10 sec are forecasted in the below section using exponential smoothing time series analysis for $\alpha=0.3$ and results are compared with Newton Difference and Dead Reckoning.

Dead Reckoning		Newton Difference		Exponential Smoothing alpha 0.3	
LONGITUDE	LATITUDE	LONGITUDE	LATITUDE	LONGITUDE	LATITUDE
80.2323	26.5189	80.2323	26.5189	80.2323	26.519
80.2323	26.5189	80.2323	26.519	80.2323	26.519
80.2323	26.5189	80.2323	26.519	80.2323	26.519
80.2323	26.519	80.2323	26.519	80.2323	26.519
80.2323	26.519	80.2323	26.5191	80.2323	26.519
80.2323	26.519	80.2323	26.5191	80.2323	26.519
80.2323	26.519	80.2323	26.5192	80.2323	26.519
80.2323	26.519	80.2323	26.5192	80.2323	26.519
80.2323	26.519	80.2323	26.5192	80.2323	26.519
80.2323	26.5191	80.2323	26.5193	80.2323	26.519
80.2324	26.5191	80.2323	26.5193	80.2323	26.519
80.2324	26.5191	80.2324	26.5194	80.2324	26.519
80.2324	26.5191	80.2324	26.5194	80.2325	26.519
80.2324	26.5191	80.2324	26.5194	80.2325	26.519
80.2324	26.5191	80.2324	26.5195	80.2325	26.519
80.2324	26.5192	80.2324	26.5195	80.2325	26.519
80.2324	26.5192	80.2324	26.5195	80.2325	26.519
80.2324	26.5192	80.2324	26.5196	80.2325	26.519
80.2324	26.5192	80.2324	26.5196	80.2325	26.519
80.2324	26.5192	80.2324	26.5197	80.2325	26.519
80.2324	26.5192	80.2324	26.5197	80.2325	26.519
80.2324	26.5193	80.2324	26.5197	80.2325	26.520
80.2324	26.5193	80.2324	26.5198	80.2325	26.520
80.2324	26.5193	80.2324	26.5198	80.2325	26.520
80.2324	26.5193	80.2324	26.5199	80.2325	26.520
80.2324	26.5193	80.2324	26.5199	80.2325	26.520
80.2324	26.5193	80.2324	26.5199	80.2325	26.520
80.2324	26.5194	80.2324	26.52	80.2325	26.520
80.2324	26.5194	80.2324	26.52	80.2325	26.520
80.2325	26.5194	80.2324	26.5201	80.2325	26.520
80.2325	26.5194	80.2324	26.5201	80.2325	26.520
80.2325	26.5194	80.2325	26.5201	80.2326	26.520
80.2325	26.5194	80.2325	26.5202	80.2326	26.520
80.2325	26.5195	80.2325	26.5202	80.2326	26.520

80.2325	26.5195	80.2325	26.5203	80.2326	26.520
80.2325	26.5195	80.2325	26.5203	80.2326	26.520
80.2325	26.5195	80.2325	26.5203	80.2326	26.520
80.2325	26.5195	80.2325	26.5204	80.2326	26.520
80.2325	26.5195	80.2325	26.5204	80.2326	26.520
80.2325	26.5196	80.2325	26.5205	80.2326	26.520
80.2325	26.5196	80.2325	26.5205	80.2326	26.520

Table 6.3: Comparison of values of Longitude, Latitude using Exponential Smoothing, Newton Difference Method, and Dead Reckoning Technique

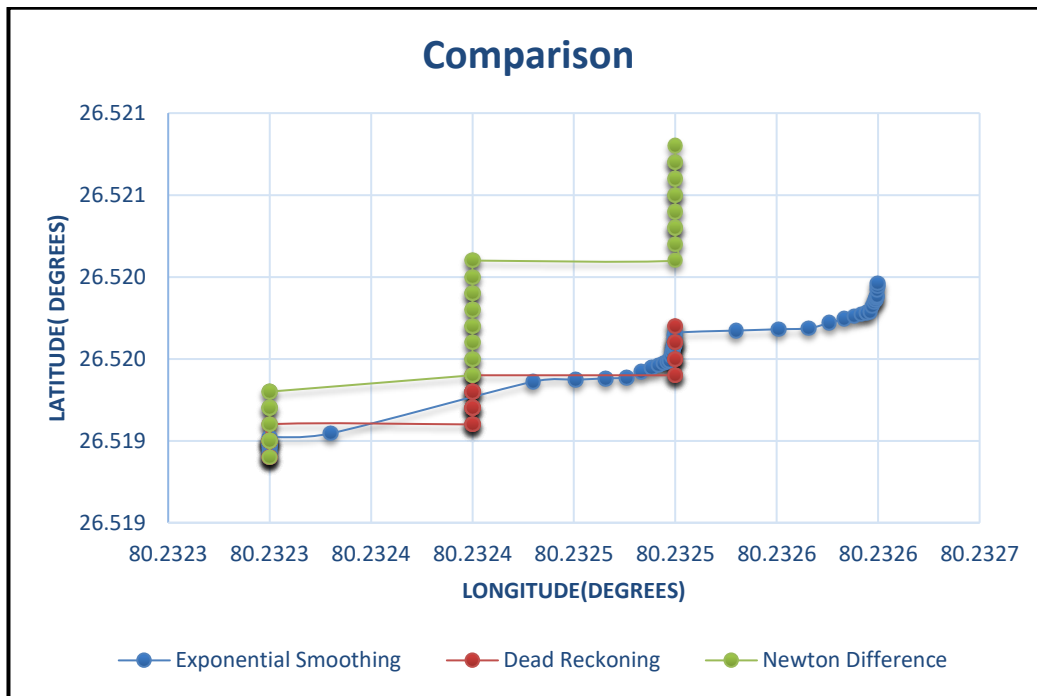


Fig 6.16 Graphical Representation of Longitude, Latitude using (D.R, ES, ND)

In contrast to the latitude of Newton difference, which is fairly distant from DR and ES, the values of longitude and latitude of dead reckoning superimpose with exponential smoothing in figure 6.16 given. As a consequence, exponential smoothing supports the outcome obtained through DR methodology. The latitude and longitude error percentages are seen to be quite low, which strongly supports the geodetic navigational conclusion.

SUMMARY

The Dead Reckoning algorithm is used in this chapter to forecast Hansa-III's current location based on its prior location over elapsed time on estimated speed. The Newton-Difference method and Exponential Smoothing Technique are used to compare and validate the Dead Reckoning data in the form of longitude, latitude, and altitude.

CHAPTER- 7

CONCLUSION AND FUTURE WORK

An autopilot is a system that controls the vehicle trajectory without manual controls. The research work emphasizes the parameter estimation of research cum trainer aircraft along with the autopilot design for pitch control of the aircraft in addition to the Integration of the Dead Reckoning approach to estimate the position of Hansa-III Aircraft for future prediction.

There is a lot of research on parameter estimation. A large researcher focused their work on parameter estimation by estimating parameters using several methodologies including OEM, FEM, and EEM, however, the study expanded not only in the parameter estimation area but also on the application side. To make the study stand out, the research effort has been expanded by constructing a pitch controller and putting a revolutionary navigational dead-reckoning approach into practice.

The methodology adopted for Parameter Estimation is Maximum likelihood and an observation is made that Aerodynamic derivative values derived with ML are fairly accurate and close to W.T values for most datasets. There is a maximum deviation in the values from Wind Tunnel result in the case of pulse Input as compared to Multi-step and Doublet thus Multi-step elevator control input is more consistent as compared to different elevator Inputs.

In the context of attitude control design in longitudinal motion, aircraft is modelled and a state-space representation of the system is developed, controllers are designed on MATLAB environment using Control System Toolbox thus performances in

Time and Frequency domain using different techniques such as Root-Locus, Pole-Placement, Linear Quadratic Regulator are analysed and compared by setting some design specifications.

In this thesis, the simulation results obtained using root-locus, pole-placement and LQR illustrate and conclude that the LQR controller settles rapidly as T_s is 0.44s as compared to pole-placement with excellent property of eliminating steady-state error to zero which justifies robust-free, good performance characteristics, the efficiency of the controller against disturbances.

It is observed that no research paper is been published related to the navigation of Hansa-III henceforth, the dead reckoning navigational technique will be implemented to study the attitude, and orientation of the system so that it can be used for surveillance in terrain-prone areas, aerial photography, monitoring of floods/droughts.

The study incorporates the implementation of the navigational approach to estimate aircraft position. The result of the Dead Reckoning approach is compared with exponential smoothing in the form of longitude, and latitude and concludes that the percentage error of Longitude, and latitude is found to be very less which validates the result dominantly. Integration Dead Reckoning and Designing autonomous control system of Hansa-III singularize the work and make study novel.

FUTURE SCOPE

The future prospects of the research on the basis of design techniques developed in this study are outlined as:

1. Parameter Estimation of an Aircraft in a non-linear state is beyond the

range of this study so the Neural Gauss-Newton method may be applied to consider non-linear aerodynamics. NGN will be more effective than ML for stall conditions, and unsteady states.

2. Non-linear MIMO Systems for controller design are beyond the scope of the research study. The proposed controller applies to SISO linear, time-variant systems.
3. An extension of the research work to design the attitude controllers (roll, Yaw) in lateral directional motion.
4. The proposed methodology to use neural networks and fuzzy logic can be extended to integrate flexibility, and the accuracy of the controller. Fuzzy logic handle system and measurement noise effectively hence considered for future application as signal processing, control system, structural health monitoring, fault-tolerant detection control system, and monitoring of environmental disasters. System Identification of Gallinaceous machines, and electric flying cars such as urban air mobility (UAM) creating new opportunities in transport engineering that need to be investigated in future(Postorino & Sarné, 2020).
5. One more extension of the research study is the incorporation of different types of aircraft as this study involves the research trainer aircraft, Hansa-III.
6. Fuzzy logic effectively handles system and measurement noise; as a result, it is being explored for use in the future in areas such as signal processing, control systems, monitoring structural health, fault-tolerant detection controls, and environmental disaster monitoring.

CHAPTER-8

REFERENCES

- Ahn, H. S., Bhambhani, V., & Chen, Y. (2009). Fractional-order integral and derivative controller for temperature profile tracking. *Sadhana - Academy Proceedings in Engineering Sciences*, 34(5), 833–850. <https://doi.org/10.1007/s12046-009-0049-2>
- Ansari, S. A., Zbikowski, R., & Knowles, K. (2006). Aerodynamic modelling of insect-like flapping flight for micro air vehicles. *Progress in Aerospace Sciences*, 42(2), 129–172. <https://doi.org/10.1016/j.paerosci.2006.07.001>
- Ashraf, A., Mei, W., Gaoyuan, L., Kamal, M. M., & Mutahir, A. (2018). Linear Feedback and LQR Controller Design for Aircraft Pitch Control. *2018 IEEE 4th International Conference on Control Science and Systems Engineering, ICCSSE 2018*, 276–278. <https://doi.org/10.1109/CCSSE.2018.8724780>
- Asraf, O., Shama, F., & Klein, I. (2022). PDRNet: A Deep-Learning Pedestrian Dead Reckoning Framework. *IEEE Sensors Journal*, 22(6), 4932–4939. <https://doi.org/10.1109/JSEN.2021.3066840>
- Basu, A., Mohanty, S., & Sharma, R. (2016). Designing of the PID and FOPID controllers using conventional tuning techniques. *Proceedings of the International Conference on Inventive Computation Technologies, ICICT 2016*, 2(1). <https://doi.org/10.1109/INVENTIVE.2016.7824789>
- Berman, Z. (1998). *The Role of Dead Reckoning and Inertial Sensors in Future General Aviation Navigation*. 0–7.
- Boeing-747*. (n.d.). https://en.wikipedia.org/wiki/Boeing_747
- BOSSERT DAVID E, & KELLY, C. (2002). AIAA 2002-4646 PID and Fuzzy Logic Pitch Attitude Hold Systems for a Fighter Jet Dr . DAVID E . BOSSERT , Lt Col , USAF * US Air Force Academy Dr . KELLY COHEN , Lt Col , Israeli Ministry of Defense % Visiting Researcher , US Air Force Academy Table 1- Pl. *Defense, August*.
- Bryan, G. . (1911). *Stability in Aviation: An Introduction to Dynamical Stability as*

Applied to Motions of Aeroplane.

- Caetano, J., De Visser, C., De Croon, G., Remes, B., De Wagter, C., Verboom, J., & Mulder, M. (2013). Linear aerodynamic model identification of a flapping wing MAV based on flight test data. *International Journal of Micro Air Vehicles*, 5(4), 273–286. <https://doi.org/10.1260/1756-8293.5.4.273>
- Chauhan, R. K., & Singh, S. (2018). Review of aerodynamic parameter estimation techniques. *2017 International Conference on Infocom Technologies and Unmanned Systems: Trends and Future Directions, ICTUS 2017, 2018-Janua*, 864–869. <https://doi.org/10.1109/ICTUS.2017.8286127>
- Chrif, L., & Kadda, Z. M. (2014). Aircraft control system using LQG and LQR controller with optimal estimation-Kalman filter design. *Procedia Engineering*, 80, 245–257. <https://doi.org/10.1016/j.proeng.2014.09.084>
- Dang, K. N., Lee, G., & Kang, T. (2015). Linear quadrotor modelling and attitude controller design based on experimental data. *ICCAS 2015 - 2015 15th International Conference on Control, Automation and Systems, Proceedings, Iccas*, 472–476. <https://doi.org/10.1109/ICCAS.2015.7364963>
- Debaleena, M., Supritam, B., Bahswati, G., & Ratna, G. (2016). Guaranteed Performance PID Controller for UAV Pitch control. In IEEE (Ed.), *IEEE first International Conference on Control, Measurement and Instrumentation (CMI)* (Issue Cmi, pp. 172–176).
- Deepa, S. N., & Sudha, G. (2016). Longitudinal control of aircraft dynamics based on optimization of PID parameters. *Thermophysics and Aeromechanics*, 23(2), 185–194. <https://doi.org/10.1134/S0869864316020049>
- Devalla, V., & Prakash, O. (2014). Developments in unmanned powered parachute aerial vehicle: A review. *IEEE Aerospace and Electronic Systems Magazine*, 29(11), 6–20. <https://doi.org/10.1109/MAES.2014.130173>
- Do Nascimento, P. P. L. L., Kimura, B. Y. L., Guidoni, D. L., & Villas, L. A. (2018). An integrated dead reckoning with cooperative positioning solution to assist GPS NLOS using vehicular communications. *Sensors (Switzerland)*, 18(9), 1–28. <https://doi.org/10.3390/s18092895>
- Dornier-228*. (n.d.). https://en.wikipedia.org/wiki/Dornier_228
- Ellington, C. P. (1984). The aerodynamics of hovering insect flight. II. Morphological parameters. *Philosophical Transactions of the Royal Society of London. B, Biological Sciences*, 305(1122), 17–40. <https://doi.org/10.1098/rstb.1984.0050>
- Finck, R. D. (1978). USAF Stability and Control DATCOM. *Flight Dynamics Laboratory*, 18(4), 3200.

<http://linkinghub.elsevier.com/retrieve/pii/0022460X71901052>

- Fusini, L., Johansen, T. A., & Fossen, T. I. (2017). Dead reckoning of a fixed-wing UAV with inertial navigation aided by optical flow. *2017 International Conference on Unmanned Aircraft Systems, ICUAS 2017*, 1250–1259. <https://doi.org/10.1109/ICUAS.2017.7991433>
- G.Mattos, P. (1994). *Integrated gps and Dead Reckoning for low-cost vehicle navigation and tracking*.
- George, V. I. (2012). *Aircraft Yaw Control System using LQR and Fuzzy Logic Controller*. 45(9), 25–30.
- Göttlicher, C., Gnoth, M., Bittner, M., & Holzapfel, F. (2016). Aircraft parameter estimation using optimal control methods. *AIAA Atmospheric Flight Mechanics Conference, January*, 1–18. <https://doi.org/10.2514/6.2016-1534>
- Grauer, J. A. (2015). Real-time data-compatibility analysis using output-error parameter estimation. *Journal of Aircraft*, 52(3), 940–947. <https://doi.org/10.2514/1.C033182>
- Greenberg, H. (1951). *A survey of methods for determining stability parameters of an airplane from dynamic flight measurements*. April. http://digital.library.unt.edu/ark:/67531/metadc55667/m2/1/high_res_d/19930082979.pdf
- Haddar, M., Chaari, R., Baslamisli, S. C., Chaari, F., & Haddar, M. (2021). Intelligent optimal controller design applied to quarter car model based on non-asymptotic observer for improved vehicle dynamics. *Proceedings of the Institution of Mechanical Engineers. Part I: Journal of Systems and Control Engineering*, 235(6), 929–942. <https://doi.org/10.1177/0959651820958831>
- Hamel, P. G. (1979). *Aircraft Parametric Identification Methods and their application Survey and future aspects*, AGARD (Issue c).
- Hamel, P. G. (2019). *Advances in Aerodynamic Modeling for Flight Simulation and Control Design* *Advances in Aerodynamic Modeling for Flight Simulation and Control Design* *. February.
- Hamel, P. G., & Jategaonkar, R. V. (1996a). Evolution of flight vehicle system identification. *Journal of Aircraft*, 33(1), 9–28. <https://doi.org/10.2514/3.46898>
- Hamel, P. G., & Jategaonkar, R. V. (1996b). Evolution of flight vehicle system identification. *Journal of Aircraft*, 33(1), 9–28. <https://doi.org/10.2514/3.46898>
- Hardier, G. (2015). An extended U-D algorithm with multiple forgetting factors for

- rls estimation of model parameters. *IFAC-PapersOnLine*, 28(21), 200–207. <https://doi.org/10.1016/j.ifacol.2015.09.528>
- Hardier, G., & Bucharles, A. (2010). On-line parameter identification for in-flight aircraft monitoring. *27th Congress of the International Council of the Aeronautical Sciences 2010, ICAS 2010*, 4, 2885–2896.
- Hardier, G., Ferreres, G., & Seren, C. (2016). A recursive estimation algorithm to track aircraft model parameters. *Conference on Control and Fault-Tolerant Systems, SysTol, 2016-Novem*, 790–797. <https://doi.org/10.1109/SYSTOL.2016.7739844>
- Harper, R. P., & Cooper, G. E. (1986). Handling qualities and pilot evaluation. *Journal of Guidance, Control, and Dynamics*, 9(5), 515–529. <https://doi.org/10.2514/3.20142>
- He, Z., & Zhao, L. (2014). A simple attitude control of quadrotor helicopter based on Ziegler-Nichols rules for tuning pd parameters. *Scientific World Journal*, 2014. <https://doi.org/10.1155/2014/280180>
- Heredia, G., & Ollero, A. (2009). Sensor fault detection in small autonomous helicopters using observer/Kalman filter identification. *IEEE 2009 International Conference on Mechatronics, ICM 2009*, 00(April). <https://doi.org/10.1109/ICMECH.2009.4957236>
- Hoffer, N. V., Coopmans, C., Jensen, A. M., & Chen, Y. (2013). Small low-cost unmanned aerial vehicle system identification: A survey and categorization. *2013 International Conference on Unmanned Aircraft Systems, ICUAS 2013 - Conference Proceedings*, 897–904. <https://doi.org/10.1109/ICUAS.2013.6564775>
- Iliff, K. W. (1989). Parameter Estimation for Flight Vehicles. *J. Guidance September-October*, 12(5).
- JAISSWAL, R., & PRAKASH, O. (2022). Classical and Modern gain estimation approach of PID controller for the pitch control of the RCTA aircraft. *INCAS BULLETIN*, 14(1), 39–56. <https://doi.org/10.13111/2066-8201.2022.14.1.4>
- Jaiswal, R., Prakash, O., & Chaturvedi, S. K. (2020). A preliminary study of parameter estimation for fixed wing aircraft and high endurance parafoil aerial vehicle. *INCAS Bulletin*, 12(4), 95–109. <https://doi.org/10.13111/2066-8201.2020.12.4.9>
- Jameson, P. D., & Cooke, A. (2012a). Developing real-time system identification for UAVs. *Proceedings of the 2012 UKACC International Conference on Control, CONTROL 2012, September*, 958–963. <https://doi.org/10.1109/CONTROL.2012.6334761>

- Jameson, P. D., & Cooke, A. (2012b). Developing real-time system identification for UAVs. *Proceedings of the 2012 UKACC International Conference on Control, CONTROL 2012, September, 958–963*. <https://doi.org/10.1109/CONTROL.2012.6334761>
- Jategaonkar, R. V. (2015). Flight Vehicle System Identification: A Time-Domain Methodology, Second Edition. In *Flight Vehicle System Identification: A Time-Domain Methodology, Second Edition*. American Institute of Aeronautics and Astronautics, Inc. <https://doi.org/10.2514/4.102790>
- Jayachandran, M., Manikandan, J., & Hwegy, Y. (2009). DESIGN OF A STAND ALONE NAVIGATION SYSTEM USING POSITION ESTIMATION ALGORITHM. *Transport, 2*, 539–542.
- Jo, D., & December, H. (2017). *LINEAR SYSTEMS THEORY* (2nd ed.).
- Juang, J. N., & Suzuki, H. (1986). An eigensystem realization algorithm in frequency domain for modal parameter identification. *Astrodynamics Conference, 1986, 8(5)*, 620–627. <https://doi.org/10.2514/6.1986-2048>
- Kasebzadeh, P. (2017). Parameter Estimation for Mobile Positioning Applications. In *Parameter Estimation for Mobile Positioning Applications* (Issue 1786). <https://doi.org/10.3384/lic.diva-141877>
- Khalid, A., Zeb, K., & Haider, A. (2019). Conventional PID, adaptive PID, and sliding mode controllers design for aircraft pitch control. *2019 International Conference on Engineering and Emerging Technologies, ICEET 2019, 1–6*. <https://doi.org/10.1109/CEET1.2019.8711871>
- Kim, E. T., Seong, K. J., & Kim, Y. C. (2015). A study on parameter estimation for general aviation canard aircraft. *International Journal of Aeronautical and Space Sciences, 16(3)*, 425–436. <https://doi.org/10.5139/IJASS.2015.16.3.425>
- Kisabo, A. (2012). Pitch Control of an Aircraft Using Artificial Intelligence. *Journal of Scientific Research and Reports, 1(1)*, 1–16. <https://doi.org/10.9734/jsrr/2012/2008>
- Klein, V. (1989). Estimation of aircraft aerodynamic parameters from flight data. *Progress in Aerospace Sciences, 26(1)*, 1–77. [https://doi.org/10.1016/0376-0421\(89\)90002-X](https://doi.org/10.1016/0376-0421(89)90002-X)
- Klien, V., & Morelli, E. A. (2006). *Aircraft System Identification: Theory and Practice*. AIAA Education series.
- Kornienko, A., & Well, K. H. (2003). Estimation of longitudinal motion of a remotely controlled airship. *AIAA Atmospheric Flight Mechanics Conference and Exhibit, August, 1–9*. <https://doi.org/10.2514/6.2003-5697>

- Kuehme, D., Alley, N. R., Phillips, C., & Cogan, B. (2014). Flight test evaluation and system identification of the Area-I Prototype-Technology-Evaluation Research Aircraft (PTERA). *AIAA Flight Testing Conference 2014, June*, 1–74. <https://doi.org/10.2514/6.2014-2577>
- Kumar, R. (2012). *Parameter Estimation Using Flight Data Of Air Vehicles At Low And Moderately High Angles Of Attack Using Conventional And Neural based Methods*. IIT Kanpur.
- Kumar, R., & Ghosh, A. K. (2014). Estimation of aerodynamic derivatives using neural network based method. In *IFAC Proceedings Volumes (IFAC-PapersOnline)* (Vol. 3, Issue PART 1). IFAC. <https://doi.org/10.3182/20140313-3-IN-3024.00057>
- Kumar, R., & Ghosh, A. K. (2015). *Nonlinear Aerodynamic Modeling from Flight Data at High Angles of Attack Using Neural-Gauss-Newton Method*. June, 1–13. <https://doi.org/10.2514/6.2015-2707>
- Kumar, V., & Patra, A. (2016). Application of Ziegler-Nichols Method for Tuning of PID Controller. *2nd International Conference on Recent Innovations in Science, Technology, Management and Environment, 2011*, 138–149. http://www.arresearchpublication.com/images/shortpdf/1479279897_127ijee.pdf
- Leontaritis, I. J., & Billings, S. A. (1985). Input-output parametric models for non-linear systems Part I: Deterministic non-linear systems. *International Journal of Control*, *41*(2), 303–328. <https://doi.org/10.1080/0020718508961129>
- Lichota, P., Dul, F., & Karbowski, A. (2020). System identification and LQR controller design with incomplete state observation for aircraft trajectory tracking. *Energies*, *13*(20). <https://doi.org/10.3390/en13205354>
- Ljung, L., & Gunnarsson, S. (1990). Adaptation and tracking in system identification-A survey. *Automatica*, *26*(1), 7–21. [https://doi.org/10.1016/0005-1098\(90\)90154-A](https://doi.org/10.1016/0005-1098(90)90154-A)
- Mahmoud, T., & Trilaksono, B. R. (2018). Integrated INS/GPS navigation system. *International Journal on Electrical Engineering and Informatics*, *10*(3), 491–512. <https://doi.org/10.15676/ijeei.2018.10.3.6>
- Maine, E., & Iliff, W. (1986). Application Estimation Stability and of Parameter to Aircraft Control Approach The Output-Error. *Nasa-Rp-1168*, 175. <http://ntrs.nasa.gov/archive/nasa/casi.ntrs.nasa.gov/19870020066.pdf>
- Melody, J. W., Basar, T., Perkins, W. R., & Voulgaris, P. G. (2000). Parameter identification for inflight detection and characterization of aircraft icing. *Control Engineering Practice*, *8*(9), 985–1001. [https://doi.org/10.1016/s0967-0661\(00\)00046-0](https://doi.org/10.1016/s0967-0661(00)00046-0)

- Milliken W.F.Jr. (2003). Progress in Dynamic stability and control research. *Journal Of The Aeronautical Sciences*, 40(6), 145–160.
- Mohammad Shahrokhi and Alireza Zomorodi. (2005). *comparison of PID controller tuning methods*. <https://doi.org/10.1002/cjce.5450830412>
- Morelli, E. A., & Grauer, J. A. (2020). Practical aspects of frequency-domain approaches for aircraft system identification. *Journal of Aircraft*, 57(2), 268–291. <https://doi.org/10.2514/1.C035599>
- Morino, L. (1974). General Theory of Unsteady Compressible Potential Aerodynamics. *NASA Contractor Reports, Cr-2464*.
- Nagoor Kani - Control System Engineering-RBA (2013).pdf*. (n.d.).
- NAL. (2000). *Hansa-3 TC&TCDS.pdf*. https://doi.org/http://164.100.60.133/type_acceptance/Hansa-3%20TC&TCDS.pdf
- NAL Hansa*. (2000). https://en.wikipedia.org/wiki/NAL_Hansa
- Nelson, R. C. (1989). Flight Stability and Automatic Control. In *Book* (Second). Tata McGraw-Hill.
- Nelson, R. C. (1998). *Flight stability and automatic control*. WCB/McGraw Hill.
- Pallett, E. H. . (1954). Aircraft electrical systems. In *Nature* (Vol. 174, Issue 4439). <https://doi.org/10.1038/1741001a0>
- Pedro Paulo Liborio Lima do Nascimento, Leandro Aparecido Villas, Bruno Yuji Lino Kimura, D. L. G. (2018). An Integrated Dead Reckoning with Cooperative Positioning Solution to Assist GPS NLOS Using Vehicular Communications. *Sensors (Switzerland)*.
- Peyada, N. K., Sen, A., & Ghosh, A. K. (2008). Aerodynamic Characterization of HANSA-3 aircraft using Equation Error, Maximum Likelihood and Filter Error Methods. *Lecture Notes in Engineering and Computer Science*, 2169(1), 1902–1907.
- Postorino, M. N., & Sarné, G. M. L. (2020). Reinventing mobility paradigms: Flying car scenarios and challenges for urban mobility. *Sustainability (Switzerland)*, 12(9), 1–16. <https://doi.org/10.3390/SU12093581>
- Psas, M. I. T., Report, T., Leveson, N., Wilkinson, C., Fleming, C., Thomas, J., & Tracy, I. (2014). *A Comparison of STPA and the ARP 4761 Safety Assessment Process I*. 1–79.
- Queijo, M. J., Wells, W. R., & Keskar, D. A. (1978). *Approximate Indicial Lift Funtion for Tapered, Swept Wings in Incompressible Flow*. August.

- Queijo, M. J., Wells, W. R., & Keskar, D. A. (1979). *Inclusion of Unsteady Aerodynamics in Longitudinal Parameter Estimation From flight data. December.*
- Radhakant Padhi, D. of A. E. (n.d.). *Advanced Control System Design*. NPTEL, IISC Bangalore. <http://nptel.iitm.ac.in>
- Radhakant Padhi Department of Aerospace Engineering, I. B. (n.d.). *Advanced Control System Design*. <http://nptel.iitm.ac.in>
- Raisinghani, S. ., & Ghosh, A. . (n.d.). Parameter Estimation of an Augmented Airplane with Unsteady Aerodynamic Modeling. *Proceedings of the 17th Int. Symp. on Space Technology and Science.*
- Raja, M., & Prakash, O. (2020). Design of high pointing accuracy NPSAT-1 satellite attitude systems of armature controlled DC motor with utilization for PD controller. *INCAS Bulletin*, 12(1), 145–156. <https://doi.org/10.13111/2066-8201.2020.12.1.14>
- Ramesh, N. G., Balaji, J., N, D. K., Dharshan, L., & Dileep, H. R. (2020). *DESIGN AND FABRICATION OF ORNITHOPTER*. 940–944.
- Reddy, G. S., & Saraswat, V. K. (2013). Advanced navigation system for aircraft applications. *Defence Science Journal*, 63(2), 131–137. <https://doi.org/10.14429/dsj.63.4254>
- Robert, J. (n.d.). *The Unsteady lift of a finite wing.*
- Robinson, J. D. (1991). *A Linear Quadratic Regulator weight selection algorithm for robust pole assignment.*
- Roudbari, A., & Saghafi, F. (2016). Generalization of ANN-based aircraft dynamics identification techniques into the entire flight envelope. *IEEE Transactions on Aerospace and Electronic Systems*, 52(4), 1866–1880. <https://doi.org/10.1109/TAES.2016.140693>
- SABHARWAL, W. C. D. (2003). *Flight : The basic book; 100 years of Aviation.*
- Saderla, S., Dhayalan, R., Singh, K., Kumar, N., & Ghosh, A. K. (2019). Longitudinal and lateral aerodynamic characterisation of reflex wing Unmanned Aerial Vehicle from flight tests using Maximum Likelihood, Least Square and Neural Gauss Newton methods. *Aeronautical Journal*, 123(1269), 1807–1839. <https://doi.org/10.1017/aer.2019.70>
- Seckel, E., & Morris, J. (1971). *the Stability Derivatives of the Havion Aircraft Estimated By Various Methods and Derived From Flight Test Data*. 35.
- Sgobba, T. (2019). B-737 MAX and the crash of the regulatory system. *Journal of Space Safety Engineering*, 6(4), 299–303.


<https://doi.org/10.1016/j.jsse.2019.09.006>

- Shinbrot, M. (1951). A Least square Curve Fitting Method with Applications to the Calculation of Stability Coefficients from Transient Response Data. *Naca Tn 2341*.
- Shurin, A., & Klein, I. (2020). QDR: A quadrotor dead reckoning framework. *IEEE Access*, 8, 204433–204440. <https://doi.org/10.1109/ACCESS.2020.3037468>
- Singh, J., & IIT Kanpur. (n.d.). *Unsteady Aerodynamic Modeling for Parameter Estimation from Flight Data*.
- SPACE india. (1988).
- Srinivasan, K. (2006). *Chapter 18 Control System Design Using State-Space Methods Quadratic Regulator Quadratic Regulator Conclusion. 2*.
- Stojiljković, B., Vasov, L., Mitrović, Č., & Cvetković, D. (2009). The application of the root locus method for the design of pitch controller of an F-104A aircraft. *Strojnicki Vestnik/Journal of Mechanical Engineering*, 55(9), 555–560.
- Sushamshushekar Doddabasappa. (2019). LQR CONTROL DESIGN FOR A DC-DC CONVERTER USING SENSITIVITY FUNCTIONS. In *Ayan* (Vol. 8, Issue 5). The Pennsylvania State University The Graduate School.
- Tang, L., Roemer, M., Ge, J., Crassidis, A., Prasad, J. V. R., & Belcastro, C. (2009a). Methodologies for adaptive flight envelope estimation and protection. *AIAA Guidance, Navigation, and Control Conference and Exhibit, August*, 1–14. <https://doi.org/10.2514/6.2009-6260>
- Tang, L., Roemer, M., Ge, J., Crassidis, A., Prasad, J. V. R., & Belcastro, C. (2009b). *Methodologies for Adaptive Flight Envelope Estimation and Protection*.
- Timeline of HAL Tejas.* (n.d.). https://en.wikipedia.org/wiki/Timeline_of_HAL_Tejas
- Tischler, M., & Remple, R. (2006). *Aircraft and Rotorcraft System Identification, Engineering Methods with Flight Test Examples*. AIAA Education series. <https://doi.org/10.2514/4.861352>
- Torabi, A., Ahari, A. A., Karsaz, A., & Kazemi, S. H. (2021). Intelligent Pitch Controller Identification and Design. *International Journal of Mathematics and Computers in Simulation*, 15, 134–140. <https://doi.org/10.46300/9102.2021.15.25>
- Usta, M. A., Akyazi, Ö., & Akpınar, A. S. (2011). Aircraft roll control system using LQR and fuzzy logic controller. *INISTA 2011 - 2011 International Symposium*

- on *INnovations in Intelligent SysTems and Applications*, 223–227. <https://doi.org/10.1109/INISTA.2011.5946069>
- Verma, H. O., & Peyada, N. K. (2021). Estimation of aerodynamic parameters near stall using maximum likelihood and extreme learning machine-based methods. *Aeronautical Journal*, 125(1285), 489–509. <https://doi.org/10.1017/aer.2020.95>
- Villarreal-Valderrama, F., Takano De La Cruz, L., Alvarez, U., Amezcuita-Brooks, L., & Liceaga-Castro, E. (2019). Design of an aircraft pitch control experimental test bench. *2018 IEEE International Autumn Meeting on Power, Electronics and Computing, ROPEC 2018, Ropec*. <https://doi.org/10.1109/ROPEC.2018.8661430>
- W. Ahmed, Z.Li, M. I. (2019). Multi-objective Eigenstructure Assignment-PID Based Controller Design for Longitudinal Motion of Aircraft. *International Conference on Control Science and System Engineering, ICCSSE, IEEE*.
- Wahid, N., & Hassan, N. (2012). Self-tuning fuzzy PID controller design for aircraft pitch control. *Proceedings - 3rd International Conference on Intelligent Systems Modelling and Simulation, ISMS 2012*, 19–24. <https://doi.org/10.1109/ISMS.2012.27>
- Wahid, N., & Rahmat, M. F. ad. (2010). Pitch control system using LQR and fuzzy logic controller. *ISIEA 2010 - 2010 IEEE Symposium on Industrial Electronics and Applications, Isiea*, 389–394. <https://doi.org/10.1109/ISIEA.2010.5679436>
- Wells, W. R., Banda, S. S., and Quam, D. L. (1979). A model for unsteady effects in Lateral Dynamics for use in Parameter Estimation. *AIAA Paper*.
- Yibo Li, Chao Chen, W. C. (n.d.). Research on Longitudinal Control Algorithm for Flying Wing UAV based on LQR Technology. *Int'l Journal on Smart Sensing and Intelligent Systems*, 6(5).
- Zadeh, L. A. (1962). From Circuit Theory to System Theory. *Proceedings of the IRE*, 50(5), 856–865. <https://doi.org/10.1109/JRPROC.1962.288302>

APPENDIX- A

CURRICULUM VITAE

<p>ROLI JAISWAL</p> <p>ADDRESS: 543/22, Antarick Complex, Badamtala, Barrackpore</p> <p>P.O. Bengal Enamel, N-24 Paragana West Bengal.</p> <p>EMAIL: rolijais89@gmail.com</p> <p>MOB: 8954686133, 9123867571</p>	
---	---

Roli is a Research Scholar with 6.5 years of teaching and Industrial experience. Her ambition is to Pursue a challenging career and be a part of progressive organization that gives scope to enhance skills, knowledge and to reach pinnacle in this field with sheer determination, hard work and dedication so that her experience can be utilized and makes good use of for the organization.

Subjects comfortable to teach includes:

Control Systems
System Identification: Includes Kalman
Filtering, ML Approaches etc. Fluid
Mechanics
Flight Mechanics
Aircraft Systems and Maintenance

Publication Summary:

- “A preliminary study of parameter estimation for fixed wing aircraft and high endurance parafoil Aerial Vehicle”, INCAS Bulletin, Vol-12, Issue-4, SCOPUS Indexed, Dec2020
- “Classical and Modern gain estimation approach of PID Controller for the pitch control of the RCTA Aircraft”, INCAS Bull., vol. 14, no. 1, pp. 39-56, 2022, Doi: 10.13111/2066-8201.2022.14.1.4
- “Estimation of Lateral Directional Aerodynamic Derivatives from Flight Data of Unmanned Powered parafoil Aerial Vehicle”, Proceedings of the AIAA Atmospheric Flight Mechanics Conference, 2018

- “Vishkira, A Gallinacious aircraft”, in International Conference of Material Science and Testing, China, 2019
- “Comparative study of longitudinal stability derivatives of Hansa-3 Aircraft Using Extended kalman Filtering Technique and ML Method” in Advances in Chemical Engineering, SCOPUS Indexed, Dehradun, Feb 2020.
- “Distinctive Navigational Approach –A Dead Reckoning for Aircraft Co-Ordinate Estimation”, 4th International Conference on Smart and Sustainable Developments in Engineering and Technology, PiCET, 22nd May 2022

Competencies and Academic Administrative Summary:

- MIS Coordinator of Aerospace Department.
- Class- Coordinator of B-Tech Second Year students.
- Guided M-Tech graduates of UAV Program in thesis writing, major projects.
- Coordinator for Industrial Visit in ISRO, ADANI, & Bharat Dynamics Limited in Hyderabad for 2019.
- Coordinator for Industrial Visit in HAL, NAL & DRDO in Bangalore for 2018.
- Mentor-Mentee Coordinator of Second and Third Year.
- Member of Organizing committee in National Space Convention 2020: Tessy Thomas, Missile Women of India was distinguished guest of the Convention.
- Summer Internship Coordinator of B-Tech Graduates.
- Technical and organizing support to students for Aero Kriti Competition.

Accreditation & Ranking Summary:

- Preparation of Criterion wise file related to teaching learning process for NAAC.
- Curriculum Design and Development and addition of value-added courses for NAAC.
- Teaching & Learning process definition, implementation and impact analysis for NAAC.
- Outcome based Education System study and generation of report for NAAC.
- PPT preparation for NAAC.

Accomplishments:

- B-tech students in their major and minor projects.
- Helping hand of placement coordinator departmental wise in UPES
- Member of “Aeronautical society of India”.
- Organized a national level seminar on “Recent trends in Aerospace Technology”.
- Technical and organizing support for engineering Events as “AERO-SAMBHODHAN” at BBDNITM, Lucknow in UTKARSH.
- Astronomy (Member of UPAAC, Lucknow)
- Participated in Workshop on “Fundamentals of robotics” from 20-10-2008 to 22-10-2008.

Organization:

Organization	Designation	Duration
University of Petroleum & Energy studies, Dehradun	Assistant Professor	14 th Aug 2017- 4 th Sep 2020
DBU University, Punjab	Technical Assistant	Sep 2015 to June 2017
BBDNITM, Lucknow	Lecturer	Dec 01, 2014 to Sep 2015.
HAL, Kanpur	Design Trainee	1 st Jan 2013 to 31 st Dec 2013

Education:

Qualification	Year of Passing	Institute/ University	Class/Division	Percentage/DGPA
PhD	2018 (Pursuing)	UPES, Dehradun	-	-
M-TECH	2017	DBU, Punjab	First Class with Distinction	81.1%
B-TECH	2012	BBDNITM, Lucknow	First Division with Honors	80%
12 TH	2007	C.B.S. E	First Class	67.7%
10 TH	2005	C.B.S. E	First Class	77.8%

Project Experience:**1. Involved in a project on comparison and analysis of AVRO class TURBO PROP Engine.**

Details: Study of AVRO class of ROLLS ROYCE DART Engine characteristics and comparisons with some suitable engines like PRATT & WHITNEY CANADA - PW123AF, PW124B, PW125B PW127E and KLIMOV COOPERATION, RUSSIA - TV7-117S, TV7-117S SERIES2 to find out engine with better SFC and Performance.

Conclusion: TV7-117S SERIES2 (RUSSIAN) Engine can replace ROLLS ROYCE Dart533-2.

- SFC is reduced which helps in saving fuel cost.
- Low engine weight.
- About 300 crores is being saved per 200 hours.

2. Involved in a project on aircraft material standards (from German std. to British, Italy, France, and USA) of aircraft parts.

- It helps in comparing & finding the substitute of parts of aircraft material.

3. **Optimization of Aerofoil** (Symmetrical, cambered) by analytical method on selection of series of Aerofoils by JAVAFOIL Software from IIT, Kanpur

Personal Details:

Date of Birth	03.11.1990
Pan card No.	AUCPJ1037E
Gender	Female
Marital Status	Married
Nationality	Indian
Language Known	English, Hindi, Bangla
Hobbies	Cooking, Travelling

APPENDIX- B

MATLAB CODES

B1. ZIEGLER NICHOLAS METHOD

```
%% Zieger nicholas method
clear all
clc

%Define plant transfer function
G_NUM=[0 0 0 55.94 103.3];
G_DEN=[1 10.07 31.18 101.8 103.3];
KU=1.34; %% ROUTH HURWITZ CRITERION
TU=1.504; %% SIMULINK BLOCK DIAGRAM
%% LOOK THE VALUE OF KP, Ti, Td
KP=0.6*KU; % CLASSIC PID
Ti=0.5*TU; % CLASSIC PID
Td=TU/8; % CLASSIC PID
%% COMPUTE Ki and Kd
Ki=1.2*KU/TU; % CLASSIC PID
Kd=0.075*KU*TU; % CLASSIC PID
%%COMPUTE Ki and Kd
Kp=0.45*KU; % PI CONTROLLER
ti=TU/1.2; %PI CONTROLLER
%% COMPUTE Ki
ki=0.54*KU/TU; %PI CONTROLLER
%% unstable characteristics using PI CONTROLLER IN SIMULINK B/D
%% %% COMPUTE Kd FOR PD CONTROLLER
kp=0.8*KU;
td=TU/8;
kd=0.1*KU*TU;
%% STABLE CHARACTERISTICS USING PD CONTROLLER IN
SIMULINK B/D
```

B2.MODIFIED ZIEGLER NICHOLAS METHOD

```
%% Modified Zieger nicholas method
clear all
```

```

clc
%Define plant transfer function
G_NUM=[0 0 0 55.94 103.3];
G_DEN=[1 10.07 31.18 101.8 103.3];
KU=0.3; %% ROUTH HURWITZ CRITERION
TU=1.873; %% SIMULINK BLOCK DIAGRAM
%% LOOK THE VALUE OF KP, Ti, Td
Kpzn=0.33*KU; % CLASSIC PID
%% COMPUTE Ki and Kd
Kimzn=0.5*TU; % CLASSIC PID
Kdmzn=0.33*TU; % CLASSIC PID

```

B3. ASTROM- HAGGULUND METHOD

```

%% Astrom-Haggulund method
clear all
clc
%Define plant transfer function
G_NUM=[0 0 0 55.94 103.3];
G_DEN=[1 10.07 31.18 101.8 103.3];
KU=0.3; %% ROUTH HURWITZ CRITERION
TU=1.873; %% SIMULINK BLOCK DIAGRAM
%% LOOK THE VALUE OF KP, Ti, Td
Kpag=0.33*KU; % CLASSIC PID
%% COMPUTE Ki and Kd
KIag=0.94*TU; % CLASSIC PID
KDag=0; % CLASSIC PID

```

B4. TYREUS LUYBEN METHOD

```

%% Tyreus luyben method
clear all
clc
%Define plant transfer function
G_NUM=[0 0 0 55.94 103.3];
G_DEN=[1 10.07 31.18 101.8 103.3];
KU=1.3400; %% ROUTH HURWITZ CRITERION
TU=1.5040; %% SIMULINK BLOCK DIAGRAM
%% LOOK THE VALUE OF KP, Ti, Td
Kpcl=0.3125*KU; % CLASSIC PID
%% COMPUTE Ki and Kd
KIcl=2.2*TU; % CLASSIC PID
KDcl=0.158*TU; % CLASSIC PID

```


B5. POLE- PLACEMENT ALGORITHM

```
clc
%define state and control matrices
A= [-1.851 0.8207 0;-4.403 -2.01 0;0 1 0];
B= [0.00562;8.95;0];
C= [0 0 1];
D= [0];
initialX = [1;0;0];
% create state space object
sys=ss(A,B,C,D);
%CHECK OPEN LOOP EIGEN VALUES
E=eig(A)
% %desired closed loop poles using butterworth polynomial equation
P= [-1.35+2.338i -1.35-2.338i -1.3];
% %solve for K using pole placement
GainK = acker(A,B,P);
disp('Feedback Gain Matrix: ');
disp(GainK);
% OR USE place to determine closed loop system gain
% GAIN= place(A,B,P)
% %CHECK for closed loop eigen values
Acl= A-B*GainK;
Ecl= eig(Acl)
% % %create closed loop system
syscl= ss(Acl,B,C,D);
% %CHECK STEP RESPONSE
step(0.2*syscl)
%solve for kr
kdc= dcgain(syscl);
kr=1/kdc
% % %create scaled input closed system
syscl_scaled = ss(Acl,B*kr,C,D);
step(syscl_scaled)
%ylabel('pitch angle (rad)');
title('Closed-Loop Step Response: pole placement');
```

B6. LINEAR QUADRATIC REGULATOR

```
A= [-1.851 0.8207 0
     -4.403 -2.01 0
     0 1 0 ];
B= [0.00562;8.95;0];
C= [0 0 1];
D= [0];
poles= eig(A)
```

```

%% poles lies in complex left side of the plane hence system is stable
%poles =
%% 0.0000 + 0.0000i
%% -1.9305 + 1.8993i
%% -1.9305 - 1.8993i
rank(ctrb(A,B));
rank(observ(A,C));
p = 400;
Q = p*C'*C;
R = 1;
[K] = lqr(A,B,Q,R)
sys_cl = ss(A-B*K, B, C, D);
step(0.2*sys_cl);
ylabel('pitch angle (rad)');
title('Closed-Loop Step Response: LQR');
% p = 400;
% Q = p*C'*C;
% R = 1;
% [K] = lqr(A,B,Q,R);
% Nbar = rscale(A,B,C,D,K)
% sys_cl = ss(A-B*K,B*Nbar,C,D)
% step(0.2*sys_cl);
% ylabel('pitch angle (rad)');
% title('Closed-Loop Step Response: LQR with Precompensation');

```

B7. CARTESIAN COORDINATES TO GEODETIC COORDINATES CONVERSION CODE

```

X=xyaS2(:,1);
Y=xyaS2(:,2);
Z=xyaS2(:,3);
X=X{:,1};
Y=Y{:,1};
Z=Z{:,1};
% Y=double(Y');
% Z=double(Z');
origin= [80.232293 ,26.518886 ,126.63];
[lat,lon]=local2latlon(X,Y,Z,origin);
%save latlon_rad.txt
zoomlevel=12;
player = geoplayer(lat(1) ,lon(1),zoomLevel);
plotRoute(player,lat,lon);

```

APPENDIX –C

C.1 EQUATIONS OF MOTION

A stationary aircraft uses an earth axes system also termed an inertial frame of reference for deriving the equation of motion in an inertial reference frame.

Expression of Newton's second law of motion:

$$\sum \vec{F} = \frac{d}{dt} m\vec{v} \quad \text{C.1}$$

$$\sum \vec{M} = \frac{d}{dt} (\vec{H}) \quad \text{C.2}$$

Where F, M, H, m, and v are the net force components (aerodynamic, structural, propulsive, gravitational), net Moment, angular momentum, the mass of the aircraft, and velocity.

Force equation in X, Y, and Z direction is expressed as follows:

$$\vec{F}_x = \frac{d}{dt} (m\vec{u}) \quad \text{C.3}$$

$$\vec{F}_y = \frac{d}{dt} (m\vec{v}) \quad \text{C.4}$$

$$\vec{F}_z = \frac{d}{dt} (m\vec{w}) \quad \text{C.5}$$

where u , v , and w are the components of forces in X, Y, Z directions respectively. Similarly, the moment equation is expressed as:

$$\vec{L} = \frac{d}{dt} (\vec{H}_x) \quad \text{C.6}$$

$$\vec{M} = \frac{d}{dt} (\vec{H}_y) \quad \text{C.7}$$

$$\vec{N} = \frac{d}{dt} (\vec{H}_z) \quad \text{C.8}$$

where L , M , and N are the rolling moment, pitching moment, yawing moment and H_x, H_y, H_z refers to angular momentum in X, Y, and Z directions.

Consider δm as the elemental mass of the airplane, v is the velocity in an inertial frame of reference, and δF stands for net force acting on δm thus

$$\vec{F} = \sum \delta F \quad \text{and} \quad \delta \vec{F} = \delta m \frac{d\vec{v}}{dt} \quad \text{C.9}$$

Thus the velocity of elemental mass δm is

$$\vec{v} = \overrightarrow{(v_c)} + \frac{d\vec{r}}{dt} \quad \text{C.10}$$

Where v_c refers to the velocity of the center of mass and $\frac{d\vec{r}}{dt}$ stands for velocity for the center of mass. Now substituting equation (3.10) into (3.9) yields

$$\vec{F} = \sum \delta F = \frac{d}{dt} \sum (\overrightarrow{v_c} + \frac{d\vec{r}}{dt}) \delta m \quad \text{C.11}$$

$$\vec{F} = m \frac{d\overrightarrow{v_c}}{dt} + \frac{d}{dt} \sum \frac{d\vec{r}}{dt} \delta m \quad \text{C.12}$$

$$\vec{F} = m \frac{d\overrightarrow{v_c}}{dt} + \frac{d^2}{dt^2} \sum r \delta m \quad \text{C.13}$$

Where r is the position vector measured from the center of mass thus $\sum r \delta m$ is zero and the new force equation formulated as

$$\vec{F} = m \frac{d\overrightarrow{v_c}}{dt} \quad \text{C.14}$$

Similarly rewriting moment equation 3.2 as the force equation as

$$\delta \vec{M} = \frac{d}{dt} \delta \vec{H} \quad \text{C.15}$$

Where M is the moment and H is angular momentum. H is written in vector form as

$$\vec{H} = \vec{r} \times \vec{p} \quad \text{and} \quad \delta \vec{H} = (\vec{r} \times \vec{v}) \delta m \quad \text{C.16}$$

Now substituting the value of $\delta \vec{H}$ from equation 3.16 to 3.15 and written as

$$\delta \vec{M} = \frac{d}{dt} (\vec{r} \times \vec{v}) \delta m \quad \text{C.17}$$

The velocity of elemental mass can be expressed in form of position vector 'r' in an inertial frame of reference as

$$\vec{v} = \overline{(v_c)} + \frac{d\vec{r}}{dt} + (\vec{\omega} \times \vec{r}) \quad \text{C.18}$$

Where v_c refers to the velocity of the center of mass, $\frac{d\vec{r}}{dt}$ stands for velocity for the center of mass, $\vec{\omega}$ is the angular velocity of the aircraft, and \vec{r} as position vector of elemental mass. The net moment can be expressed by substituting the value of equation 3.18 to 3.16 as

$$\vec{H} = \sum \delta \vec{H} = \sum r \delta m \times v_c + \sum [r \times (\vec{\omega} \times \vec{r})] \delta m \quad \text{C.19}$$

The first term of equation 3.19 $\sum r \delta m$ is substituted as zero as r is the position vector measured from the center of mass. Now the equation is reduced to

$$\vec{H} = \sum [\vec{r} \times (\vec{\omega} \times \vec{r})] \delta m \quad \text{C.20}$$

Where $\vec{r} = x\hat{i} + y\hat{j} + z\hat{k}$

$$\vec{\omega} = p\hat{i} + q\hat{j} + r\hat{k}$$

Solving equation 3.20 using \vec{r} , $\vec{\omega}$ is expressed as

$$(\vec{\omega} \times \vec{r}) = \begin{bmatrix} \hat{i} & \hat{j} & \hat{k} \\ p & q & r \\ x & y & z \end{bmatrix} \quad \text{C.21}$$

$$(\vec{\omega} \times \vec{r}) = \hat{i}[qz - ry] - \hat{j}[pz - xr] + \hat{k}[py - qx]$$

$$[\vec{r} \times (\vec{\omega} \times \vec{r})] = \begin{bmatrix} \hat{i} & \hat{j} & \hat{k} \\ x & y & z \\ qz - ry & xr - pz & py - qx \end{bmatrix}$$

$$= \hat{i}[py^2 - qxy - rxz + pz^2] - \hat{j}[pxy - qx^2 - qz^2 + ryz] + \hat{k}[px^2 - pzx - qyz + ry^2]$$

Substituting the above equation in equation no (3.20) to get moment equations in X, Y, and Z direction

$$H_x = p \sum (y^2 + z^2) \delta m - q \sum xy \delta m - r \sum xz \delta m \quad \text{C.22}$$

$$H_y = q \sum (x^2 + z^2) \delta m - p \sum xy \delta m - r \sum yz \delta m \quad \text{C.23}$$

$$H_z = r \sum (x^2 + y^2) \delta m - q \sum yz \delta m - p \sum xz \delta m \quad \text{C.24}$$

The moment and product of inertia of aircraft are defined in the below section:

$$\begin{aligned}
 I_x &= \iiint (y^2 + z^2) \delta m & I_{xy} &= \iiint (xy) \delta m \\
 I_y &= \iiint (x^2 + z^2) \delta m & I_{xz} &= \iiint (xz) \delta m \\
 I_z &= \iiint (x^2 + y^2) \delta m & I_{yz} &= \iiint (yz) \delta m
 \end{aligned} \tag{C.25}$$

Where I_x, I_y, I_z are the mass moment of inertia of the system in x, y, and z directions respectively. While substituting equation 3.23 in equation 3.22 the moment of momentum equation is expressed as

$$H_x = pI_x - qI_{xy} - rI_{xz} \tag{C.26}$$

$$H_y = qI_y - pI_{xy} - rI_{yz} \tag{C.27}$$

$$H_z = rI_z - qI_{yz} - pI_{xz} \tag{C.28}$$

C.2 Transformation of equations in a rotational frame from an inertial frame of reference

The vector identity used to transform the inertial frame of reference to the body fixed frame of reference is represented as:

$$\left. \frac{dA}{dt} \right|_{IF} = \left. \frac{dA}{dt} \right|_{BF} + \omega \times A \tag{C.29}$$

Where ω is the angular velocity of vector A, IF is the inertial frame of reference, and BF is the body-fixed frame of reference. The identity applied to an aircraft for axes transformation is written as:

$$\vec{F} = m \left. \frac{dV_C}{dt} \right|_{BF} + m (\omega \times V_C) \tag{C.30}$$

$$\vec{M} = \left. \frac{d\vec{H}}{dt} \right|_{BF} + (\omega \times H) \tag{C.31}$$

Solving the equations 3.26 and 3.27 to deduce force and moment equations in scalar form is represented as

$$V_C = u \hat{i} + v \hat{j} + w \hat{k} \tag{C.32}$$

$$\vec{\omega} = p \hat{i} + q \hat{j} + r \hat{k} \tag{C.33}$$

$$(\omega \times V_C) = \begin{bmatrix} \hat{i} & \hat{j} & \hat{k} \\ p & q & r \\ u & v & w \end{bmatrix} \tag{C.34}$$

$$(\omega \times V_C) = \hat{i}[qw - rv] - \hat{j}[pw - ur] + \hat{k}[pv - qu] \tag{C.35}$$

The force equations in X, Y, and Z direction while substituting the value of curl ($\omega \times V_C$) in below equations are given by

$$F_x = m[\dot{u} + qw - rv] \quad \text{C.36}$$

$$F_y = m[\dot{v} + ru - pw] \quad \text{C.37}$$

$$F_z = m[\dot{w} + pv - qu] \quad \text{C.38}$$

The moment equations in X, Y, and Z direction while substituting the value of curl ($\omega \times H$) in equation 3.27 is given by

$$\vec{\omega} = p\hat{i} + q\hat{j} + r\hat{k} \quad \text{C.39}$$

$$\vec{H} = H_x\hat{i} + H_y\hat{j} + H_z\hat{k} \quad \text{C.40}$$

$$(\omega \times H) = \begin{bmatrix} \hat{i} & \hat{j} & \hat{k} \\ p & q & r \\ H_x & H_y & H_z \end{bmatrix} \quad \text{C.41}$$

$$(\omega \times H) = \hat{i}[qH_z - rH_y] - \hat{j}[pH_z - rH_x] + \hat{k}[pH_y - qH_x] \quad \text{C.42}$$

Recalling Scaler moment equation 3.24 as discussed in the previous section

$$H_x = pI_x - qI_{xy} - rI_{xz}$$

$$H_y = qI_y - pI_{xy} - rI_{yz} \quad \text{C.43}$$

$$H_z = rI_z - qI_{yz} - pI_{xz}$$

$$L = m[\dot{H}_x + qH_z - rH_y]$$

$$M = m[\dot{H}_y + rH_x - pH_z] \quad \text{C.44}$$

$$N = m[\dot{H}_z + pH_y - qH_x]$$

Substituting the values of H_x , H_y , H_z into equation 3.38 to deduce rolling, pitching, and yawing moment along the X, Y, and Z axes and assuming the XZ plane as the symmetry of the airplane thus $I_{yz} = I_{xy} = 0$.

The moment equation of an airplane in an XZ plane can be written as

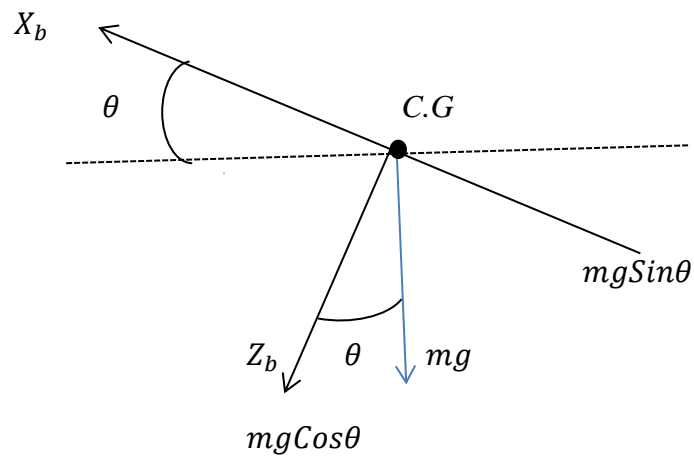
$$L = I_x \dot{p} - I_{xz} \dot{r} + qr(I_z - I_y) - I_{xz}pq \quad \text{C.45}$$

$$M = I_y \dot{q} + rp(I_x - I_z) + I_{xz}(p^2 - r^2) \quad \text{C.46}$$

$$N = -I_{xz} \dot{p} + I_z \dot{r} + pq(I_y - I_x) + I_{xz}qr \quad \text{C.47}$$

Rewriting Force equation by considering Gravitational, and thrust effects on Aircraft:

Gravitational Force (mg) lies at the center of gravity position of the airplane in body fixed axes as shown in fig1. The resolved components are written as:



$$F_{x_{gravity}} = -mg \sin \theta \quad C.48$$

By comparing both figures $F_{y_{gravity}}, F_{z_{gravity}}$ can be resolved as shown below

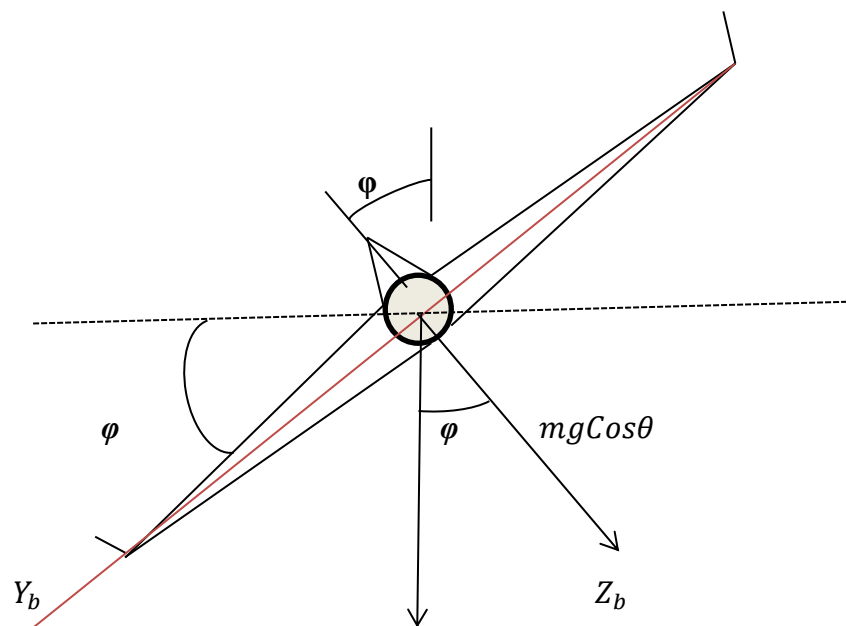


Fig C.1: Components of gravitational force in body axis

$$F_{y_{gravity}} = mg \cos \theta \sin \phi \quad C.49$$

$$F_{z_{gravity}} = mg \cos \theta \cos \phi \quad C.50$$

The thrust forces acting on an airplane in X, Y, and Z directions can be written as

$$\begin{aligned}
F_{x_T} &= X_T \\
F_{y_T} &= Y_T \\
F_{z_T} &= Z_T
\end{aligned}
\tag{C.51}$$

The thrust moments acting on an airplane in X, Y, and Z directions can be written as L_T, M_T, N_T

The finalized set of force equations is expressed as:

$$X - mg\sin\theta = m[\dot{u} + qw - rv] \tag{C.52}$$

$$Y + mg\cos\theta\sin\phi = m[\dot{v} + ru - pw] \tag{C.53}$$

$$Z + mg\cos\theta\cos\phi = m[\dot{w} + pv - qu] \tag{C.54}$$

Where X, Y, and Z indicate the net forces (Propulsive force, gravitational force, thrust force, etc) acting in X, Y, and Z direction

$$m\dot{u} = m(rv - qw) + \bar{q}C_xS - mg\sin\theta + T \tag{C.55}$$

$$m\dot{v} = m(pw - ru) + \bar{q}C_yS + mg\cos\theta\sin\phi \tag{C.56}$$

$$m\dot{w} = m(qu - pv) + \bar{q}C_zS + mg\cos\theta\cos\phi \tag{C.57}$$

APPENDIX -D

GAIN & COORDINATE ESTIMATION

D1. GAIN ESTIMATION OF CONTROLLERS USING TRADITIONAL APPROACHES ZN, MZN, AH, TL OF DIFFERENT DATASETS

D1.1 PID CONTROLLER

KP -PID

Data Set	ZN	MZN	AH	TL
H0	0.618	0.3399	0.3399	0.3219
H1	0.42	0.231	0.231	0.2188
H2	0.804	0.4422	0.4422	0.4188
H3	0.414	0.2277	0.2277	0.2156
H4	0.588	0.3234	0.3234	0.3063
H5	0.468	0.2574	0.2574	0.2438
H6	0.93	0.5115	0.5115	0.4844
H7	0.162	0.0891	0.0891	0.0844
H8	2.58	1.419	1.419	1.3438
H9	0.72	0.396	0.396	0.375
H10	1.062	0.5841	0.5841	0.5531
H11	0.402	0.2211	0.2211	0.2094
H12	2.58	1.419	1.419	1.3438
HP1	0.522	0.2871	0.2871	0.2719
HP2	0.528	0.2904	0.2904	0.275
HD1	0.18	0.099	0.099	0.0938

Twelve datasets of Multistep Input, one dataset of Doublet Input, and 2 dataset of Pulse Input are used for Proportional gain estimation of PID Controller using traditional approach such as ZN, MZN, AH and TL

KI-PID

Dataset	ZN	MZN	AH	TL
H0	0.7774	0.795	1.4946	3.498
H1	0.4841	0.8675	1.6309	3.817
H2	1.072	0.752	1.4138	3.3088

H3	0.5156	0.803	1.5096	3.5332
H4	0.7323	0.803	1.5096	3.5332
H5	0.6671	0.7015	1.3188	3.0866
H6	1.3248	0.702	1.3198	3.0888
H7	0.2017	0.803	1.5096	3.5332
H8	6.45	0.4	0.752	1.76
H9	0.8933	0.806	1.5153	3.5464
H10	1.5128	0.702	1.3198	3.0888
H11	0.4988	0.806	1.5153	3.5464
H12	4.219	0.6115	1.1496	2.6906
HP1	0.582	0.8965	1.6854	3.9446
HP2	0.598	0.883	1.66	3.8852
HD1	0.1922	0.9365	1.7606	4.1206

Twelve datasets of Multistep Input, one dataset of Doublet Input, and 2 dataset of Pulse Input are used for Integral gain estimation of PID Controller using traditional approach such as ZN, MZN, AH and TL

KD-PID

Dataset	ZN	MZN	AH	TL
H0	0.1228	0.5247	0	0.2523
H1	0.0911	0.5726	0	0.2753
H2	0.1508	0.4963	0	0.2387
H3	0.0831	0.53	0	0.2549
H4	0.118	0.53	0	0.2549
H5	0.0821	0.463	0	0.2227
H6	0.1632	0.4633	0	0.2228
H7	0.0325	0.53	0	0.2549
H8	0.258	0.264	0	0.127
H9	0.1451	0.532	0	0.2558
H10	0.1864	0.4633	0	0.2228
H11	0.081	0.532	0	0.2558
H12	0.3944	0.4036	0	0.1941
HP1	0.117	0.5917	0	0.2845
HP2	0.1166	0.5828	0	0.2803
HD1	0.0421	0.6181	0	0.2972

Twelve datasets of Multistep Input, one dataset of Doublet Input, and 2 dataset of Pulse Input are used for Integral gain estimation of PID Controller using traditional approach such as ZN, MZN, AH and TL

D1.2 PI CONTROLLER

KP-PI

Dataset	ZN	TL
H0	0.4635	0.3219
H1	0.315	0.2188
H2	0.603	0.4188
H3	0.3105	0.2156
H4	0.441	0.3063
H5	0.351	0.2438
H6	0.6975	0.4844
H7	0.1215	0.0844
H8	1.935	1.3438
H9	0.54	0.375
H10	0.7965	0.5531
H11	0.3015	0.2094
H12	1.935	1.3438
HP1	0.315	0.2719
HP2	0.396	0.275
HD1	0.135	0.0938

Twelve datasets of Multistep Input, one dataset of Doublet Input, and 2 dataset of Pulse Input are used for Proportional gain estimation of PI Controller using traditional approach such as ZN, MZN, AH and TL

KI-PI

Dataset	ZN	TL
H0	0.3512	3.498
H1	0.2187	3.817
H2	0.4843	3.3088
H3	0.2329	3.5332
H4	0.3308	3.5332
H5	0.3014	3.0866
H6	0.5985	3.0888

H7	0.0911	3.5332
H8	2.9138	1.76
H9	0.4035	3.5464
H10	0.6834	3.0888
H11	0.2253	3.5464
H12	1.906	2.6906
HP1	0.263	3.9446
HP2	0.2701	3.8852
HD1	0.0868	4.1206

Twelve datasets of Multistep Input, one dataset of Doublet Input, and 2 dataset of Pulse Input are used for Integral gain estimation of PI Controller using traditional approach such as ZN, MZN, AH and TL

D1.3 PD CONTROLLER

PD using ZN Tuning

Dataset	Kp	Kd
H0	0.824	0.1638
H1	0.56	0.1214
H2	1.072	0.201
H3	0.552	0.1108
H4	0.784	0.1574
H5	0.624	0.1094
H6	1.24	0.2176
H7	0.216	0.0434
H8	3.44	0.344
H9	0.96	0.1934
H10	1.416	0.2485
H11	0.536	0.108
H12	3.44	0.5259
HP1	0.696	0.156
HP2	0.704	0.1554
HD1	0.24	0.0562

Twelve datasets of Multistep Input, one dataset of Doublet Input, and 2 dataset of Pulse Input are used for Proportional, Integral gain estimation of PD Controller using traditional approach such as ZN

D2. MULTI-STEP 3211 INPUT DATASETS (H0-H12)

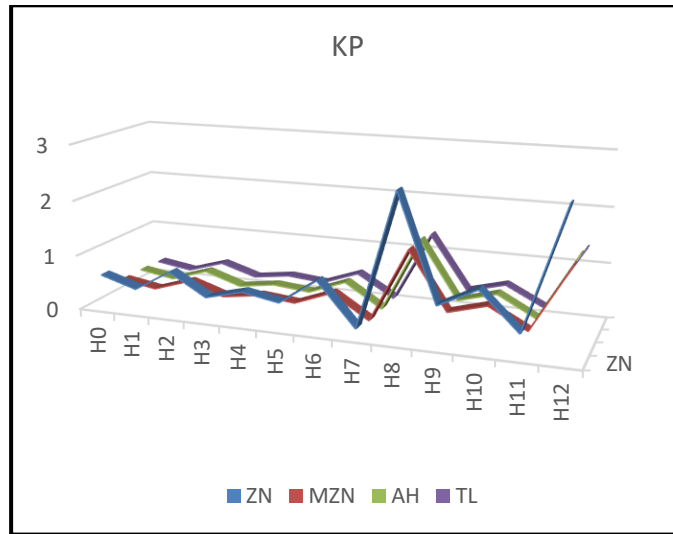


Fig D.1 Comparison of Proportional gain value of Multi-step datasets using Tuning approaches such as: ZN, MZN, TL, and AH

Proportional gain value of twelve datasets of multistep Input form using PID tuning approaches are compared and observed H7 dataset has highest gain value while using ZN Technique. Moreover, gain values of all datasets using various tuning methods superimposes each other

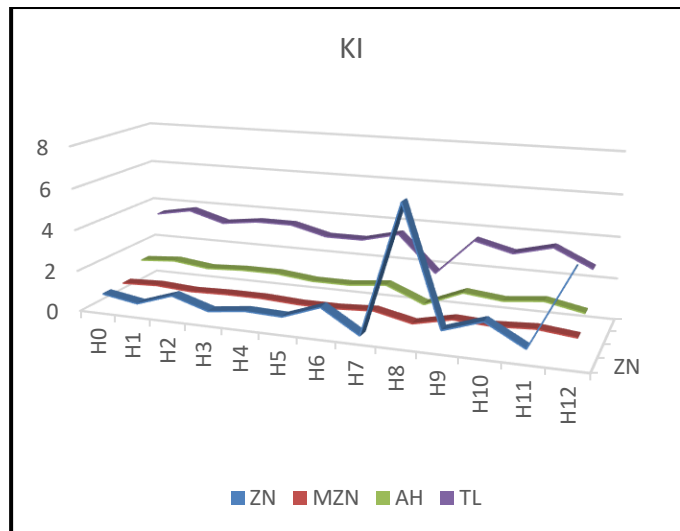


Fig D.2 Comparison of Integral gain value of Multi-step datasets using Tuning approaches such as: ZN, MZN, TL, and AH

Integral gain value of twelve datasets of multistep Input form using PID tuning approaches are compared and observed H7 and H9 dataset has highest gain value while using ZN Technique. Moreover, gain values of all datasets using various tuning methods superimposes each other.

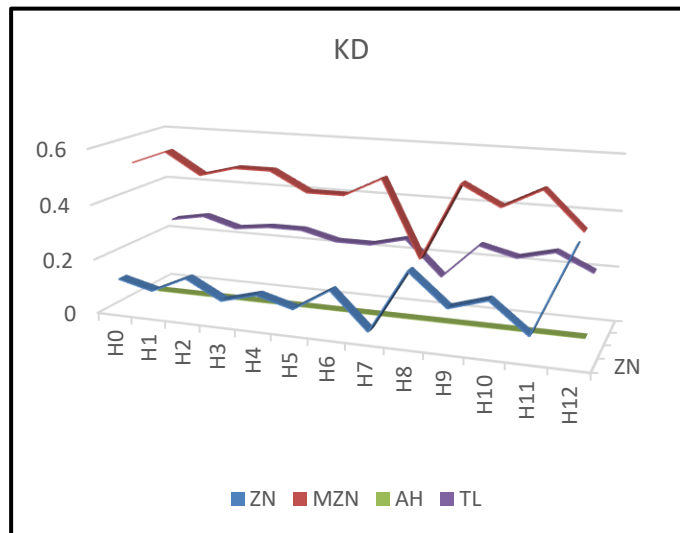


Fig D.3 Comparison of Derivative gain value of Multi-step datasets using Tuning approaches such as: ZN, MZN, TL, and AH

Derivative gain value of twelve datasets of multistep Input form using PID tuning approaches are compared and observed H1 dataset has highest gain value while using MZN Technique

PULSE INPUT DATASETS (HP1-HP2)

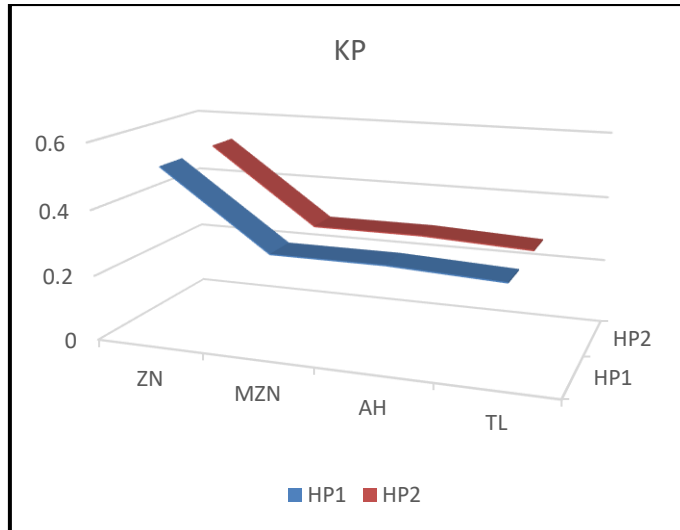


Fig D.4 Comparison of Proportional gain value of Pulse Input datasets using Tuning approaches such as: ZN, MZN, TL, and AH

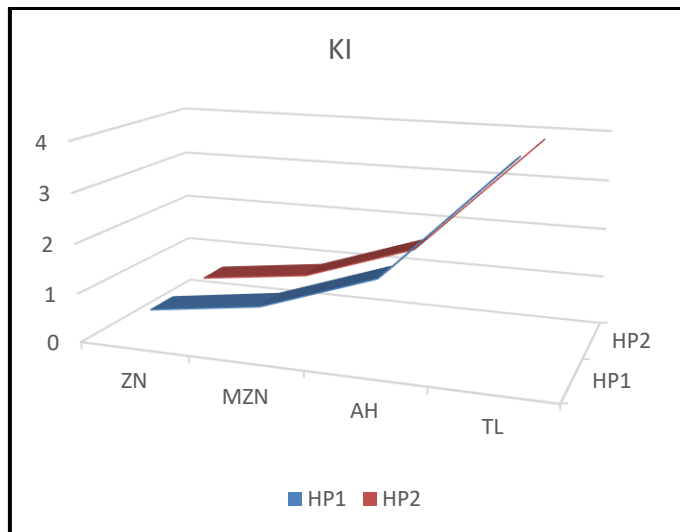


Fig D.5 Comparison of Integral gain value of Pulse Input datasets using Tuning approaches such as: ZN, MZN, TL, and AH

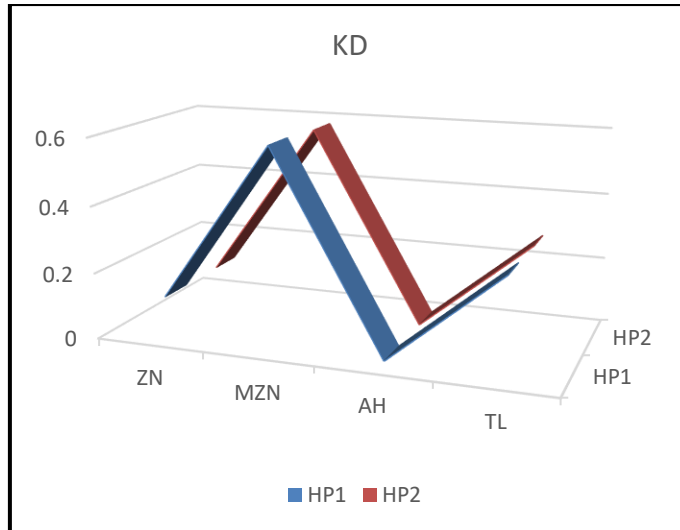


Fig D.6 Comparison of Derivative gain value of Pulse Input datasets using Tuning approaches such as: ZN, MZN, TL, and AH

Proportional, Derivative and Integral gain value of two datasets of Pulse Input form using PID tuning approaches are compared in above figure (D.4-6)

DOUBLET INPUT DATASETS (HD1)

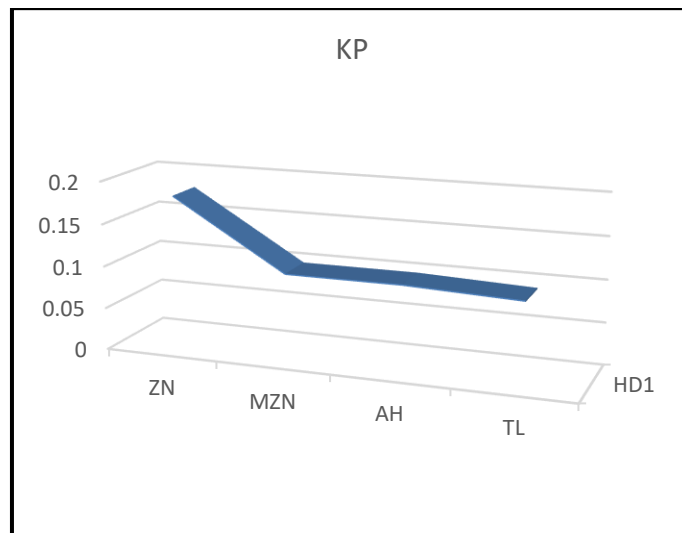


Fig D.7 Comparison of Proportional gain value of Doublet Input datasets using Tuning approaches such as: ZN, MZN, TL, and AH

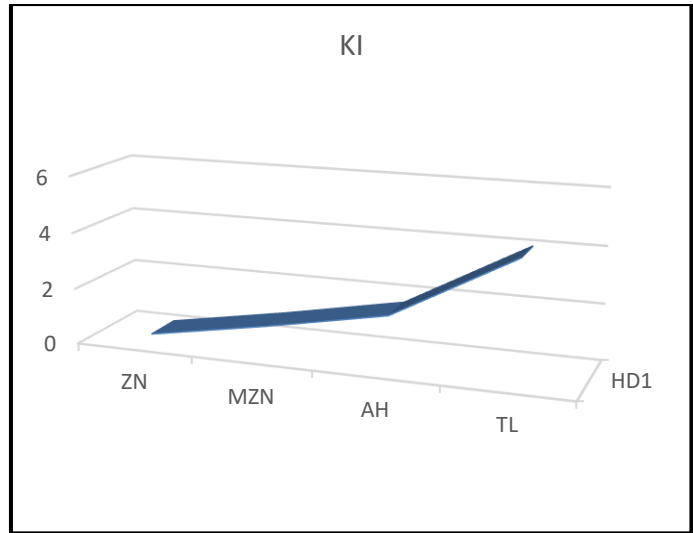


Fig D.8 Comparison of Integral gain value of Doublet Input datasets using Tuning approaches such as: ZN, MZN, TL, and AH

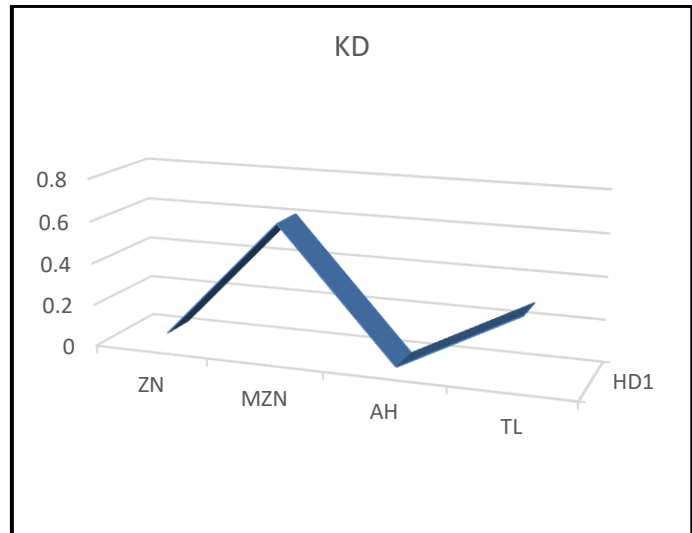


Fig D.9 Comparison of Derivative gain value of Doublet Input datasets using Tuning approaches such as: ZN, MZN, TL, and AH

Proportional, Derivative and Integral gain value of one datasets of Pulse Input-form using PID tuning approaches are compared in above figure (D.7-9)

COMPARE MULTI STEP, DOUBLET, AND PULSE INPUT DATASETS OF PID CONTROLLER

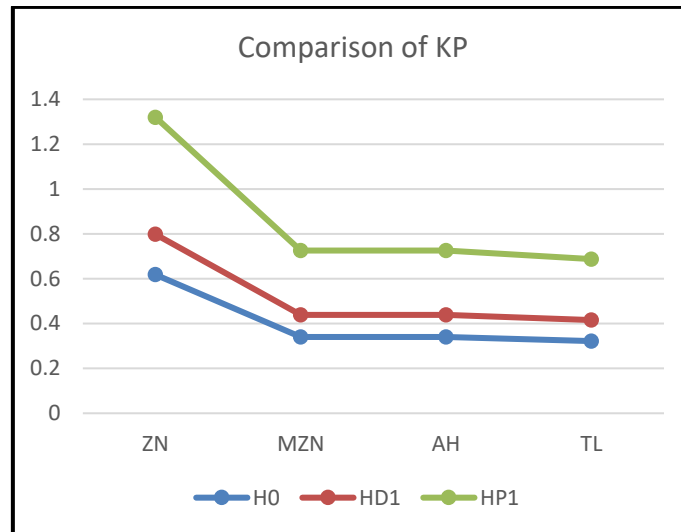


Fig D.10 Comparison of Proportional gain value of Multi-step, Doublet, and Pulse input datasets using Tuning approaches such as: ZN, MZN, TL, and AH

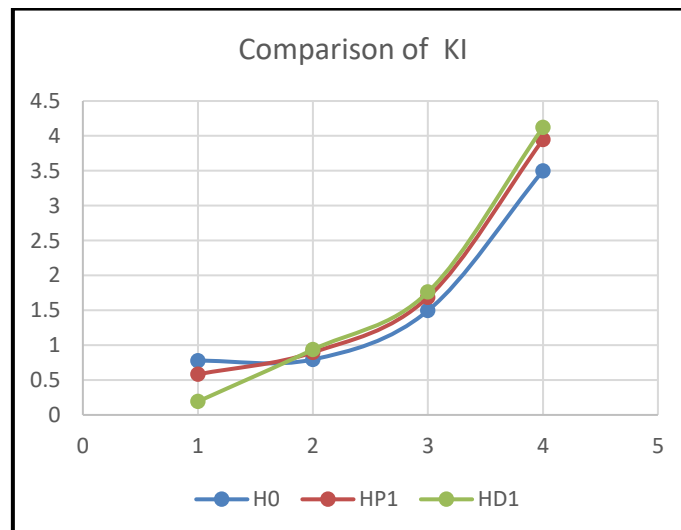


Fig D.11 Comparison of Integral gain value of Multi-step, Doublet, and Pulse input datasets using Tuning approaches such as: ZN, MZN, TL, and AH

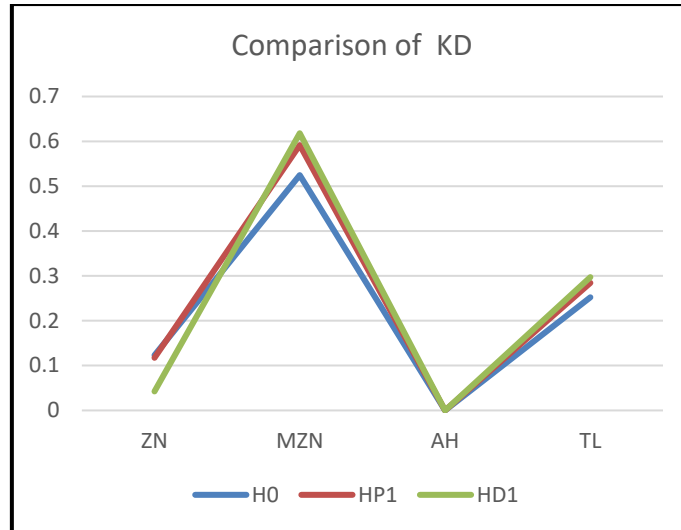


Fig D.12 Comparison of Derivative gain value of Multi-step, Doublet, and Pulse input datasets using Tuning approaches such as: ZN, MZN, TL, and AH

COMPARE MULTI STEP, DOUBLET, AND PULSE INPUT DATASETS OF PD CONTROLLER

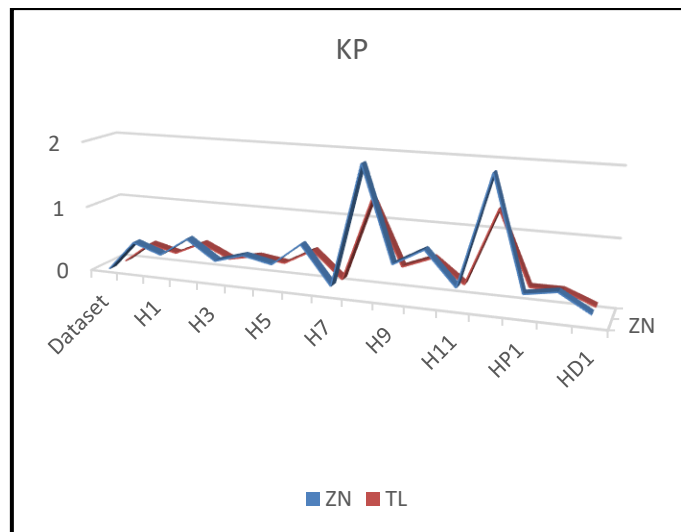


Fig D.13 Comparison of Proportional gain value of Multi-step, Doublet, and Pulse input datasets of PD Controller using Tuning approaches such as: ZN, and TL

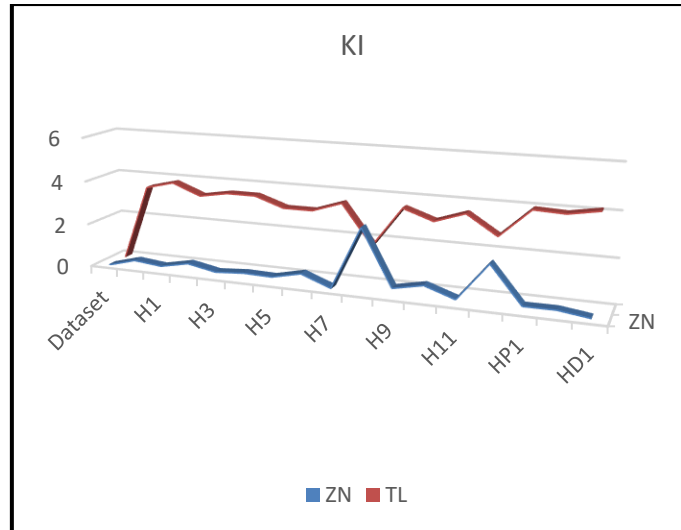


Fig D.14 Comparison of Integral gain value of Multi-step, Doublet, and Pulse input datasets of PD Controller using Tuning approaches such as: ZN, and TL

COMPARE MULTI STEP, DOUBLET, AND PULSE INPUT DATASETS OF PD CONTROLLER

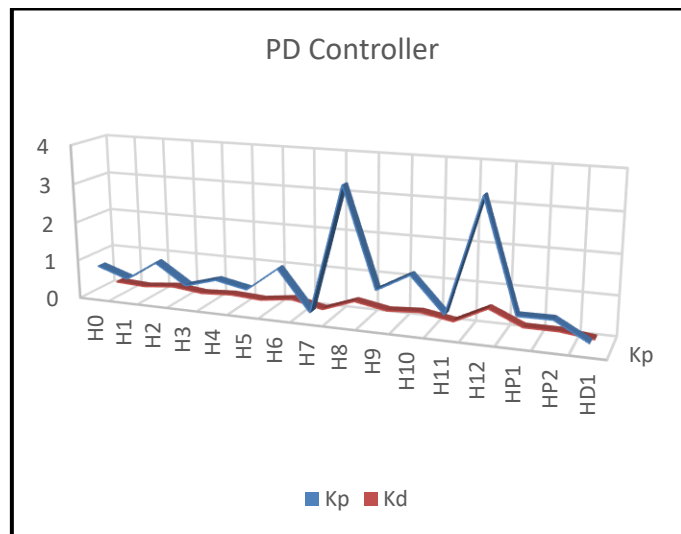
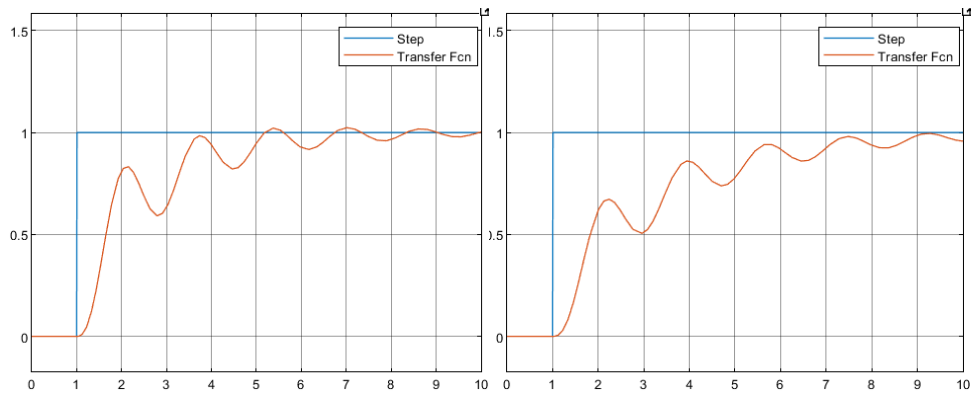


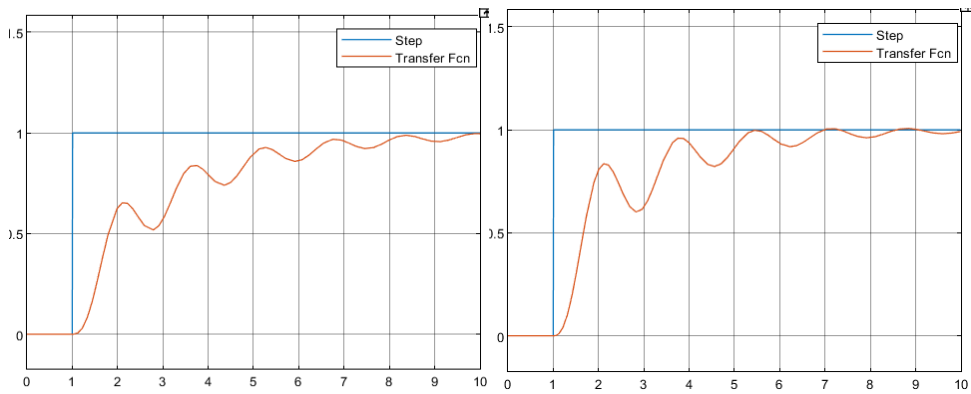
Fig D.15 Comparison of Proportional Integral gain value of Multi-step, Doublet, and Pulse input datasets of PD Controller

ZIEGLER NICHOLAS FIGURES OF MULTI-STEP, DOUBLET, AND PULSE INPUT



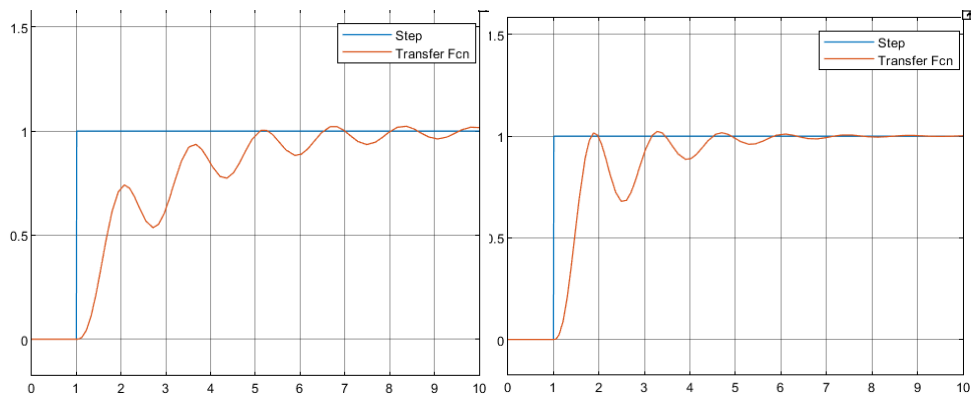
DATA SET H0

DATA SET H1



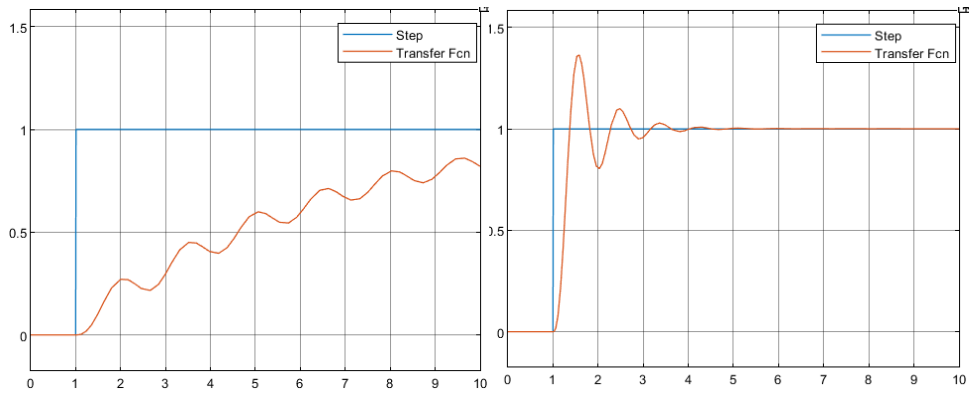
DATA SET H2

DATA SET H4



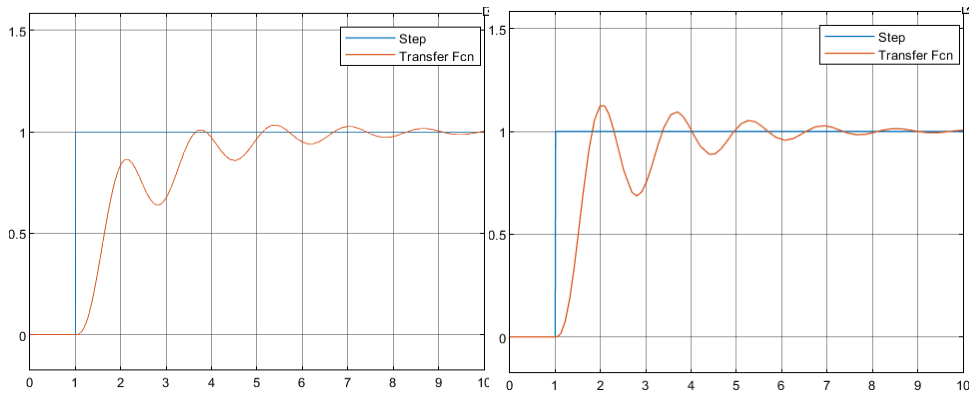
DATA SET H5

DATA SET H6



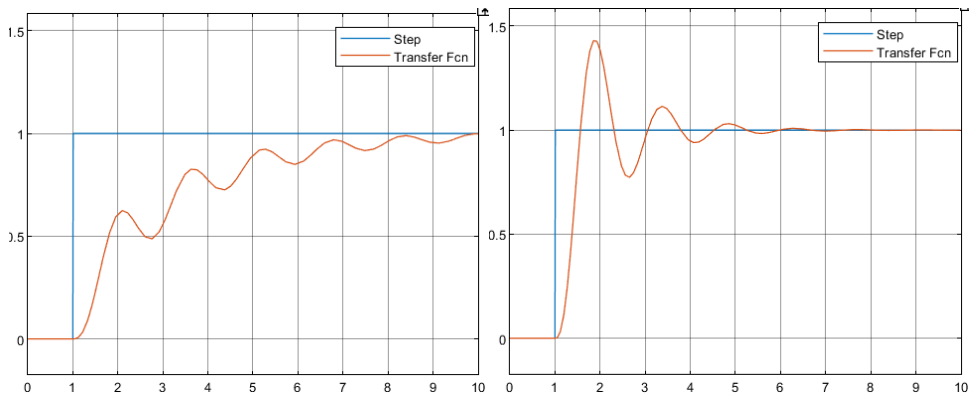
DATA SET H7

DATA SET H8



DATA SET H9

DATA SET H10

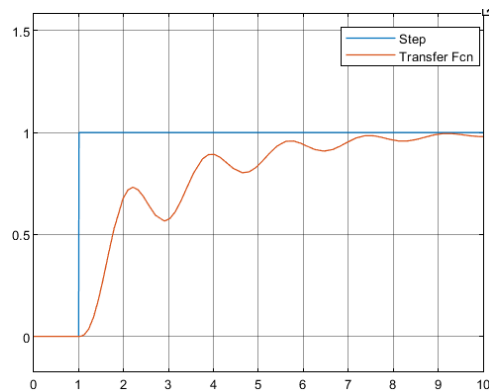


DATA SET H11

DATA SET H12

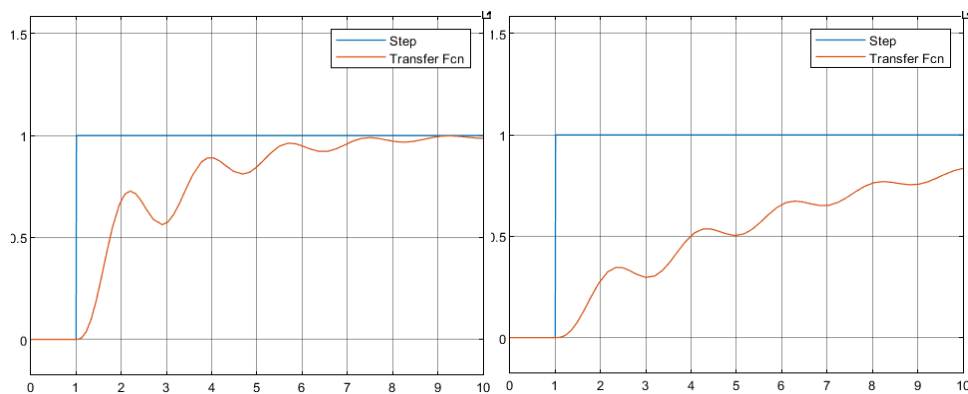
Fig D.16 Step response of Multi-step Input Dataset H0-H12 using Ziegler Nicholas tuning technique

DOUBLET INPUT



DATA SET D1

PULSE INPUT



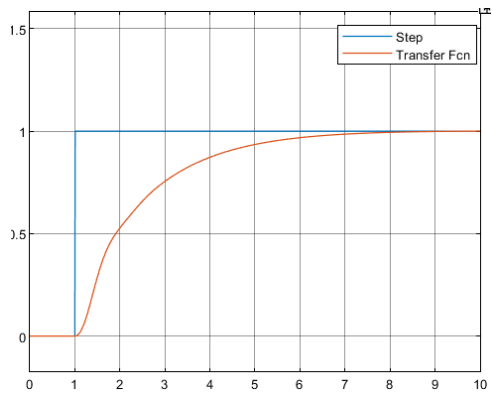
DATA SET HP1

DATA SET HP2

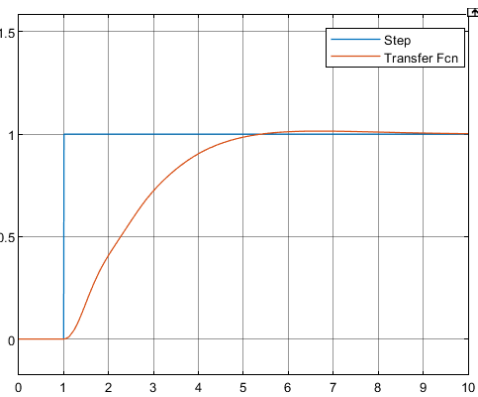
Fig D.17 Step response of Doublet, and Pulse Input Dataset D1, HP1, and HP2 using Ziegler Nicholas tuning technique

Various datasets are used for gain optimization to design controller using PID tuning Approach. In this figure, X axes denotes time(sec) and Y axes as amplitude. The step response shows oscillatory behaviour of input form which gets damped after short interval. Dataset H12 shows optimal response among all datasets.

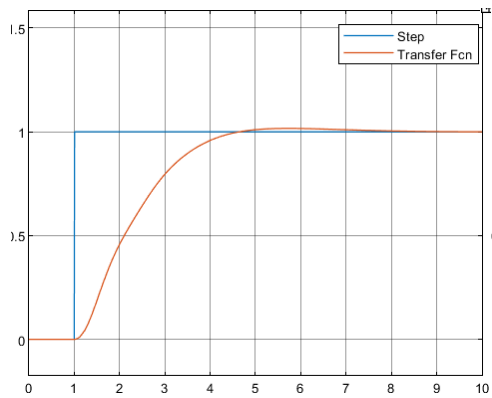
MODIFIED ZIEGLER NICHOLAS FIGURES OF MULTI-STEP, DOUBLET, AND PULSE INPUT



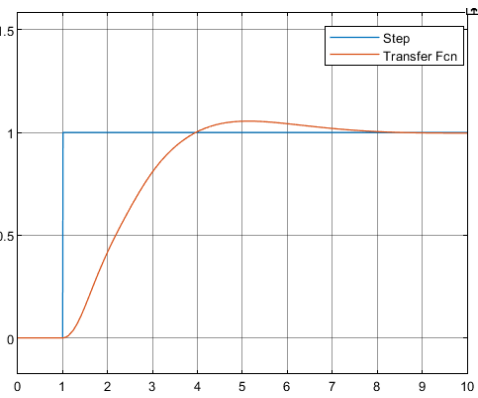
DATA SET H0



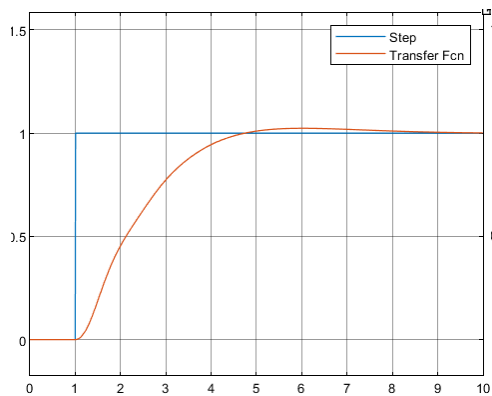
DATA SET H1



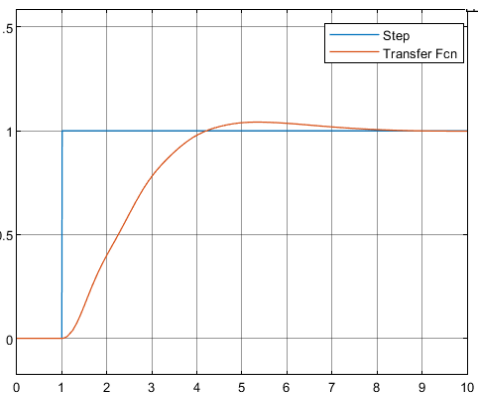
DATA SET H2



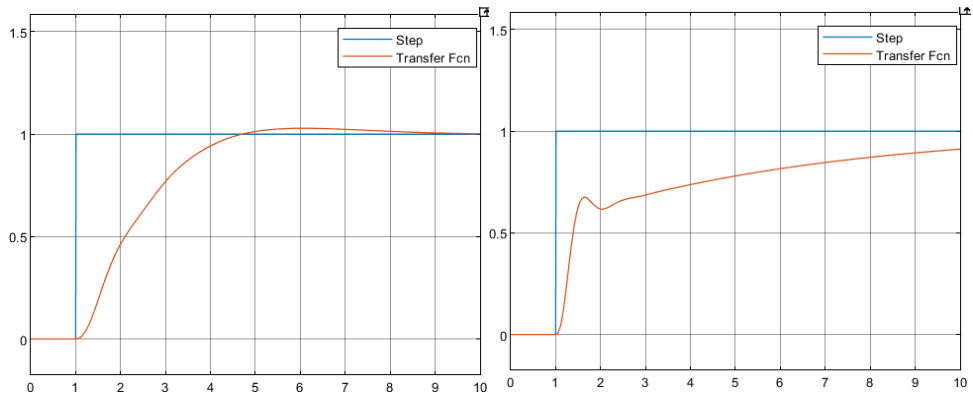
DATA SET H4



DATA SET H5

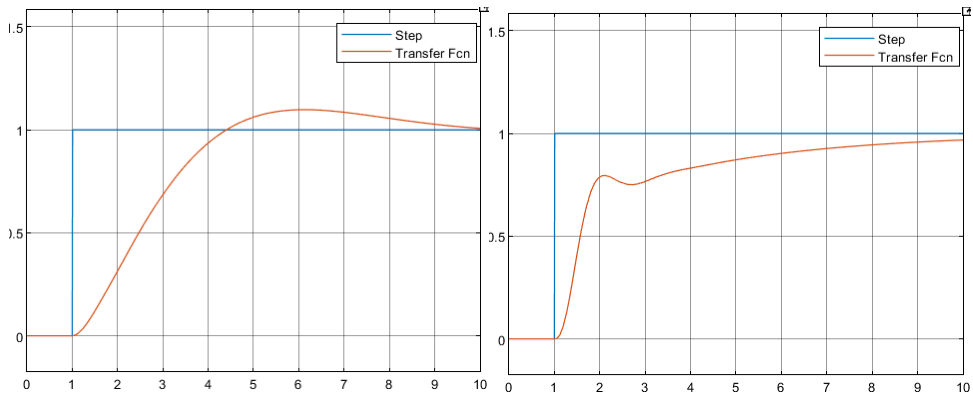


DATA SET H6



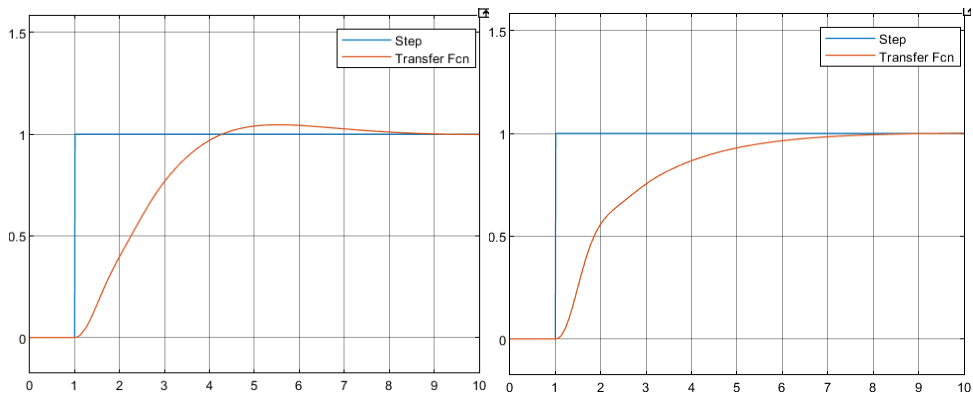
DATA SET H7

DATA SET H8



DATA SET H9

DATA SET H1

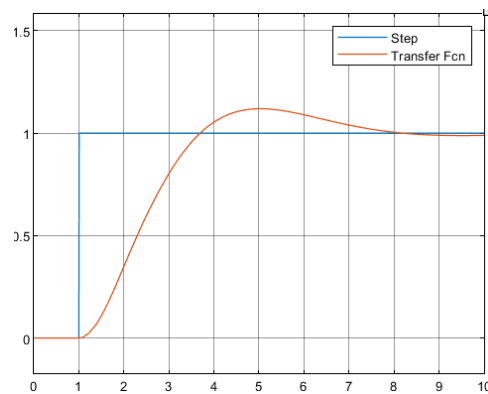


DATA SET H11

DATA SET H12

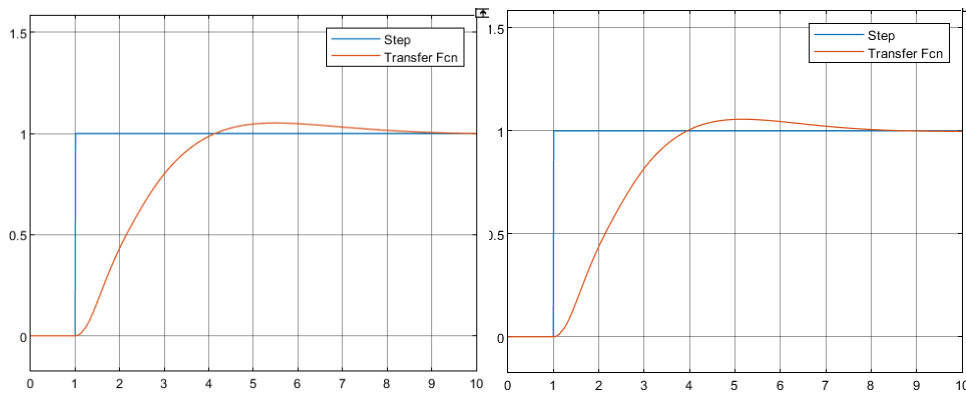
Fig D.18 Step response of Multi-step Input Dataset H0-H12 using Modified Ziegler Nicholas tuning technique

DOUBLET INPUT



DATA SET HD1

PULSE INPUT



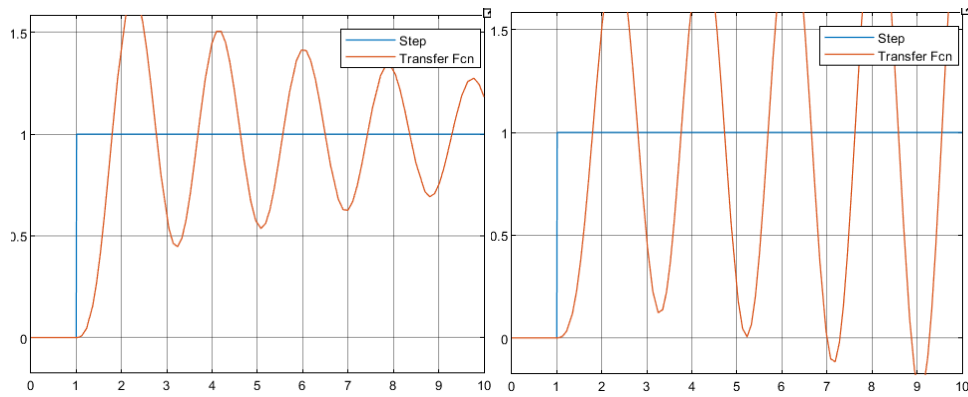
DATA SET HP1

DATA SET HP2

Fig D.19 Step response of Multi-step Input Dataset H0-H12 using Modified Ziegler Nicholas tuning technique

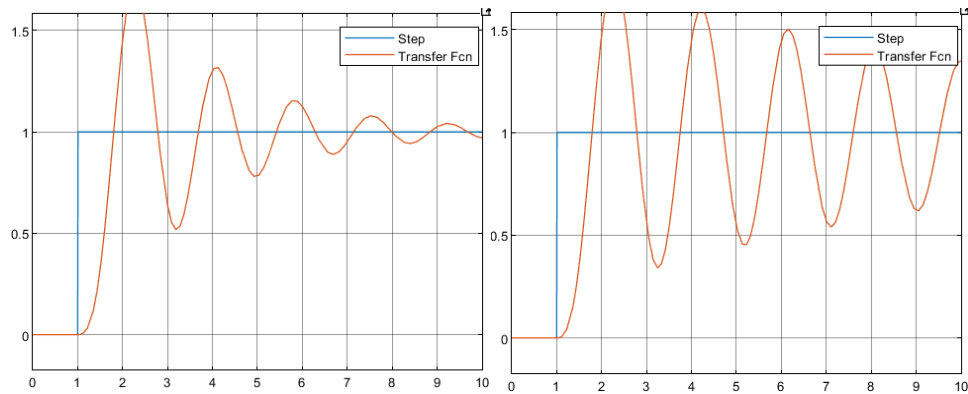
Various datasets are used for gain optimization to design controller using PID tuning Approach. In this figure, X axes denotes time(sec) and Y axes as amplitude. The step response shows oscillatory behaviour of input form which gets damped after short interval. Dataset H5 shows optimal response among all datasets as meeting all control system design requirements

TYREUS-LUYBEN FIGURES OF MULTI-STEP, DOUBLET, AND PULSE INPUT



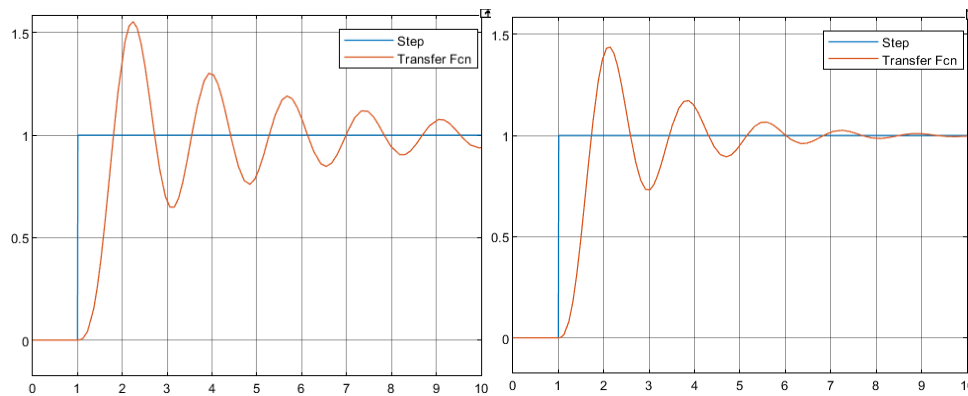
DATA SET H0

DATA SET H1



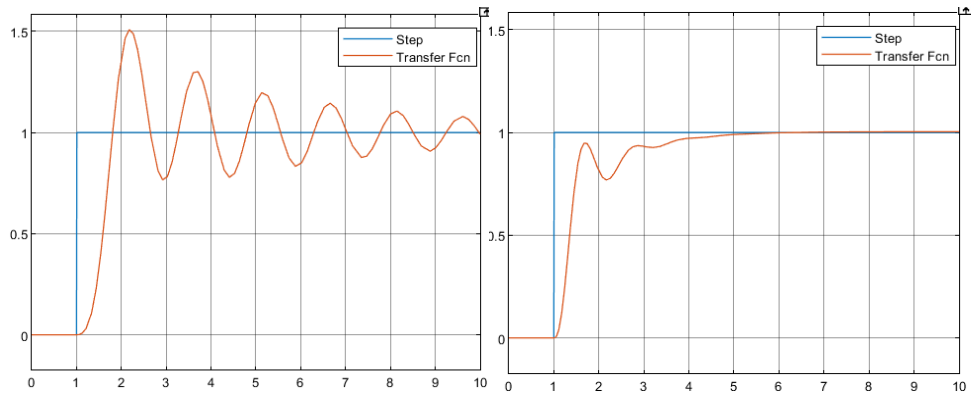
DATA SET H2

DATA SET H4



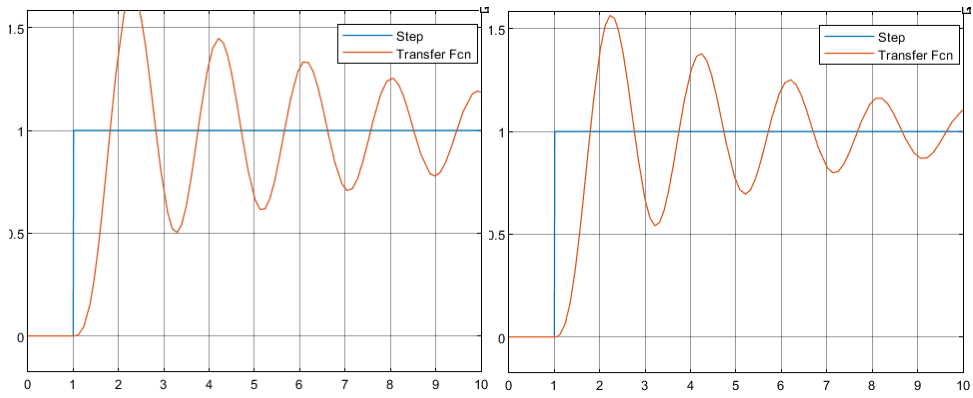
DATA SET H5

DATA SET H6



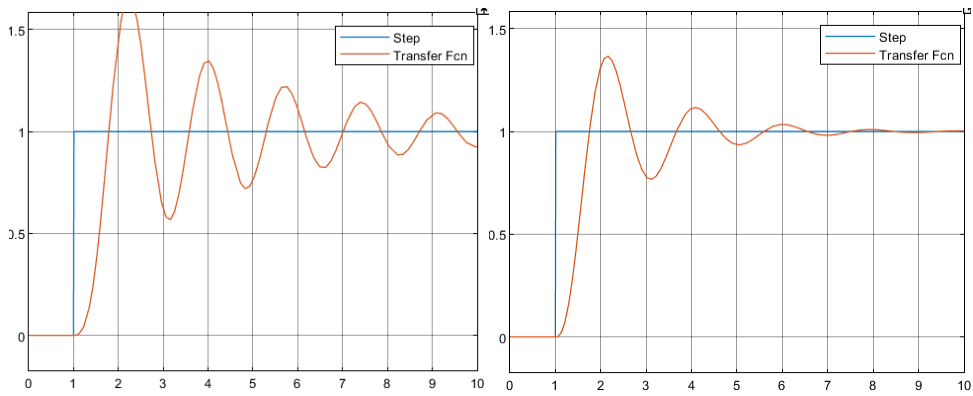
DATA SET H7

DATA SET H8



DATA SET H9

DATA SET H10

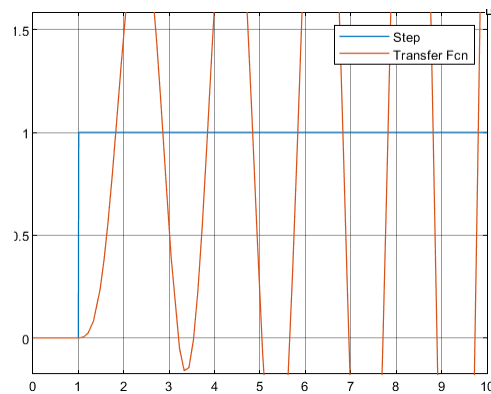


DATA SET H11

DATA SET H12

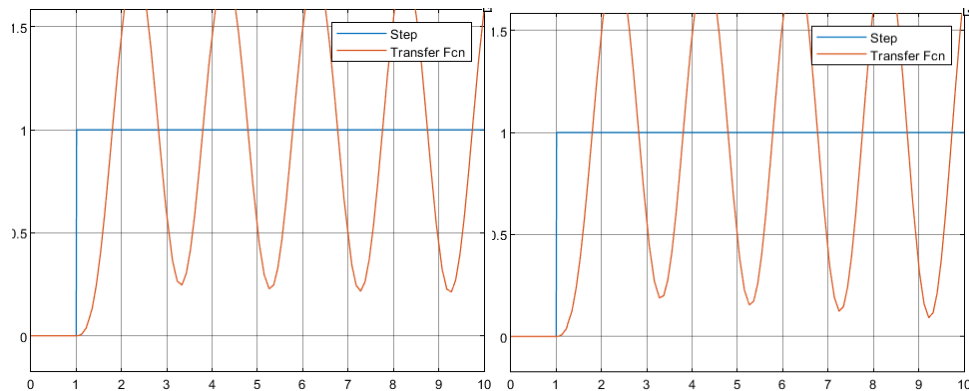
Fig D.20 Step response of Multi-step Input Dataset H0-H12 using Tyreus-Luyben tuning technique

DOUBLET INPUT



DATA SET HD1

PULSE INPUT



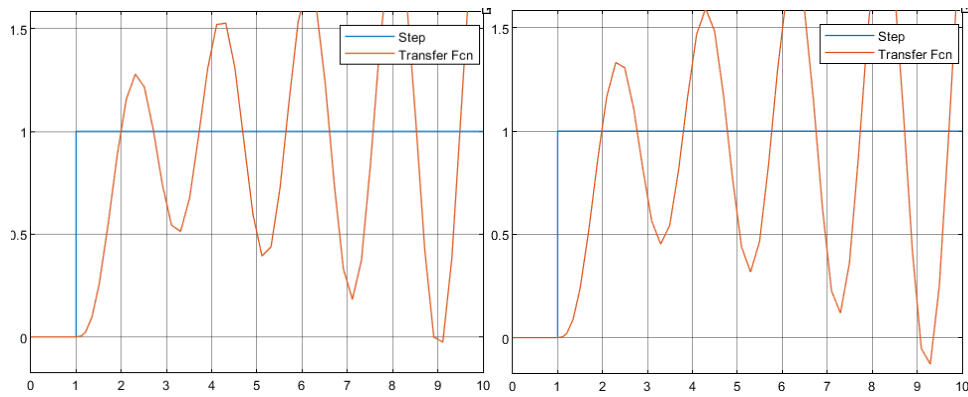
DATA SET HP1

DATA SET HP2

Fig D.21 Step response of Doublet, Pulse Input Dataset HD1, HP1, and HP2 using Tyreus-Luyben tuning technique

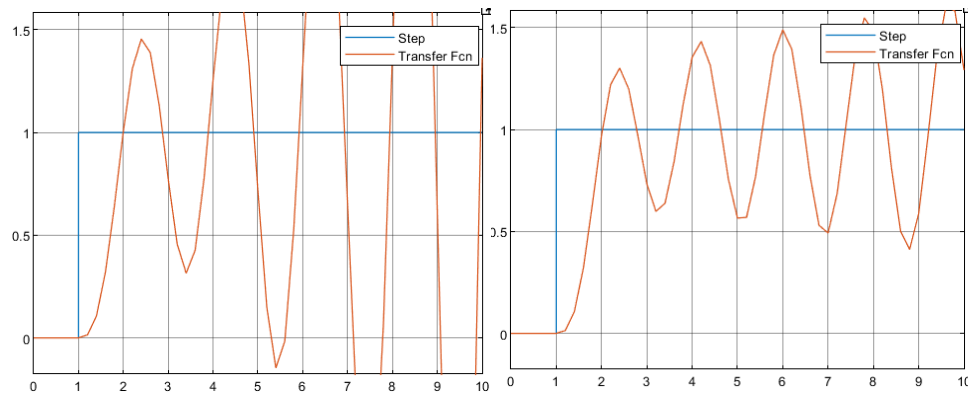
Various datasets are used for gain optimization to design controller using PID tuning Approach. In this figure, X axes denotes time(sec) and Y axes as amplitude. The amplitude of the step response shows oscillatory behaviour of input form which gets damped after short interval. Dataset H12 shows optimal response among all datasets whereas amplitude goes on increasing with respect to time of doublet and pulse input dataset

ASTROM-HAGGLUND FIGURES OF MULTI-STEP, DOUBLET, AND PULSE INPUT



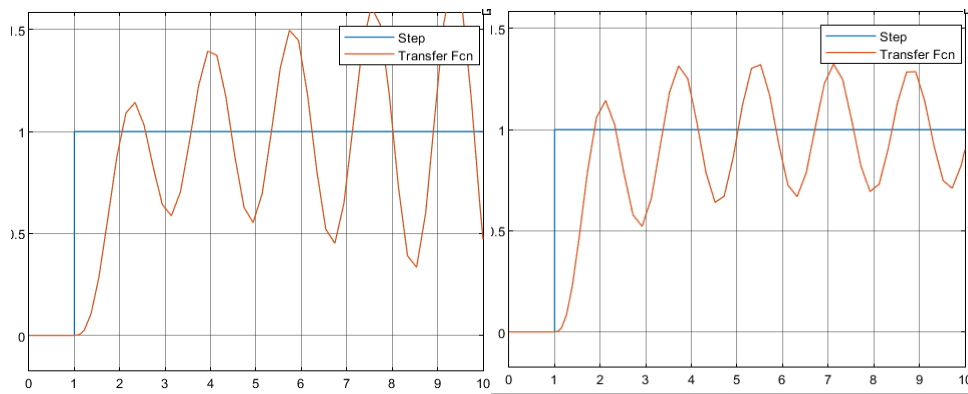
DATA SET H0

DATA SET H1



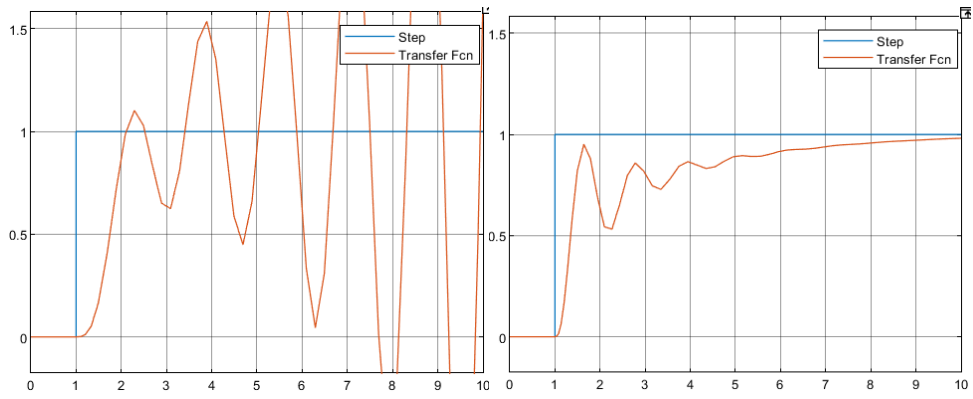
DATA SET H2

DATA SET H4



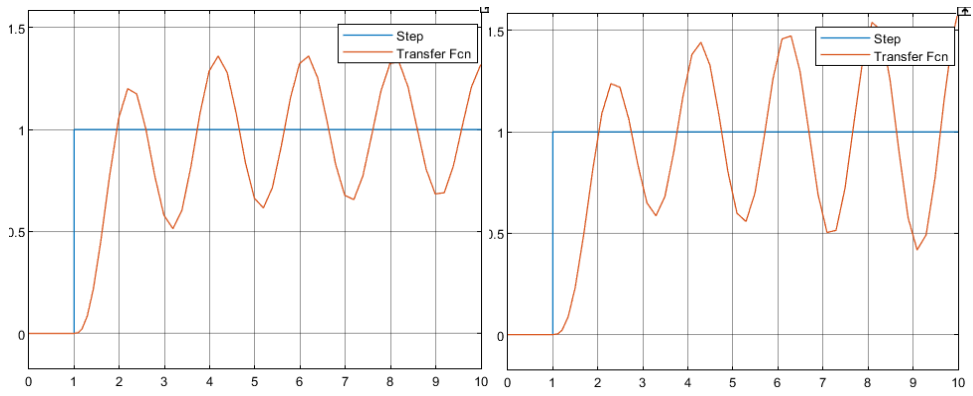
DATA SET H5

DATA SET H6



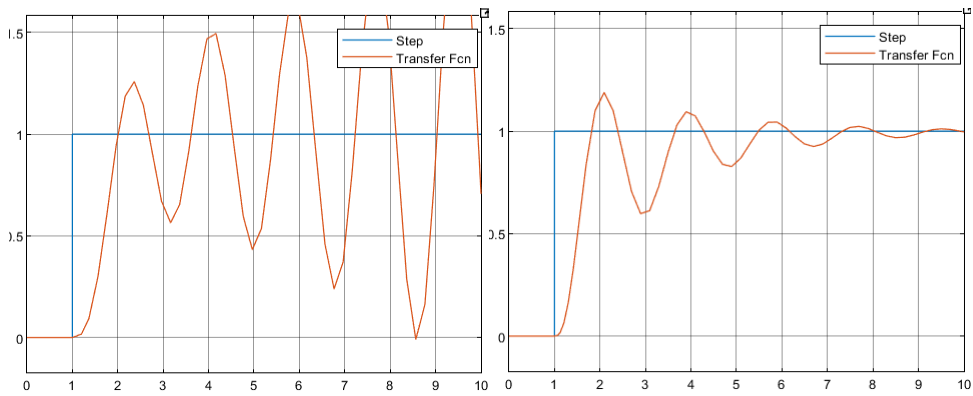
DATA SET H7

DATA SET H8



DATA SET H9

DATA SET H10

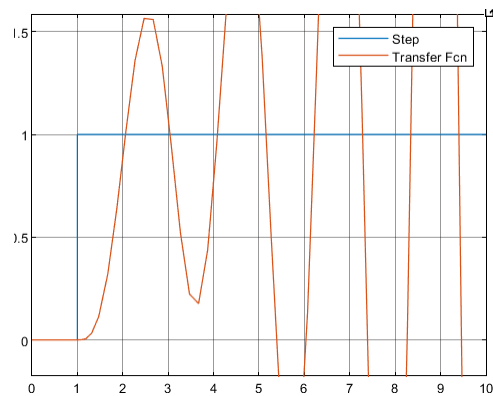


DATA SET H11

DATA SET H12

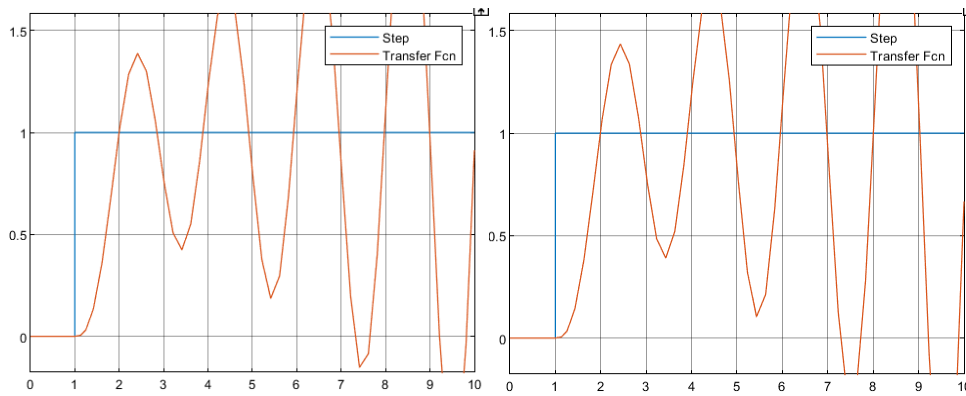
Fig D.22 Step response of Multi-step Input Dataset H0-H12 using Astrum-Hagglund tuning technique

DOUBLET INPUT



DATA SET HD1

PULSE INPUT



DATA SET HP1

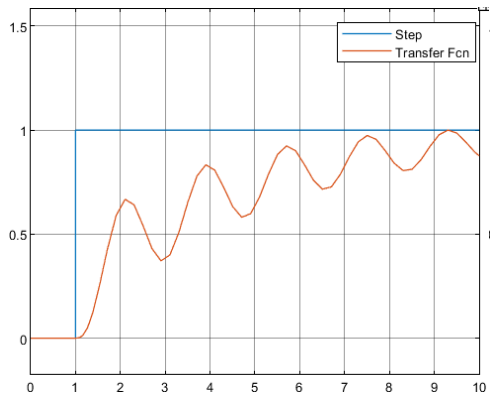
DATA SET HP2

Fig D.23 Step response of Doublet, Pulse Input Dataset HD1, HP1, and HP2 using Astrum- Hagglund tuning technique

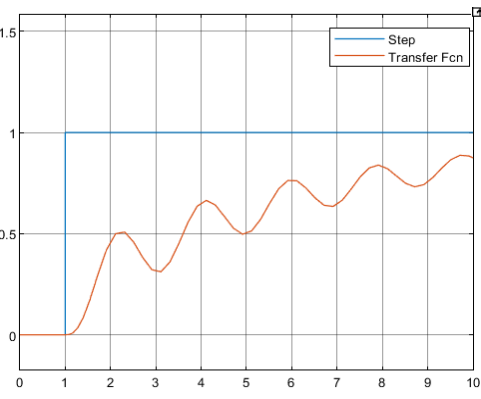
Various datasets are used for gain optimization to design controller using PID tuning Approach. In this figure, X axes denotes time(sec) and Y axes as amplitude. The amplitude of the step response shows oscillatory behaviour of input form which gets damped after short interval. Dataset H12 shows optimal response among all datasets whereas amplitude goes on increasing with respect to time of doublet and pulse input data

ZIEGLER NICHOLAS FIGURES OF MULTI STEP, DOUBLET, AND PULSE INPUT DATASETS OF PI CONTROLLER

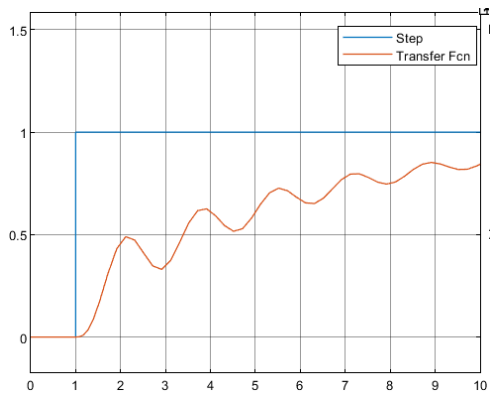
MULTISTEP INPUT



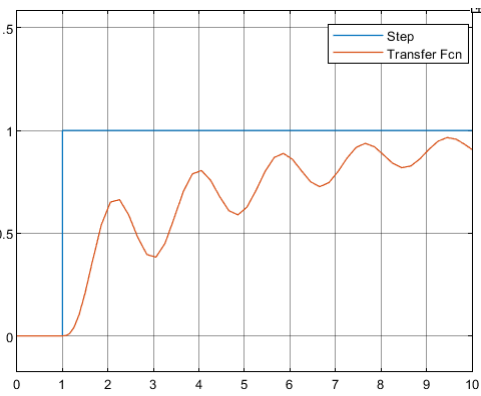
DATA SET H0



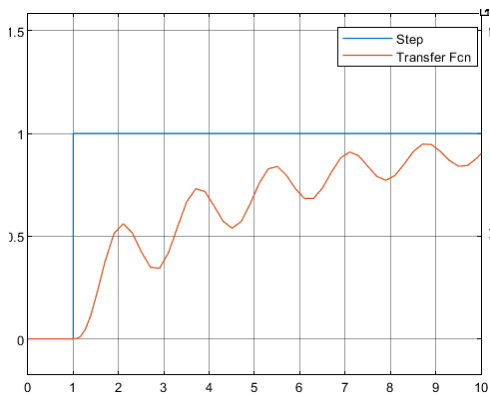
DATA SET H1



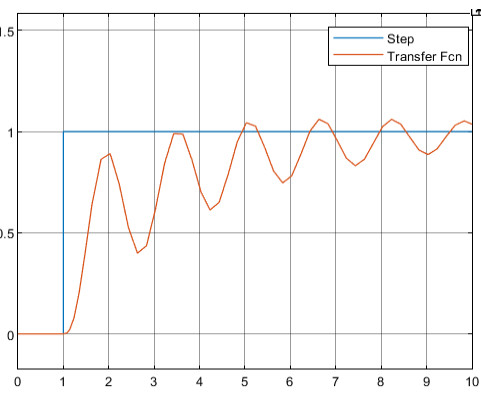
DATA SET H2



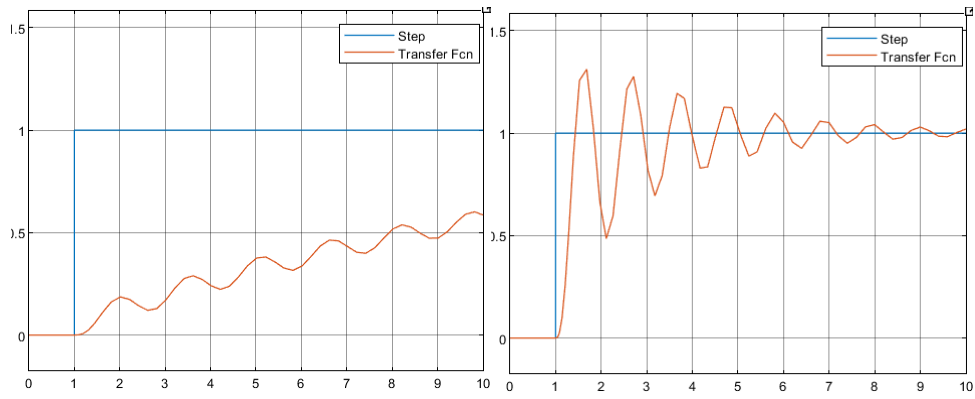
DATA SET H4



DATA SET H5

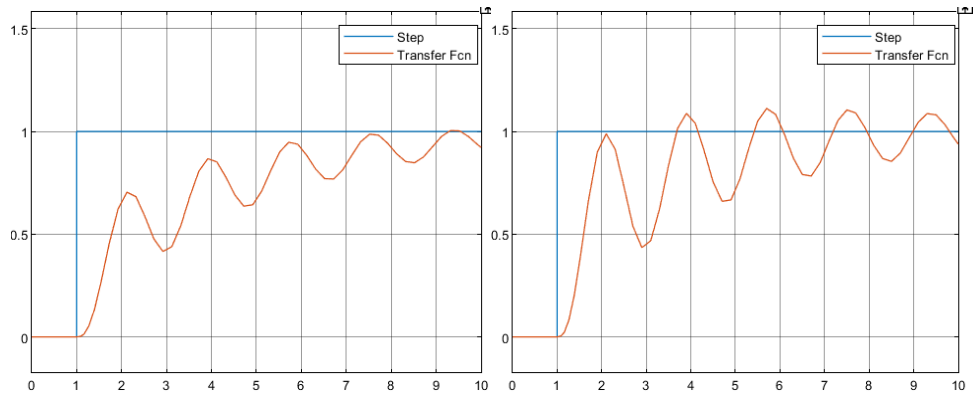


DATA SET H6



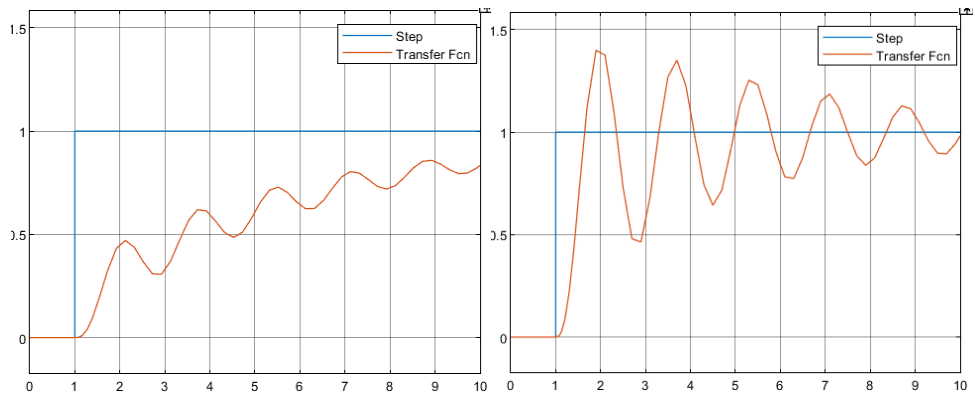
DATA SET H7

DATA SET H8



DATA SET H9

DATA SET H10

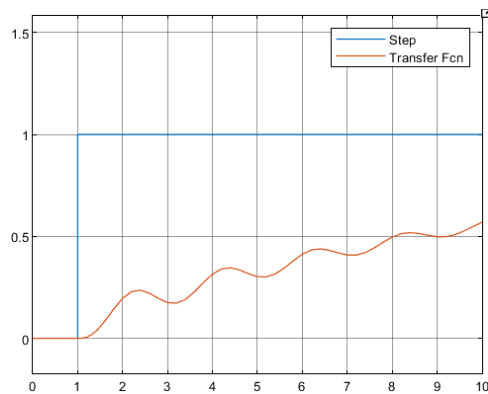


DATA SET H11

DATA SET H12

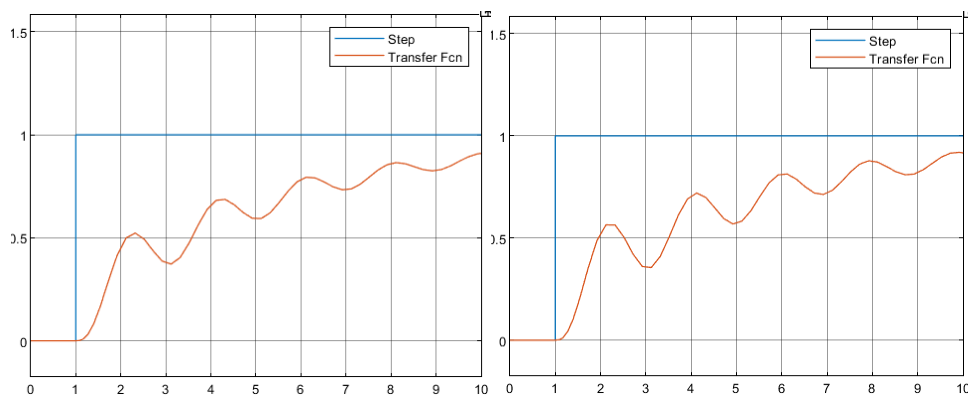
Fig D.24 Step response of Multi-step Input Dataset H0-H12 using Ziegler Nicholas tuning technique of PI Controller

DOUBLET INPUT



DATA SET HD1

PULSE INPUT



DATA SET HP1

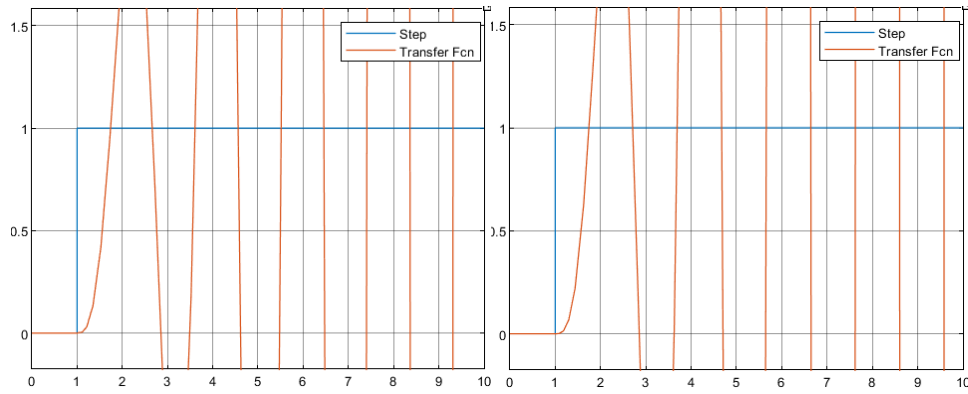
DATA SET HP2

Fig D.25 Step response of Doublet, Pulse Input Dataset HD1, HP1, and HP2 using Astrum- Hagglund tuning technique

Various datasets are used for gain optimization to design controller using PI tuning Approach. In this figure, X axes denotes time(sec) and Y axes as amplitude. The amplitude of the step response shows oscillatory behaviour of input form which gets damped after short interval. Dataset H12 shows optimal response among all datasets

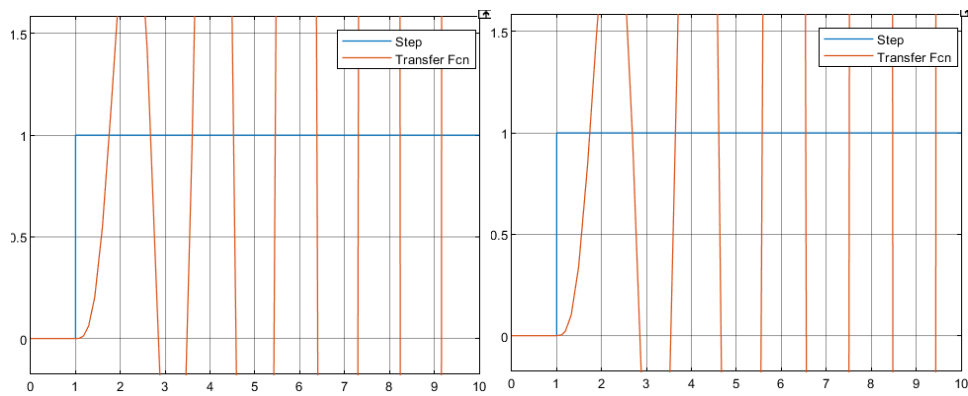
TYREUS-LUYBEN FIGURES OF MULTI STEP, DOUBLET, AND PULSE INPUT DATASETS OF PI CONTROLLER

MULTI STEP INPUT



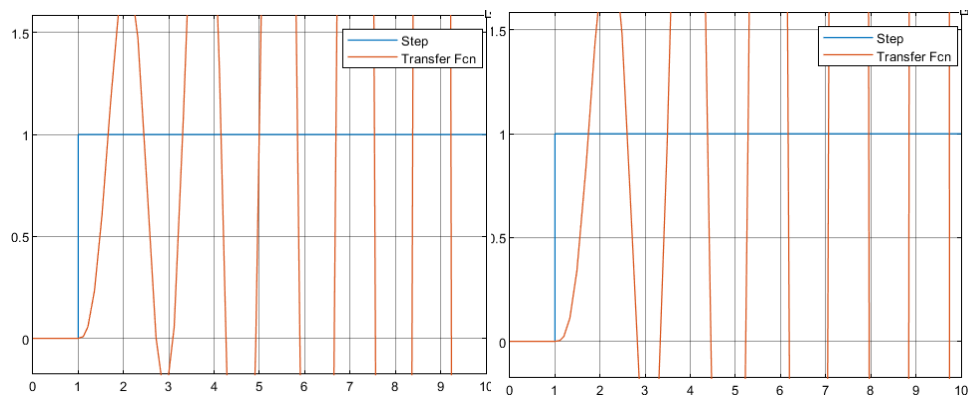
DATA SET H0

DATA SET H1



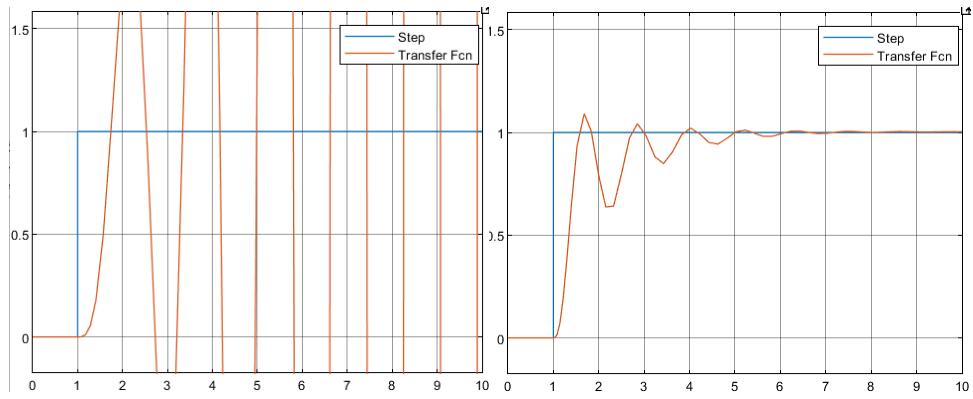
DATA SET H2

DATA SET H4



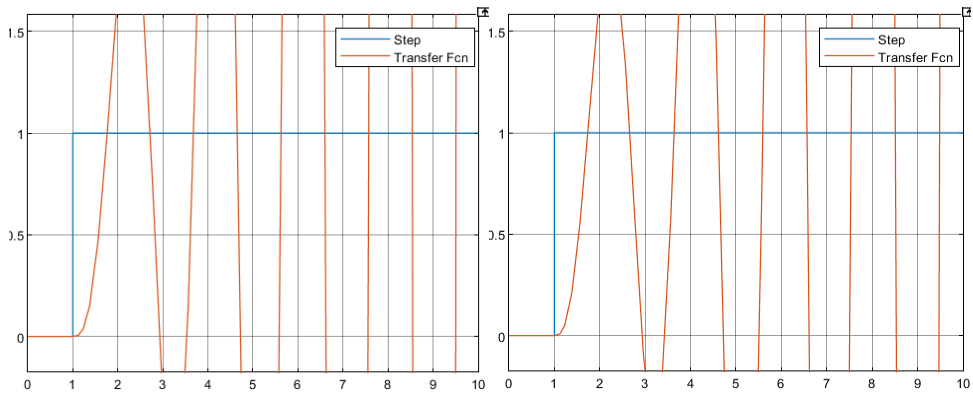
DATA SET H5

DATA SET H6



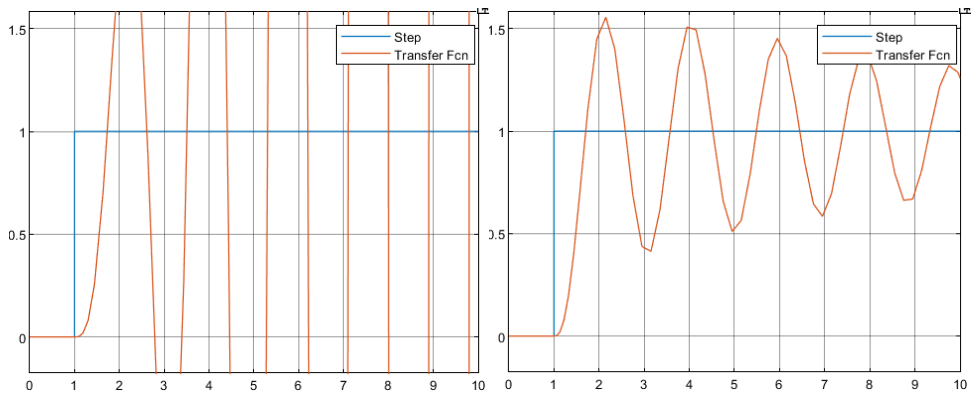
DATA SET H7

DATA SET H8



DATA SET H9

DATA SET H10

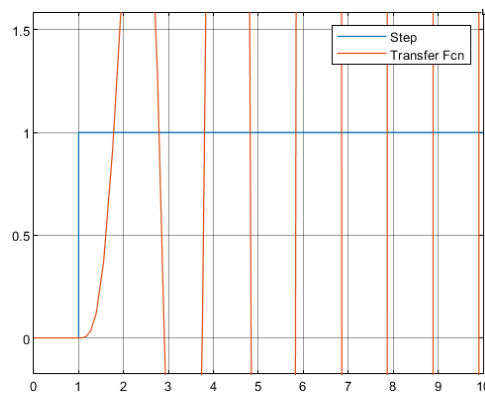


DATA SET H11

DATA SET H12

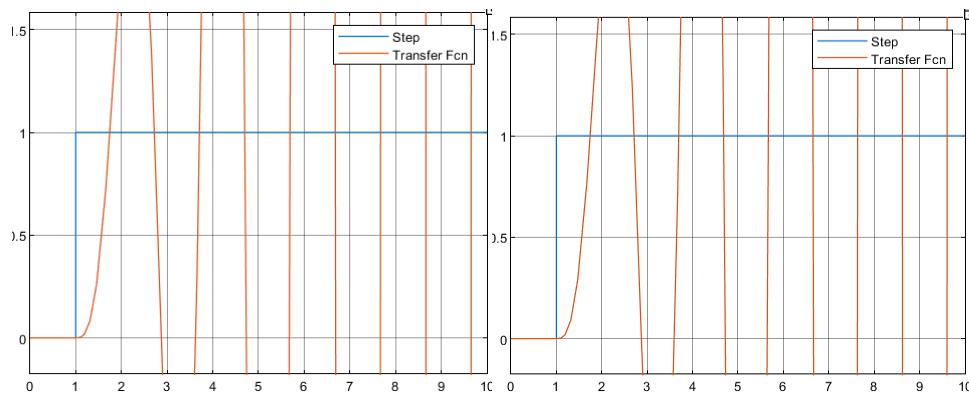
Fig D.26 Step response of Multi-step Input Dataset H0-H12 using Tyreus-Luyben tuning technique of PI Controller

DOUBLET INPUT



DATA SET HD1

PULSE INPUT



DATA SET HP1

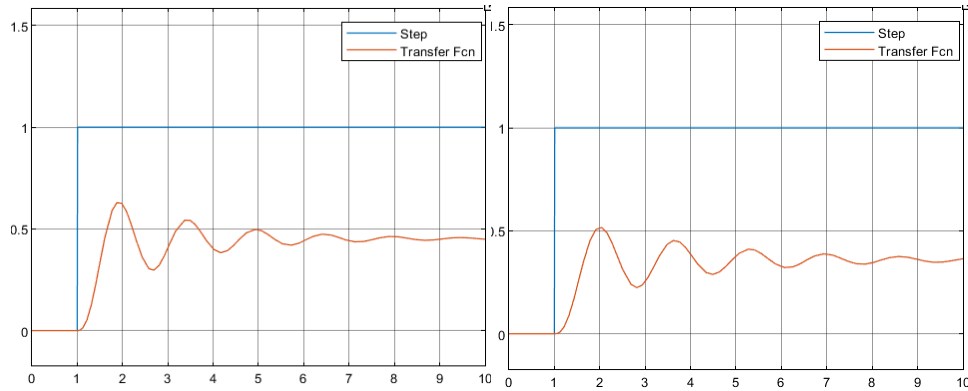
DATA SET HP2

Fig D.27 Step response of Doublet, Pulse Input Dataset HD1, HP1, and HP2 using Astrum- Haggglund tuning technique

Various datasets are used for gain optimization to design controller using PI tuning Approach. In this figure, X axes denotes time(sec) and Y axes as amplitude. The amplitude of the step response shows oscillatory behaviour of input form which gets damped after short interval. Dataset H8 shows optimal response among all datasets. Moreover, all other datasets have ever increasing amplitude.

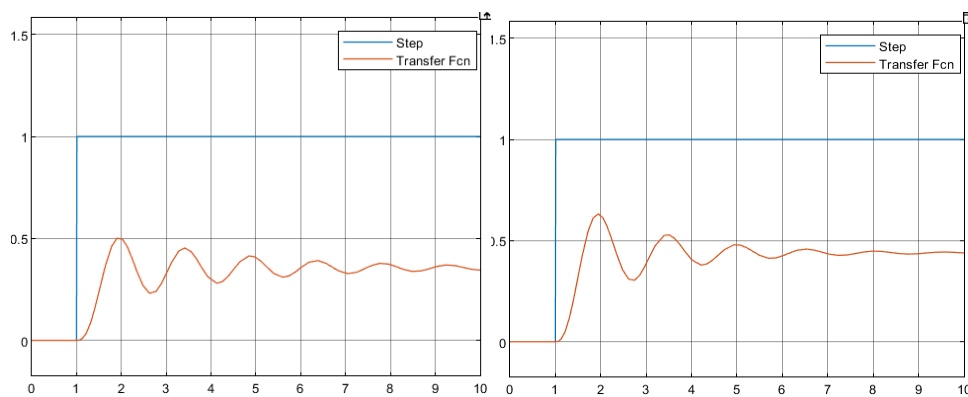
ZIEGLER NICHOLAS FIGURES OF MULTI STEP, DOUBLET, AND PULSE INPUT DATASETS OF PD CONTROLLER

MULTISTEP INPUT



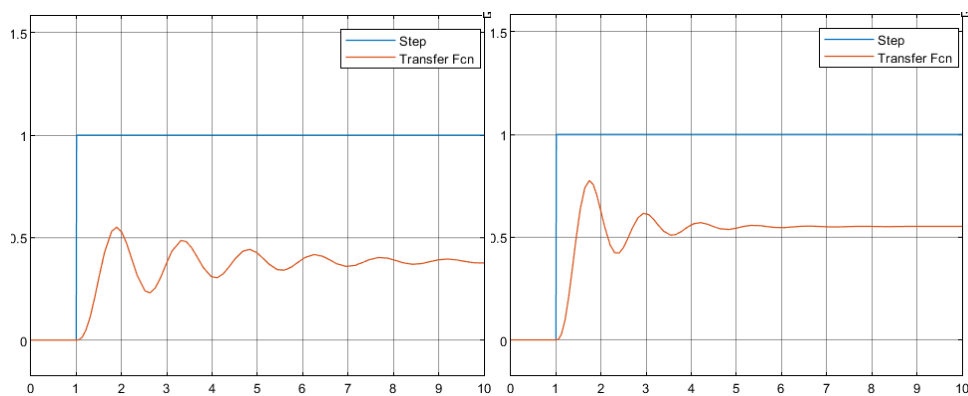
DATA SET H0

DATA SET H1



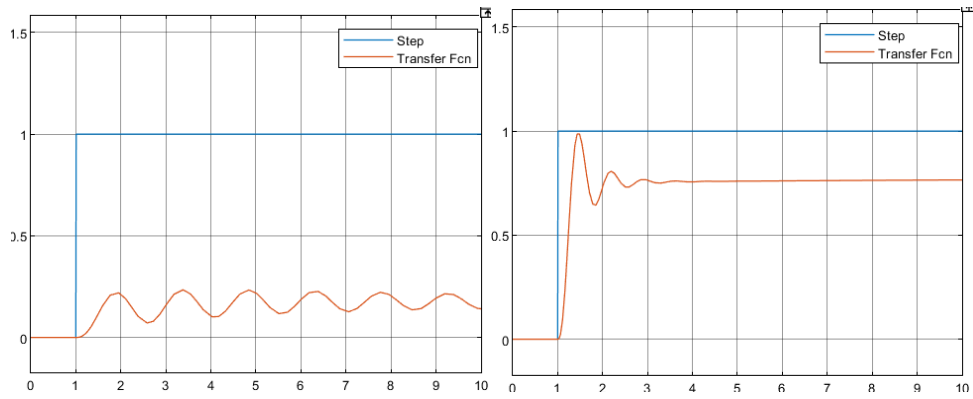
DATA SET H2

DATA SET H4



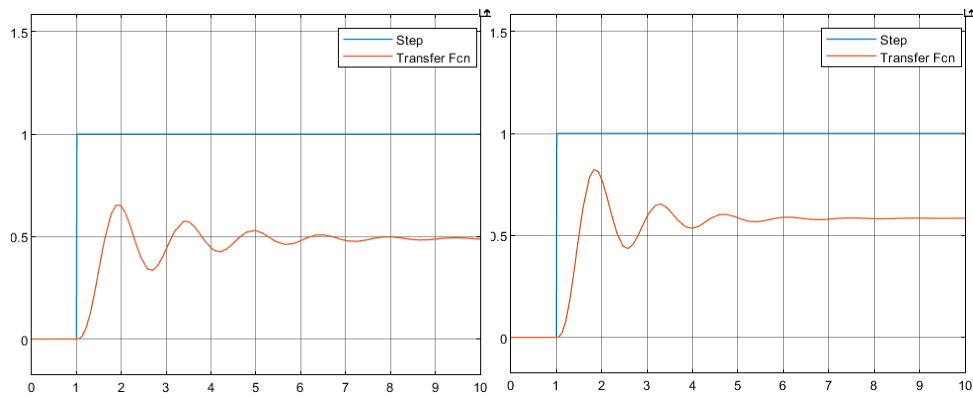
DATA SET H5

DATA SET H6



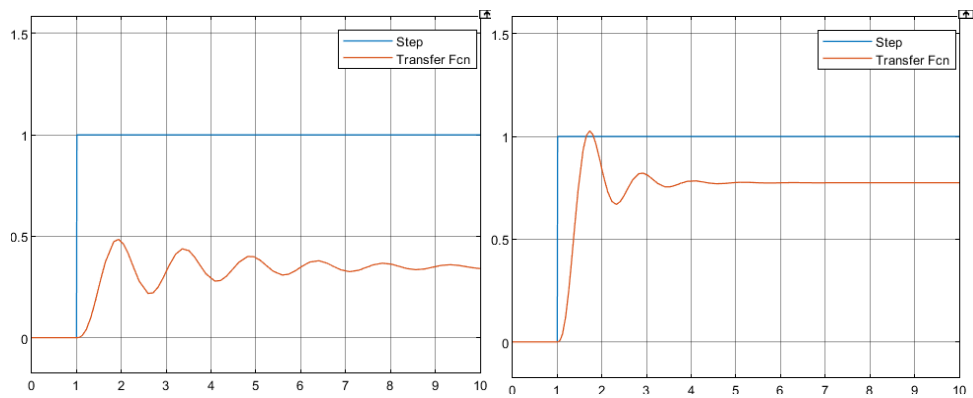
DATA SET H7

DATA SET H8



DATA SET H9

DATA SET H10

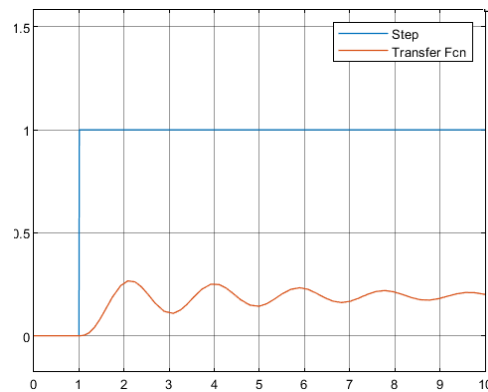


DATA SET H11

DATA SET H12

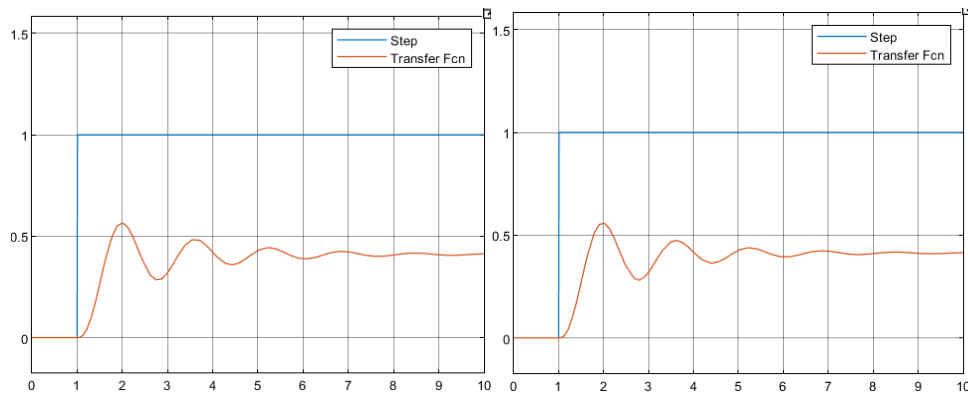
Fig D.28 Step response of Multi-step Input Dataset H0-H12 using Ziegler Nicholas tuning technique of PD Controller

DOUBLET INPUT



DATA SET D1

PULSE INPUT



DATA SET P1

DATA SET P2

Fig D.29 Step response of Doublet, Pulse Input Dataset D1, P1, and P2 using Ziegler Nicholas tuning technique

Various datasets are used for gain optimization to design controller using PD tuning Approach. In this figure, X axes denotes time(sec) and Y axes as amplitude. The amplitude of the step response shows oscillatory behaviour of input form which gets damped after short interval.

D3. ESTIMATION OF CARTESIAN COORDINATES USING FLIGHT DATA

Δt	ax	az	vx(k-1)	vx(k)	vz(k-1)	vz(k)	X(K-1)	Z(K-1)	Altitude(Y)	X(k)	Z(K)
0.02	2.474977	3.31304	36.5718	36.6213	26.682	26.74826	0	0	30540.65268	0.732426	0.534965
0.02	2.443499	3.326073	36.6213	36.67017	26.74826	26.81478	0.732426	0.534965	30540.65591	1.465829	1.071261
0.02	2.430449	3.315653	36.67017	36.71878	26.81478	26.8811	1.465829	1.071261	30540.65915	2.200205	1.608883
0.02	2.460625	3.335148	36.71878	36.76799	26.8811	26.9478	2.200205	1.608883	30540.66239	2.935565	2.147839
0.02	2.474912	3.320663	36.76799	36.81749	26.9478	27.01421	2.935565	2.147839	30540.66563	3.671915	2.688123
0.02	2.443434	3.312962	36.81749	36.86636	27.01421	27.08047	3.671915	2.688123	30540.66886	4.409242	3.229732
0.02	2.430385	3.318601	36.86636	36.91497	27.08047	27.14684	4.409242	3.229732	30540.6721	5.147541	3.772669
0.02	2.46056	3.302547	36.91497	36.96418	27.14684	27.21289	5.147541	3.772669	30540.67534	5.886825	4.316927
0.02	2.474847	3.337831	36.96418	37.01367	27.21289	27.27965	5.886825	4.316927	30540.67858	6.627098	4.86252
0.02	2.44337	3.311102	37.01367	37.06254	27.27965	27.34587	6.627098	4.86252	30540.68182	7.368349	5.409438
0.02	2.43032	3.305892	37.06254	37.11115	27.34587	27.41199	7.368349	5.409438	30540.68505	8.110572	5.957677
0.02	2.460496	3.310376	37.11115	37.16036	27.41199	27.4782	8.110572	5.957677	30540.68829	8.853779	6.507241
0.02	2.474782	3.31665	37.16036	37.20985	27.4782	27.54453	8.853779	6.507241	30540.69153	9.597976	7.058132
0.02	2.443305	3.317889	37.20985	37.25872	27.54453	27.61089	9.597976	7.058132	30540.69477	10.34315	7.61035
0.02	2.430255	3.298646	37.25872	37.30732	27.61089	27.67686	10.34315	7.61035	30540.698	11.0893	8.163887
0.02	2.460431	3.299971	37.30732	37.35653	27.67686	27.74286	11.0893	8.163887	30540.70124	11.83643	8.718744
0.02	2.474717	3.294893	37.35653	37.40603	27.74286	27.80876	11.83643	8.718744	30540.70448	12.58455	9.274919
0.02	2.44324	3.316298	37.40603	37.45489	27.80876	27.87508	12.58455	9.274919	30540.70772	13.33365	9.832421
0.02	2.43019	3.286346	37.45489	37.5035	27.87508	27.94081	13.33365	9.832421	30540.71095	14.08372	10.39124
0.02	2.460366	3.301883	37.5035	37.5527	27.94081	28.00685	14.08372	10.39124	30540.71419	14.83477	10.95137
0.02	2.474653	3.285324	37.5527	37.6022	28.00685	28.07256	14.83477	10.95137	30540.71743	15.58681	11.51283
0.02	2.443175	3.289663	37.6022	37.65106	28.07256	28.13835	15.58681	11.51283	30540.72067	16.33984	12.07559

Table D.3 Cartesian Coordinates Estimation Using Flight Data

APPENDIX- E

LIST OF PUBLICATIONS

SCOPUS INDEXED JOURNALS

1. “A preliminary study of parameter estimation for fixed wing aircraft and high endurance parafoil Aerial Vehicle”, *INCAS Bulletin*, Vol-12, Issue-4, SCOPUS Indexed, Dec2020
2. “Classical and Modern gain estimation approach of PID Controller for the pitch control of the RCTA Aircraft”, *INCAS Bull.*, vol. 14, no. 1, pp. 39-56, SCOPUS Indexed, 2022, Doi: 10.13111/2066-8201.2022.14.1.4

CONFERENCES

1. “Estimation of Lateral Directional Aerodynamic Derivatives from Flight Data of Unmanned Powered parafoil Aerial Vehicle”, *Proceedings of the AIAA Atmospheric Flight Mechanics Conference*, 2018
2. “Comparative study of longitudinal stability derivatives of Hansa-3 Aircraft Using Extended Kalman Filtering Technique and ML Method” in *Advances in Chemical Engineering*, SCOPUS Indexed, Dehradun, Feb2020.
3. “Distinctive Navigational Approach –A Dead Reckoning for Aircraft Co-Ordinate Estimation”, 4th International Conference on Smart and Sustainable Developments in Engineering and Technology, PiCET, 22nd May 2022.
4. “Comparative assessment of stochastic approaches-EKF, ML to determine parameters of an RCTA aircraft for autopilot design” is submitted on International Conference on Engineering and Technology, PiCET 2023

PhD Thesis

ORIGINALITY REPORT

5%

SIMILARITY INDEX

3%

INTERNET SOURCES

4%

PUBLICATIONS

2%

STUDENT PAPERS

PRIMARY SOURCES

1

Submitted to Indian Institute of Technology,
Kanpur

Student Paper

<1 %

2

Ravindra V. Jategaonkar. "Flight Vehicle
System Identification: A Time-Domain
Methodology, Second Edition", American
Institute of Aeronautics and Astronautics
(AIAA), 2015

Publication

<1 %

3

Submitted to University of Petroleum and
Energy Studies

Student Paper

<1 %

4

Ying Bai, Zvi S. Roth. "Classical and Modern
Controls with Microcontrollers", Springer
Science and Business Media LLC, 2019

Publication

<1 %

5

documents.mx

Internet Source

<1 %

6

"Handbook of Unmanned Aerial Vehicles",
Springer Nature, 2015

Publication

<1 %
